Cost-Effective Strategies for Wind Farm O&M: Topics in Structural Reliability, Load Analysis, Predictive Maintenance and Decision Making

Colone, Lorenzo

Link to article, DOI:
10.11581/DTU:00000033

Publication date:
2018

Document Version
Publisher's PDF, also known as Version of record

Cost-effective Strategies for Wind Farm O&M

Topics in Structural Reliability, Load Analysis, Predictive Maintenance and Decision Making

Department of Wind Energy
PhD Report 2018

Lorenzo Colone

DTU Wind Energy PhD-0088(EN)
DOI number: 10.11581/DTU:00000033

September 2018

DTU Wind Energy
Department of Wind Energy

Authors: Lorenzo Colone

Title: Cost-Effective Strategies for Wind Farm O&M Topics in Structural Reliability, Load Analysis, Predictive Maintenance and Decision Making.

2018

Project Period:
July 2015 – Sept. 2018

Education:
PhD

Acknowledgement:
This project has received funding from the European Union's Horizon 2020 research and innovation programme under the Marie Sklodowska-Curie grant agreement No 642108 (Advanced Wind Energy Systems Operation and Maintenance Expertise, http://awesome-h2020.eu/).

Supervisor:
Senior Scientist Anand Natarajan, DTU Wind Energy
Co-supervisor:
Senior Scientist Nikolay Krasimirov, DTU Wind Energy

Examiners:
Professor Po Wen Cheng, University of Stuttgart
Professor Lance Manuel, The University of Texas, Austin
Senior Scientist Gunner Chr. Hansen, DTU Wind Energy

DTU Wind Energy is a department of the Technical University of Denmark with a unique integration of research, education, innovation and public/private sector consulting in the field of wind energy. Our activities develop new opportunities and technology for the global and Danish exploitation of wind energy. Research focuses on key technical-scientific fields, which are central for the development, innovation and use of wind energy and provides the basis for advanced education.

DTU Wind Energy has a staff of approximately 240 and a further 35 PhD-students, spread across 38 different nationalities. The variety of research, education, innovation, testing and consultancy is reflected in the employment profile which includes faculty with research and teaching responsibilities, researchers and technical academic staff, highly skilled technicians and administrative staff.

Our facilities are situated at DTU Risø Campus and at DTU Lyngby Campus. Furthermore the department is running the national test stations in Høvsøre and Østerild.

Technical University of Denmark
Department of Wind Energy
Frederiksborgvej 399
Building 118
4000 Roskilde
Denmark

www.vindenergi.dtu.dk

Technical University of Denmark, Department of Wind Energy

PhD thesis report

A dissertation submitted in fulfillment of
the requirements for the degree of
Doctor of Philosophy

Preface

The transition from conventional energy generation technologies to renewable energies is an ambitious plan steered by the threat of human-driven global warming, causing climate change [1]. At its present state, this global responsibility is formalized under a long-term deal named as *Paris Agreement*, which engages 195 participating Countries worldwide. The primary goal of the agreement is to reduce the amount of carbon dioxide present into the atmosphere by mitigating the release of greenhouse gases, along with countermeasures for its capture and storage. To boost the shift to renewable energies were also the first signs of crisis of conventional energy sources, such as oil, coal and nuclear. Therefore, wind energy, especially offshore, plays a key role in the transition to low-carbon economies.

As a result of considerable efforts by the scientific community and supportive political decisions, significant steps ahead have been made during the latest years to lower the cost of energy from wind resources. However, several issues still need to be addressed to keep pace with a fast growing market and adapt to strategic business decisions. Nowadays, the scenario around industrial development of the wind energy market portrays European Countries in a leading position. This burden motivates active research to achieve cost-effective solutions without drastically harming the economy.

Wind farms are strategic facilities designed to meet the global energy demand and let future generations benefit from a sustainable world. For such large scale projects, it is of primary importance to ascertain adequate safety levels in balance with economical aspects throughout the entire lifetime of the assets. Maintenance is a fundamental practice from this standpoint. Successful maintenance reduces the risk of unforeseen failures, thus avoiding potential negative impact on the economical viability of the project as well as on society.

This work is a small contribution towards the development of intelligent maintenance practice of wind farms. It embraces different aspects concerning the whole turbine as a system and as a cluster of systems, leaving a realistic impression of the scale of the problem. My intention is to provide the backbone for future advanced studies in this area, and serve as inspiration for future researchers. This dissertation has been carried out between July 1st, 2015 and August 15th, 2018 at the Technical University of Denmark, under the financial support of the Marie Curie Action, H2020 European Research framework, which funding is greatly appreciated. Furthermore, the project is part of a consortium of academic and industrial bodies named as AWESOME (Advanced Wind Energy Systems Operation and Maintenance Expertise). The collaboration with Vattenfall Vindkraft A/S and the Technical University of Munich has been fundamental for the final delivery of this dissertation.

L. Colone
Copenhagen, June 2018

Summary (Danish)

Væsentlige teknologiske fremskridt har, I årtiet forud for denne udgivelse, pavet vejen for stor fremgang I antallet af større offshore vindkraft farme. Problemstillingen I fokus er p.t. ved at skifte væk fra at optimere designet og øge effektiviteten, og over til hvordan disse installationer kan drives og vedligeholdes på økonomisk mest hensigtsmæssig vis. Denne forskning fokuserer primært på udvikling af emner relateret til vindmølleparkers drift og vedligeholdelse (Eng: Operations & Maintenance, forkortet O&M). Dette område er på nuværende tidspunkt allerede inkluderende af de seneste teknologiske udviklinger inden for sikkerhedsteori og Big-data, hvilke under tiden tranformerer måderne hvorpå tekniske installationer bør drives, I konteksten af den nye industrielle revulotion. I vindenergisektoren findes en stærk motivation for at reducere omkosting af vindenergi, herunder med særlig fokus på innovationer inden for drift og vedligehold, hvilke betragtes til at være blandt de mest relevante mhp. At nå målet. Indeværende afhandling adresserer relevante problemstillinger relateret til drift og vedligehold af vindmølleparker, herunder specifikke målsætninger 1) evaluering af egnetheden af modeller for de naturlige omgivelser mhp. Evaluering af belastningseffekter I offshore konstruktioner 2) evaluering af den økonomiske levedygtighed af moniteringssystemer baseret på eksisterende machine learning metoder 3) kombinationsbelastninger med observerede nedbrud (eller strukturelle svigt) på en vindmøllepark-skala. Med hensyn til lastanalyse, er design lasttilfælde (DLC) svarende til operationelle tilstande samt tilstande I driftstop betragtet I dette studie, sammen med normale turbulensmodeller og normale bølgetilfælde. Til udviklingen af forudsigende vedligeholdelsesteknikker, er ikke-operationelle tilstande fjernet fra datasættet. De originale bidrag I denne afhandling er opgivet herunder. Listen er ikke inddelt I kategorier, med hensyn til de forskellige emner som behandles.

- Undersøgelse af egnetheden af den udmattelsestilsvarende turbulens percentil for monopæle, som defineret I IEC61400-1 [2], ved brug af Monte Carlo (MC) simuleringer af den fælles sandsynlighedsfordeling for miljøets variable, herunder middel vindhastighed, turbulens, betydende bølgehøjde og periode for maksimalbølge. Bidrag fra vindmølleparkers turbulensslipstrøm betragted ligeledes, baseret på modellen udviklet af Frandsen [3].

- Udledelse af den analytiske fejl I Wheeler Stretching på begrænsede vanddybder, brugt som korrektionsfaktor I det oprindelige udtryk for at tilfredstille Laplace ligningen som beskriver den todimensionale bølgebevægelse.

- Kvantificering af usikkerheden af den kinematiske model for bølger, med hensyn til udmattelsesskade I driftstop- og operationelle tilstande. Ikke-liniære bølger og Wheeler Stretching korrektion medtages I betragtningerne. Denne usikkerhed defineres som forholdet imellem damage equivalent loads (DELs). I de to tilfælde, divideret med den

DEL som fremkommer ved brug af den liniære bølgemodel og Wheeler Stretching.

- En pålidelighedsanalyse baseret på udmattelsesgrænsetilstanden af det mest udmattelsesbelastede snit af en monopæl, med hensyn til variabiliteten af modeller af miljøet for lastansættelse, herunder turbulens og bølger. Svigtgrænsefunktionen inkludere skade I stoptilstandende samt I operationelle tilstande, med deres respektive usikkerheder medtaget. Usikkerhed betragtes både I last- og I modstandsdelen af svigtgrænsefunktionen. Analysen udføres over hele møllens levetid, ved at beregne det akkumulerede samt det årlige pålidelighedsindeks udfra overlevelsessandsynligheden for det forrige år.

- En kvantificerende analyse om mulig korrelation imellem vinge-rods DEL'er og registrerede nødstop forsaget af funktionsfejl I pictch mekanismen på en offshore vindmøllepark. Dette opnås ved at genskabe udmattelseslasthistorikken for bøjningsmoment ved vinge-rod for en vindmøllepark, og herefter sammenligne denne med registrede nødstop, som følge af funktionsfejl.

- En metode som benytter "least absolute shrinkage and selection operator (LASSO)"-regularisering til at finde det mindst mulige sæt af signaler som muliggør prædiktion af skade forklarende variable i regressionsmodeller. Modellen er baseret på opbygning af normalbilledet af udsving i temperaturen i hovedlejet.

- Klassifikation af SCADA alarmer med henblik på tidlig erkendelse af fejl. Metoden baserer sig på at undgå hændelser med kritiske fejl ved at prædiktere mindre alvorlige SCADA alarmer, der potentielt set kunne forbedre driften af vindmølleparken. Neurale netværk og Naïve Bayes modeller er implementeret og Receiver Operator Characteristics (ROC) kurver er bygget på baggrund af output. En multi-test tilgang blev brugt til at generere flere ROC kurver med henblik på at kunne kvantificere prædiktionsusikkerheden.

- En metodik til vurdering af den økonomiske levedygtighed af klassificeringsbaserede forudsigelsesmodeller ved at kombinere Machine Learning og begivenhedstræ analyse, medtagende risikoen for svigt og falske alarmer. En effektivitetsparameter introduceres for at modellere den reducerede sandsynlighed for svigt af mekaniske komponenter givet vedligeholdelseshandlinger udført følgelig til en alarm. På denne måde er kvantificeringen af dens virkning på det samlede udbytte medtaget. Effektiviteten virker på sandsynligheden for fiasko givet en vedligeholdelseshandlin fra operatøren, og øges lineært fra 0 til 1. Den samme fremgangsmåde benyttes til regressionsbaserede forudsigelsesmodeller.

I forbindelse med den tidligere liste over udviklinger, kan de vigtigste resultater og konsekvenser af dette arbejde således angives som følger:

- Den udmattelsestilsvarende turbulens percentil for monopæle, som defineret I IEC standarden, er egnet til mekaniske komponenter, som f.eks. vinger, men er for konservativ for monopæle

- Den probabilistiske analyse af de hydrodynamiske koefficienter viser, at DEL fordelingenerne ikke er følsomme over for variabilitet af inerti og drag-koefficienterne, hvilket er en relevant information i pålidelighedsanalyser.

- Monopælens usikkerhedsanalyse af bølgemodellen viste, at der var en væsentlig forskel mellem stoppede- og driftsbelastninger. Disse stiger dramatisk ved stilstand på grund af fraværet af aerodynamisk dæmpning.

- De vigtighedsfaktorer, der beregnes ved hjælp af første ordens pålidelighedsmetoden, viste, at på trods af at bølgemodellens usikkerheder ikke er de vigtigste drivkræfter for udmattelsessikkerhed, er de signifikante forskelle i levetid og årlig sandsynlighed for svigt, når forskellige modeller kombineres. Dette har indflydelse på designbelastningsanalyser samt levetidsfolængelse gennem aeroelastiske simuleringer.

- Den kvalitative vurdering mellem vingerodens bøjningsmoment DEL og sandsynlighedsplottet over funktionsfejl i pitch systemet viser, at pitch-hændelserne er mere tilbøjelige til at forekomme i et konturområde større end 0,95 for normaliseret flapvis DEL. Da vurderingen ikke er kvantitativ, kan disse resultater ikke bekræfte en direkte korrelation mellem belastninger og svigt, men snarere et potentiale for at bruge belastningsplots til opnåelse af en forbedret park-konfiguration, der reducerer kritiske svigt.

- En analyse af skadesfølsomme egenskaber ved svigt af hovedlejet viser, at tårntoppens acceleration i for-akter retning og hovedlejets lodrette acceleration viser samtidig variation, der angiver progressive fejl. Disse oplysninger kan bruges til at opbygge multivariate outputlag for at dedektere fejl ved hjælp af regressionsmodeller.

- LASSO-reguleringen muliggør en stor reduktion af datasætets dimensioner og giver en fysisk fortolkning af svigtprocessen. Beslutningsanalysen udført på dette problem viste, at en reparationspolitik er omkostningseffektiv i forhold til udskiftningspolitik, samt at den førstnævnte varierer som funktion af reperationshandlingernes effektivitet. Metoden hjælper således med at beslutte om tekniske systemers økonomiske levedygtighed før deres implementering.

- Koblingen mellem Machine Learning med hændelses-træer for at kvantificere pålideligheden af datadrevne moniteringssystemer giver kriterier for at vælge en risikobaseret tærskel for online-forudsigelsesmodeller. Tilgangen kan føre til forbedret drift af vindmølleparker og gode driftsvilkår.

- Træning af klassificeringsalgoritmerne flere gange med en tilfældige testbatch for hver hold/out muliggør en kvantificering af forudsigelsesusikkerheden på ROC-kurven. Disse oplysninger er nyttige for at fastslå pålideligheden af den benyttede algoritme. Modellering af den reducerede sandsynlighed for fejl, antaget brugerens indgriben, gør det muligt at evaluere effektiviteten ved forskellige lede tider, hvilket vil bidrage til at træffe beslutninger om typen af system, der skal implementeres. Endelig afslørede analysen af SCADA-data forud for en nedlukningshendelse, at vindhastighedsstatistik højere end gennemsnittet, kombineret med unormal drift, kan øge risikoen for svigt.

Fremtidig forskning bør komplementere de væsenligste aspekter af denne afhandling, fra at undersøge virkningen af at forbedrede statistiske analyser for at give en mere generel konklusion om pålideligheden af vindmøllefundamenter under forskellige miljømodeller til belastningsvurdering, herunder følgende, inddragelse af detaljeret analyse af vibrationsdata i forudsigelsesmodeller og kvantificering af dennes økonomiske gevinst, standardisering af

moniteringssystem ved sammenlægning af SCADA- og vibrationsdata, opskalere moniteringssystemerne til vindmølleparkniveau og tillade fleksibel læring af disse, udvidelse af beslutningsmodeller til at omfatte længere lede tider, mere robuste forudsigelser og mere nøjagtige omkostningsmodeller; belastningsplots bør udvides med reelle komponentfejl kombineret med målte vibrationsdata og SCADA-data.

Summary (English)

Over the decade preceding this writing, important technological advancements in wind turbine design have enabled a massive deployment of large scale offshore wind farm projects. The main question is now shifting from enhancing turbine and farm design characteristics to optimize the energy capture, to operating and maintaining these facilities in an economically convenient manner. This research primarily concentrates on the development of aspects related to wind farm Operation and Maintenance (O&M). This field is by now an established discipline embracing the latest developments in reliability and Big-data, which are transforming the way to operate in the context of the new industrial revolution. There is a considerable drive in decreasing wind energy costs, where innovations in O&M are targeted among the most relevant to achieve the goal. This thesis addresses relevant issues related to wind farm O&M, which specific targets are 1) evaluation of the suitability of environmental models for load assessment of offshore substructure 2) assessment the economic viability of monitoring systems based on current machine learning techniques and 3) correlating loads with experienced failures on a wind farm scale. With regards to load analyses, design load cases (DLC) corresponding to operational states and standstill conditions are considered throughout this work along with normal turbulence models and normal sea states. For development of predictive maintenance techniques, non-operational states are taken out from the dataset. The original contributions of this thesis are readily listed below. The list is uncategorized with respect to the different topics treated.

- Investigation of the suitability of the fatigue equivalent turbulence percentile for monopiles as defined by IEC61400-1 [2] through Monte Carlo (MC) simulations of the joint probability distribution of the environmental variables, such as mean wind speed, turbulence, significant wave height and wave peak period. Contribution from wind farm wakes is also considered based on the model developed by Frandsen [3].

- Derivation of the analytical error of Wheeler stretching at finite water depths, used as corrective factor in the original formulation to satisfy the Laplace equation describing the two dimensional wave motion.

- Quantification of the wave kinematic model uncertainty with respect to fatigue damage in standstill and operational conditions. Nonlinear waves and Wheeler stretching correction are considered. This uncertainty is defined as the ratio between DELs in the two cases divided by the DEL resulting from using the linear wave model and Wheeler stretching.

- A reliability analysis based on fatigue damage limit state of the most fatigue-loaded section of the monopile is performed, with respect to the variability of environmental models for load assessment, namely turbulence and waves. The limit state function

includes standstill and operational damage, where their respective uncertainties are adopted in both the load and resistance term of the limit state function. The analysis is performed over the turbine lifetime.

- A qualitative analysis about possible correlation between blade root DELs and experienced shut-down events due to malfunctions in the pitch mechanism on an offshore wind farm. This is achieved by recreating the fatigue load map of the blade root bending moments of a wind farm, and compare it with recorded shut-downs due to malfunctions.

- A methodology based on least absolute shrinkage and selection operator (LASSO) regularization to select the minimum necessary number of signals to predict damage-sensitive features for regression-based prediction models. The model is based on tracking the normal behaviour fluctuations of main bearing temperatures.

- Classification of SCADA alarms for early fault detection. The method is based on avoiding the occurrence of critical failures by predicting low-severity SCADA alarms, which could potentially lead to improved wind farm operations. Neural network and Naïve Bayes classifiers are implemented and their probabilistic output is used to build Receiver Operator Characteristic (ROC) curves. A multi-testing approach is used to generate several ROC curves, in order to quantify the prediction uncertainty.

- A methodology to assess the economic viability of classification-based prediction models by coupling machine learning and event tree analysis, considering risk of failures and false alarms. An efficiency parameter is introduced to model the reduced probability of failure of mechanical components given maintenance interventions performed consequently to an alarm. Thus, the quantification of its effect on the total utility is addressed. The efficiency acts on the probability of failure given an intervention from the operator and increases linearly from 0 to 1. The same approach is used for regression-based prediction models.

Thus, in connection to the previous list of developments, the main findings and implications of this work can be listed as follows:

- The fatigue equivalent percentile defined by IEC standards is suitable for mechanical components like blades but too conservative for monopiles.

- The probabilistic analysis on the hydrodynamic coefficients shows that the DEL distributions are not sensitive to the variability of inertia and drag coefficients, which is an relevant information in reliability analyses.

- The wave model uncertainty analysis of the monopile revealed that a substantial difference between standstill and operational loads. These increases dramatically in standstill, due to absence of aerodynamic damping.

- The importance factors computed through the first order reliability method revealed that despite the wave model uncertainties are not the major drivers for fatigue reliability, the analysis shows significant differences in terms of lifetime and annual probability of failure when different models are combined. This has impact on design load analyses as well as lifetime reassessment through aeroelastic simulations.

- The qualitative assessment between blade root flapwise DEL normalized with respect to its maximum value and probability map of pitch system malfunctions, reveal that the in this case it is not possible to predict these malfunctions through a load map. However, since the assessment is not quantitative, these study cannot confirm a direct correlation between loads and failures, but rather a potential for using the load maps for achieving an improved farm configuration to mitigate the occurrence of critical failures.

- The analysis of damage-sensitive features in case of main bearing failures shows that the tower-top acceleration in the fore-aft direction and main bearing vertical acceleration show variation when a failure is present. This information can be used for building multivariate output models based on regression.

- The LASSO regularization enables a significant reduction of the dimensionality of the dataset as well as providing a physical interpretation of the failure process. The decision analysis carried out on this problem, revealed that a repair policy is cost-effective compared to replacement, and the first varies as function of the efficiency of intervention. The method thus helps decide on the economic viability of intelligent systems before their implementation.

- Coupling machine learning based predictive models with event-trees to quantify the reliability of data-driven monitoring systems provides a criteria to select a risk-based threshold for online classifiers. The approach could lead to improved wind farm operations and smooth running conditions.

- Training the classifiers multiple times with a random testing batch for each hold/out enables a quantification of the prediction uncertainty on the ROC curve. This information is useful to ascertain the reliability of the algorithm adopted. Thus, modeling of the reduced probability of failure given intervention by the user, allows to evaluate the efficiency at different lead times, which will help making decisions about the type of system to implement. At last, the analysis of the SCADA data prior a shut-down event revealed that wind speed statistics higher than those normal conditions and abnormal operation may increase the risk of failures.

Future research should complement key-aspects of this dissertation, from investigating the effect of improved statistical analyses to provide a more general conclusion about the reliability of wind turbine foundations under different environmental models for load assessment; inclusion of detailed analysis of vibration data into prediction models and quantification of their benefit; standardization of monitoring system by merging SCADA and vibration data; scale-up the monitoring systems to a wind farm level and allow flexible learning; extension of decision models to comprise longer lead times, more robust predictions and more accurate cost models; the load maps should be extended with real component failures coupled with measured vibration features and SCADA data.

Acknowledgements

Should I mention all the important people I came across along the way, it would clearly require more than one page. But a complete dissertation is not only written by brain, but also by heart.

A first acknowledgment goes back to the origin of this work, to Thomas Buhl, Anand Natarajan and Nikolay Dimitrov for believing in my capabilities to join a high-level educational environment, and to Ignacio Marti' for the moral support during the final part of the studies.

A special thank to Mads Hovgaard for enabling the opportunity to take part of this project and for supporting the idea of accepting the challenge.

Because no book or thesis is written without being inspired by other books, I would like to thank Daniel Straub, Micheal Faber, Tim Bedford, Nikolay Dimitrov for providing the basic concepts that inspired the ideas of this work.

I greatly appreciated the ever-surprising facts and motivating discussions with Michael Muskulus and the remarkable wisdom, experience and competences of Anders Melchior Hansen.

Thanks to Maik Reder, Jannis Tautz-Weinert, Elena Gonzales, Lisa Ziegler, Laura Valdecabres, Estefania Artigao, Emmanuil Nanos, Nurseda and Helene Seyr for the magnificent group and daily dose supply of positive charge to perform our duties, and for all the experiences we shared, from the cold and welcoming Norwegian mountains to the warm and shining Spanish shores.

Thanks to Mario Berk for whatever we call friendship that links us, to the colors of the Walchensee lake and the whole Engineering Risk Analysis group at the Technical University of Munich. In particular to Daniel Straub for his natural drive for engineering rationality, analytical mindset and pragmatism.

I learned from Davide Conti how to be more empathic and how to be more careful in delicated situation, certainly necessary along the way. Thanks to Peggy Friis, for treating me like a son during these years, and for the amazing time we had together. I am also gratefull to all those remarkable people in the SAC section at DTU Wind Energy that strive for integrity and transparency that enrich the professional environment and promotes scientific progress. Thanks to Alexander Verbart and Njomo Wandji for the mutual advices and rich conversations.

Thanks to Vattenfall for showing resilience to my repeated pushes for obtaining operational data. But also, for everything I learned from your valuable competences. In particular, thanks to Christian Pavese for teaching me strategic tips related to the content of this dissertation, and to Pierre Julien Trombe for making me notice that statistical problems have always a different perspective from which to look. Thanks to Thomas Pedersen for his patience and commitment in providing the necessary data. Finally, thanks to my family for learning and accepting many aspects of life not necessarily in agreement with their preferences. I hope you can all benefit from all the strange facts you will not understand of this document.

Contents

List of Figures

Acronyms

ADC Actuator Duty Cycles

AI Artificial Intelligence

BEM Blade Element Momentum

BN Bayesian Network

CBM Condition Based Maintenance

CMS Condition Monitoring Systems

COV Coefficient of Variation

DEL Damage Equivalent Load

DLC Design Load Case

DOF Degrees of Freedom

EOM Equation of Motion

FAR False Alarm Rate

FORM First Order Reliability Method

IS Importance Sampling

LASSO Least Absolute Shrinkage and Selection Operator

LDA Linear Discriminant Analysis

LM Linear Model

LTI Linear Time Invariant

MAE Mean Absolute Error

MC Monte Carlo

MSE Mean Squared Error

NB Naive Bayes

NBM Normal Behaviour Model

NN Neural Networks

O&M Operation and Maintenance

PCE Polynomial Chaos Expansion

PDF Probability Density Function

PFA Probability of False Alarms

PHM Prognostic Health Management

POD Probability of Detection

RBI Risk Based Inspection

RCM Reliability Centered Maintenance

RF Random Forrests

RMS Root Mean Square

RMSE Root Mean Squared Error

ROC Receiver Operator Characteristic

SCADA Supervisory Control and Data Acquisition

TF Transfer Function

WT Wind Turbine

List of articles

This is the list of articles attached to this thesis. The list refers to their corresponding status at the time of publishing. Article VI and V are collaborative works that are not part of the author's main contribution to this thesis.

- **Article I** Impact of turbulence induced loads and wave kinematic models on fatigue reliability estimates of offshore wind turbine monopiles - Published.
- **Article II** Predictive repair of wind turbine drive-train components based on machine learning - Under review.
- **Article III** - Assessing the Utility of Early Warning Systems for Detecting Failures in Major Wind Turbine Components - Published.
- **Article IV** - Optimisation of Data Acquisition in Wind Turbines with Data-Driven Conversion Functions for Sensor Measurements - Published.
- **Article V** Automated fault detection for wind turbines based on SCADA and CMS data - Under review.

Chapter 1

Introduction

An investment in knowledge pays the best interest.

B. Franklin

1.1 Background

1.1.1 Reliability and Big-data

According to the World Economic Forum [7], it is by now acknowledged that the modern period of history and development of human kind signs the dawn of the 4th industrial revolution. As every other revolution in history, also the contemporary brings systemic changes. These changes are featured by a myriad of electronic devices, machines and equipment in general, becoming increasingly ”smart”, thanks to their ability to adapt to external inputs through advanced control systems and provide real-time information through sensor networks, under the form of data. In addition, digital connectivity has further enabled immediate access to this information in a way never seen before. To certain extents, connectivity positively affects communities and interaction among people, supports societal and scientific progress and improves the quality of life. Consequently, this implies that data is a far valuable and ubiquitous resource. From an economic standpoint, data is currently valued as the *oil of the digital era* [8], and the advent of the new millennium has somehow warmly welcomed a new form of ”oil-rush”.

In fact, it is sufficient to think of how many digital enterprises employ data to support their business. Today’s tech giants as for instance Amazon, Facebook and Google among the most popular, are striking examples of this trend. Their dominant presence in the market is allowed by continuous development of up-to-date methodologies and applications for increasing the value of customers’ data. Or aviation engineers working with data records, who some decades ago would consider the job done by merely filling in a one-page document of flight information. Strict business requirements on aircraft reliability made it necessary to enable an efficient and fast interpretation of data. This made exclusive reliance on manual human capabilities soon outdated, leaving space to automated data processing techniques capable of giving answers in a profitable time span. Today, the amount of data coming from daily flights easily fills up

several gigabytes of memory, which is indicative of the significant steps ahead made over time in this area.

However, to make data a valuable resource it is necessary to process, interpret and turn them into actionable information. This is where engineering practice and analytical skills come into play. In the recent years, this concept is becoming prominent also within medium-small enterprises, thanks to open-source availability of statical tools that are making data analysis the bottom line of the new industrial revolution.

In general terms, the scientific community refers to as Big-data to indicate the extensive use of data as source of information. This use comprise all actions and challenges related to their capture, generation, processing, graphical visualization, storage and transfer. There is a growing interest in combining data with reliability engineering, which has by now become a new established discipline [9].

1.1.2 Maintenance engineering

The flow of technological changes achieved in the last decades has indubitably had a resonant impact on the mechanical industry too, especially in those area where a correct interpretation of data could potentially make a difference. One of those applications is Operation and Maintenance (O&M). Maintenance can be defined as the set of actions necessary to guarantee the required safety level of high-value assets, and fulfill the scope for which they were originally designed, throughout their lifetime. It is clear to notice the direct relation of maintenance to reliability of mechanical and electrical sub-assemblies constituting the asset. Nevertheless, determining the reliability level of operating assets is far from trivial, mostly because of multiple factors involved among which machine models, quality of design and manufacturing, operating environments, inaccessibility and so forth. Relevant literature for industrial applications broadly categorizes maintenance into three main types, as listed below [10, 11, 12].

- **Run to failure** This is historically the first maintenance approach, based on running the machine until a failure, often catastrophic, would occur. The low-frequent failure event implies long downtimes with significant production losses in this case. This method is still employed in cases of large fleets consisting of small machines, where the loss of one machine does not sensibly compromise the safety of other machines and personnel, and production losses are negligible.

- **Preventive** This strategy is based on performing maintenance regularly according to certain time intervals, typically smaller than the mean time before failure (MTBF). Thus, this approach relies on knowledge of the lifetime distribution of specific components. If this was true, preventive maintenance would have great advantages thanks to the possibility to plan maintenance largely in advance. Thus, it finds large applications in cases of steady operational conditions and known statistics of component lifetime.

- **Predictive** As a result of the daily variation of the operational regime, a predictive policy allows to perform maintenance when required, by constant monitoring specific damage-sensitive parameters. This is also known as condition based maintenance (CBM)

Presently, there exist a substantial amount of literature proving that CBM has led to significant benefits in several industrial sectors [13]. This maintenance type requires reliable

monitoring systems providing the information necessary to assess the health of operating machines. In broad terms, a maintenance program should incorporate fault diagnosis and intervention with repair or replacement to reduce the risk of future failures. However, regardless how efficiently an intervention can be performed, the risk of developing unforeseen failure modes is always present.

Historically, maintenance has developed under different names to indicate the same common scope. In some engineering fields such as aerospace and precision manufacturing industries, this discipline was originally established and still known as Prognostic Health Management (PHM) [14, 15]. PHM is a wide maintenance concept encompassing multiple levels of support actions, such as fault diagnosis and estimation remaining life of the asset's critical components. Besides, it extends this process to electrical and mechanical components, storage units, hydraulic circuits, pipes and so on. Another popular maintenance concept developed at the beginning of the '60s was Reliability Centered Maintenance (RCM), ordinarily adopted by airlines starting from the '70s and by the nuclear power industry [16]. This type of maintenance approach is based on the implementation of different strategies to optimize the productivity of the asset. Furthermore, it answers key questions such the identification of critical failure modes, analysis of their consequences and prediction. A more recent approach well suited for offshore structures, especially foundations, is risk-based maintenance based on inspections (RBI). Major work is given by Straub [17], Nielsen [18], Hovegaard [19]. This methodology combines information from inspections and any other kinds of evidence on the real state of the system, to update a model-based inference of the real structural degradation. Typically Bayesian networks (BNs) are used to achieve this goal. BNs are acyclic graphs that describe the conditional dependency between stochastic variables [20]. In particular they model causal relationship, that is why they are often refereed to as causal networks. Fatigue damage for instance, is a stochastic process that cannot be directly measured, but rather calculated through mechanical models. Thus, uncertainty on the estimated model parameters can be reduced by exploiting new evidence, such as measurements from monitoring systems, expert opinions or subjective judgment [12]. RBI is a good candidate for fatigue-driven failures of substructures and became popular within the offshore industry. However, a main concern for wind turbines (WTs) are mechanical components, which often lack of physical models and deep knowledge of operational parameters to describe their degradation leading to failures.

At present, maintenance is a continuously developing field ready to embrace new technological trends such as artificial intelligence (AI) and the Internet of Things. Maintenance is concerned with prediction, identification of anomalies in a timely manner, intervention based on dedicated schedules and decisions by taking into account uncertain environmental conditions. In particular, these latter are of main concern for offshore wind farms, because wind speed is an uncontrollable and unsteady input. A dynamic environment determines the level of mechanical stress that components need to withstand [21]. These in turn become more prone to failure than expected.

Wind energy poses unique challenges compared to other industries that will be discussed throughout this dissertation, from which the necessity of further research in this area. This thesis covers some technical aspects related to wind farm O&M, which are briefly summarized and discussed in the next sections of this chapter. Challenges associated with monitoring, reliability and load assessment are discussed and treated in the perspective of reducing costs by improving current methodologies and models proposed by current design standards and guidelines.

1.1.3 Wind power economics

As a consequence of strong restrictions and large-scale limitations such as lack of exploitable land space, environmental impact, public opposition and noise emission, especially when it comes to large multi-megawatt machines and favorable wind resources the future of wind power generation shows an incresing trend towards offshore, as opposed to onshore. Recent annual statistics based on European wind energy generation [4] clearly show this trend, Fig.1.1. Top advantages of the offshore market are less turbulent wind speed thanks to the absence of rough terrains, which offers better exploitation of the wind resources and less fatigue loads. In [22] a throughout discussion on technical and societal challenges related to the transition to renewable energies is provided.

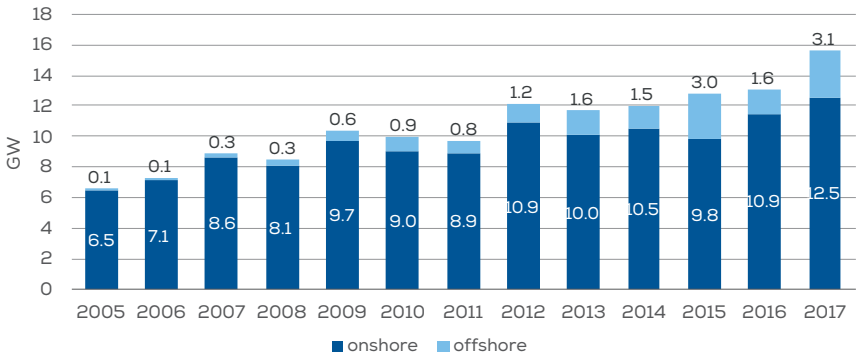

Figure 1.1: Annual power installation in GW in EU, onshore and offshore [4].

However, the elevated costs per megawatt (MW) installed capacity is still a clear disadvantage compared to onshore. It is not trivial to find in literature updated numbers, although some statistics from are available from the US offshore wind industry provided by the National Renewable Energy Laboratory (NREL) dating back to 2016 [23] (approximately 42 €/MWh onshore vs. 145 €/MWh bottom-fixed offshore and 174 €/MWh floating offshore). The levelised cost of energy (LCOE) is a measure of the economic assessment of an asset generating revenues from producing electricity. The LCOE is defined as the total lifetime costs to construct and operate the production facility at year N_y divided by the total energy produced throughout its lifetimes [24], as

$$\mathrm{LCOE} = \frac{\sum_{i=1}^{N_y} (\mathrm{CapEx} + \mathrm{OpEx})/(1+r)^i}{\sum_{i=1}^{N_y} \frac{\mathrm{AEP}}{1000}/(1+r)^i} \tag{1.1}$$

where the capital expenditures (CapEx) [€/kW] comprise design, construction and installation costs of the asset. The operational expenditures (OpEx) [€/kW/yr] sum up the costs of running the business throughout the asset's lifetime, which in case of wind farms include fixed and variable O&M costs. The latter in turn depend on the number of maintenance interventions performed, which is directly related to the failure rate of mechanical and electrical components of the turbines as well as auxiliary facilities such as array cables, substations and

so on. The LCOE can be regarded as an average cost of energy that would be delivered steadily by an equivalent plant during its lifetime. In case of offshore wind farms, the variable costs also depend on the site availability for maintenance, costs of hiring vessels and overall power losses due to downtime. In Eq.1.1, AEP is the annual energy production [MWh/MW/yr] and r the discount rate for the capitalised costs [23].

O&M is identified as a major cost-driver, landing somewhere between 20% and 40% LCOE, and the significant variation depends on a number of factors such as turbine technology, distance from shore, capacity factor and so forth. An extreme example documented by Besnard [25], shows that the O&M costs of the Horns Rev I offshore wind farm, in Denmark, reached 40% of the LCOE. These costs were broken down into categories such as corrective maintenance (43%), serial failures (25%), retrofits and refurbishment, preventive maintenance, vessels and helicopter overheads.

Cost reductions are achievable by improving the turbine reliability and thus increasing availability, or minimizing unscheduled maintenance. Since increasing reliability also increases CapEx, this increase should be lower than the reduction of OpEx. However, decreasing the LCOE requires acting from different sides, such as improving load predictions and design, enhanced knowledge of the failure process and development of tools for predicting critical failures. However, predicting failures becomes more challenging when failure rates are not constant, and their modelling must be based on condition of both environmental and operational variables. Tavner et al. [26] demonstrated that some failures are predictable based on the assumptions of constant failure rates, or failure rates following the bathtub curve. However, more recent studies by Reder et al. [27] have shown that the buthtub curve is not suitable for describing WT component failures over time, which justifies the usefulness of predictive strategies for monitoring turbines.

It is estimated that in the near future, lowering-cost technologies will enable an increasing installed capacity worldwide and less reliance on government subsidies [28].

1.2 State-of-art and problem statement

This section provides a throughout review of previous work carried out within the specialised topics of this dissertation, and highlights the research gap which is addressed as novel contribution.

1.2.1 Load assessment models

One major problem the offshore industry is facing is how to make cheaper foundations. Despite the enormous cost reduction compared to few years ago, foundation design, manufacturing, transport and construction of offshore WTs still account for a percentage of the overall costs in the range 25-34% [29]. Although new concepts such as floating turbines will enable the deployment of wind farms located at high water depths, bottom-fixed substructures are still a prominent solution in shallow and moderate waters [30]. This kind of foundation will remain attractive especially for large scale project in the north sea, thanks to their ease of installation and established technology and experience inherited from previous offshore industries.

Besides design, manufacture and installation, in the recent years, older wind farms reaching their end-of-life have led practitioners to consider actions such as lifetime extension, repowering

or decommissioning of WTs [31]. These actions require a throughout assessment of structural integrity through load reassessment, inspections and SCADA history. SCADA (supervisory control and data acquisition) system is a DNV-GL [32] provide guidelines for extending lifetime all load transferring components and structures. The primary focus of the guidelines is towards fatigue reassessment, including an analytical as well as a practical approach. Since foundations have a drastic economic impact in this perspective, their extension of life has been under strong focus in the recent years. For example, let us imagine we were able to establish that the monopiles a 20-year old wind farm are still able to support the support the turbine above. If yes, for how long? How much fatigue life is left? It is clear that taking decisions according to well defined criteria and with a certain degree of confidence would imply large economic benefits for the business. The state of the art in this area is documented in [31, 33, 34]. Their research highlights methodologies to approach the problem of estimating remaining lifetime of critical WT components. Depending of the type of information or data available, this assessment can be performed by using single sources of data available or a combination of them, such as on-site inspections, analytical models and data driven models derived from condition monitoring data. From a technical standpoint, estimating lifetime is bounded to a physical description of the fatigue damage accumulated over time. Therefore, it important to establish a good knowledge of the loads and mechanical stress concentrated in particular hot-spots. On this regard, a load monitoring approach seems an appealing solutions. This is performed through sensors conveniently placed on the structures to allow direct accessibility in case of maintenance. Interesting work on monitoring vibrations of offshore WT foundations is provided by Weijtjens et al. [35, 36], along with an sensitivity study of the environmental effects such as turbulence and wakes on vibration. The authors in [37] proposed a hybrid approach based on strain measurements on the tower bottom and a simple physical model of the turbine structure to predict loads of neighboring turbines.

The assessment of remaining life of substructures however, in the majority of cases relies on numerical simulations based on aeroelastic load analyses. Mathematical formulations to reproduce the environmental forces acting on the turbine throughout its lifetime are typically implemented in the solver. Assumptions and simplification are made in order to make it possible to carry out a number of simulations which is indicative for the entire lifetime, which will be explained in detail throughout this thesis. Some of the environmental models and techniques were originally developed by the oil and gas industry [38], as for example wave kinematic models and soil, because offshore WTs are located at relatively shallow waters compared to offshore oil platforms. Accurate prediction of cycling loads on offshore WTs foundations becomes of primary importance for two main reasons: a) bottom-fixed foundations are moment resisting and b) fatigue is a design driver due to their high sensitivity to dynamic loading [29]. Thus, one issue addressed in this work is to investigate the suitability of wave kinematic models currently available for WT monopiles, typically located at shallow water sites. Moreover, the fatigue equivalent turbulence level set by current standards [2] is investigated for WT monopiles.

As per the DNV-GL guidelines [32], the load reassessment for lifetime extension and in design, should be best performed according to fully probabilistic approaches. These analyses require multiple steps, among which the identification of critical failure modes, derivation of limit state functions, specification of model and statistical uncertainties and target a reliability level. In most cases, a sensitivity study on the model parameters shall also be of interest. Fatigue and extreme load reassessment are of main interest for extending the turbine lifetime

[37].

1.2.2 Failure-load correlation

Previous work on WT reliability has confirmed that a correlation between reliability and wind speed characteristics exists, as the study conducted in [39] based 10 years of whether data. Lately, more advanced models have conditioned WT reliability to both weather and operational parameters [40]. However, a direct correlation may further exist between failures and loads, fatigue or extreme, within the wind farm. Literature provides some examples of this connection. Some experimental work has observed patterns between specific running conditions and gearbox failures [41]. The study suggested that planetary bearings are susceptible to physical damage during under-loading, which may eventually lead to failure due non-torque loads. In general, high fatigue loads or higher accumulated damage, is an indication of higher probability of failure [42]. Also overloading, resulting for instance from extreme events, may be responsible for increasing the probability of initiating a crack, as it is the case for gear teeth.

Therefore, this study attempts to compare load maps, as originally developed by Galinos et al. [43], with real experienced malfunctions in order to find possible patterns between them. These malfunctions can be retrieved by the SCADA alarm history and typically stored in an alarm-log of the wind farm. However, it should be remarked that this type of analysis makes sense only after several years of operation. Since the numerical case treated in this thesis has an operational life is of 5 years, the investigation the wind farm fatigue loads is only intended to be used as indication of possible increased probability of failure, and not as a direct correlation to failures. This latter in fact, if any, would imply a inadequate initial design after such a short operational time. In any case, a description of the load variation within a wind farm can indicate critical components and provide a criteria for deciding which turbine should be inspected [43], e.g. based on fatigue damage.

The importance of this comparison is to understand if failures are connected to not optimal wind farm configurations. In fact, the layout configuration is currently primarily driven by power optimization requirements [44], or considering also loads [45], while failures and the effect of maintenance actions on them are not yet considered. In-service failures increase O&M costs and thus the LCOE, (see Eq.1.1). Unlike failures though, wind farm loads can be estimated in the design phase through aeroelastic simulations. This means that if a correlation between loads and failure exists, additional constraints could be used in the farm layout optimization problem, which accounts for reduced LCOE by reducing the failure rate. The LCOE is currently used as objective function for these types of optimization problems [46].

In the case study of a real wind farm, pitch and drive-train components malfunctions were identified. The pitch system is a mechanisms often subject to failures, due to adverse environmental conditions and mechanical degradation processes such as friction [47]. Research in this area may help explain what are the drivers of common pitch malfunctions. Load maps are then compared respectively with the event maps of the recorded malfunctions.

1.2.3 Predictive maintenance

It was mentioned that in-service failures, excluding events beyond the design envelope of the turbine, are undesired events which play an important role in wind farm O&M, in that they decrease the reliability of the power plant resulting in significant economic losses, which

in turn influence the overall cost of electricity from wind resources. Failures can be predicted and handled implementing suitable maintenance programs based on health assessment of mechanical components through active monitoring.

Monitoring is the process that allows understanding the status of a system through direct observation or inference of its state. In a general context, the value of monitoring resides in the physical inaccessibility of an object of interest. The analysis of data makes up for or the inability to interpret its behaviour by human perceptive capabilities only. For this reason, the term "remote" often precedes the word monitoring or sensing. To clarify, the reader should think of different examples ranging from atomic scale operations such as biological tests, detection of radioactivity and all kinds of medical analyses, to large scale examples such as operating engines, spacecraft, tunnels, bridges and so on. It is evident that these examples present practical challenges in terms of direct accessibility for inspection, or direct experimental testing. In case of wind farms, remote location and frequent adverse weather are the main factors justifying the use of remote sensing and the massive research in this area. Owing to a number of factors such as wind farm configuration, wakes, climate, seabed variation and operational conditions and poor maintenance, some components may experience higher damage while others would still be running in optimal conditions. Consequently, a preventive maintenance policy (see Section 1.1.2) does not seem to be the best suitable strategy for major parts in WTs, except for less important components which can still be checked opportunistically. It is more straightforward then, to think on maintenance based on condition, especially for major mechanical parts or sub-assemblies.

Part of this thesis is dedicated to fully data-driven methods for failure prediction. Current literature in this area primarily focuses at improving the performance of algorithms for typical failure modes in gear-boxes, main bearings, generators. Regression models are typically used to track the normal behaviour trend of damage-sensitive features, as for instance used in [48, 49]. These are continuous variables, like temperatures or vibrations features among the most employed. Other recent studies have demonstrated that the turbine under-performance can be detected indicating the presence of failure [50]. These models are based on linear or nonlinear regression and can be parametric or non-parametric supervised learning techniques. This approach is known as normal behaviour modelling (NBM). The model is set to issue an alarm as soon as a threshold is exceeded. This threshold is based on a degradation measure defined over the set of output variables, as difference between real measurements and the model output. A constructive review is provided in [51]. An input set is needed, selected to be sufficiently correlated with the damage-sensitive feature to be tracked. In this approach, the question of selecting the best performing input set arise. While there is a vast amount of research dealing with boosting the predictive power of these systems, or even exploring their capabilities and flexibility on large scales [52], a statistical interpretation of the input variables and a criteria to select the best predictive input subset is still missing. This will help practitioners decide on the the number of input variables to be employed in the prediction model, thus reducing the amount of data processing and manual interpretation. The authors in [48] for example used an autocorrelation-based approach to achieve this target. Other techniques may be based on simple Pearson cross-correlation matrix and set a threshold to a minimum correlation coefficient between the output variable and the input. As learned from industrial experience in fact, data processing and maintenance of online running predictive systems are among the major cost-drivers for the organizations.

An alternative approach is prediction of frequent events, as opposed to rare. This distinction

is primarily made in terms of severity of the event and frequency of occurrence. For instance, the failure of a gearbox is not as frequent as a daily SCADA alarm, which in turn can be defined as frequent. These alarms are triggered whenever a certain variable surpasses a defined operational threshold, typically set by the manufacturer or the operators. Since these shut-down events can be several, a classifier can be used to train the prediction model. Repeated small events however, were observed in this work to lead or be related to the occurrence of rare events. Previous work on this subject was carried out in [53], where a SCADA-based classifier of labeled classes was set-up. A closer look to this problem from the point of view of the performance of advanced AI-based classifiers is given by Bach et al. [54], who employed vibration features to predict different class of bearing failures. As it will be argued later in Ch. 5, the use of vibration data compared to SCADA data only can substantially improve the lead time, defined as the time lag between the first warning issued by the prediction model and the failure itself, or any other reference point in time.

As it emerges from the the cases exemplified above, predicting a failure event also implies dealing with the level of confidence of the prediction system employed. This means the monitoring system can fail recognising whether an event is true or not. Depending on the severity of the warning, the operator will perform an action associated with a cost. The benefit can be for instance avoiding the cost associated with the occurrence of a failure such as replacement costs, mobilization time required by the crew to prepare the operation while the turbine is standing still and power losses. Consequences of all the actions triggered by an early alarm must be considered and decisions are then taken based on the most convenient outcome. Therefore, the utility has to be evaluated from a risk perspective, which in practice can be achieved through a cost-benefit analysis. The latter quantifies the benefit of implementing the system against its running costs. This thesis provides two examples of decision trees developed for regression and classification types of predictions. Only a financial risk is considered, following the assumption that only economical losses are associated with WT failures. However, it is worth noting that risk can be associated to multiple attributes. For instance, in the example of the airlines, maintenance practice would also involve low customers' satisfaction and company's reputation besides financial losses, because of possible delays or corrective actions [55]. The further research contribution of this work is therefore towards a utility assessment through decision trees.

This analyses are based on real experienced failure events, and the decision tools developed have the aim to reveal the primary maintenance cost-drivers making it possible to raise awareness within the organization. This represent a potential for future cost reductions in wind farm O&M. The research gap in this area is still significantly large and the wind energy industry is currently facing a number of obstacles that prevent operators from taking informed decision. Among the most significant, is a lack of open communication, information sharing and issue on data ownerships between energy operators and turbine manufactures. Wind energy operators are fully liable of performing maintenance on their operating machines after the warranty period, often set to 5 years [56], making it necessary for them to develop in-house tools for data analysis, hire suitable personnel and schedule maintenance activities. All the risks associated with lifetime management of an asset must be incorporated in a maintenance program.

1.3 Main wind turbine components

It is preliminary to visualize under which conditions WT components are subject to degradation, wear and thus increased risk of failure. Besides normal aging, external factors affect their durability. With respect to offshore sites, turbines are located in places dominated by an abundance of wind resources. These implies the presence of harsh and aggressive site conditions, such as high and low temperatures, frequent storms, corrosive environments due to salinity, waves, currents, humidity, turbulence, marine growth, ice, sea-spray and so on. Mechanical and electrical equipment are indeed sensitive to the variability of those parameters, or a combination of them. The picture in Fig.1.2 shows a typical example of operating offshore turbines.

Figure 1.2: Example of an offshore wind farm, Block Island, USA [5]

DNV-GL [57] provide useful design guidelines to account for these physical phenomena while designing. However, it is far from attainable to believe that all possible real conditions will likely to be predicted during design, due to the stochastic nature of the mentioned phenomena and, in general, lack of exhaustive knowledge of the physical parameters into play. Ideally, if these were deterministic, it would be possible to achieve safe designs at relatively low costs, thanks to lower uncertainty and more accurate prediction of operational loads.

Fig.1.3 displays a typical nacelle configuration of a geared WT machine. The main component of a WT rotor nacelle assembly are rotor blades, main bearings (typically 1 or 2), main shaft, gearbox and generator. Some types do not implement a gearbox in a configuration called direct-drive. The structural parts supporting the rotor nacelle assembly, the substructures, are the tower, transition piece and foundation. The connections between different structural members and mechanical components are made of mechanisms and constraints to allow motion where required. Examples are, pitch and yaw mechanisms, drive-train couplings, grouted joints etc.

1.4 Scope

In connection to this introduction and review of related literature, a description of the novel research questions is here summarised. The work is divided into three main area depicted in Fig.1.4.

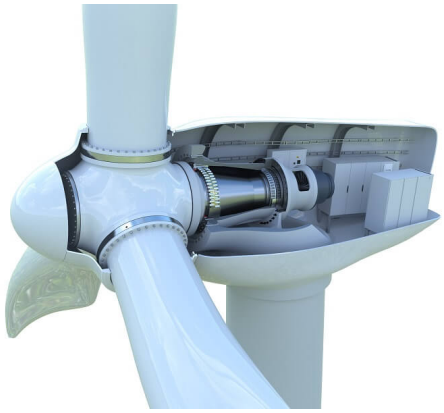

Figure 1.3: Example of drive-train configuration [6]

- **Are environmental models for fatigue load analysis of offshore WT monopiles suitable for all site conditions?** Based on fully coupled aeroelastic simulations, the impact of different environmental models on fatigue lifetime of offshore WT monopiles is investigated using probabilistic reliability formulations of the fatigue limit state. Three different wave kinematic models and less conservative level of equivalent turbulence calibrated for fatigue loads monopiles are taken under consideration. Wake effects are taken into account too. The advantage of using equivalent turbulence levels is to have a basis for preliminary designs of WT components, which are are lose as possible to the final design and strongly reduce the number of simulations to achieve this. However, equivalent turbulence may often lead to over conservative estimates. The influence of uncertainty in the hydrodynamic coefficients in the Morrison equation is investigated. When using linear waves, a correction term to account for the mathematical error of the Wheeler stretching at finite water depths is derived.

- **How does the reliability of offshore WT monopiles vary under different environmental models?** The study discusses the consequences of using the right environmental models for load assessment in accordance with real site configurations, with the scope to reduce the safety margins in the design of foundation as well life reassessment towards the end-of-life. The novel contribution of this study is the assessment of environmental models from the perspective of fatigue reliability, which translates theoretical formulations into practical numbers for wind farm designers and operators.

- **Can a qualitative assessment of the wind farm load map indicate a possible correlation with failure?** Knowledge of the loading conditions across a wind farm is part of a maintenance program for assessing lifetime of mechanical components and structural members. Based on a case study, the fatigue load history within a wind farm is reconstructed using real environmental conditions and aeroelastic simulations based on tools already developed. Alarm-logs of the wind farm revealed several issues with hydraulic pitch system and drive-train components such as bearings, gear-boxes and generators. The initial idea was to compare pitch errors deriving from the introduction of the friction torque into the equations of motion (EOM). Unfortunately this modeling resulted in convergence problems. Instead, results are shown in terms of pitch duty

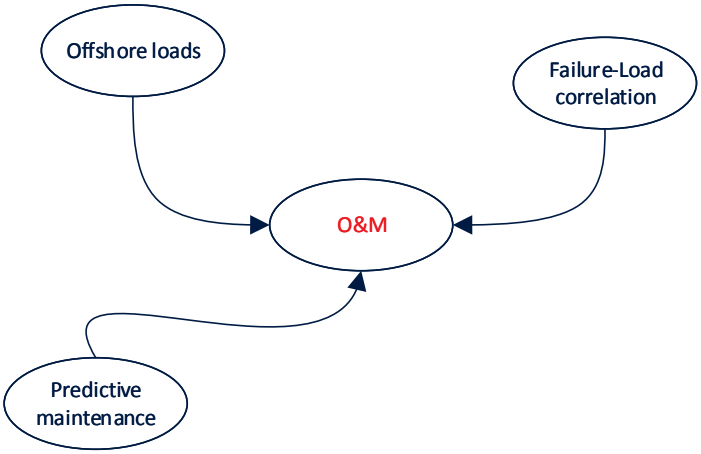

Figure 1.4: Main structure of the thesis.

cycle maps, blade root fatigue loads and main shaft torque fatigue loads and frequency of event maps of the wind farm.

- **Are classification-based predictive systems cost-effective, and how can their utility be analysed?** Classification techniques are used to model and predict SCADA alarms. A decision model based on event tree is developed, which enables the assessment of the monitoring system in economical terms. CBM is modelled through a parameter which takes into account the efficiency of intervention performed when the system predicts a malfunction. The effect of the efficiency is to decrease the probability of failure of the sub-assembly affected. The model devises the optimal configuration of the classifier in order to obtain maximum benefit, as a trade-off between false alarms and correctly classified events. The novel contribution resides in the combination of the output obtained from prediction systems based on machine learning with decision/event trees, which will represent an area of open research in the future. The overall aim of the work is to provide simple practical tools to assess the cost-effectiveness of prediction models before their implementation based on prior information, as well as modeling the performance of the maintenance practice.

- **Are regression-based predictive systems cost-effective, and how can their utility be analyzed?** Improvements to NBMs with respect to available literature are developed. The usefulness of prediction models and how they can be effectively employed for decision making is quantified by constructing an event tree suited for regression-based NBM to predict the occurrence of rare events. Two maintenance strategies of repair and replacement are considered and their expected utility is quantified through the decision tree. In the repair policy, the same approach as in the classification-based technique is used, namely the effect of a successful repair action is modeled through an efficiency that decreases the probability of failure.

- **Which variables among SCADA and CMS systems should be included in a prediction model based on NBM?** In the example of the main bearing failures, a sensitivity analysis based on least absolute shrinkage and selection operator (LASSO) is proposed, which has the scope to reduce the dimensionality of the input dataset and eliminate unnecessary covariates.

1.5 Outline

The remainder of this thesis is organized as follows. Ch.2 introduces the fundamental concept of structural analysis and multi-body dynamics, with the aim to provide sufficient knowledge to understand fully coupled aeroelastic models. Then offshore WT are described along with basic principles of hydrodynamic and aerodynamic, as well as design load cases (DLC) defined by current standards. The area of structural reliability is introduced along with numerical models to estimate the probability of failure in case of complex limit state functions and an explanation of the uncertainties to be considered in a reliability study. Ch.3 is dedicated at describing how to develop load maps of a wind farm starting from assessment of site conditions and aeroelastic simulations. The mathematical formulation of the second order pitch system is presented along with friction models for pitch bearings. Ch.4 is entirely dedicated at introducing the topics of AI, differences between predicting and explaining a certain phenomena through predictive models, learning algorithms used in this work and other topics typical of machine learning. The knowledge gained through this chapter is preparatory to understand Ch.5, where the notions of predictive modeling are applied on CBM and basic decision models, along with a constructive review of SCADA and vibration data applied for condition monitor WTs. These two chapters are clearly linked together, but for the sake of clarity they presented separately, in that more general discussions and considerations are given in the first.

Each chapter contains a recall of the scientific background preliminary to understand the overall work-flow as well as analytical details, along with an explanations of how the information has been used in the related articles, where necessary. If not, specific motivation is given. Each chapter may refer to scientific notions presented in other chapters when necessary. The descriptions are as brief as possible, leaving the reader space for deepening into more advanced details through relevant references. Intentionally, the same information already contained in the scientific publications are not repeated in the main text, unless deemed necessary to understand the work-flow. For convenience, nomenclature and definition of mathematical quantities may be similar across different topics and in general differ from the one adopted in the scientific articles.

This thesis is built-up around 3 main scientific papers (Articles I,II,III) and further research summarized in a thesis chapter (Ch.3). The contribution of the coauthors of this work has been necessary for the final delivery of the thesis. In Article I, nonlinear wave time series were available from a database created by A. Natarajan, and the reliability analysis was based on implemented computational tools developed in other Universities freely available for researchers. In Article III, the computations of the sensitivity analysis were performed by M. Reder. In Ch.3, the PID controller for the pitch torque has been developed in collaboration with A. Melchior Hansen. The derivation of free wind speed statistics within and the fitting functions using the polynomial chaos expansion (PCE) method were obtained using codes developed by N. Dimitrov. When required, all the coauthors contributed with general enhancement

of methodologies and interpretation of results to be presented in a scientific manner, as well as with providing a critical review of the manuscripts. The remaining content, such as all the conceptual ideas, data collection and processing, computations, technical details, interpretation of results and writing are direct contributions of the main author of this thesis.

O&M remains a multidisciplinary field, which embraces a wide range of engineering disciplines. As stated in [58], it is unrealistic to think of going through all the details in a limited time frame allowed for a doctoral program. Thus, the approaches are either to narrow to scope of the research or to stay general without digging into many details while contributing in more areas. This dissertation best fits the second approach.

Chapter 2

Environmental models for load assessment

Uncertainty is that thing that disappears when you are certain

T. Bedford

This chapter introduces the reader to the basic notions of WT loads, DLCs defined by IEC standards, concepts design and safety and describes the most common types of offshore foundations, reliability analyses and related analytical tools.

2.1 Wind turbine loads

2.1.1 Aerodynamic

Some theoretical aspects in this section are retrieved from [59]. WTs are machines designed for the primary aim of extracting power from wind. The aerodynamic profile of the blades, the airfoil, allows the balance of lift and drag forces necessary to generate rotational kinetic energy. Airfoils generate lift as a result of a pressure difference. These forces can be derived by a the Blade Element Momentum (BEM) theory. This simplified approach combines the linear momentum theory, which concerns the derivation of forces acting on at the blade based on a control volume, and the blade element theory, which concern the derivation of 2-dimensional forces acting on the blade profile. Assuming an annular control volume described by a radial variable r and thickness dr, the BEM theory expressed the differential aerodynamic thrust force dT and torque dQ, as

$$dT = \varrho U^2 4a(1-a)\pi r dr \tag{2.1}$$

$$dQ = 4a'(1-a)\varrho U \pi r^3 \Omega dr \tag{2.2}$$

where a is the induction factor, ϱ the air density, U the wind speed, Ω the blade rotational speed and $a' = \omega/2\Omega$ is the angular induction factor, where ω is the induced angular velocity. The Betz linear momentum theory originally developed for ship propellers, assumes the fluid being homogeneous and incompressible, a steady state fluid flow and no friction.

Such models represent a complex interaction between aerodynamics, structural dynamics and control systems under the external forcing of the turbulent wind field(including wakes from other turbines), and possibly other external forces from waves and ice

Commercial aeroelastic codes implement the BEM theory extended to include unsteady inflow conditions. These solvers are based on fully coupled aero-hydro-servo-elastic simulators, meaning that the complex interaction between aerodynamics, structural dynamics and power control is considered simultaneously under the stochastic excitation of the wind and wave, in case of offshore WTs and wake turbulence from neighbor turbines [60] . The term fully-coupled means that the acting forces depend on the actual structural response making the problem nonlinear. In this work, the simulator will be simply referred to as aeroelastic. The WT dynamic concerns the solution of a differential equations where $\mathbf{x}$ is the response vector. In the commercial aeroelastic code used in this work, HAWC2 [61], the formulation is based multibody dynamics approach, which included finite element formulations. Other approaches can be based solely on finite elements or participating modes. A common feature of aeroelastic codes is their modular formulation [62]. These modules comprise soil conditions, turbine geometry and constraints, control unit, external loading (wind and waves) and structural response.

Fig. 2.1 exemplifies the difference between the response below and above rated wind speed of a variable speed pitch regulated WT. The example refers to Article I. In the first case, the varying rotational speed Ω modulates the thrust force acting in the fore-aft direction, while in the second case the turbine operates at constant speed. The fluctuations increase at higher wind speeds due to larger turbulence.

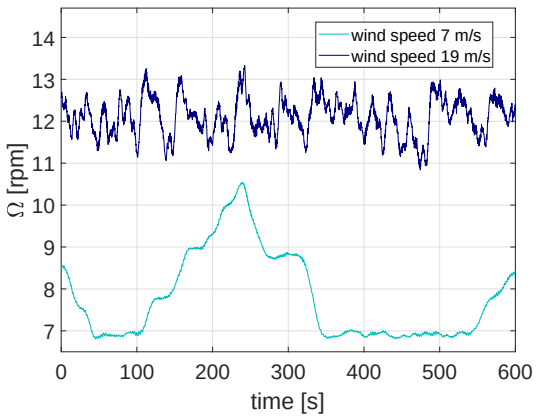

Figure 2.1: Example of rotational speed at mean wind speeds 7 m/s and 19 m/s (5MW NREL reference turbine).

2.1.2 Hydrodynamic

The theoretical background in this section is partly retrieved from [63]. WT hydrodynamic concerns the description of the dynamic interaction between ocean waves and substructures. This interaction is played by wave kinematics and wave loads acting on the structure, the latter estimated through the Morison equation. Regular and irregular waves refer to respectively a unimodal wave and a composition of modes at different frequencies, amplitudes and phases.

Most commonly, the linear theory is used to approximate the wave particle kinematics, starting from the definition of the Laplace equation for the potential flow, as

$$\begin{aligned} &\nabla^2\phi = 0 \quad in\ \Theta \\ &\tfrac{\partial\phi}{\partial z} = 0 \quad on\ \Gamma_1 \\ &\tfrac{\partial\phi}{\partial t} + \tfrac{1}{2}(u^2+w^2) + \tfrac{p}{g} + gz = C \quad on\ \Gamma_2 \end{aligned} \tag{2.3}$$

where Θ is the 2-dimensional continuous domain, Γ_1 is the sea bottom at a water depth $z=-h$, Γ_2 is the water surface, u and w the horizontal and vertical particle velocity respectively. The quantity p is the atmospheric pressure and C is a constant. The solution of Eq.2.3 is the potential flow for the velocity field at finite water depths which satisfies the free kinematic boundary conditions, as

$$\phi(x,z,t) = \frac{\eta_a}{k\omega}\ \frac{\cosh[k(h+z)]}{\sinh(kh)}\ \sin(kx-\omega t) \tag{2.4}$$

where $\eta_a \approx H/2$ is the wave amplitude, with H being the linear wave height. Often, the stretching is used to extend the validity of the linear theory to the water particles above the mean sea level. From Eq.2.4, the velocity field in the two directions $\mathbf{v}=(u,v)$ considered can be expressed as

$$\mathbf{v} = \nabla\phi. \tag{2.5}$$

From the previous considerations, the wave profile of an irregular wave has the following expression

$$\eta(x,z,t) = \sum_{i=1}^{N} A_i(\omega_i)\ \cos(k_i x - \omega_i t + \varepsilon_i) \tag{2.6}$$

where the input parameters are the wave amplitude $A_i(\omega_i)$, the spectral frequency ω_i, the wave number k_i and the random phase ε_i. Eq.2.7 expresses the horizontal particle velocity field derived from Eq.2.6 where Wheeler stretching is applied. The second order non linear wave kinematic model applied here is described [64]. The nonlinear horizontal velocity field u_{nlin} is expressed by Eq.2.8.

$$u_{lin}(x,z,t) = \sum_{i=1}^{N} A_i\ \omega_i\ \frac{\cosh\left[k_i h\left(\frac{h+z}{h+\eta}\right)\right]}{\sinh(k_i h)}\ \cos(k_i x - \omega_i t + \varepsilon_{ij}) \tag{2.7}$$

$$\begin{aligned} u_{nlin}(x,z,t) =& \frac{\cosh[k_i(z+h)]}{\sinh(k_i h)}\ \cos(k_i x - \omega_i t) + \\ &+ \sum_{i=1}^{N}\sum_{j=1}^{N}[B_{ij}^{+}(z)\cos(k_{ij}^{+}x - \omega_{ij}^{+}t + \varepsilon_{ij}) + B_{ij}^{-}(z)\cos(k_{ij}^{-}x - \omega_{ij}^{-}t + \varepsilon_{ij})] \end{aligned} \tag{2.8}$$

The expressions for the linear and nonlinear horizontal accelerations in the vertical direction can be expressed similarly. The second order transfer functions $B_{ij}^{+}(z)$, $B_{ij}^{-}(z)$, $C_{ij}^{+}(z)$, $C_{ij}^{-}(z)$ rearranged in Eq.2.8 are function of wave amplitude, frequency, wave number, water depth

and vertical coordinate, their explicit formulation is fully documented in [65]. The second order expansion is evaluated at $i \neq j$. The superscripts $+$ and $-$ refer to a summation or difference between frequencies. The nonlinear second order wave model takes into account higher order frequency contributions to better describe nonlinearities of the natural wave profile, which is a stochastic process.

To generate wave kinematic times series, spectra information must be known. This define the significant wave height H_s and the peak period T_s. From these quantities, a spectrum generates the amplitudes as function of the frequencies. The phases can be assumed as random variables in the general case. Typical parametric spectra available are Pierson–Moskowitz and JONSWAP [66]. To predict the wave loads on the substructure, the Morison equation is used [67],

$$F(t) = \frac{1}{2}\varrho C_d D_m \mid u(t) - \dot{q}(t) \mid (u(t) - \dot{q}(t)) + \frac{\pi D_m^2}{4}\varrho C_m \dot{u}(t) - \frac{\pi D_m^2}{4}\varrho(C_m - 1)\ddot{q}(t) \tag{2.9}$$

where $F(t)$ is the wave force per unit length, C_m and C_d are respectively inertia and drag coefficients, D_m the monopile diameter, ϱ the water mass density and q denotes the structural displacement in the horizontal direction. The hydrodynamic coefficients may vary significantly according to several physical phenomena, and thus affecting the load distribution in the long term. Often, the wave directional spreading is employed along with the two dimensional wave kinematic field [2].

2.1.3 Turbulence

Wind turbines are exposed to ambient turbulence from the free stream, as well as turbulence generated by wind farm wakes. Wake turbulence is an important design driver both for the single turbine and for the wind farm layout, since it is the main responsible for fatigue loading. Therefore, this variable is important not only for design purposes, but also for load reassessment.

One of the first models to predict wake turbulence within a wind farm was built by Frandsen [3]. This model is based on the hypothesis that ambient and wake-induced turbulence can be represented by an equivalent turbulence level. This equivalence is expressed in terms of fatigue loading. The formulation is formalized in the IEC standards [2], as

$$\sigma_e = \left[(1 - N_t\ p_w)\hat{\sigma}_c^m + p_w \sum_{i=1}^{N_t} \hat{\sigma}_{iw}^m(d_i)\right]^{1/m} \tag{2.10}$$

where D_m and a uniform wind direction distribution $f(\vartheta \mid U)$ are assumed. In Eq.2.10, p_w is the probability of wake condition, N_t is the number neighboring turbines, $\hat{\sigma}_c$ is the free ambient characteristic turbulence and $\hat{\sigma}_w$ the characteristic value of the maximum center wake turbulence standard deviation at the hub height, expressed as

$$\hat{\sigma}_w = \sqrt{\frac{U^2}{(1.5 + 0.8d/\sqrt{C_T(U)})^2} + \hat{\sigma}_c^2} \tag{2.11}$$

where $C_T(U)$ is the thrust coefficient known as function of the mean wind speed in case of a pitch regulated variable speed turbine. Thanks to the definition of an equivalent turbulence level, the number of aeroelastic simulations can be greatly reduced in some practical cases. Although this approach of modelling turbulence is simple, it may lead to conservative load

estimates. Also, it is imporant to mention that this formulation assumes a constant Wöhler exponent, and it is not in general valid for multiple Wöhler exponents. Therefore, this represent an approximation.

A more sophisticated method is the Dynamic Wake Meandering (DWM) model [68]. The DWM model is based on heuristic engineering considerations about the nature of wakes and how they affect nearby turbines. In DWM, the wake on a downstream turbine aligned with the wind flow is considered as acting on a circular area with reduced wind speed and modified turbulence. In this scenario, the load variation associated with the presence of wake turbulence will depend on the relative position of the turbines and the size of the wake. Based on the assumptions of the DWM, the wake center position will be affected by transverse wind. The wake center location is a random variable, and its standard deviation increases with the distance from the wake source. It is possible to estimate this variance as a function of the transverse wind speed standard deviation, by taking into account the covariance between longitudinal and transversal wind speed components. This variance in turn depends on the type of spectrum employed for generating the wind field. These are the main ingredients to be able to model the turbulent flow conditions containing contributions from farm wakes that can be implemented on aeroelastic codes. The topic however, contains domain knowledge, which goes beyond the scope of this thesis. The reader is therefore adviced to refer to specialised literature for further details, since this paragraph has the only aim to provide a general description of the phenomena.

2.1.4 Design load cases

From the previous considerations, the structural response of complex multibody systems can be described, once the external excitation is known. Apart from gravity loads, the remaining source of excitation are summarised below

- Aerodynamic, resulting from the wind-rotor interaction.
- Actuation, originated from the turbine control system such as yaw, breaks, pitch, torque and so forth.
- Hydrodynamic, resulting from wave-substructures interaction.
- Sea ice, in case of ice clusters hitting the substructures.
- Earthquakes and impacts.
- Wakes, resulting from the wind farm configuration and affects downstream turbines.
- Tower passing loading, veer, sheer and yaw error.

The DLCs define a set of loading situations relevant for the operational lifetime of the turbine, as defined in IEC64100-1 [2]. These conditions are necessary for the evaluation of the design characteristics of a WT, and are divided into the following categories

- Normal power production
- Power production in combination with grid loss or electric network faults
- Start-up, normal and emergency shut-down

- Standstill
- Standstill in combination with faults
- Transport, maintenance and repair
- Icing and sea ice loads

Along with these load cases, the input environmental conditions should also cover all the possible scenarios, with the help of extrapolation of extreme events from site observations at a given return period. Among the most important sea and wind conditions are

- Normal turbulence and normal wind shear
- Extreme turbulence and extreme wind shear
- Extreme wind speed
- Gusts and sudden wind direction change
- Extreme gusts
- Normal, severe and extreme sea state
- Breaking waves
- Sea currents

Further environmental conditions that are considered extreme and must be assessed in extreme sites are temperature, earthquakes, lightning and ice.

In this work, DLC 1.1, 1.2 and 6.4 (see [2]) are considered, because they concern the estimation of fatigue loads during operation and standstill. For an offshore WT, the main environmental parameters to be considered are mean wind speed U, turbulence σ_u, significant wave height H_s and wave peak period T_p. In more specialised analyses, other variables may be considered as random, such as wind shear, air density, wakes and so forth [69], as it will be shown in Chap. 3. The probability of occurrence of each combination of environmental variables has to be taken into account, according its joint probability distribution

$$f(U, \sigma_u, H_s, T_p) = f(U)\ f(H_s \mid U)\ f(T_p \mid U, H_s)\ f(\sigma_u \mid U). \tag{2.12}$$

DLCs should be selected if relevant for the structural integrity of the turbine following specific site assessments. For instance, a combination of extreme and fault conditions may be found to be a critical situation. In this cases it is clear that particular combinations of DLCs and environmental parameters may lead to structural failures. However, to achieve economical and safe designs, the designer should account for the probability of occurrence of these critical events within the turbine lifetime, and accept a certain target probability of failure. Based on these considerations, partial safety factors are introduced in the design equations to compensate for uncertainty in both loads and resistance, associated with specific failure modes. DNV [70] provides a categorization into safety classes, namely low, normal and high, as well as limit states such as ultimate strength, fatigue, serviceability and so forth. For each safety class, a target probability of failure is associated. The scope of the reliability analysis is then to ensure e a safe design under uncertain inputs.

2.1.5 Types of foundations

The aim of this subsection is to describe different types of offshore WT support structures. As documented in [71], WT support structures can be categorised into 4 classes:

- **Piled** structures provide easy manufacturing and installation, thanks to several years of experience in other sectors such as oil and gas. Their stability relies on tangential forces established between soil and structure due to friction.
- **Gravity base** structures simply rely on compressive soil strength and dead loads, which ensure their stability. Thus, gravity based foundations are designed to avoid tensile forces.
- **Suction bucket** are based on the principle of removing water from the skirt, thus to guarantee stability thanks to negative pressure.
- **Floating** structures can be of different types and their design is currently under strong research focus. The floating concept could turn out to be a game changer for very high water depths.

Thus, with respect to their structural configuration, these categories are further divided into monopiles, tripod, jacket, gravity and floating. In particular monopiles are mostly suitable for moderate and shallow waters. However, thanks to a series of advantages [72], their adoption is becoming prominent for larger water depths, as also confirmed by recent research [73].

One major concern associated to pushing monopiles towards deeper waters, is that the first natural frequency in the fore-aft direction decreases sensibly due to their high flexibility, and thus shifting the spectral peak towards the wave dominant frequency range, typically around 0.22 Hz for the North Sea. These in turn become detrimental especially for fatigue lifetime. As argued in [72], if the well established supply chain for manufacturing and installation of WT monopiles could be transferred at high water depths, there would be great potential for economic benefits than starting a new supply chain of other types. This concept is well linked to standardization of WT foundations. Thus, the motivation of treating monopiles as research objective results from the considerable drive to improve their technology, which also includes load analysis.

Offshore WT foundations are unmanned structures, and so they belong to a normal safety class corresponding to a target annual probability of failure of 10^{-4} [70].

2.2 Uncertainties

In the context of reliability and risk analysis, uncertainties are commonly categorized according to their type. The discussion in this section is inspired by [74]. *Aleatory* uncertainties are those originating from the inherent variability of natural processes, as for example the air temperature in a specific region, the annual variation of a river water depth, the amount of wind solar particles into the atmosphere in January etc. They concerns the inherent randomness of all stochastic processes observable in nature. Model and statistical uncertainties are referred to as *epistemic*, originating from mathematical models used to describe an observed natural process, partial lack of knowledge or unknown values of certain estimated quantities because of limited observations.

The example of the weather for [74] makes the concept clear. Even though a model exists to predict future occurrences of a certain event, its intensity and so on, aleatory uncertainty makes it rather difficult to obtain reliable prediction far in future. Model uncertainties will depend by the amount of information that was available at the time of modeling.

In WT load analysis, different sources of uncertainty are present, and in a reliability context they must be taken into account. These originate from the mathematical description of the wind-wave interaction through the BEM theory, structural response through mechanical models, mathematical equations to model external inputs such as wind and waves. The natural variability is taken into account by stochastic input parameters, whose statistics are estimated from observations.

2.2.1 Lower-order wind turbine model

For the quantification of the wave model uncertainties, a reduced-order WT model was used, similarly to the ones developed by Schløer et al. [75]. The reason for this is to eliminate other sources of uncertainty in the model, such as wind-structure interaction, soil-structure interaction due to soil flexibility and controller effects. The forcing term in the EOM is the wave load hitting the structure computed through the Morison equation. The Newmark method is used to solve the differential equation. Fig.2.2 shows the in-plane mode shapes of the system, as well as a comparison in terms of dynamic response at a monopile section and its spectra, Fig.2.3.

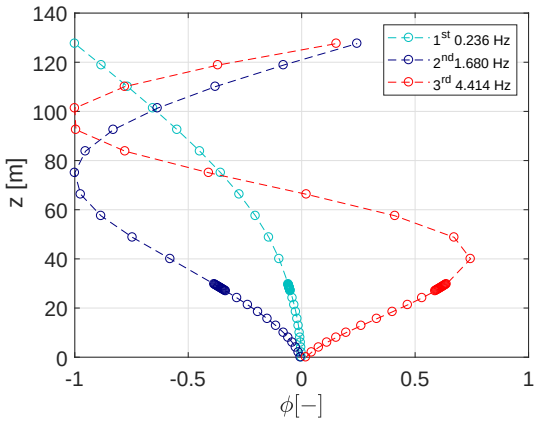

Figure 2.2: Normalised in-plane mode shapes of the lower order WT model.

Fig.2.3b, shows the agreement the agreement in terms of spectral energy content between the full aerodynamic model and the reduced one. When the turbine is in operation, a large percentage of the total damping in the first mode is provided by aerodynamic effects. The damping level substantially affect the fatigue loads [73], especially on tower and foundations and therefore it needs particular focus. There is a considerable amount of literature dedicated at estimating operational and standstill damping. In this work, an experimental estimate was given by computing the logarithmic decrement damping of the tower-top acceleration, by giving as input a step wind speed, as shown in Fig.2.4.

The homogeneous oscillating solution of an under-damped single DOF (free vibrations), with φ_0 the phase angle, ω_0 its natural frequency and $A(t)$ the time varying amplitude, can

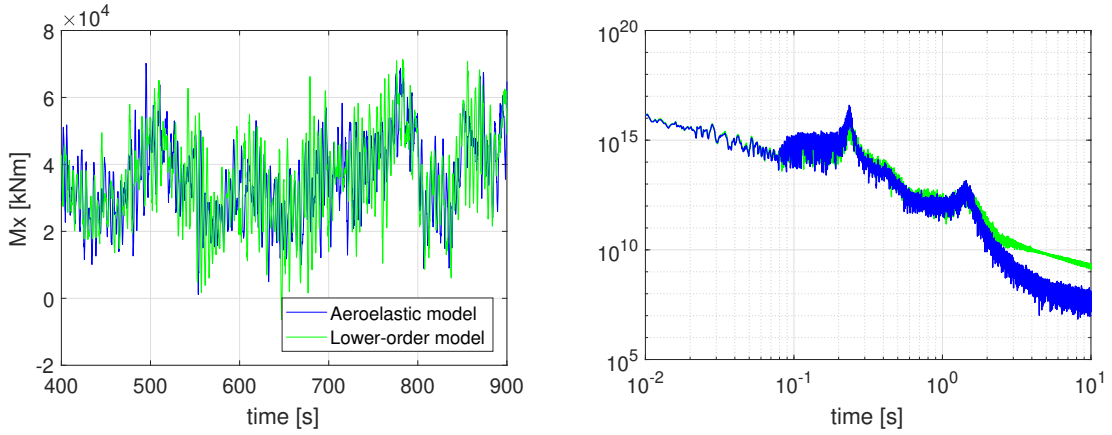

Figure 2.3: Comparison between mudline fore-aft bending moment response in time domain and spectrum for lower-order and full aeroelastic models.

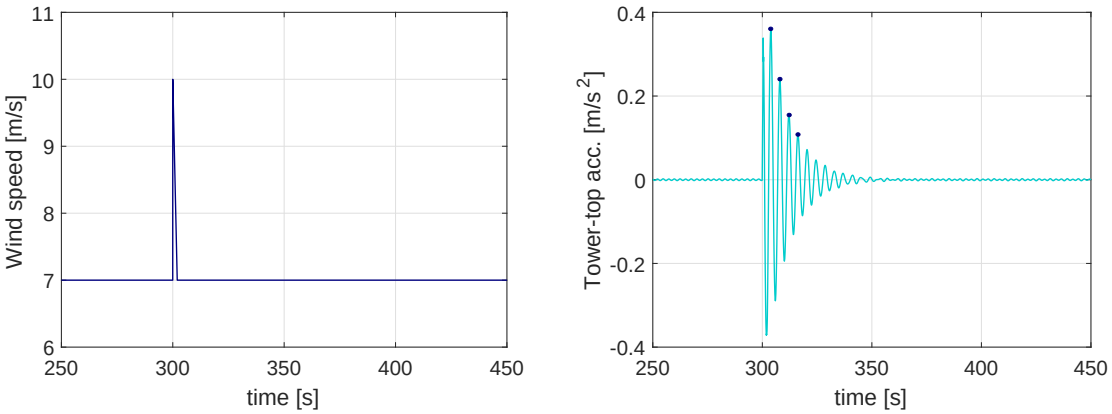

Figure 2.4: Wind step excitation to a constant wind speed and corresponding free decay response of the tower-top acceleration for experimental determination of the aerodynamic damping.

be expressed as

$$y(t) = A(t)\cos(\omega_0 t + \varphi_0). \tag{2.13}$$

Thus, the amplitude $A(t) = A_0 e^{-\zeta t}$, where ζ is the damping ratio. The amplitude at two different times t_1 and t_2, can be expressed as

$$A(t_1) = A_0 e^{-\zeta t_1}, \qquad A(t_1) = A_0 e^{-\zeta t_2} \tag{2.14}$$

thus,

$$\frac{A(t_1)}{A(t_1)} = e^{-\zeta(t_1 - t_2)} = e^{-\zeta NT} \tag{2.15}$$

where N is the number of complete oscillation, and $T = (t_1 - t_2)/N$, their period. By taking the logarithm of both sides of Eq.2.15, it can be verified that the logarithmic decrement

damping is estimated as

$$\delta = \zeta T = \frac{1}{N} \ln \frac{A(t_1)}{A(t_1)}. \tag{2.16}$$

2.3 Fatigue reliability

As a result of cycling loading, fatigue is a measure of the cumulative physical damage. When the cumulative damage reaches a critical value, a physical crack initiates, which leads to loss of fatigue strength and ultimately a structural collapse. From a mathematical standpoint, fatigue is a mapping function from mechanical stress onto damage. This function operates through a cycle counter, the rainflow cycle counting, and an empirical relationship between the number of cycles to failure and the corresponding amplitude, the SN-curve [70]. The cumulative damage can be computed as

$$D = \sum_{i}^{N} \frac{n_i}{a_i} \Delta\sigma_i^m \tag{2.17}$$

where N is the total number of binned load ranges, m the Wöhler exponent, $log(a)$ the intercept of the SN-curve, n and $\Delta\sigma$ respectively number of cycles and stress range obtained by rainflow cycle counting. Similarly to Eq.2.17, the DEL is defined as

$$\text{DEL} = \left(\frac{1}{n_{eq}} \sum_{i}^{N} \Delta L_i^m n_i \right)^{1/m} \tag{2.18}$$

where ΔL is the load range and n_{eq} is the equivalent number of 1-Hz cycles with respect to the specific time frame of the load. Thus, given Eq.2.18, the DEL can be defined as the load range at a frequency of 1-Hz, which results in the same fatigue load as the original time series. The total accumulated damage over a certain period of time can be found through Palmgren-Miner's rule, Eq.2.19, which assumes that the stress is a stationary stochastic process within this time frame the hypothesis of linear cumulative damage holds.

$$D_t = \sum_{i}^{N} \Delta D_i \tag{2.19}$$

As defined by DNV guidelines [70], *a limit state is a condition beyond which a structure or structural component will no longer satisfy the design requirements.* A reliability analysis of level III [76], requires a full probabilistic approach both in the demand and capacity terms. The fatigue limit state function can be in this case formulated as

$$g(\mathbf{X}) = \Delta - D_t(\mathbf{X}) \tag{2.20}$$

where Δ is the capacity term corresponding to the upper damage limit, typically modeled as a Gaussian distribution to account for the statistical uncertainty in the Miner's rule, due to the deviations between fatigue tests and real loading conditions. A constructive review on the work carried out around the quantification of this uncertainty is provided by Straub [17], mainly based on offshore oil-and-gas structures. There it is reported that the coefficient of variation (COV) of this parameter has a wide spread, between of 20 to 60%. In Article I this

was set to be 10% in order to have a better balance with the remaining model uncertainties and quantify their effect. The vector of stochastic input variables $\mathbf{X}$, representing the uncertainties in the model. The condition $g(\mathbf{X}) = 0$ represents the failure surface, while $g(\mathbf{X}) \leq 0$ is the entire failure domain. Thus, an estimate of the probability of failure is given through the following integral

$$P_f = P[g(\mathbf{X}) \leq 0] = \int \mathbf{1}_{g(\mathbf{X})\leq 0} f_x(\mathbf{X})\ d\mathbf{X} \tag{2.21}$$

where $\mathbf{1}$ denotes the zero-one indicator function and $f_x(\mathbf{X})$ is the joint PDF of the random variables. In some cases, the failure surface may be strongly nonlinear depending on the complexity of the model, and thus the integration of Eq.2.25 is not always straightforward. Furthermore, it is important to notice that the stochastic input variables may be of different orders of magnitudes and have different distribution. This may lead to inconsistencies in the reliability model. Thus, is common practice to transform the variables into a standard space of independent and identically distributed (i.i.d.) through the exact transformation [77]

$$U = \Phi^{-1}(F(X)) \tag{2.22}$$

where $\Phi()$ is the normal cumulative distribution function (CDF) and $F(X)$ the CDF of the real variable. Eq.2.22 transform the variable into a standardized space with zero mean and unit variance. The Hasofer-Lind's reliability index is defined in the standard space as the minimum distance between the design point $\mathbf{u}^*$ on the failure surface $g(\mathbf{U}) = 0$ and the origin, simply calculated through the Euclidean distance

$$\beta = \min_{g(\mathbf{U})=0} \sqrt{\sum_{i=1}^{n} \mathbf{u}_i^2} \tag{2.23}$$

2.3.1 First order reliability method

First order reliability method (FORM) is a gradient based methods for estimating the reliability index (see e.g. Ditlevsen & Madsen [78]). FORM is usually very fast and is based on approximating the failure domain around the design point with a hyperplane. Indicating as $\mathbf{U}$ the normalized variable space, the linear parameters of the hyperplane are estimated as

$$\boldsymbol{\alpha} = -\frac{\nabla g(\mathbf{U})}{\|\nabla g(\mathbf{U})\|}\bigg|_{\mathbf{U}=\mathbf{u}^*} \tag{2.24}$$

The elements of the vector $\boldsymbol{\alpha}$ are the normalized derivatives of the failure surface around the design point, thus they indicate the sensitivity of the surface with respect to the normalized parameters. For this reason, $\boldsymbol{\alpha}$ is the vector of importance factors. Thus, the probability confined by the hyperplane can well approximate the failure probability, as

$$P_f = P[g(\mathbf{U}) \leq 0] \sim P(\beta - \boldsymbol{\alpha}^T \mathbf{U}) = \Phi(-\beta) \tag{2.25}$$

Given the numerical the analytical expression of Eq.2.24, the importance factors can be found iteratively. Note that the inverse problem can also be used, namely given a certain reliability target, to find the configuration of the parameters $\mathbf{U}$ that satisfies such constrain. This is known as IFORM (inverse FORM). This is used for instance to calibrate partial safety

factors or to analyze the contour surfaces of the environmental parameters given a fixed return period.

Higher order models approximate the failure domain around the design point with a polynomial function, also called as SORM, second order reliability models.

2.3.2 Monte Carlo

MC simulations directly computes the integral in Eq.2.25 through realization of the function $g(\mathbf{X})$ by random sampling from the vector of random variables. Since it is a pure numerical approach, MCS is an unbiased estimator. The probability of failure is estimated as

$$\hat{P}_f = \sum_{j=1}^{N} \mathbf{1}_{g(\mathbf{X_j})\leq 0} = \frac{N_f}{N} \tag{2.26}$$

where N is the total number of samples and N_f is the number of samples in the failed domain. MCS also provides an estimate of the numerical error in the estimation of Eq.2.26, by noting that in this case $\mathbf{1}_{g(\mathbf{X})}$ follows a Bernoulli distribution with mean and variance respectively found as

$$\mu_{\mathbf{1}_{g(\mathbf{X})}} = P_f \tag{2.27}$$

$$\sigma^2_{\mathbf{1}_{g(\mathbf{X})}} = P_f(1 - P_f) \tag{2.28}$$

which, for a large number of trials N, P_f can be approximated by a normal distribution with parameters

$$\mu_{P_f} \sim \hat{P}_f \tag{2.29}$$

$$\sigma_{P_f} \sim \frac{\sigma_{\mathbf{1}_{g(\mathbf{X})}}}{N}. \tag{2.30}$$

Thus, the numerical COV is found as

$$COV_{P_f} = \sqrt{\frac{1 - \hat{P}_f}{N\hat{P}_f}} \tag{2.31}$$

In this way, the number of samples necessary to reach a certain precision on the estimation can be found through Eq.2.31, thus representing a convergence criterion. The drawback of MC simulations is that converge depends on the magnitude of the probability of failure. For instance, in Paper I, a 2% precision is set. This required a number of MC simulations for a $P_f \sim 10^{-4}$ approximately equal to $N \sim 2 \cdot 10^6$, which is already a very large number of cases.

2.3.3 Importance Sampling

Importance sampling (IS) is a MC based technique, which provides a robust estimate when dealing with small probability of failures and nonlinear failure surfaces. The probability of failure is expressed as

$$P_f = P[g(\mathbf{U}) \leq 0] = \int \mathbf{1}_{g(\mathbf{U})\leq 0} \frac{f_u(\mathbf{U})}{\Psi(\mathbf{U})} \Psi(\mathbf{X})\ d\mathbf{U} \tag{2.32}$$

where the function $\Psi(\mathbf{U})$ is the *importance distribution*. Thus, the estimate is found analogously to Eq.2.26. The importance distribution increases the chances to sample around an arbitrary region, rather than in the entire domain. Confidence bounds can be found as in the MSC method. IS can be used in combination to other techniques to increase the robustness of the estimation of the probability of failure by sampling closer to the design point $\mathbf{u}^*$. For instance, in Article I, a FORM is first used to obtain an estimate of the design point and thus IS refines the estimation.

Ocean Engineering 155 (2018) 295–309

Contents lists available at ScienceDirect

Ocean Engineering

journal homepage: www.elsevier.com/locate/oceaneng

Impact of turbulence induced loads and wave kinematic models on fatigue reliability estimates of offshore wind turbine monopiles

Lorenzo Colone *, Anand Natarajan, Nikolay Dimitrov

Technical University of Denmark, Department of Wind Energy, Frederiksborgvej 399, 4000 Roskilde, Denmark

ARTICLE INFO

Keywords:
Offshore wind turbine
Monopile foundation
Turbulence
Nonlinear waves
Model uncertainty
Fatigue reliability

ABSTRACT

The cost of offshore wind turbine substructures has a significant impact on competitiveness of the wind energy market and is affected by conservative safety margins adopted in the design phase. This implies that an accurate design load prediction, especially of those resulting in fatigue damage accumulation, may help achieve more cost-effective solutions. In this article, the impact of turbulence and wave loads on fatigue reliability of pile foundations is investigated for a 5-MW offshore wind turbine. Loads obtained by varying turbulence percentiles are compared with those obtained from the full joint probability distribution of wind speed and turbulence through Monte Carlo (MC) simulations, and from the equivalent turbulence level currently adopted by IEC standards. The analyses demonstrate that a lower equivalent turbulence percentile leads to a more realistic and less conservative estimation of fatigue loads. Subsequently, the research focuses on studying the effects of uncertain marine environments on the fatigue load distribution, showing that the latter is insensitive to the random variability of the hydrodynamic coefficients. With respect to the wave kinematic model, a comparison between nonlinear and linear waves clearly suggests that hydrodynamic forces depend significantly on the kinematic model adopted and the operational conditions of the turbine. Furthermore, a term is derived to correct the error introduced by Wheeler stretching at finite water depths. The respective model uncertainties that originate from the nonlinear irregular wave model and Wheeler correction are quantified and employed in a reliability analysis. In a case study, the results are finally compared in terms of estimated probability of failure, with the aim to quantify the influence of environmental models on monopile reliability.

1. Introduction

Wind is an affordable and sustainable source energy which represents a strong alternative to traditional methods of energy production. Over the recent years, the offshore wind industry has seen considerable growth, thanks to a greater exploitation of wind resources located far from the shore, in addition to other important advantages compared to onshore sites (L Petersen et al.,). However, offshore wind turbines are constantly exposed to significant loads, due to highly fluctuating environment. The profitability of a wind farm depends substantially on the cost associated with material, construction and installation of the substructures and, these costs may rise significantly as the industry moves towards larger turbines (Bhattacharya). Thus, the probability of failure, typically expressed over a period of one year, provides an indication of the investment needed to perform the mentioned activities successfully. This quantity measures the structural safety level ensured by applying design factors to compensate for uncertainties. Hence, it is evident that more accurate predictions of operational loads and improved knowledge of the physical parameters governing the structural reliability are of paramount importance in balancing the economic aspects against safety standards, (Hahn, 1999).

The wind turbine international design standards, IEC 61400-1, describe how to use a simplified equivalent wind conditions for the assessment of the design loads for each wind turbine components. For turbulence intensity, a characteristic value corresponding to the 90th percentile of the lognormal distribution is required. This definition is based on experimental work by Frandsen (2007) on blade loads, which describes the effective turbulence as a design quantity resulting in the same fatigue damage as the random variable. Sørensen et al. (2008) quantified the model uncertainty that originates by applying this formulation, and compared the results in terms of reliability in the presence of wind farm wakes. The study concluded that the model describes satisfactorily the random wind speed fluctuations. In more recent work carried out by Toft et al. (2016), it was found that for pile

* Corresponding author.
E-mail addresses: lcol@dtu.dk (L. Colone), anat@dtu.dk (A. Natarajan), nkdi@dtu.dk (N. Dimitrov).

https://doi.org/10.1016/j.oceaneng.2018.02.045
Received 6 July 2017; Received in revised form 13 February 2018; Accepted 21 February 2018

foundations in free ambient turbulent flow, a lower characteristic value may lead to more realistic and less conservative lifetime fatigue loads. In the same work, it was found that for blade root flapwise bending moments, results varied significantly from site to site. Thus turbulence being the main fatigue driver, its equivalent values need careful evaluation based on site specific load assessment in order to avoid overly conservative estimations.

Besides loads from the rotor, wave loads are significant contributors to the design of offshore substructures. The current practice recommend the assessment of wave loads to be performed based on simulated linear irregular waves generated from conventional spectra, typically Pierson-Moskovitz (PM) or JONSWAP. The linear wave theory is built on the hypothesis of small perturbation of the mean sea level (MSL) from which the potential flow is derived satisfying the normal boundary conditions (Journée and Massie, 2000). Along with linear waves, stretching methods are usually employed, among which the most popular is Wheeler (Wheeleret al, 1969), which is used to extend the validity of the linear theory to water particles above the MSL. For several decades, the linear theory has been successfully applied for predicting wave forces acting on offshore platforms. The latter are often located at very deep waters, where the wave kinematic are well approximated by the linear theory (Moan et al., 2007). However, most onshore wind turbines supported by pile foundations are sited in medium-shallow waters [1] (Arapogianni et al., 2013) where nonlinear effects are commonly encountered due to high steepness (cf. Veldkamp (Veldkamp and Van Der Tempel, 2005)).

Ocean waves are, by nature, non-Gaussian stochastic processes, (Natarajan, 2014). DNV-GL design guidelines for offshore wind turbines (DNV), suggest a fifth-order Stokes wave theory as an alternative to the linear model, which is only suitable for deep waters. Fully nonlinear models (cf Schløer et al. (2016),), although accurate, are computationally very expensive and therefore not desirable for offshore industrial applications. For this reason, the model that has received the most attention so far is the one developed by Sharma and Dean (Sharma, 1980), based on a second order expansion of the potential flow at finite water depths. Using this model, several studies have provided evidence that nonlinearities have an influence on loads of the substructure. In a study conducted by Agarwal and Manuel (2011), it was argued that the load difference is primarily due to the higher energy content present in the spectrum of nonlinear waves compared to that of conventional waves, which may affect the overall dynamic response. Consequently, long term fatigue damage is also influenced, as demonstrated by Michael et al. (Van Der Meulen et al., 2012), and Veldkamp et al. (Veldkamp and Van Der Tempel, 2005). In more practical terms, Marino et al. (2013), argued that nonlinearities may alter the load significantly when the contribution from aerodynamic damping is absent. This occurs during standstill and in the side-to-side (SS) dynamic response of the turbine during normal power production. In these cases, the main source of excitation for the substructure is from direct longitudinal waves, wave directional spreading and wind-wave misalignment, which is also discussed in for instance in (Kim and Natarajan, 2013). Standstill or idling occur because of unplanned downtime, normal shut-down due to maintenance, wind speed outside the operational range (e.g. storm) or no power requirement. Some statistics from UK offshore sites (Feng et al., 2010), reported that the typical availability of an offshore turbine may range between 60% and 95%. Since the assessment of lifetime fatigue damage is strongly dependent on the turbine availability, as discussed by Ziegler et al., (Ziegler and Muskulus, 2016), loads during standstill and idling need careful evaluation, especially in cases where significant resonance phenomena may occur.

However, from an operational perspective, it is of interest to quantify what is the impact of different environmental models on reliability and fatigue lifetime of monopiles, with respect to idling and operational conditions of the wind turbine. Therefore, the purpose of this research is to analyse the variation of structural loads by considering modified equivalent turbulence levels in free ambient flow, wind farm wakes and the effect of different wave kinematic models. The influence of the latter is quantified based on a lower-order wind turbine structure with coupled interaction of Morison forces, rotor forces and structural response. Subsequently, first and second-order statistics of the wave model uncertainties are used in the fatigue reliability analysis. The damage model used is based on Palmgren-Miner's cumulative law and bilinear SN-curve, as recommended in relevant standard practice (DNV). For the reliability analysis as well as load estimation, time domain aeroelastic simulations are employed. This work has the aim to evaluate and reduce the uncertainty in wind turbine damage equivalent loads and enhance lifespan assessment of offshore pile foundations.

The remainder for this article is as follows. The first section analyses the influence of varying turbulence levels in terms of fatigue loads under free ambient and wake conditions. Subsequently, Wheeler correction and the sensitivity of fatigue loads to the random variability of the hydrodynamic coefficients are studied. In the next section, a second order wave model is benchmarked against the linear wave theory combined with Wheeler stretching to evaluate their model uncertainty. Finally, a reliability analysis is performed combining different turbulence levels and wave models.

2. Site and model description

2.1. Wind and wave statistics

The 10-min hub height mean wind speed distribution used, corresponds to a IEC wind class 1B, with scale and shape parameters of the Weibull distribution being respectively $A = 11$, $c = 2$. Wave statistical data are based on site specific measurements from the research platform FINO (Mittendorf, 2009), located in the North Sea. The significant wave height H_s and zero-crossing wave period T_z are given at their expected values conditional on the mean wind speed U. The turbulence σ_u is taken at its characteristic value defined as

$$\sigma_u = I_{ref}(0.75U + 5.6) \tag{1}$$

where $I_{ref} = 0.14$ for the wind class selected. Alternatively, the IEC standards provide a formulation which allows to consider the turbulence as a log-normal distributed random variable conditional to mean wind speed $f(\sigma_u|U)$. The mean and standard deviation of the turbulence are defined in Eq. (2)

$$\mu_\sigma = I_{ref}(0.75U + 3.8), \qquad \sigma_\sigma = 1.4I_{ref} \tag{2}$$

MC simulations are used to sample from the joint probability distribution of the environmental variables

$$f(U, H_s, T_p, \sigma_u) = f(U)\, f(H_s|U)\, f(T_p|U, H_s)\, f(\sigma_u|U) \tag{3}$$

where $f(U)$ and $f(H_s|U)$ are Weibull probability density functions. The derivation of the expected spectral peak period T_p is found by Eq. (4) assuming a PM spectrum for the generation of random waves. The zero crossing period is given as log-normally distributed. The range of variability of the environmental variables is listed in Table 1.

Table 1
Environmental variable ranges for normal operating conditions.

Variable	Min	Max	Unit
U	3	25	m/s
H_s	0.8	7.3	m
T_p	5	12	s
σ_u	0.5	3.5	m/s

[1] The majority of European offshore sites located between 5 and 30 m, 74% of the total number installed on monopiles with an average water depth of 22 m.

Table 2
5MW NREL pitch regulate variable speed reference turbine characteristics.

Variable	Value	Unit
Rated power	5	MW
Cut-in wind speed	3	m/s
Cut-out wind speed	25	m/s
Rated wind speed	11.4	m/s
Rated rotor speed	12.1	rpm
Hub height, from MSL	90	m
Rotor diameter	126	m

$$T_p^4 = \frac{5\pi}{4} T_z^4 \tag{4}$$

2.2. Turbine

The NREL-5MW reference turbine described in detail in (Jonkman et al., 2009), is considered as installed on a monopile located at 20 m water depth in an elastic stiff sand soil. The monopile was configured so that the natural frequencies would correspond to the ones obtained in the reference project OC3 phase II (Jonkman and Musial, 2010), in order to avoid structural resonances. The first natural frequency corresponding to the fore-aft (FA) mode is $f_0 = 0.237$ Hz. The soil is modelled by nonlinear springs distributed along the soil portion of the pile. The soil stiffness is based on p-y-curve as recommended by the American Petroleum Institute, (RP2A-LRFD).

Numerical simulations are performed using the commercially available fully coupled aero-hydro-servo-elastic code HAWC2, (Larsen and Hansen, 2007) (see Table 2). The load cases considered in this work are summarized in Table 3. DLC 1.2 (b) and 6.4 are used for the reliability analysis, while DLC 1.2 (a) is used for MC simulations, according to the DLC definition in the IEC 61400-3. Loads from ocean currents are not considered. Unless clearly specified, the simulation time assumed is $T_s =$ 600 s. Initial simulation transients were removed from the analysis, by computing time series over 720 s and discarding the initial 120 s. Since the study aims at fatigue loads and fatigue damage assessments, normal sea state (NSS) and normal turbulence model (NTM) are used. These conditions prevail throughout the turbine lifetime.

The estimated 1-Hz damage equivalent load (DEL) is used as measure quantity throughout the analyses, defined as

$$L(U) = \left(\frac{1}{n_{eq}} \sum_{i=1}^{N} \Delta L_i^m n_i \right)^{1/m} \tag{5}$$

where L is the DEL defined over 600 s, n_{eq} the equivalent number of cycles, ΔL_i and n_i are respectively load range and associated number of cycles. N is the total number of Rainflow counted load ranges. Linear SN-curve is adopted for structural steel with a Wöhler exponent $m = 4$. The results from the aeroelastic simulations are expressed in terms of accumulated equivalent load L_l computed by Eq. (6)

$$L_{life} = \left(\sum_{j=1}^{N_u} \mu\left[L(U_j)\right]^m P(U_j) \right)^{1/m} \tag{6}$$

where N_u the number of discrete wind speeds, $\mu\left[L(U_j)\right]$ is the DEL averaged over a certain number of seeds per mean wind speed U_j and $P(U_j)$ its probability of occurrence.

3. Turbulence induced fatigue loads

This section shows a comparative study in terms of fatigue equivalence between different characteristic values of the turbulence intensity. The scope ot the analysis is to define a turbulence level which results in the same fatigue load as that obtained from the random turbulence. This is achieved by first deriving an equivalent turbulence intensity by pure analytical considerations based on simplified assumptions (see A). The analytical approach consists of an extension to the monopile of the idea presented in (Frandsen, 2007), where the wind turbine structure is reduced to an upright cantilever beam with a lumped mass at the tower top to model the rotor nacelle assembly mass and loaded by a dynamic thrust load. The simplified formulation shows that the monopile fatigue DEL is proportional to the standard deviation of the wind velocity at a given mean wind speed and Wöhler exponent. Subsequently, the effective turbulence level predicted by the simplified approach is compared with the results obtained by numerical simulations, using the aeroelastic wind turbine model. The probabilistic approach considers the full joint probability distribution of mean wind speed and turbulence $f(U, \sigma_u)$, as alternative to an equivalent turbulence. Furthermore, in order to focus on turbulence loads, the effect of wave loads is neglected for this analysis.

3.1. Free ambient turbulence

Under the approximated hypothesis of linearity between turbulence intensity and monopile fatigue loads, (Troldborg et al., 2014), the analytical formulation of the equivalent turbulence intensity I_e can be adopted, as

$$I_e^m = \int I^m f(I|U)\, dI \tag{7}$$

where I indicates the random variable. The integral in Eq. (7) is solved numerically assuming a log-normal distribution for $f(\sigma_u|U)$ as per Eq. (2), for the turbulence class here adopted. Fig. 2a displays a comparison between effective turbulence intensity, Eq. (7), and different turbulence percentiles using the formulation defined by IEC, Eq. (2). It is shown that for steel (m = 4), the effective turbulence is closer to the 60th percentile defined by IEC.

To demonstrate the validity of the values predicted by Eq. (7), a numerical case is set up where 5 sets of aeroelastic simulations are performed adopting a constant turbulence level for each case, varying between the 90th and the 50th percentile with a step of ten. The turbulence percentiles are defined based on the distribution in Eq. (2). The DELs obtained are averaged over 6 turbulence seeds for each mean wind speed in order to reduce the statistical uncertainty, following the recommendations given by IEC, (IEC, 61400-1). From the definition of the effective turbulence, these results are compared against 2000 MC simulations where random samples are drawn from the joint probability distribution $f(U, \sigma_u)$. The design load case DLC 1.2 (a) is considered, Table 3.

In Fig. 1, only loads corresponding to the 60th and 90th percentiles are displayed. The 60th percentile is the closest to the results provided by the crude MC approach in terms of fatigue equivalence, as seen from Table 4. The 90th percentile defined by IEC shows conservative results for the pile foundation where the accumulated DEL is increased by 13% in the FA direction and 11% in the SS direction. A lower turbulence level is also observed for the blade root bending moment, which is an agreement with some of the findings in (Toft et al., 2016), where a significant

Table 3
Selected design load cases and definition of environmental parameters (IEC 61400-3).

Design case	DLC	Wind	Wave	$\theta_{wind}, \theta_{wave}$	Conditions
Power production	1.2 (a)	NTM, $U_{in} < U_{hub} < U_{out}$	NSS, $f(U, H_s, T_p, \sigma_u)$	UNI,MUL	Fatigue
Power production	1.2 (b)	NTM, $U_{in} < U_{hub} < U_{out}$	NSS, $H_s = E(H_s\|U)$	UNI,MUL	Fatigue
Idling (standstill)	6.4	NTM, $U_{in} < U_{hub} < U_{out}$	NSS, $H_s = E(H_s\|U)$	UNI,MUL	Fatigue

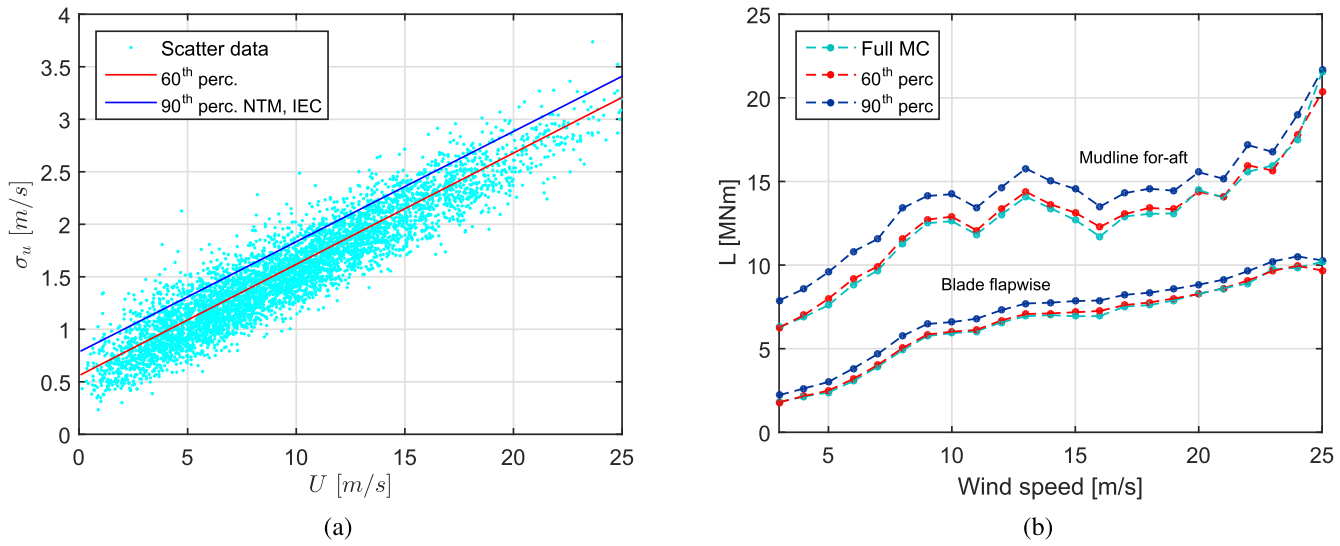

Fig. 1. *a)* Scatter mean wind speed and turbulence *b)* DEL for monopile FA and blade root flapwise bending moments at different values of the turbulence percentile.

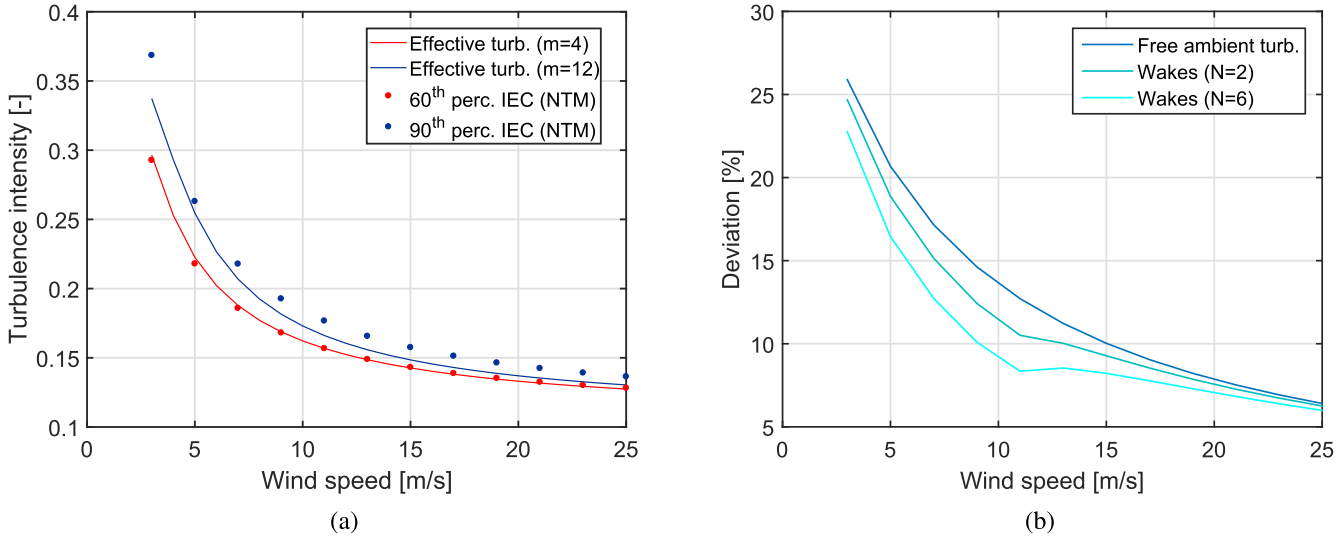

Fig. 2. *a)* Comparison between turbulence intensity at different percentiles of the lognormal distribution and effective turbulence at different Wöhler exponents *b)* Difference in percentage between 90th and 60th for free ambient turbulence and wake conditions.

Table 4
Normalized accumulated DEL at different turbulence quantiles. Blade root flapwise and mudline bending moments.

Sensor	Crude MC	60th perc.	90th perc.
Blade Flapwise	1.00	1.01	1.06
Mudline FA	1.00	1.01	1.13
Mudline SS	1.00	1.02	1.11

variability for this response is encountered at different site conditions. For the blade root, the fatigue load coming from the 90th percentile is slightly more conservative by 6% in this study. For the monopile, the lower fatigue equivalent percentile found here is directly used as characteristic value of the free ambient turbulence $\widehat{\sigma}_c$, where an additional contribution from wind farm wakes has to be considered.

3.2. Contribution from farm wakes

In order to quantify the effect of wakes, a case study is performed based on the formulation described in the amendment of IEC standards, (IEC, 2005). Wake generated turbulence increases the overall turbulence level. These are taken into account for fatigue calculations as combination of free ambient and farm wake turbulence in operational conditions, Eq. (8).

$$\sigma_e = \left[(1 - N_t\, p_w)\widehat{\sigma}_c^{\,m} + p_w \sum_{i=1}^{N_t} \widehat{\sigma}_{iw}^{\,m}(d_i) \right]^{1/m} \tag{8}$$

A distance between turbines equal to five times the rotor diameter $d = 5D_m$ and a uniform wind direction distribution $f(\theta|U)$ are assumed. In Eq. (8), $p_w = 0.06$ is the probability of wake condition, N_t is the number neighbouring turbines, $\widehat{\sigma}_c$ is the free ambient characteristic turbulence and $\widehat{\sigma}_w$ the characteristic value of the maximum center wake turbulence standard deviation at the hub height (Sørensen et al., 2008), expressed as

$$\widehat{\sigma}_w = \sqrt{\frac{U^2}{\left(1.5 + 0.8d/\sqrt{C_T(U)}\right)^2} + \widehat{\sigma}_c^2} \tag{9}$$

where $C_T(U)$ is the thrust coefficient known as function of the mean wind speed in case of a pitch regulated variable speed turbine. Table 5 shows

Table 5
Accumulated DEL computed using the 60th percentile normalized with respect to the corresponding DEL computed using the 90th percentile.

Case	FA	SS
$N_t = 2$	0.91	0.95
$N_t = 6$	0.92	0.95

the normalized accumulated DEL computed using the 60th percentile characteristic turbulence with respect to 90th percentile currently used. The results are averaged over 6 turbulence seeds for each wind speed bin in the operational range with step of 2 m/s. Two cases with $N_t = 2$ and case $N_t = 6$ are analysed.

Using the 60th turbulence percentile leads lower accumulated DELs by approximately 10% in the FA direction and 5% in the SS direction. As expected, the FA bending moment is more affected by the reduction being mainly governed by longitudinal turbulence. Fig. 2b shows that the difference between the 90th and 60th percentiles decreases as the number of neighbouring turbines increases. This confirms that in the presence of strong wakes, the ambient turbulence effect vanishes. Fig. 3 displays examples of monopile FA bending moment from aeroelastic simulations adopting different turbulence levels, below and above rated wind speed. The SS bending moment is only slightly affected by the number of neighbouring turbines.

4. Wheeler correction at finite water depths

According to the linear superposition principle, ocean waves can be approximated as a sum of regular sinusoidal harmonics and random phase to form an irregular wave (Journée and Massie, 2000). The empirical relation introduced by Wheeler to extend the kinematic above the mean sea level, introduces a mathematical error at finite water depth which is herein derived. In the equations below, a regular unimodal wave is considered. Under the hypothesis of small wave amplitudes $\eta(x,t)$ the field equation in the two dimensional case is described by Eq. (10), reported here for the sake of clarity

$$\begin{aligned} &\nabla^2\phi = 0 \quad in\ \Omega \\ &\frac{\partial\phi}{\partial z} = 0 \quad on\ \Gamma_1 \\ &\frac{\partial\phi}{\partial t} + \frac{1}{2}\left(u^2 + w^2\right) + \frac{p}{g} + gz = C \quad on\ \Gamma_2 \end{aligned} \tag{10}$$

where Ω is the field domain, Γ_1 is the sea bottom at a water depth $z = -h$, Γ_2 is the wave surface and u and w the horizontal and vertical particle velocity respectively. The quantity p is the atmospheric pressure and C is a constant. From Eq. (10) the solution of the Laplace equation is the potential flow for the velocity field for finite water depths which satisfies the free kinematic boundary conditions (Cauchy-Poisson) (Journée and Massie, 2000)

$$\phi(x,z,t) = \frac{\eta_a}{k\omega}\,\frac{\cosh[k(h+z)]}{\sinh(kh)}\,\sin(kx - \omega t) \tag{11}$$

where $\eta_a \approx H/2$ is the wave amplitude, with H being the linear wave height. The stretching consists in replacing the physical vertical coordinate z in z', as

$$z' = h\left(\frac{h+z}{h+\eta}\right) - h, \qquad -h \le z' \le 0, \qquad -h \le z \le \eta \tag{12}$$

Introducing Eq. (12) into Eq. (11) the residual term of the Laplace equation can be computed, as

$$\nabla^2\phi_w = k\left(\alpha^2 - 1\right)\phi_w \tag{13}$$

where it has been indicated with

$$\alpha = \frac{h}{h+\eta} \tag{14}$$

The residual term in Eq. (13) vanishes as the water depth increases meaning that no error is present at infinite water depths. Thus, at finite water depths, a correction can be introduced on the argument of the sinusoidal function

$$\widehat{\phi}_w(x,z,t) = \frac{\eta_a}{k\omega}\,\frac{\cosh\left[kh\left(\frac{h+z}{h+\eta}\right)\right]}{\sinh(kh)}\,\sin(\alpha kx - \omega t) \tag{15}$$

where $\widehat{\phi}_w(x,z,t)$ is the potential flow function with corrected Wheeler stretching. It can be verified that the new potential function satisfies the two dimensional field equation, as

$$\nabla^2\widehat{\phi}_w = 0 \tag{16}$$

It is worth noting that for $h \to \infty$, the following relations are valid

$$kh\left(\frac{h+z}{h+\eta}\right) \to kh, \qquad \alpha \to 1 \tag{17}$$

To quantify the deviation in particle velocity from Wheeler stretching, the new kinematics are derived from the corrected potential flow expressed by Eq. (15) leading to the linear velocity and acceleration in the horizontal direction, where the corrective term is applied

$$u = \frac{\partial\phi}{\partial x}, \qquad a = \frac{\partial u}{\partial t} \tag{18}$$

$$\widehat{u}(x,z,t) = \alpha\,\eta_a\,\omega\,\frac{\cosh\left[h\left(\frac{h+z}{h+\eta}\right)\right]}{\sinh(kh)}\cos(\alpha kx - \omega t) \tag{19}$$

$$\widehat{a}(x,z,t) = \alpha\,\eta_a\,\omega^2\,\frac{\cosh\left[kh\left(\frac{h+z}{h+\eta}\right)\right]}{\sinh(kh)}\sin(\alpha kx - \omega t) \tag{20}$$

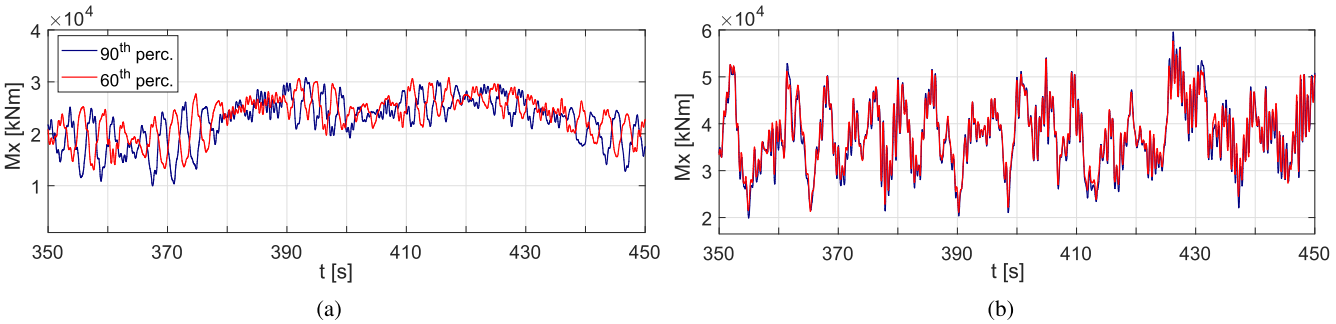

Fig. 3. Mudline FA bending moment at *a)*$U = 7$ m/s and *b)* $U = 19$ *m/s* in wake conditions ($N_t = 2$), showing the difference between the selected turbulence percentiles.

The numerical example displayed in Fig. 4a, shows a velocity profile of a unimodal wave assuming a period $T_w = 8$ s, a water depth $h = 20$ m and a wave height η_a varying in the interval $\frac{0}{3}$ m. As displayed in Fig. 4a, the correction in the potential function leads to lower velocities for positive wave heights, Fig. 4. Furthermore, the deviation increases with the wave height. In the following discussions and figures, this model will be referred to as Wheeler correction.

It is important to remark that this derivation has the aim to only quantify the effects of satisfying the Laplace equation at finite water depths. Since it is not based on any experimental work, the approach has not been validated and it is not certain that it will necessarily lead to more accurate load predictions.

5. Uncertainty of drag and inertia coefficients

The sensitivity of DEL due to wave forces during normal operation is analysed in this section, in order to quantify the effect of random variability of the hydrodynamic coefficients employed to compute wave forces. The empirical formulation introduced by Morison (Morison et al., 1950), is by far the most common way of predicting unidirectional wave load acting on an immerse slender body in an unsteady flow, in this case the monopile being a hollow cylinder. As described in (DNV), above the range defined as the limit $D_m/\lambda \leq 0.2$ where D_m is the pile diameter and λ the wave length, the pile affects the wave flow leading to wave diffraction phenomena. This can be taken into account by the MacCamyFuchs correction on the inertia coefficient C_m. Other environmental factors are responsible for a variation of the hydrodynamic coefficients. Marine growth for instance, which is a biological accumulation of microorganisms and algea on wetted surfaces, results in increased of inertia and drag forces as a consequence of increased surface roughness and cross-section area (Shi et al., 2012). In fact, roughness due to marine growth modifies the transition laminar to turbulent flow at lower Reynold's numbers resulting in increased drag. In consequence of the natural variability of the oceanic environment, the validity of the Morison equation may not always be respected. In structural reliability, the uncertainty on the hydrodynamic forces exerted on a pile foundation turns into a load variation due to wave-structure interaction. For computing loads on the substructure, inertia and drag coefficients can be treated as normally distributed random variables, chosen here as $C_m \sim \mathcal{N}(\mu_m, \sigma_m) = (1.9, 0.1)$ and $C_d \sim \mathcal{N}(\mu_d, \sigma_d) = (0.9, 0.1)$, with μ and σ being respectively their mean and standard deviation. Although higher values of the uncertainty in the hydrodynamic coefficients can be found in practice, values provided in literature for fatigue analyses were used, (Veldkamp, Burrows et al., 1997). Thus, two parallel studies are performed respectively considering the hydrodynamic coefficients as random and deterministic variables, the latter corresponding to their mean values. Under normal operating conditions, the load case DLC 1.2 (b) is used. A set of 2000 randomly sampled environmental conditions from Eq. (3) are used as input parameters to aeroelastic simulations. Waves are modelled as irregular linear random waves and Wheeler stretching. A side analysis is performed to quantify the statistical impact of wave forces on the DEL by only including wind forces. Thus, in order to show the influence of the wave load on the SS direction, wave directional spreading is included in this analysis along with a wave misalignment of 10 deg. Results are displayed in Fig. 5 in terms of probability distributions of the mudline bending moments.

As shown in Fig. 5 the wave force increases the mode of the DEL distribution by nearly 20% of the total fatigue loads in the FA direction and 28% in the SS direction as summarized in Table 6. The values are normalized with respect to the bending moments in the corresponding direction of the deterministic case.

In Fig. 5 the smoothing was obtained by kernel density estimator (Sheather and Jones, 1991). As it can be inferred, the distribution of the DEL in both SS and FA directions is insensitive to the uncertainty introduced on the hydrodynamic coefficients. A slight increase of 2% and 4% respectively are encountered as seen from Table 6. Although this small variation, their deterministic expected values can be conveniently adopted without significant impact. However, larger uncertainties if present in the hydrodynamic coefficients than the ones considered in this study may have larger impact on fatigue loads. The analysis also shows the statistical contribution of wave loads. The latter increase the mean DEL compared to the case where only wind excitation is present. The difference displayed in Fig. 5 between wind only and combined wind-wave excitation has to be interpreted qualitatively, since wind and wave forces are coupled with the dynamic response of the structure and their effect cannot in principle be studied separately.

6. Damage model

6.1. Cumulative damage

For the assessment of fatigue damage, a linear cumulative law based SN-curve and Palmgren-Miner's method is used. The SN-curve is a relationship between number of stress cycles to failure and the associated

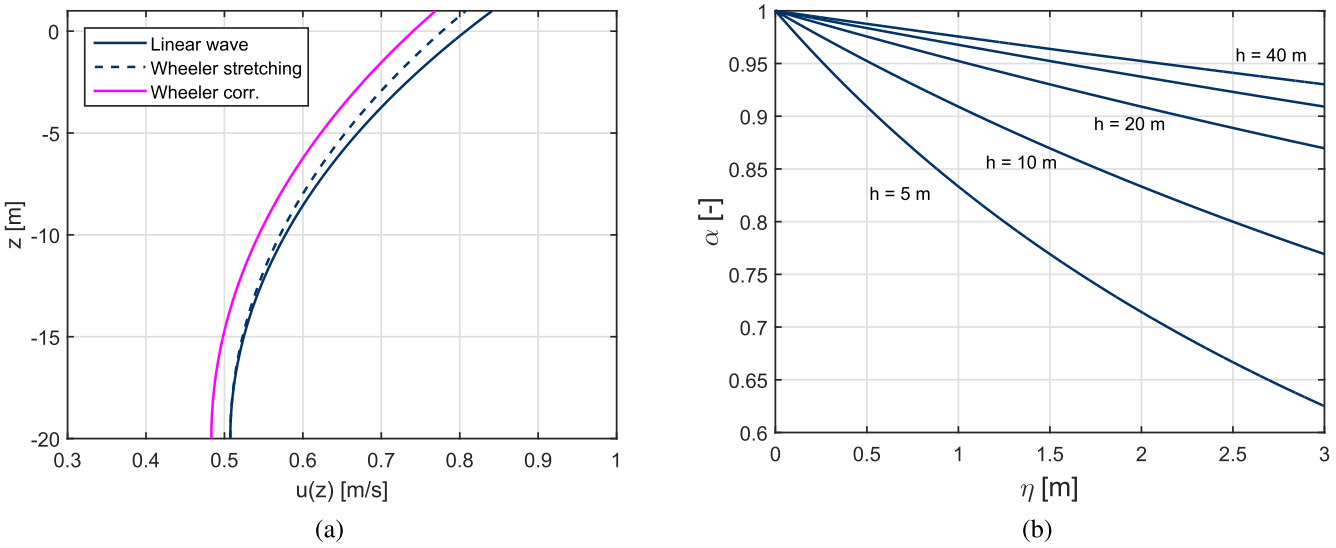

Fig. 4. *a)* Velocity field $u(z)$ along the vertical coordinate at a given point in time and fixed abscissa. Wave height $\eta_a = 1$ m. *b)* Wheeler stretching error at different water depths as a function of wave height.

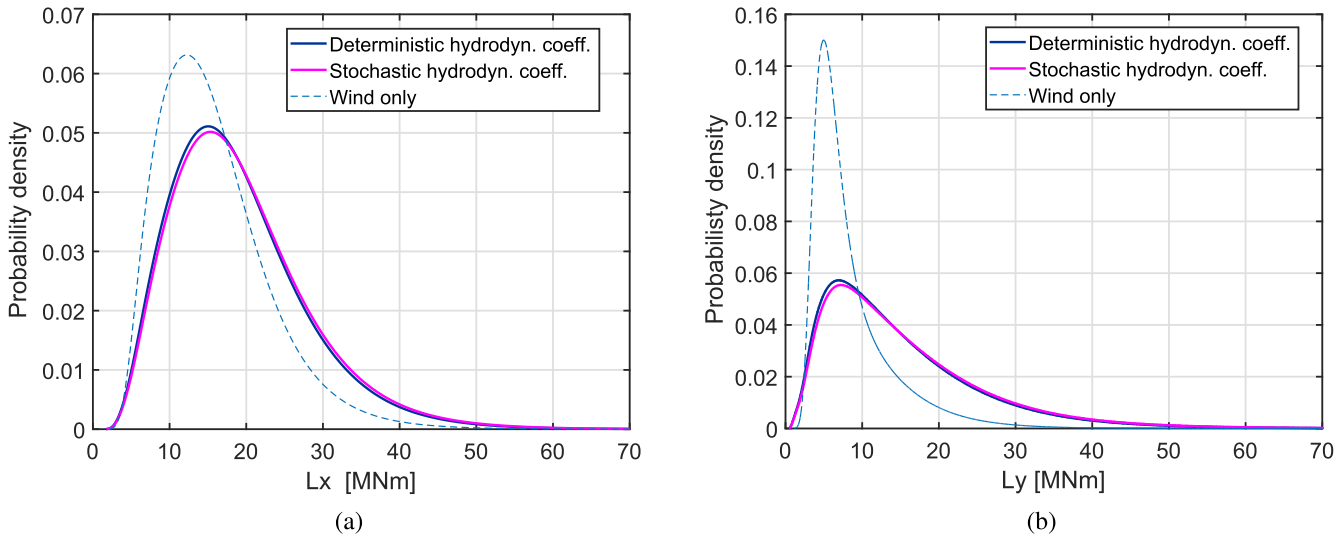

Fig. 5. DEL distribution at the mudline for random and deterministic variability of hydrodynamic coefficients and wind forces only. FA and SS directions are displayed.

Table 6
Normalized mode of the DEL distribution for deterministic and random variation of the hydrodynamic coefficients.

C_m, C_d	FA	SS
Deterministic	1.00	1.00
Random	1.02	1.04
Wind only	0.81	0.72

stress amplitude. The expected short term cumulative damage $D_s(U)$ can be expressed in the integral and discrete forms, as

$$D_s = \frac{N}{a}\int_0^{\infty} \Delta\sigma(U)^m f(\Delta\sigma)\, d\sigma = \sum_i^{N_{\Delta\sigma}} \frac{n_i}{a_i} \Delta\sigma(U)_i^m \tag{21}$$

where $N_{\Delta\sigma}$ is the total number of cycles experienced during the simulation time T_s, $log(a)$ the intercept of the SN-curve and $f(\Delta\sigma(U))$ the stress ranges distribution conditional on the mean wind speed obtained from Rainflow counting. In literature, as for instance in (Sørensen et al., 2008) and (Nejad et al., 2014), there are several formulations assuming a closed form of the integral in Eq. (21). This is in practice accomplished by assuming a model for the stress range distribution $f(\Delta\sigma)$, typically two parameters Weibull distribution. Here the long term expected damage D is obtained by Palmgren-Miner's rule by integrating the short term damage conditional to the mean wind speed over the long term mean wind speed distribution $f(U)$. For offshore substructures, the full sea and wind state has to be considered through the joint probability distribution of the environmental variables $f(U,H_s,T_p,\sigma_u)$. However, in this work only discrete states are considered for fatigue damage, which means that the environmental variables are all conditional to the mean wind speed U.

6.2. Fatigue reliability

Fatigue life of a structural component is the time spent under ordinary loading conditions necessary to initiate a physical crack which would result in a loss of ultimate fatigue strength of the member. The fatigue damage limit state function $g(\mathbf{X})$ can be formulated according to the SN approach, where $\mathbf{X} = [X_1, X_2, \ldots X_n]$ is a collection of random variables in the load and resistance model. The condition $g(\mathbf{X}) \leq 0$ indicates a failure occurrence. In this work, the cumulative damage during operation and standstill is considered, indicated respectively as D_{op} and D_{ss}.

$$g(\mathbf{X}) = \Delta - D_{op}(X_{op}) - D_{st}(X_{st}) \tag{22}$$

The turbine lifetime is taken as reference period for computing the cumulative damage by means of Eq. (33). In case of offshore turbines, the service life is set to $T_{life} = 25$ years, which comprises a contribution to damage from operational conditions computed through DLC 1.2 (b), and from idling computed through DLC 6.4 (see Table 3). In Eq. (22), the term Δ represents the failure limit modelled as a stochastic variable associated with Miner's rule, i.e. the degree of uncertainty in predicting variable amplitude fatigue loads usually conducted from constant amplitude tests. The vector $\mathbf{X}$ denotes the set of uncertainties considered. Once the limit state function is known explicitly through Eq. (22), the probability of failure P_f is defined as

$$\widehat{P}_f = P[g(\mathbf{X}) \leq 0] = \int_{g(\mathbf{X})\leq 0} f_x(\mathbf{X})\, dx \tag{23}$$

where $f_x(\mathbf{X})$ is the joint probability density function of the random variables $\mathbf{X}$. From reliability theory, the estimated generalised reliability index $\widehat{\beta}$, simply indicated as β, is linked to the estimated probability of failure $\widehat{P}_f$, as

$$\beta = -\Phi^{-1}(\widehat{P}_f) \tag{24}$$

where Φ is the standard normal probability distribution function. Given the complexity of the limit state function $g(\mathbf{X})$, the integral in Eq. (24) is calculated through first order reliability method (FORM) followed by re-evaluation with importance sampling (IS) based on a Gaussian sampling distribution, (Dimitrov et al., 2013). The FORM method assumes a linear safety margin, which in some cases may lead to inaccurate estimation of the reliability index. On the other hand, FORM is an efficient way to find the most likely failure point. Importance sampling centered at the design point $\mathbf{X}_d$ determined by a FORM analysis can serve as verification and improvement of the FORM results, since IS, as most simulation methods, is not strongly affected by nonlinearity in the safety margin. This technique was more computationally efficient than crude MC simulations, as confirmed by preliminary attempts.

6.3. Uncertainties

A review of the major uncertainties typically considered in reliability of offshore structures can be found in (Hahn, 1999; Sørensen et al., 2008; DNV; Tarp-Johansen, 2003; Rangel-Ramírez and Sørensen, 2012). The

uncertainties considered contain a statistical uncertainty related to wind and wave climate assessment X_{st}, model uncertainty in the simulation of the dynamic response X_{dyn}, blade aerodynamic model X_{aero}, wake turbulence model X_{wk} and stress calculation from finite elements models or others X_{str}. An uncertainty is also considered to account for the limited simulation time, X_{sim}, representative for the entire lifetime. Numerical values of the aforementioned quantities are retrieved from available literature and listed in Table 8. An additional contribution is introduced to model the uncertainty associated with the wave kinematic model adopted. These are specified for standstill and operational condition separately, respectively indicated as $X_{h,ss}$, $X_{h,op}$. The cumulative damage is a nonlinear function of these quantities because the uncertainties are applied to the respective parameters on which they produce effect.

7. Wave induced fatigue loads

7.1. Wave kinematic models

The surface elevation process $\eta(t)$ of a long crested unidirectional sea wave can be expressed as linear superposition

$$\eta(x,z,t) = \sum_{i=1}^{N} A_i(\omega_i)\cos(k_i x - \omega_i t + \varepsilon_i) \tag{25}$$

where the input parameters are the wave amplitude $A_i(\omega_i)$, the spectral frequency ω_i, the wave number k_i and the random phase ε_i. Three different wave kinematic models are compared. Eq. (26) expresses the horizontal particle velocity field derived from Eq. (25) where Wheeler stretching is applied. The second order non linear wave kinematic model applied here is described (Natarajan, 2014). The nonlinear horizontal velocity field u_{nl} is expressed by Eq. (27). Furthermore, a third kinematic model uses velocity and acceleration obtained by the generation of linear random waves corrected by the factor derived in section 4 as $\widehat{u}_l(t) = \alpha\, u_l(t)$.

$$u_l(x,z,t) = \sum_{i=1}^{N} A_i\,\omega_i\,\frac{\cosh\left[k_i h\left(\frac{h+z}{h+\eta}\right)\right]}{\sinh(k_i h)}\cos(k_i x - \omega_i t + \varepsilon_{ij}) \tag{26}$$

$$u_{nl}(x,z,t) = \sum_{i=1}^{N} A_i\,\omega_i\,\frac{\cosh[k_i(z+h)]}{\sinh(k_i h)}\cos(k_i x - \omega_i t) + \sum_{i=1}^{N}\sum_{j=1}^{N}\left[B_{ij}^{+}(z)\cos\left(k_{ij}^{+}x - \omega_{ij}^{+}t + \varepsilon_{ij}\right) + B_{ij}^{-}(z)\cos\left(k_{ij}^{-}x - \omega_{ij}^{-}t + \varepsilon_{ij}\right)\right] \tag{27}$$

Likewise, the expressions for the horizontal acceleration and kinematics in the vertical direction can be written. The second order transfer functions $B_{ij}^{+}(z), B_{ij}^{-}(z), C_{ij}^{+}(z), C_{ij}^{-}(z)$ rearranged in Eq. (27) are function of wave amplitude, frequency, wave number, water depth and vertical coordinate, their explicit formulation is reported for instance in (Agarwal and Manuel, 2011). The second order expansion is evaluated at $i \neq j$. The superscripts + and − refer to a summation or difference between frequencies.

Table 8
Stochastic model for fatigue reliability - welded steel (LN = lognormal, N = normal, D = deterministic).

Description	Variable	Distribution	Value	Mean	Std
Miner's rule	Δ	N	–	1.00	0.10
Wind climate	X_{st}	LN	–	1.00	0.05
Aerodynamic	X_{aero}	GB	–	1.00	0.10
Structural dynamic	X_{dyn}	LN	–	1.00	0.03
Farm wakes	X_{wk}	LN	–	1.00	0.10
Simulation time	X_{sim}	N	–	1.00	0.02
Stress computation	X_{sc}	LN	–	1.00	0.03
Intercept SN-curve ($m_1 = 3$)	$\log(a_1)$	D	12.05	–	–
Intercept SN-curve ($m_2 = 5$)	$\log(a_2)$	D	16.08	–	–
Interia coeff.	C_m	D	1.9	–	–
Drag coeff.	C_d	D	1.0	–	–

7.2. Assessment of the wave model uncertainty

This analysis has the aim to quantify the model uncertainties in fatigue loads associated with the wave kinematic model adopted. Model uncertainties are epistemic and originate from imperfect knowledge or idealizations of the mathematical formulation used to predict a natural process. In other words, it is a measure of the ability of a mathematical model to reproduce a natural phenomena. For example, Ambühl et al. (2015), explicitly expressed this bias by evaluating the performance of different mathematical models against real wave measurements. In this work, due to absence of measurements, the second order wave kinematic model and Wheeler correction at finite water depth are compared against the linear wave model in Eq. (26). The load variation is then expressed as a relative ratio X_h between the equivalent stress $\sigma'_{\psi,eq}$ computed from the different wave kinematic models and from the linear wave model $\sigma_{\psi,eq}$, as in Eq. (28). The equivalent stress is defined similarly to Eq. (5), considering stress time series instead of loads.

$$X_h = \frac{\sigma'_{\psi,eq}}{\sigma_{\psi,eq}} \tag{28}$$

The nominal stress parametrised with respect to the radial position on a specific section of the monopile ψ, is expressed by Eq. (29). Given the monopile geometry and dimensions, the stress can be well approximated by a longitudinal membrane stress as defined by DNV-GL (AS,). The contribution from the vertical force is neglected due to of its small load range, which does not contribute to fatigue. It is assumed that shear stresses are also negligible.

$$\sigma_\psi(t) = \frac{M_x(t)}{I}\,R\sin(\psi) - \frac{M_y(t)}{I}\,R\cos(\psi) \tag{29}$$

In Eq. (29), $R = 3$ m is the medium radius of the monopile and $I = 4.12\ \mathrm{m}^4$ the area and the area moment of inertia of the circular hollow section. In Eq. (29) the dependency from the environmental parameters

Table 7
Environmental parameters used for the assessment of the wave load variation. P_i is the probability of occurrence of each state.

Variable	s1	s2	s3	s4	s5	s6	s7	s8	s9	s10	s11	s12
U [m/s]	3	5	7	9	11	13	15	17	19	21	23	25
H_s [m]	1.00	1.52	3.12	3.72	4.10	4.63	5.06	5.33	6.04	6.64	7.10	7.33
T_p [s]	6.00	6.50	6.72	7.08	7.43	7.90	8.26	8.48	9.02	9.46	9.78	9.94
P_i [−]	0.132	0.142	0.146	0.160	0.152	0.127	0.094	0.062	0.036	0.019	0.009	0.004

is omitted. The first two statistical moments of X_h provide a measure of the relative model uncertainty.

Table 7 shows the discrete set of environmental parameters. To compare the wave kinematic models, only the states $s3$ to $s12$ are used due to data availability. The states $s1$ and $s2$ will be used in the next section and reported here for completeness. The probability of occurrence is taken according to the wind speed Weibull distribution in the range 7–25 m/s, with step of 2 m/s resulting in 10 discrete states. The turbulence level as expressed by Eq. (1) is used. The hydrodynamic load acting on the substructure is computed by the Morison formula with coupled wave-structure interaction, as

$$F(t) = \frac{1}{2}\rho C_d D_m \left| u(t) - \dot{q}(t) \right| (u(t) - \dot{q}(t)) + \frac{\pi D_m^2}{4}\rho C_m \dot{u}(t) - \frac{\pi D^2}{4}\rho (C_m - 1)\ddot{q}(t) \tag{30}$$

where $F(t)$ is the wave force per unit length, C_m and C_d are respectively inertia and drag coefficients, D_m the monopile diameter, ρ the water mass density and q denotes the structural displacement in the FA direction. Due to the random variability of the hydrodynamic coefficients not significantly affecting the load distribution in the long term, C_m and C_d are considered constant.

The load case DLC 6.4 defined by IEC design standards for offshore turbines (IEC, 61400-3) concerns fatigue analysis during idling. According to the description, resonant loading of the substructure from wave excitation has to be taken into account assuming NSS and wave misalignment. In this analysis a wave misalignment of 10 deg is considered. Resonance effects are caused by the wave spectral energy typically concentrated in a frequency band close to the first natural frequencies of the turbine (FA, SS).

Damping is an important player for fatigue. Several experimental studies on offshore turbines have shown the variation of the additional damping provided by the rotor. In (Koukoura et al., 2015) this value was found to be approximately 12% in idling in the FA direction while when the turbine is operating, it may rise up to 60% (logarithmic decrement). Although aerodynamic damping represents a large portion of the total damping in operation, this latter is a sum of additional contributions given by soil, hydrodynamic interaction, structure and controller. Hereby, two different states of the turbine are analysed, namely idling or standstill and normal operation. The flow chart in Fig. 7 explains the procedure to estimate the model uncertainty of the wave forces associated with the defined wind turbine states.

7.3. Lower-order turbine model

In order to specify X_h, a set of nonlinear waves based on the second order kinematic model is generated using the statistical parameters listed in Table 7. Since the aim of the analysis is to quantify the wave kinematic model uncertainty, the effect of other uncertainties must be neglected. These include aerodynamic interaction, structural model, rotor excitation, controller unit and soil model. For this reason, a lower order three-dimensional numerical model of a wind turbine structure is set-up, where the rotor nacelle assembly is replaced by a lumped mass at the tower top m_{top} and a bottom fixed monopile. The portion of soil pile is calibrated in length to match the first natural frequency of the areroelastic model, the latter being $f_0 = 0.237$ Hz in both FA and SS directions (apparent fixity). The system is modelled with Timoshenko beam elements (Friswell, 2010). This set-up ensures coherence with the dynamic response of the full aeroelastic model.

7.4. Standstill loads

First an analysis is performed on the full aeroelastic and equivalent model in idling conditions, where only hydrodynamic forces are exerted on the structures given the negligible contribution of the wind force acting on the system. These are applied in the two directions x and y according to the misalignment applied. A logarithmic decrement damping $\delta_{ss} = 7\%$ is considered representative for standstill. Because the turbine is not operating, the damping can be assumed constant for all the environmental states defined in Table 7. In both systems, a stiffness proportional Rayleigh damping matrix $\mathbf{C} = \alpha\mathbf{K}$ is tuned by varying the structural damping of the support structure and then computing the analytical logarithmic decrement as ratio between real and imaginary part of the eigenvalue λ, as

$$\delta = 2\pi \frac{\mathscr{R}(\lambda)}{\mathscr{I}(\lambda)} \tag{31}$$

This value includes contributions from soil and structure damping. A comparison of the response in time domain of the two systems in standstill is displayed in Fig. 8.

7.5. Operational loads

To quantify the hydrodynamic load variation during operation, an estimate of the aerodynamic damping at different mean wind speeds is needed (see Fig. 9). This is accomplished by computing the logarithmic decrement damping δ_{op} of the tower-top acceleration to a small perturbation of a constant mean wind speed, using the full aeroelastic model. No turbulence and waves are applied. The resulting free decay response is used to estimate the logarithmic decrement and damping ratio as indicated in Eq. (32). This procedure provides an engineering estimate of the damping available during normal power production (see e.g. Tempel (2006)). Fig. 12 displays the damping ratio estimated by this procedure.

$$\delta = \frac{1}{n}\log\left(\frac{p_0}{p_n}\right), \qquad \zeta = \frac{1}{\sqrt{1 + \left(\frac{2\pi}{\delta}\right)^2}} \tag{32}$$

In Eq. (32), p_0 is the first peak response while p_n is the peak response after n periods. Subsequently, the estimated aerodynamic damping in the FA direction, is used as input to the simplified system as additional contribution applied at the tower-top mass as shown in Fig. 6, and modelled with an internal viscous damper. The damping coefficient is found as $c = 2\zeta\sqrt{km}$, where m and k are respectively modal mass and modal stiffness of the considered modes in the FA and SS directions. Thus, the aerodynamic forces applied on the simplified model are the tower-top bending moments in the two directions x and y, the thrust force and the horizontal force in the y direction. The hydrodynamic forces are applied as in the standstill case. All these components are extracted from aeroelastic simulations using the full model. The thrust force was obtained from an aeroelastic model with stiff tower and rotor, in order to eliminate the wind-structure interaction.

Fig. 8 shows the good agreement between the structural response of

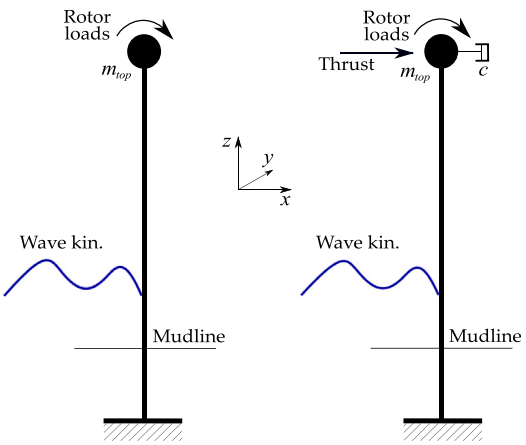

Fig. 6. Simplified mechanical system for estimating the wave model uncertainty in standstill and operating conditions.

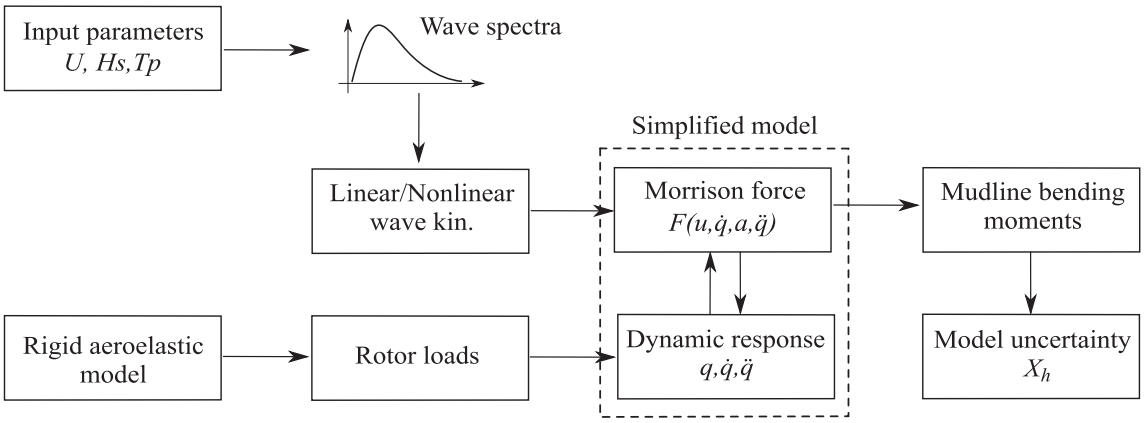

Fig. 7. Estimation of the model uncertainty from the wave kinematic models adopted.

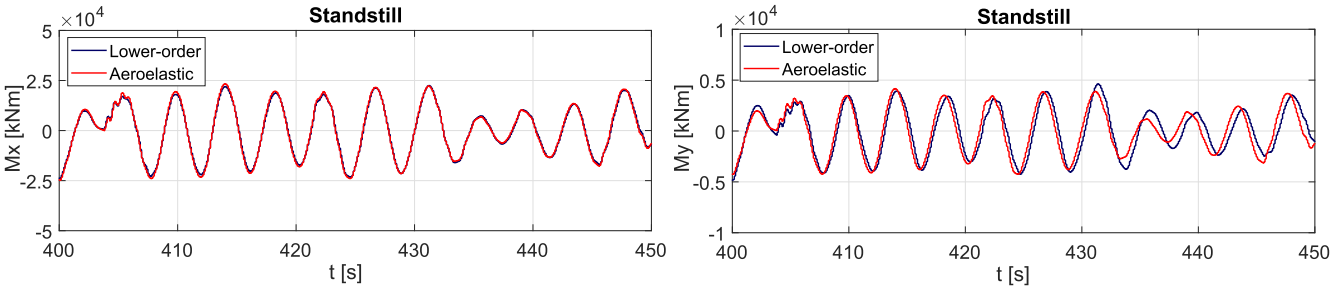

Fig. 8. Comparison lower-order model vs. full aeroelastic model of the mudline FA and SS bending moments in standstill.

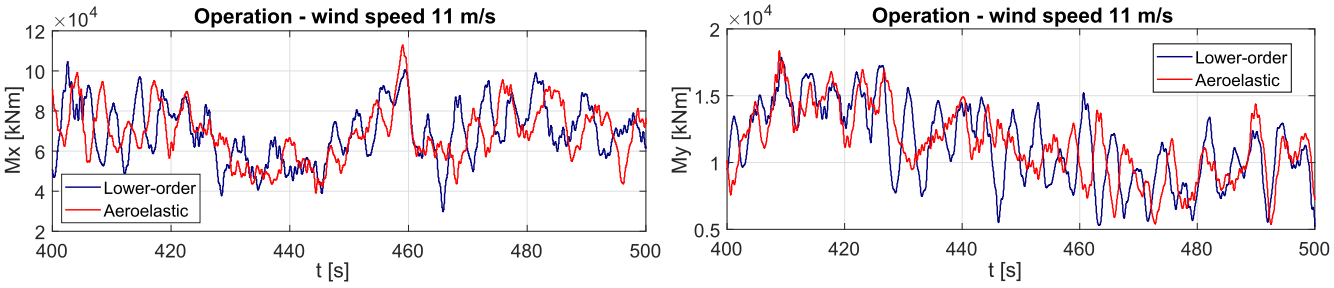

Fig. 9. Comparison lower-order model vs. full aeroelastic model of the mudline FA and SS bending moments in operation.

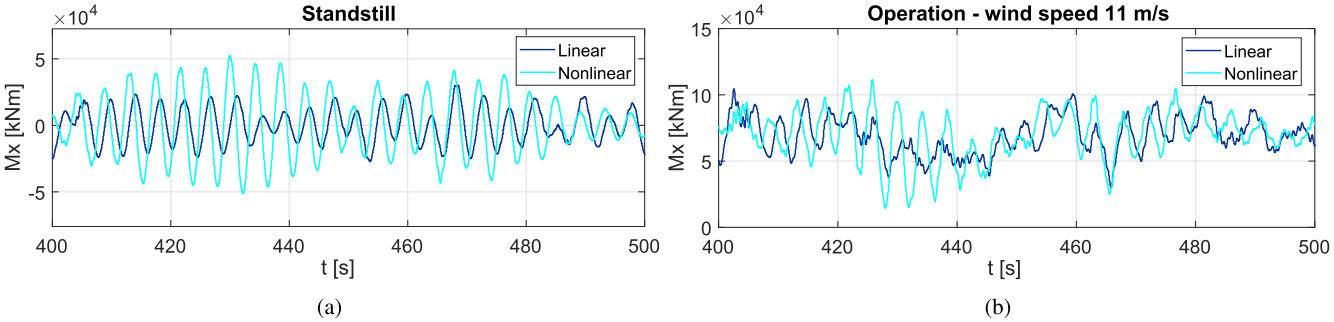

Fig. 10. Comparison between mudline FA bending moments from linear and nonlinear wave excitation. In *a)* idling and *b)* operational conditions computed from the lower-order model.

the simplified and the full aeroelastic model. A better match is seen for standstill conditions than in operation. This is not surprising because the structural response in operation is influenced by the controller, which is absent in the simplified model.

Fig. 10 shows an example of transient load in standstill and operation where the load difference can be visually perceived. As it can be inferred, nonlinear waves result in higher structural loads and become more important at low damping values. Their effect almost vanishes when the response is sufficiently damped by aerodynamic contributions, Fig. 13, as also found for instance in (Marino et al., 2013). This means that modelling nonlinear waves is important for standstill or idling conditions where resonances due to nonlinear interaction phenomena between waves and structure occur. The high load difference captured in Fig. 10 between 420 and 440 s is due to different wave used seed between linear and nonlinear waves.

The Wheeler correction at finite water depth slightly decreases the load as displayed in Fig. 13. Note that, at 20 m water depth this becomes visible but not significant, Fig. 11. The mudline FA and SS bending moments obtained from the input parameters listed in Table 7 have a duration of approximately 1 h. Due to this, the load variation statistics were determined by windowing with a sliding period of 10 min starting from every third minute. This resulted in 18 time series for each state. The ratio X_h defined in Eq. (28) is then computed in the two directions using a bilinear SN-curve (see Table 8). Coherently, the same set of input data is used to calculate the load variation when finite water depth correction is applied. Statistics are reported in Table 8.

Fig. 13a and b displays the wave model uncertainty as function of the mean wind speed compute at an angular point $\psi = \pi/4$ *rad*. When nonlinear waves are modelled, the ratio X_h shows a positive trend with the mean wind speed in operational conditions. Moreover, the figures highlight the variation in fatigue loads in the two states considered. In standstill the equivalent stress variation can reach 30% to 40% at high wind speeds, while in operation this effect is clearly attenuated by high damping to 10% to 20%. Because the ratio X_h shows a slightly decreasing trend when the correction at finite water depth is applied, its dependence on the mean wind speed is considered constant in the reliability analysis. Table 9 shows the statistics determined based on the results discussed above, where a linear fit is performed to obtain the trend. Only one single value of the standard deviation is adopted, corresponding to the mean value of the standard deviations computed at each mean wind speed. The wave model uncertainties are all assumed log-normally distributed.

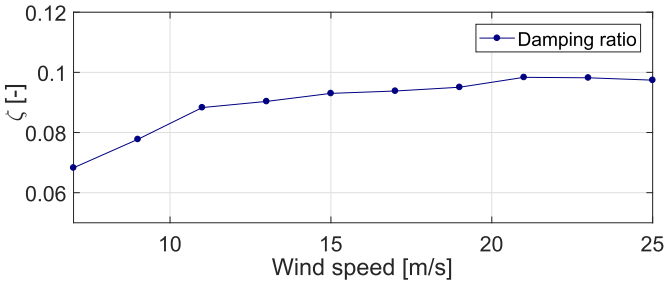

Fig. 12. Estimated damping ratio from free decays of the tower-top acceleration.

8. Stochastic model for fatigue reliability

The load variation coefficients obtained from different wave kinematic models and the different equivalent turbulence level in wake conditions are employed in the lifetime reliability analysis. The cumulative damage combines the contributions of the design load cases DLC 1.2 (b) and 6.4 with reference to Table 3, respectively operation and standstill (idling) conditions. Table 8 describes the stochastic model. The mechanical properties of the monopile steel are defined in (Veritas,), which provide a variety of cases corresponding to different marine exposures. In this example, a bilinear SN-curve in seawater with cathodic protection for butt welded elements is selected. In Table 9 the coefficients $a = 0.01$, $b = 0.02$ and $c = 0.87$ are obtained from Fig. 13.

The expression of the cumulative damage as function of wave misalignment φ, wind direction θ, mean wind speed U, the radial angle ψ, random variables $\mathbf{X}$ and time t can be readily expressed as

$$D_\psi(t,\mathbf{X}) = \frac{t}{T_s}\sum_{i=1}^{N_U}\sum_{j=1}^{N_\theta}\sum_{k=1}^{N_\varphi} D_s\left(U_i,\theta_j,\varphi_k,\mathbf{X}_{op}\right)P\left(U_i,\theta_j\right)P(\varphi_k) + \frac{t}{T_s}\sum_{i=1}^{N_U}\sum_{j=1}^{N_\theta}\sum_{k=1}^{N_\varphi} D_s\left(U_i,\theta_j,\varphi_k,\mathbf{X}_{ss}\right)P\left(U_i,\theta_j\right)P(\varphi_k) \tag{33}$$

where t is taken at one year steps. The random variables are specified in operational and standstill conditions, as

$$\mathbf{X}_{op} = \left[X_{st}, X_{dyn}, X_{aero}, X_{wk}, X_{sim}, X_{str}, X_{h,op}\right]$$
$$\mathbf{X}_{ss} = \left[X_{st}, X_{dyn}, X_{sim}, X_{str}, X_{h,ss}\right] \tag{34}$$

Note that in standstill the uncertainty due to wakes and aerodynamic computations are not considered, since wind loads do not significantly affect fatigue when the turbine is not operating. To account for the difference between the wave model uncertainty, it is assumed that $X_{h,op}$ and $X_{h,ss}$ are average multiplicative factors reflecting the load variation when

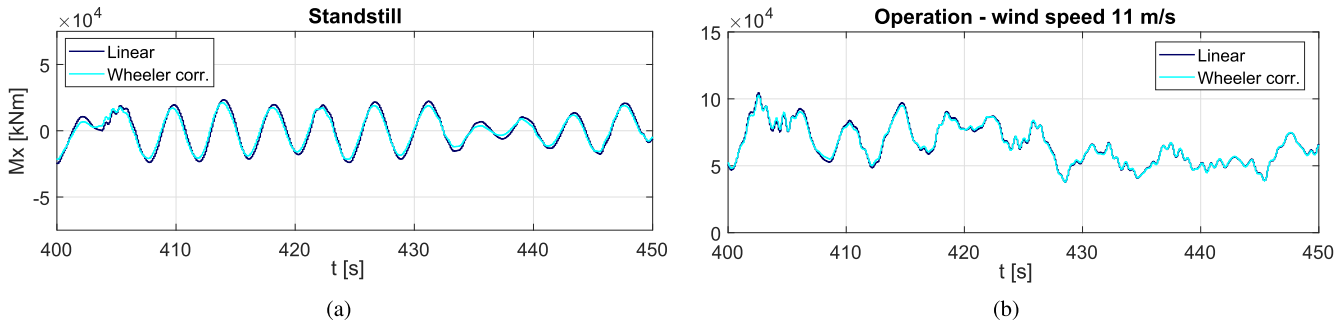

(a) (b)

Fig. 11. Comparison between mudline FA bending moments with and without linear wave correction at finite water depths. In *a)* idling and *b)* operational conditions computed from the lower-order model.

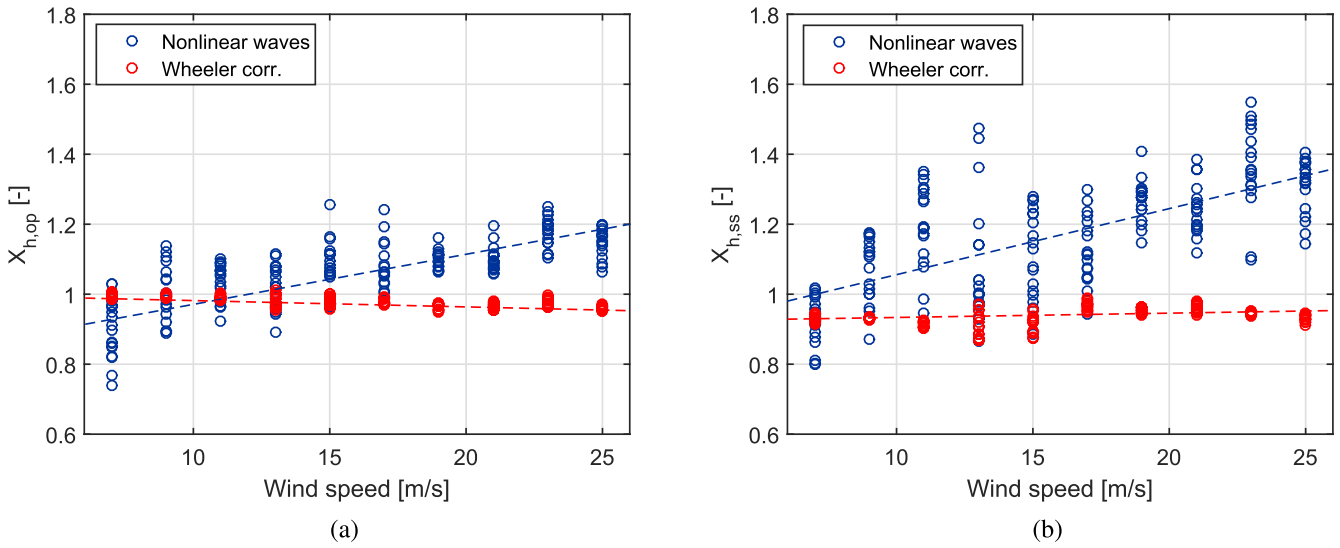

Fig. 13. Model uncertainty for the nonlinear wave kinematic model and correction at finite water depths as function of the mean wind speed. *a)* Operational conditions *b)* Standstill.

Table 9
Statistics of the wave model uncertainty in operation $X_{h,op}$ and in standstill $X_{h,ss}$ (log-normal).

	Nonlinear waves		Wheeler corr.	
Variable	mean	std	mean	std
$X_{h,op}$	$aU + c$	0.06	0.97	0.01
$X_{h,ss}$	$bU + c$	0.10	0.91	0.01

different kinematic models than the linear model are used. With this in mind, the damage is computed by Eq. (21), where the following transformation is applied

$$\Delta\sigma' = X_h\, \Delta\sigma \tag{35}$$

by noting that

$$D \propto \sigma_{eq}^{m} \tag{36}$$

where $\Delta\sigma'$ is the stress range when wave model uncertainties are applied and $\Delta\sigma$ is the stress range resulting from linear waves. The mechanical stress is computed at an angular point $\psi = \pi/4$ rad of the most fatigue loaded section, which turned out to be located 7 m below the mudline. The model uncertainties derived at the mudline section are valid at every vertical station along the monopile height, which is a deterministic geometrical dimension. The reference period T is thus partitioned into the two periods, $T = T_{ss} + T_{op}$. It is assumed that the annual turbine availability is 92%. For simplicity, the frequency of occurrence of the mean wind speed is assumed to be the same for both standstill and operation in this particular case, although without compromising the validity of the results. Standstill conditions are simulated with rotor blades pitched at 82 deg and the rotor let free to rotate.

According to the local hot spot model, a stress concentration factor $SCF = 1$ is adopted as suggested by (DNV), in case of no change of thickness and no imperfections. As a consequence, an uncertainty due to SCFs was not included in the stochastic model. Thickness correction for the stress distribution is applied as recommended in (Veritas,). In total, 8 wind directions are considered and for each wind direction 3 cases of wave misalignment are modelled, being respectively $\varphi = [-10, 0, +10]$ deg with respective probability of occurrence $P(\varphi) = [0.25, 0.5, 0.25]$. A uniform wind direction probability $P(\theta_w)$ is considered in order keep the numerical case more general, although realistic. Indicating with m_x and m_y the bending moments at each wind direction, the FA and SS bending moments can found as

$$\begin{aligned} M_x(t,\theta_w) &= m_x(t)\cos(\theta_w) - m_y(t)\sin(\theta_w) \\ M_y(t,\theta_w) &= m_x(t)\sin(\theta_w) + m_y(t)\cos(\theta_w) \end{aligned} \tag{37}$$

9. Results

A study case of a turbine in a wind farm is considered, where the number of neighbouring turbines is $N_t = 6$ positioned radially with respect to the turbine analysed at a distance of 5 rotor diameters. A set 12 discrete environmental states is employed for the estimation of the cumulative damage and their respective frequency of occurrence is shown in Table 7. The fatigue damage is computed from numerical simulations using the full aeroelastic model.

The reliability analysis is performed on a reference period of one year throughout the entire lifetime. The reliability index at time t is computed from the cumulative probability of failure $\widehat{P}_f(t)$ expressed by Eq. (24), where the number of trials simulated by IS ensures convergence on the probability of failure until a $CoV = 0.02$ is reached, (Marelli et al., 2017). In order to compare the annual reliability level at the end of life for all the cases studied, Eq. (24) is computed where the annual probability of failure is given by

$$\Delta\widehat{P}_f(t) = \frac{\widehat{P}_f(t) - \widehat{P}_f(t-\Delta t)}{\left(1 - \widehat{P}_f(t)\right)\Delta t} \tag{38}$$

where $(1 - \widehat{P}_f(t))$ is the survival probability at time t, (Rangel-Ramírez and Sørensen, 2012) and $\widehat{P}_f(t)$ is the cumulative probability of failure at time t, displayed in Fig. 14a. Today's standards recommend an annual reliability index $\beta \geq 3.3$ for offshore substructures, corresponding to minor or moderate consequences of failure. A preliminary analysis showed that under the loading conditions assumed the structure reaches an annual reliability index at 25 years of $\beta_{ref} = 2.4$ in the baseline case calculated by Eq. (38), which implies that the design requirements at the end of life are not met. Thus, in order to have a safe baseline for comparison, a design factor $z = 1.3$ was introduced. This parameter is a multiplicative factor of the monopile thickness τ, of which the approximated area moment of inertia of a tubular section is a linear variable

$$I \approx \pi R^3 \tau \tag{39}$$

By doing so, the annual reliability index calculated by Eq. (38) in the reference case reaches $\beta_{ref} = 3.45$ at 25 years, which is considered

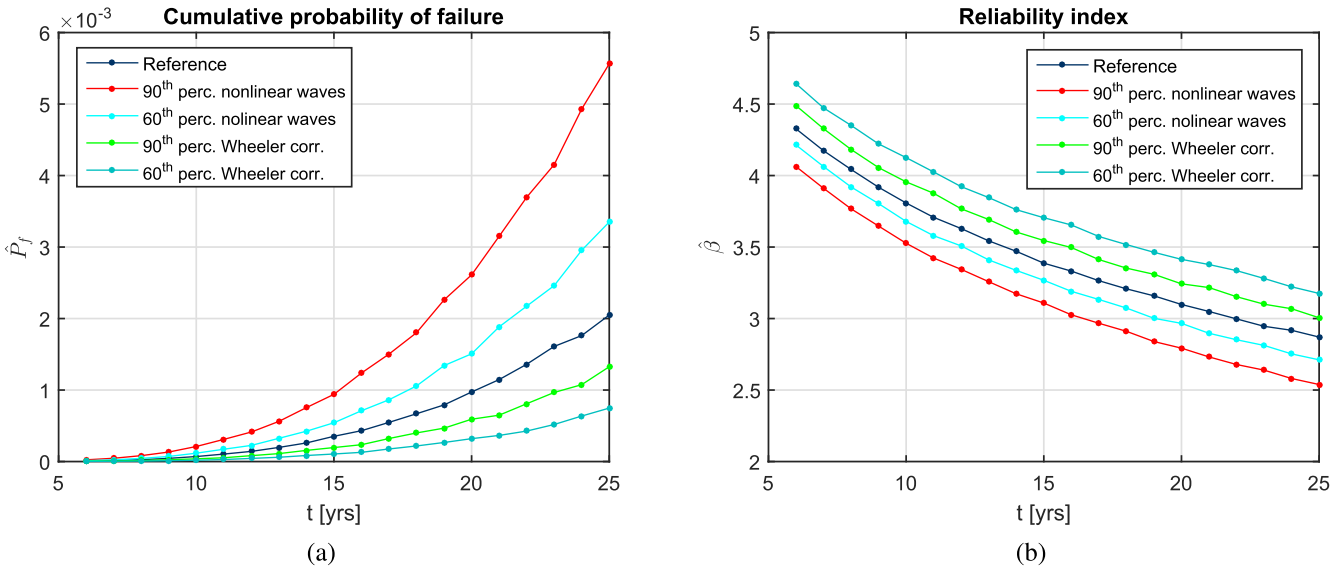

Fig. 14. *a)* Cumulative probability of failure as a function of time for different wave kinematic models and turbulence levels, based on the SN-curve approach. *b)* Corresponding reliability index.

Table 10
Annual reliability index at the end of life for different turbulence percentiles and wave kinematic models.

		Nonlinear w.		Wheeler corr.	
Lifetime	β_{ref}	60th	90th	60th	90th
25yrs	3.45	3.35	3.22	3.70	3.48
20yrs	3.70	3.60	3.39	3.92	3.75

Table 11
Impact of the environmental models on fatigue reliability in terms of percentage of variation of the annual reliability index, χ, from the baseline case.

	Nonlinear w.		Wheeler corr.	
Lifetime	60th	90th	60th	90th
25 yrs	−3%	−7%	+8%	+1%
20 yrs	−3%	−9%	+6%	+1%

satisfactory for this case.

In Fig. 14, the cumulative probability of failure and reliability index are visualised where the reference case corresponds to the 90^{th} percentile of the turbulence and linear waves. These results are obtained by running a reliability analysis using Eq. (33) where $t = \frac{5}{25}$ years with a step of one year. The impact of the environmental models becomes more evident over time because fatigue damage is a cumulative process. The results in Table 11 show this variation in terms of percentage indicated as χ defined in Eq. (40), between the end of life annual reliability indices when different models are used, against the baseline case. In order to quantify the significance between the cases analysed, a 5% variation threshold against the baseline case is set. Note that the reliability values shown in Table 10 and Fig. 14 differ because in Fig. 14 the cumulative reliability index computed at time t takes into account the survival probability at time $t-1$.

$$\chi = 100\left(1 - \frac{\beta}{\beta_{ref}}\right) \tag{40}$$

As inferred from Table 11, not all cases are significantly affecting the reliability, when compared to the baseline case. Nonlinear waves and lower percentile play an opposite effect, and their combined case results in a slight variation below the threshold defined. Also the Wheeler correction alone is not significant in this case of 20 m water depth. In this latter case it is possible to notice the high impact of the turbulence percentile.

Additionally, the importance factors of the random variables are computed from the FORM analysis showing that the model uncertainties due to the wave kinematic models have less impact compared to the remaining model uncertainties, as reported in Table 12. This can be explained by the dependency of the wave model uncertainty on the mean wind speed, and noting that the most frequent significant wave heights occur in the medium range (Table 7) according to the wind speed distribution, at which the model uncertainties are moderate (Fig. 13). The reported values in Table 12 have been computed using 90th turbulence percentile. The wave model uncertainties are given as a summation over all the mean wind speeds, including standstill and operational conditions.

10. Discussion

Although the effect of the investigated environmental models is important on structural loads, they are not the primary drivers for fatigue reliability as also confirmed by the analysis of the importance factors. In fact, the reliability index level seems to be mostly sensitive to the type of damage model used. For instance, by eliminating the thickness correction defined by DNV-GL standard practice, the annual reliability at 25 years in the baseline case increases noticeably from $\beta_{ref} = 3.45$ to $\beta_{ref} = 3.90$. However, the meaning of this type of analysis is to provide evidence of the degree of variation of the reliability index under the different factors

Table 12
Importance factors for the fatigue reliability models.

Case	Δ	X_{st}	X_{aero}	X_{dyn}	X_{wk}	X_{sim}	X_{str}	$\sum_i X_h(U_i)$
Linear waves	0.012	0.003	0.688	0.011	0.265	0.011	0.011	–
Nonlinear waves	0.012	0.003	0.674	0.011	0.268	0.011	0.011	0.009
Wheeler corr.	0.011	0.003	0.696	0.011	0.256	0.010	0.011	0.003

considered.

Despite the effect not being drastic, this is still easily observable. For instance, the Wheeler correction at finite water depth combined with the 60th percentile results in an increased annual reliability index by 15% at 25 and 20 years, which corresponds to circa 6 times lower probability of failure, compared to the case where nonlinear waves and the 90th percentile are used. Therefore, this confirms that the choice of the environmental models used has an impact on the design as well as the estimation of the remaining life after several years of operation. In the industry, this procedure still substantially relies on analytical models implemented in aero-hydro-servo-elastic codes, due to several impracticalities connected to a direct load measurement throughout the entire service life, especially in the foundation. As a consequence, monitoring the availability and the climate during different operational states is very important for load assessment. In cases of deep waters, nonlinear effects vanish making it realistic to use linear models.

The correction to the Wheeler stretching formulation is seen to reduce the particle velocities and acceleration in the horizontal direction, leading to lower fatigue loads. It should be noted that this formulation is not intended to replace the original model, but rather only to quantify the effects of satisfying the Laplace equation. Its validity in real applications has not been tested, and additional future experimental investigations could be made to prove the validity of this approach.

The wave model uncertainties generally depend on the joint distribution of the main environmental parameters, namely mean wind speed and significant wave height. In this work, due to lack of wave measurements, only mean wind speed was considered as driving parameter. Instead, a wider range of sea states should be considered with their respective probability of occurrence. Furthermore, since most offshore site are located in highly irregular sea bottoms at shallow waters causing breaking phenomena, further interesting research may be carried out to quantify their impact on long term loads.

In general, it is important to remark that the reliability assessment is case specific and cannot be represented by one case study only, as the one analysed in this paper. Therefore, in order to decide on what type of environmental model to employ, it is recommended to perform a careful evaluation of the expected turbine loads in connection to the specific site characteristics and preliminary structural analyses.

Standstill loads and wind farm wakes considered in this analysis contribute considerably to fatigue damage and this could explain the lower reliability level obtained compared to the original design. Consequently, in order to achieve the desired target reliability level in the reference case, a design factor was introduced. It is important to notice that the right calibration of the design parameter would require a reliability-based design optimization, which is outside the scope of this work.

In the reliability analysis, the uncertainty in the Wöhler exponent has not been considered. In connection to this study, since fatigue damage is a nonlinear function of the mechanical stress through the Wöhler exponent, it is expected that its uncertainty would amplify the effect of wave nonlinearities on the monopile loads, especially in standstill.

11. Conclusions

This research highlights the importance of modelling turbulence and waves for the assessment of fatigue loads on offshore wind turbine monopiles. With respect to the environmental models, nonlinear waves, correction at finite water depth, uncertainty in the hydrodynamic coefficients and turbulence level have been analysed. The influence of nonlinear waves is more pronounced during standstill and its effect is conditional to the operational damping and the wind speed distribution. The load calculated when correction at finite water depth is applied shows some degree of variation by decreasing the load estimation, which is expected to increase at lower water depths. Uncertainty introduced in the hydrodynamic coefficients does not seem to affect significantly the probability distribution of the equivalent loads on the monopile. This has been quantified by numerical MC simulations where uncertain hydrodynamic coefficients were used.

The importance of estimating a correct equivalent value of the turbulence intensity has been discussed. The turbulence level defined by IEC standards is in general conservative for the assessment of the monopile fatigue loads. In this specific case, a 60th percentile was found to be more realistic, namely closer to the full MC approach. However, the influence of the free ambient turbulence decreases in the presence of strong farm wakes. For the analysis, a realistic case of 6 neighbouring turbines equidistant from the objective one was considered. Further investigation is needed to quantify how different wind and turbulence classes affect the choice of this parameter. In general, the fatigue load reduction resulting from the application of lower equivalent turbulence could potentially lead in lighter structures, saving material and installation costs on large scales. Future research should quantify this reduction in practical and economical terms.

Acknowledgements

This project has received funding from the European Unions Horizon 2020 research and innovation programme under the Marie Sklodowska-Curie grant agreement No 642108 (Advanced Wind Energy Systems Operation and Maintenance Expertise, http://awesome-h2020.eu/).

Appendix A. Derivation of the linear relationship between turbulence and damage equivalent loads

In the following steps, previous studies were followed by Arani et al., (Troldborg et al., 2014). The external force is represented by a thrust $T(t)$ acting at the tower top. Denoting by A the rotor area and C_T the thrust coefficient, the thrust force can be approximated as

$$T(t) = \frac{1}{2}\rho A C_T U(t)^2 \tag{A.1}$$

where the wind speed $U(t)$ can be expressed by the sum of a time invariant mean wind speed U and a turbulent term $u(t)$. The thrust can then be linearised using quasi-steady assumptions where the turbulent term $u(t)$ is considered small

$$T(t) = \frac{1}{2}\rho A C_T (U + u(t))^2 \approx \frac{1}{2}\rho A C_T \left[U^2 + 2Uu(t)\right] \tag{A.2}$$

According to Eq. (A.2), the second order term of the turbulence $u(t)$ has been omitted by linear approximation. This implies a direct proportionality between the linearised standard deviation of the thrust force σ_T and the standard deviation of the wind speed fluctuations given a constant mean wind speed U, as

$$\sigma_T \propto \sigma_u \tag{A.3}$$

Furthermore, to simplify the scheme, only the first mode corresponding to the FA direction is considered. In frequency domain, the response

spectrum of an output through a linear and time invariant system exited by a random load, can be expressed as

$$S_{yy}(\omega) = |H(\omega)|^2 S_{uu}(\omega) \tag{A.4}$$

where $S_{yy}(\omega)$ is the spectrum of the response $y(t)$, $H(\omega)$ is the energy transfer function of the linear structural system and $S_{uu}(\omega)$ spectrum of the excitation. The wind field generated by the aeroelastic code used is based on the Mann turbulence model (Larsen and Hansen, 2007) while DNV-GL guidelines (DNV) suggest a Kaimal spectrum. The standard deviation of the response σ_y is proportional to the standard deviation of the turbulence term σ_u at a constant mean wind speed U. Under certain assumptions the approach can be demonstrated analytically as shown in reference (Troldborg et al., 2014) for a Kaimal spectrum.

$$\sigma_y \propto \sigma_u \tag{A.5}$$

which, in turn, using Eq. (A.3) implies a direct proportionality between $\sigma_y \propto \sigma_T$. As shown in (Frandsen, 2007), if the response $y(t)$ can be considered narrow banded where the dominant natural frequency is ω_0 and linear SN-curve are assumed, the DEL is also proportional to σ_y conditionally on the Wöhler exponent and the mean wind speed.

$$L(U) \propto \sigma_u \tag{A.6}$$

This relation can also be extended to the Mann turbulence model, by noting that the latter is built on the Kaimal spectrum, (Mann, 1998). However, since the proportionality is determined by the transfer function which is outside the spectrum, the formulation should in principle be valid for any spectrum.

References

Agarwal, P., Manuel, L., 2011. Incorporating irregular nonlinear waves in coupled simulation and reliability studies of offshore wind turbines. Appl. Ocean Res. 33 (3), 215–227.

Ambühl, S., Ferri, F., Kofoed, J.P., Sørensen, J.D., 2015. Fatigue reliability and calibration of fatigue design factors of wave energy converters. Int. J. Marine Energy 10, 17–38.

Arapogianni, A., Genachte, A., Ochagavia, R.M., Vergara, J., Castell, D., Tsouroukdissian, A.R., Korbijn, J., Bolleman, N., Huera-Huarte, F., Schuon, F., et al., 2013. Deep Water - the Next Step for Offshore Wind Energy, European Wind Energy Association (EWEA). ISBN, Brussels, Belgium, pp. 978–982.

D. N. V. AS, Buckling Strength of Shells.

S. Bhattacharya, Challenges in design of foundations for offshore wind turbines, Eng. Technol. Ref. 1(1).

Burrows, R., Tickell, R., Hames, D., Najafian, G., 1997. Morison wave force coefficients for application to random seas. Appl. Ocean Res. 19 (3–4), 183–199.

Dimitrov, N., Friis-Hansen, P., Berggreen, C., 2013. Reliability analysis of a composite wind turbine blade section using the model correction factor method: numerical study and validation. Appl. Compos. Mater. 20 (1), 17–39.

G. DNV, DNV-OS-J101–design of Offshore Wind Turbine Structures, DNV GL.

Feng, Y., Tavner, P., Long, H., 2010. Early experiences with UK Round 1 offshore wind farms. Proc. Inst. Civ. Eng.Energy 163 (4), 167–181.

Frandsen, S.T., 2007. Turbulence and Turbulence-generated Structural Loading in Wind Turbine Clusters. Technical University of Denmark, Risø National Laboratory for Sustainable Energy.

Friswell, M.I., 2010. Dynamics of Rotating Machines. Cambridge University Press.

Hahn, B., 1999. Reliability assessment of wind turbines in Germany. In: 1999 European Wind Energy Conference, pp. 1–5.

I. E. C. IEC, Wind Turbines - Part I: Design Requirements - IEC 61400–1.

I. E. C. IEC, Wind Turbines - Part III: Design Requirements for Offshore Wind Turbines - IEC 61400–3.

IEC, I.E.C., 2005. Amendment to IEC 61400-1, p. 2008.

Jonkman, J., Musial, W., 2010. Offshore Code Comparison Collaboration (OC3) for Iea Wind Task 23 Offshore Wind Technology and Deployment. Tech. rep.. National Renewable Energy Lab. (NREL), Golden, CO (United States).

Jonkman, J., Butterfield, S., Musial, W., Scott, G., 2009. Definition of a 5-MW Reference Wind Turbine for Offshore System Development. Tech. rep.. National Renewable Energy Laboratory (NREL), Golden, CO.

Journée, J., Massie, W., 2000. Offshore Hydromechanics. TU Delft.

Kim, T., Natarajan, A., 2013. Effect of coupled nonlinear wave kinematics and soil flexibility on the design loads of offshore wind turbines. In: Proceedings of 51st AIAA Aerospace Sciences Meeting Including the New Horizons Forum and Aerospace Exposition.

Koukoura, C., Natarajan, A., Vesth, A., 2015. Identification of support structure damping of a full scale offshore wind turbine in normal operation. Renew. Energy 81, 882–895.

E. L Petersen, C. B. Hasager, M. Courtney, A. Natarajan, T. J. Larsen, H. Bredmose, G. C. Larsen, P. E. Sørensen, N. A. Cutululis, N. Erik-Clausen, et al., Offshore wind farms, Handbook of Clean Energy Systems.

Larsen, T.J., Hansen, A.M., 2007. How 2 Hawc2, the User's Manual. Tech. rep.. Risø National Laboratory.

Mann, J., 1998. Wind field simulation. Probabilist. Eng. Mech. 13 (4), 269–282.

Marelli, S., Schöbi, R., Sudret, B., 2017. Uqlab User Manual–structural Reliability. Tech. rep., Technical report, Chair of Risk, Safety and Uncertainty Quantification, ETH Zurich. Report UQLab-V1. 0-107.

Marino, E., Lugni, C., Borri, C., 2013. The role of the nonlinear wave kinematics on the global responses of an OWT in parked and operating conditions. J. Wind Eng. Ind. Aerod. 123, 363–376.

Mittendorf, K.E., 2009. Joint description methods of wind and waves for the design of offshore wind turbines. Mar. Technol. Soc. J. 43 (3), 23–33.

Moan, T., Zheng, X.Y., Quek, S.T., 2007. Frequency-domain analysis of non-linear wave effects on offshore platform responses. Int. J. Non Lin. Mech. 42 (3), 555–565.

Morison, J., Johnson, J., Schaaf, S., et al., 1950. The force exerted by surface waves on piles. J. Petrol. Technol. 2 (05), 149–154.

Natarajan, A., 2014. Influence of second-order random wave kinematics on the design loads of offshore wind turbine support structures. Renew. Energy 68, 829–841.

Nejad, A.R., Gao, Z., Moan, T., 2014. On long-term fatigue damage and reliability analysis of gears under wind loads in offshore wind turbine drivetrains. Int. J. Fatig. 61, 116–128.

Rangel-Ramírez, J.G., Sørensen, J.D., 2012. Risk-based inspection planning optimisation of offshore wind turbines. Struct. Infrastruct. Eng. 8 (5), 473–481.

A. RP2A-LRFD, Recommended Practice for Planning, Designing and Constructing Fixed Offshore Platforms-load'and Resistance Factor Design, American Petroleum Institute, Washington.

Schløer, S., Bredmose, H., Bingham, H.B., 2016. The influence of fully nonlinear wave forces on aero-hydro-elastic calculations of monopile wind turbines. Mar. Struct. 50, 162–188.

Sharma, J.N., 1980. Development and Evaluation of a Procedure for Simulating a Random Directional Second-order Sea Surface and Associated Wave Forces.

Sheather, S.J., Jones, M.C., 1991. A reliable data-based bandwidth selection method for kernel density estimation. J. Roy. Stat. Soc. B 683–690.

Shi, W., Park, H.-C., Baek, J.-H., Kim, C.-W., Kim, Y.-C., Shin, H.-K., 2012. Study on the marine growth effect on the dynamic response of offshore wind turbines. Int. J. Precis. Eng. Manuf. 13 (7), 1167–1176.

Sørensen, J.D., Frandsen, S., Tarp-Johansen, N., 2008. Effective turbulence models and fatigue reliability in wind farms. Probabilist. Eng. Mech. 23 (4), 531–538.

Tarp-Johansen, N.J., 2003. Examples of Fatigue Lifetime and Reliability Evaluation of Larger Wind Turbine Components. Tech. rep.

Tempel, J.V.D., 2006. Design of Support Structures for Offshore Wind Turbines no. april.

Toft, H.S., Svenningsen, L., Moser, W., Sørensen, J.D., Thøgersen, M.L., 2016. Wind climate parameters for wind turbine fatigue load assessment. J. Sol. Energy Eng. 138 (3), 031010.

Troldborg, N., Sørensen, J.N., Mikkelsen, R., Sørensen, N.N., 2014. A simple atmospheric boundary layer model applied to large eddy simulations of wind turbine wakes. Wind Energy 17 (4), 657–669.

Van Der Meulen, M.B., Ashuri, T., Van Bussel, G.J., Molenaar, D.P., 2012. Influence of nonlinear irregular waves on the fatigue loads of an offshore wind turbine. In: The Science of Making Torque from Wind; 4th Scientific Conference, Oldenburg (Germany), 9-12 Oct, 2012.

H. F. Veldkamp, Chances in Wind Energy: a Probabilistic Approach to Wind Turbine Fatigue Design.

Veldkamp, H., Van Der Tempel, J., 2005. Influence of wave modelling on the prediction of fatigue for offshore wind turbines. Wind Energy 8 (1), 49–65.

D. N. Veritas, Fatigue Design of Offshore Steel Structures, No. DNV-RP-C203 30.

Wheeler, J., et al., 1969. Methods for calculating forces produced by irregular waves. In: Offshore Technology Conference, Offshore Technology Conference.

Ziegler, L., Muskulus, M., 2016. Fatigue reassessment for lifetime extension of offshore wind monopile substructures. J. Phys. Conf. 753, 092010. IOP Publishing.

Chapter 3

Coupling load and failure maps

Never look down while climbing.

The author

The research question addressed in this chapter is the attempt to predict wind farm failures by looking at the distribution of critical components and experienced loads within a wind farm as indication of physical damage.

The case study considered is a wind farm in operation for 5 years, where several records of pitch malfunctions were experienced and recorded in the alarm logs. The idea is to combine the frequency of occurrence of these multifunction within the wind farm with suitable damage indicators commonly derived from wind farm load simulations, including the effect of wake turbulence generated by neighbor turbines. The final aim is to provide these indicators under the form of "maps", to be compared with a probability map of the malfunctions.

Given the nature of the recorded alarms, which will be clearer in the following, it was initially thought that the pitch bearing friction effect may be a good candidate to explain the occurrence of the alarms. In fact, the bearing friction can cause a deviation between the reference pitch communicated by the control system and the actual pitch delivered by the actuator through a torque. On this purpose, the pitch error originating from the presence of a friction torque is selected as best indicator. In the attempt of quantifying this effect, a methodology to include the pitch friction into the EOM of the pitch system used in the aeroelastic solver is developed. This model is composed by two steps. The first step concerns the development of a frictionless torque-based pitch controller, meaning that the dynamic of the pitch actuator results in a torque that is in reality supplied by the pitch actuator.

The stability of this system is tested in a open and closed loop set-up and the initial part of this chapter is dedicated at explaining the steps upon which the model is built, starting from basic notions of control theory. The second step consists of including the friction torque as an additional contribution to the frictionless torque that appears in the EOMs. This second step however, turned out to be unsuccessful due to convergence problems. Although the model developed here has not been eventually used in the analysis, its derivation is reported for completeness.

Instead of the pitch error due to friction torque, other indicators of possible malfunctions are selected. These are the flapwise blade root bending moment DEL, the mean friction moment and actuator duty cycle (ADC). The reason for the flapwise bending moment is its

direct relation to the friction moment on the pitch bearing, and the DEL is used as indication of damage at the blade root section, where the pitch bearing is located. The friction moment is chosen since it comprises the contribution of the in-plane bending moment and the longitudinal force. Finally, the ADC is a measure of the intensity of the pitch activity.

The main idea upon which the analysis is based, is that these quantities may vary significantly within the wind farm due to wake effects, and from the fact that turbulence is the major driver for pitch activity and cycling loads. The final aim is to understand whether an initial load map assessment can reveal critical areas within the wind farm with increased risk of failure.

The indicator maps are obtained using an in-house developed tool based on PCE, although some adjustments were needed for its calibration for the specific case study. The development of a stable dynamic pitch system based on frictionless torque and the introduction of the friction torque into the EOM, can also be considered a further contribution, despite its convergence problems.

3.1 Failure-load correlation

In Ch.1 it was mentioned that wind turbines are subject to highly fluctuating environments, thus becoming more prone to fatigue-driven failures, meaning by cycling loading. A throughout based on a significant databased on failure observations in several components work by Reder & Melero, Reder et al. [27, 40, 79, 80] has shown important correlations between environmental factors such as relative humidity, temperatures and turbulence and reliability of main wind turbine components. Besides weather conditions, reliability may also depend directly on mechanical loads. It is important to notice that harsh weather is often associated with high power production, thus increasing wear and degradation of mechanical parts. However, computing loads requires an aeroelastic model and computation of wind farm loads based on the its configuration. The aim of this analysis is to correlate wind farm load maps with failure maps, obtained respectively using the the methodologies adopted in [43] and real event recorded.

3.2 Linear time invariant systems

In this section some theoretical knowledge of control theory is recalled, which is preliminary to the next sections, in particular PID (proportional, integral, derivative) controllers. The theory recalled here is based on [81]. These techniques are also applied in experimental modal analysis.

First, it is important to make clear that the systems considered in this chapter are linear time invariant (LTI). Given a LTI system with input $x(t)$ and output $y(t)$, the transfer function (TF), denoted by $H(s)$, is defined as the Laplace transform of the impulse response function $h(t)$. The Laplace transform of a function $x(t)$ is an improper integral defined as

$$X(s) = \mathcal{L}[x(t)] = \int x(t)e^{st}\, dt \tag{3.1}$$

where $s = \sigma + j\omega$ is the Laplace variable. The response of a LTI system to an input can be found through the convolution integral, as

$$y(t) = \int_0^t h(\tau)x(t-\tau)\ d\tau \tag{3.2}$$

In frequency domain, after applying the Laplace transformation, Eq.3.3 simply becomes

$$Y(s) = H(s)X(s) \tag{3.3}$$

The impulse response is the response of the system to a Dirac delta $\delta(t)$, in time domain. The reason why a Delta is used as input function is because it is able to excite the entire frequency band of a system at equal energy, ideally from 0 to infinity. In fact, the Laplace (or Fourier) transform of a Delta is equal to 1. In this way, the properties of the system can be suitably characterized (amplitude and phase).

The frequency response function (FRF) is the steady-state response of a LTI system to a harmonic input, namely when the transient response vanishes. By varying the frequency of the harmonic input, it is possible to explore the behaviour of the output through the entire frequency band of interest, thus obtaining a picture of the system's behaviour. The FRF can be obtained by the TF by substituting $s = j\omega$.

Finally, the unit step response is the response of a system to a unit step input. This method can be used to analyze the damping properties of a system and overshoot to a sudden perturbation.

3.3 Controllers

In the Laplace domain, the TF of a PID becomes

$$H(s) = K_p\Big(1 + \frac{1}{T_i s} + T_d s\Big) \tag{3.4}$$

Ziegler and Nichols, proposed an experimental rule to determine the values of the parameters K_p, K_i and K_d. The method is based on deriving an experimental step response of the PID through an open loop system, trying to limit the maximum overshoot. The method is only applicable if the system is stable with dominant negative poles and thus unit step response close to an S-shape. The step response is generated experimentally, as in Fig.3.1.

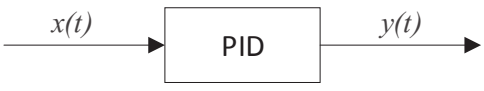

Figure 3.1: Open loop diagram for PID controller parameter tuning based on Ziegler-Nichols method.

Under this assumptions, the TF can be approximated by a first order TF, as

$$\frac{X(s)}{Y(s)} = \frac{K_1 e^{-Ls}}{Ts + 1} \tag{3.5}$$

where L and T are the time delay and time constant respectively. Thus, the tuning rules for the first order step response PID controller according to Ziegler and Nichols are found as

$$K_p = 1.2\frac{T}{L}, \quad T_i = 2L, \quad T_d = 0.5L \tag{3.6}$$

3.4 Blade pitch actuator

In pitch-regulated-variable-speed wind turbines, the pitch angle in the full load region is regulated to balance aerodynamic thrust and torque in order to achieve the desired power output. The pitch mechanism consists of an actuator, which controls and moves the system. This movement is a rotation around the longitudinal axis of the blade, the pitch angle. Modern wind turbines implement a collective pitch system, where the blades pitch simultaneously and the same reference pitch angle ϑ_{ref} is communicated by the controller unit to the actuator. Another possibility which is gaining more focus in the recent years is individual pitch, [82]. Common commercial pitch actuators can be hydraulic or electromechanical. In aeroelastic simulations, the dynamic motion of the actuator, the servo system, can be modeled either through a first order filter, as second order filter [83], or through actuator forces. The first two types are based on specifying a body-to-body constrain acting as a bearing and controlling position, velocity and acceleration by a servo mechanism. When ϑ_{ref} is communicated to the actuator by the controller, the actual pitch angle ϑ reaches the value ϑ_{ref} through a TF. Eq.3.7 is the mathematical expression of a first order filter, which typically models electromechanical actuators [84], as

$$\dot{\vartheta} = \frac{1}{\tau}(\vartheta - \vartheta_{ref}) \tag{3.7}$$

where τ is the time constant. This topics are well presented for instance in [85]. The second order second filter, Eq.3.8, is used to model hydraulic actuators[86]. The FRF in Eq.3.10 can be determined by giving as input a harmonic excitation ϑ_{ref} with a frequency ω.

$$\ddot{\vartheta} + 2\zeta\omega_0\dot{\vartheta} + \omega_0^2\vartheta = \vartheta_0 e^{j\omega t} \tag{3.8}$$

$$\vartheta(t) = |H(j\omega)|\vartheta_0 e^{j(\omega t - \phi)} \tag{3.9}$$

where ϕ is a phase term and the complex FRF is

$$H(j\omega) = \frac{\omega_0^2}{\omega_0^2 - \omega^2 + 2j\zeta\omega_0\omega} \tag{3.10}$$

Typically in a damping ratio $\zeta \leq 1$ is chosen, in order to model a underdamped or critically damped response. The frequency ω_0 is set according to the specific purpose. Note that the parameters of the TF can be used to simulate a possible pitch fault [83].

3.5 Actuator motion based on forces

In practice, the motion around the blade longitudinal axis is enabled by a slewing bearing located between the hub and the blade root. An example of this type of roller bearing is displayed in Fig.3.3, similarly used for the yaw mechanism. The main disadvantage of using first and second order filters to model the pitch actuator as explained in the previous section, resides in the inability to explicitly control a pitch torque, by limiting the analysis only at describing the dynamic motion of the pitch angle through a FRF. An alternative way to control the pitch angle is by controlling the actuator forces through a servo. An example provided in [87] shows a system based on a two cascade PI units from which the frictionless

pitch torque can be derived and given as input in the rigid body EOM, which include the pitch angle variation due to the blade's inertia forces. The tuning of this system provided a sufficiently damped response. More detailed approaches are based on direct modelling of the actuator internal mechanism as for instance in [86] where the system's dynamic is triggered by the compressibility of the hydraulic oil.

To model this system in HAWC2 a similar approach as in [87] is followed. The difference is that a constraint between the shaft and the blades is introduced through an external system dll (dynamic link library). The constrain consists of a set of equations describing a spatial node where the only free DOF is the rotation around the longitudinal axis of the blade, as shown in Fig.3.2.

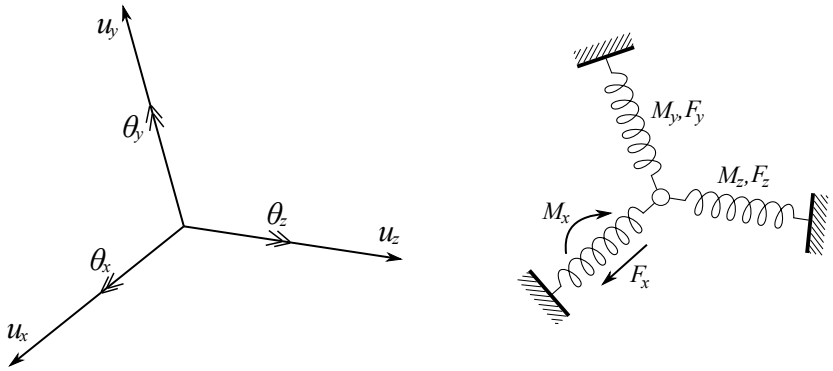

Figure 3.2: Degrees of freedom and forces of the node between shaft and blades to model the pitch motion.

The vector of DOFs $\mathbf{q} = \{u_x, u_y, u_z, \vartheta_x, \vartheta_y, \vartheta_z\}$, where ϑ_z is the pitch angle, simply indicated as ϑ. The vector $\mathbf{r} = \{F_x, F_y, F_z, M_x, M_y, M_z\}$ are the reaction forces obtained by linear and rotational springs. The moment M_z is the frictionless pitch torque, indicated as Q_c. The subset of equations comprising the first five EOM are stiff reaction forces of the body in Fig.3.2 and can be written in matrix form, as

$$\bar{\mathbf{r}} = \bar{\mathrm{K}}\bar{\mathbf{q}} \tag{3.11}$$

with $\bar{\mathrm{K}} = k\mathrm{I}$ is a diagonal matrix where I is a 5×5 identity matrix and the stiffness k is set big enough to provide rigid reactions. The torque Q_c is function of the pitch error $e = \vartheta - \vartheta_{ref}$, which can be controlled by a PID unit, by using the following set of equations

$$\begin{aligned} Q_c &= K_p e + K_i \int e \; dt + K_d \dot{\vartheta} \\ \vartheta - e &= \vartheta_{ref} \\ \dot{e} - \vartheta &= 0 \end{aligned} \tag{3.12}$$

where the second and third equations in Eq.3.12 are additional states introduced to stabilise and control the system.

As pointed out in [87], the pitch motion is fully coupled with external loads and inertia of the system, such as blade and bearing. Therefore, in operation, the equilibrium at the node between the two bodies, shaft and blade, is satisfied according to the following equation

Figure 3.3: Example of slewing bearing for wind turbine pitch systems.

$$I + Q_c + Q_a + Q_g + Q_f = 0 \tag{3.13}$$

where I is the contribution from inertia forces of the blade and bearing, Q_a the resultant moment from the aerodynamic forces, Q_g the resultant moment from gravitational forces, and Q_f is a friction term. Note that Q_c is a controlled force, which is applied to allow the pitch motion. In operation, the total pitch torque will need to balance the contribution of all the remaining terms in order to keep the pitch angle at the desired position.

3.5.1 Calibration of the motor torque in standstill

To analyse the frictionless motor torque only and tune the PID parameters, standstill conditions are considered, meaning that Eq.3.17 becomes Eq.3.14, where only the system's intertia inertia J is taken into account [87].

$$J\ddot{\vartheta} = Q_c(t) \tag{3.14}$$

The parameters of the PID can be found experimentally using the first method proposed by Ziegler and Nichols described in Sec.3.3. Fig.3.4 shows the step response of the PID. As can be seen, the tuning provides a maximum overshoot of 15% while the response is sufficiently damped.

By inserting Eq.3.12 into Eq.3.14, the resulting closed loop equation is obtained (Eq.3.15. The block diagram of the closed loop system for the pitch actuator is shown in Fig.3.5.

$$J\ddot{\vartheta} + K_p(\vartheta - \vartheta_{ref}) + K_i \int (\vartheta - \vartheta_{ref})\, dt + K_d\dot{\vartheta} = 0 \tag{3.15}$$

In the Laplace domain, the TF becomes

$$\frac{\vartheta(s)}{\vartheta_{ref}(s)} = \frac{K_p + K_i/s}{Js^2 + K_p + K_i/s + K_d s} \tag{3.16}$$

Based on the PID parameters tuned before, Eq.3.16 provides a Bode diagram as shown in Fig.3.6. As can be noticed, the response of the system equals a critically damped response of a second order system [85]. For a frequency range below 1 Hz, the system provides a damped response with no amplifications and sufficiently in phase with the input ϑ_{ref} which in this case set at 0.5 Hz.

Fig.3.7 shows the response of the system implemented in HAWC2 using the full aeroelastic model in standstill conditions, where a step pitch is given as reference. Note the similarity with Fig.3.4.

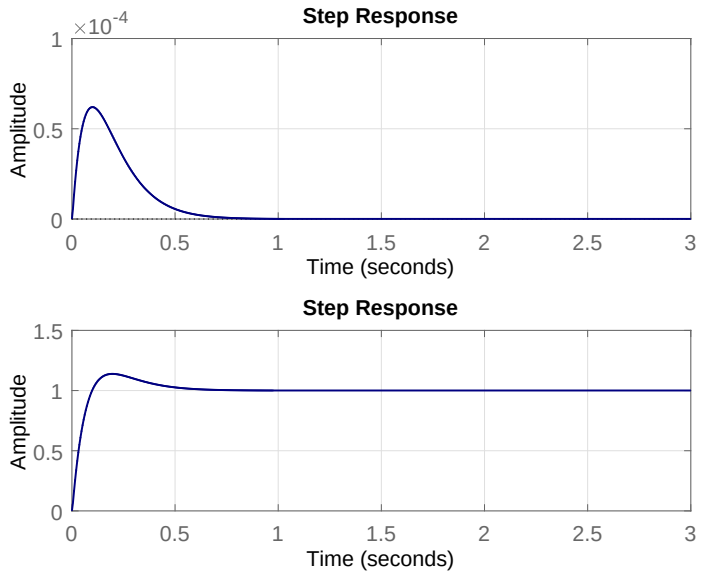

Figure 3.4: Step response of the PID system controlling the pitch torque.

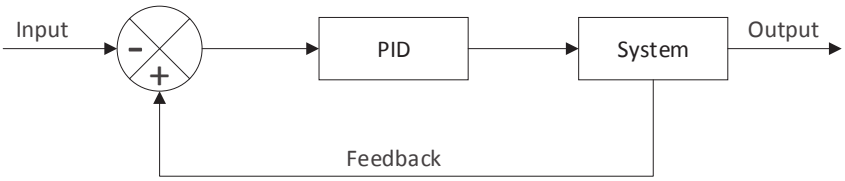

Figure 3.5: Closed loop diagram of the pitch actuator based on forces.

Afterwards, a harmonic pitch excitation is given as input to the system, where the only contribution to the pitch torque comes from the inertia, as per Eq.3.14. Results are displayed in Fig.3.8, where the motor torque corresponds to the blade's inertia forces driven by the pitch acceleration $\ddot{\vartheta}$.

3.5.2 Operational tests

After calibrating the model and the proved the stability of the system, further tests are carried out here. Fig.3.9 shows the motor torque to a constant step wind speed ranging from 4 to 25 m/s. No turbulence is considered. Note that the equilibrium follows Eq.3.13, where all contribution are now embedded. The aerodynamic forces mainly govern the reaction of the pitch torque, as a result of the full dynamic coupling. This can be verified by comparing Fig.3.9a and 3.10a, which displays the blade root torsional moment for the same simulation.

Fig.3.9b and 3.11b highlight the effect of gravitational forces, which shifts the response by 120 degrees for each blade. This effect cannot be encountered in Fig.3.8b, since gravitational forces are neglected.

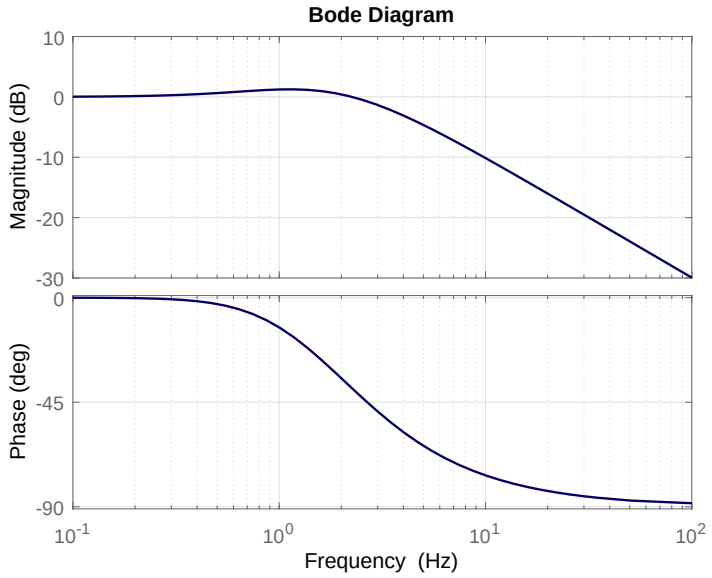

Figure 3.6: Amplitude and phase of the closed loop response of the pitch actuator.

3.5.3 Bearing friction

Besides the frictionless turning moment Q_c necessary to actuate the pitch motion, the bearing will experience an additional friction torque, which is addressed in this section. Once able to control Q_c through a controller PID, an additional contribution Q_f due to friction can be introduced (Eq.3.17). This quantity is typically calculated according to physical models and it generally depends on the system's states and forces described in the previous section. With reference to Eq.3.14, which represent the EOM when the turbine is standing still, the equation becomes

$$J\ddot{\vartheta} = Q_c(t) + Q_f(t, \mathbf{q}, \dot{\mathbf{q}}, \mathbf{r}). \tag{3.17}$$

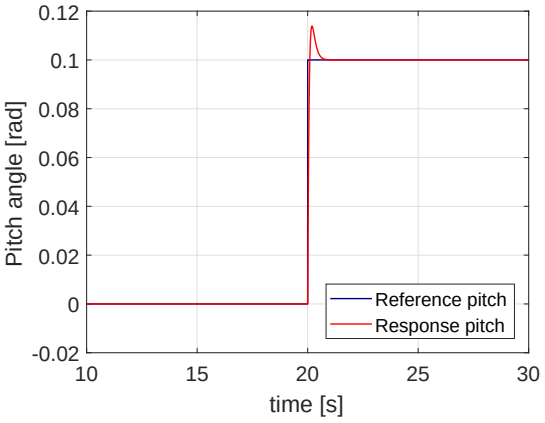

Figure 3.7: Step pitch response of the actuator system based on forces.

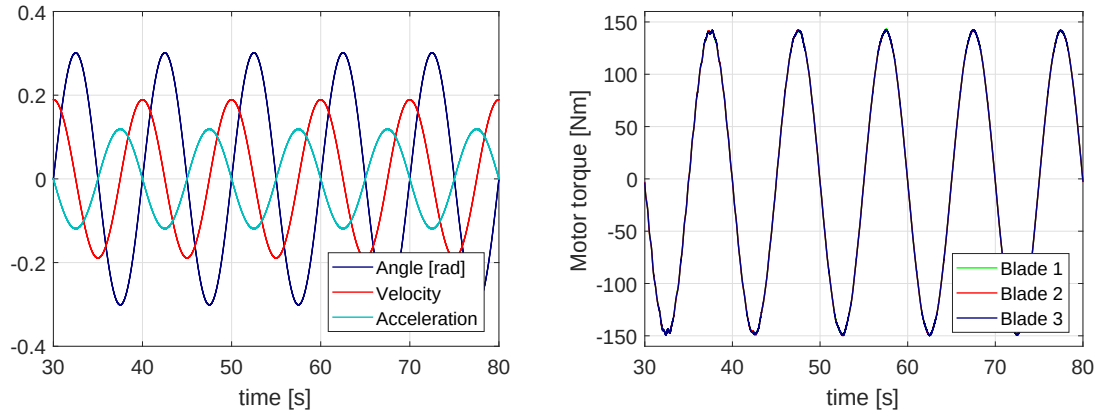

Figure 3.8: Pitch response to a harmonic pitch excitation. No aerodynamic and gravitational forces are considered.

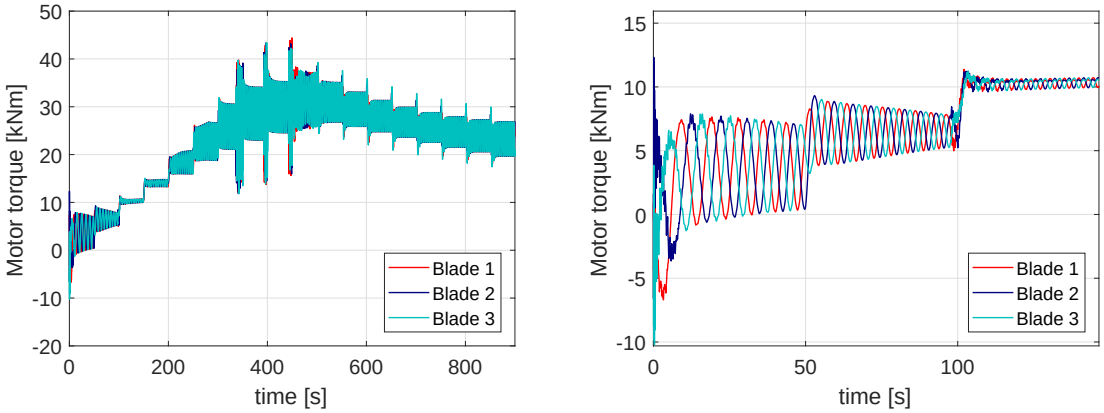

Figure 3.9: Pitch torque for a step wind speed varying within the operational range 4 to 25 m/s.

It is important to notice that the direction of friction moment follows the pitch velocity. To solve this problem, the authors in [88] expressed the friction moment as function of the pitch velocity $\dot{\vartheta}$, through a piecewise activation function. Herein however, in order to ensure numerical convergence in the aeroelastic code, the activation function requires continuous differentiability.

$$Q_f(t, \mathbf{q}, \dot{\mathbf{q}}, \mathbf{r}) = \frac{2}{\pi} f(\mathbf{r}) f(\dot{\vartheta}) \tag{3.18}$$

In Eq.3.18, $f(\dot{\vartheta}) = \arctan(K\dot{\vartheta})$ where the constant K is large enough to provide a sufficiently smooth and fast transition from negative to positive pitch velocities. An example of this function is displayed in Fig.3.12 for different values of the parameter K in a typical range of pitch velocities for a wind speed at 17 m/s. The y-axis shows dimensionless function $\frac{2}{\pi} f(\dot{\vartheta}$ in Eq.3.18.

The function $f(\mathbf{r})$ contains the load dependent and independent contributions to the friction moment. Here, the model proposed by [89] is employed. This model only considers the Coulomb friction, namely only the load dependent contribution. Other models can be found in [90], or more specifically [91]. Eq.3.19 displays such model, where the coefficients α,

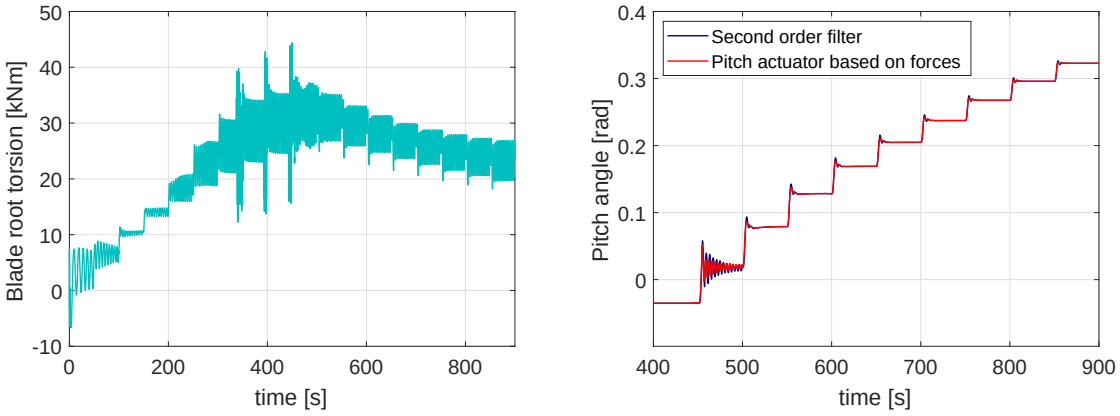

Figure 3.10: *a*) Blade root torsional moment and *b*) pitch comparison between second order filter and pitch actuator based on forces for a step wind speed varying within the operational range 4 to 25 m/s.

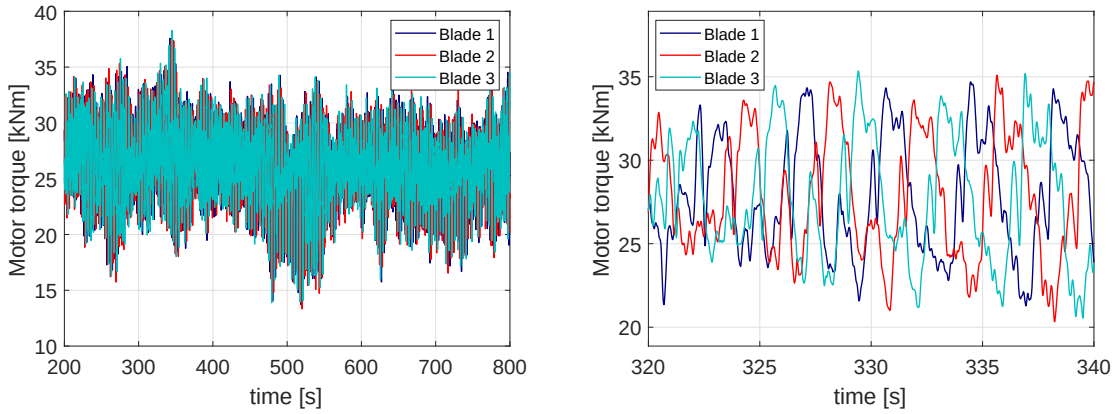

Figure 3.11: Pitch torque for a turbulent case at 17 m/s mean wind speed.

β and γ depend on the the friction coefficients, bearing geometry and mechanical properties, while M_{xy} is the in-plane resulting bending moment, F_{xy} the in plane resulting force found through Eq.3.20 and F_z is the axial force (see Fig.3.2).

$$f(\mathbf{r}) = \alpha M_{xy} + \beta F_{xy} + \gamma F_z \tag{3.19}$$

$$M_{xy} = \sqrt{M_x^2 + M_y^2}, \quad F_{xy} = \sqrt{F_x^2 + F_y^2} \tag{3.20}$$

However, in order to observe the effect of a real pitch system controlled by forces, a limitation to amount of torque provided by the motor should be set. This can be done by setting a maximum allowable torque delivered by the actuator. After that limit, the pitch bearing basically slides. This was modelled through a symmetric function between the theoretical demanded torque Q_d and the real one delivered by the actuator Q_c. In this way, the effect of the friction would be visible, in that the maximum level would reach it's value earlier, due to the additional friction torque Q_f. Otherwise, the system would always be able to deliver infinite amount of torque.

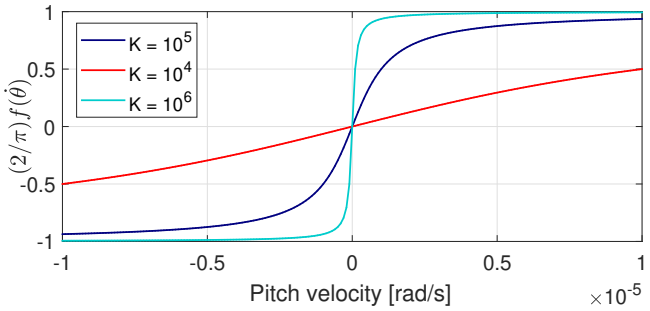

Figure 3.12: Friction activation as function of the pitch velocity.

However, by putting an upper threshold to the torque, resulted in convergence problems for the solver. Therefore, at this point of the thesis, a decision was taken. The numerical results obtained in the following sections compare the wind farm pitch activity map, rather than the pitch error resulting from modelling the friction torque into the EOMs, as initially planned. However, the model described above in this chapter is still valid and exploitable for further research. Unfortunately due to time constraints, it was not possible to find a solution to make the solver converge.

3.5.4 Pitch duty activity

The ADC is the percentage of time the actuator needs to deliver a motion relative to its maximum allowable motion. Because of this definition, the pitch duty cycle of hydraulic actuators can be used as an indication of the amount of work required by the actuator before occurring malfunctions, such as overheating, sliding, oil-leaking etc. The formulation reported by Tibaldi et al. [92] is herein used, which expresses the pitch duty cycle as function the pitch velocity, as

$$\mathrm{ADC} = \frac{1}{T}\int_0^T \frac{\dot{\beta}(t,U)}{\dot{\beta}_{max}} dt \tag{3.21}$$

where T is the simulation time and $\dot{\beta}$ the pitch velocity. The maximum pitch velocity $\dot{\beta}_{max}$ is defined in the controller unit, which computes the optimal pitch reference.

3.6 Wind farm load mapping

Loads on turbines within a wind farm depend on the farm configuration and need to be assessed based on full probabilistic aeroelastic simulations [69]. 5 load channels are considered, 3 blade root bending moments, ADC and mean friction. These quantities will be referred to as indicators. The aeroelastic model of the real turbine was available for the analysis. The water depth is considered fixed at 20 m and no soil model is included. For the wind farm maps, the indicators are computed distinctly on the three blades for each simulation and the average value is taken. Unless specified, 12 turbulence seeds are considered for each simulation case. The DLC 1.2 is used.

3.6.1 Assessment of site conditions

Data are available as 10-minute average values from an offshore wind farm during an operational periods of 5 years. Periods of turbine inactivity were removed from the dataset by applying two filters. These are power less or equal than zero to filter out non operational wind speed records. To reconstruct the fatigue load map through aeroelastic simulations, a statistical characterization of the site data is first needed. Based on available data, the analysis requires the following ingredients:

- Assessment of free wind speed conditions from nacelle anemometers
- Determination of the free wind speed wind rose
- Mean wind speed directional distribution
- Shear and density distributions
- Mean and standard deviation of the turbulence
- Wave statistical parameters such as significant wave height and peak period

Some of the quantities listed above are expressed as function of the mean wind speed, given their significant variation. The standard deviation of the turbulence corresponds to the standard deviation of the 10 min turbulence. Since the failure analyzed happen during operation, only operational loads are considered (DLC 1.2, see Sec. 2.3). Fig.3.13 display the wind roses for the wind farm analysed by using 36 and 12 bins. The coherence between the two roses makes is reasonable to use 12 bins for the analyses.

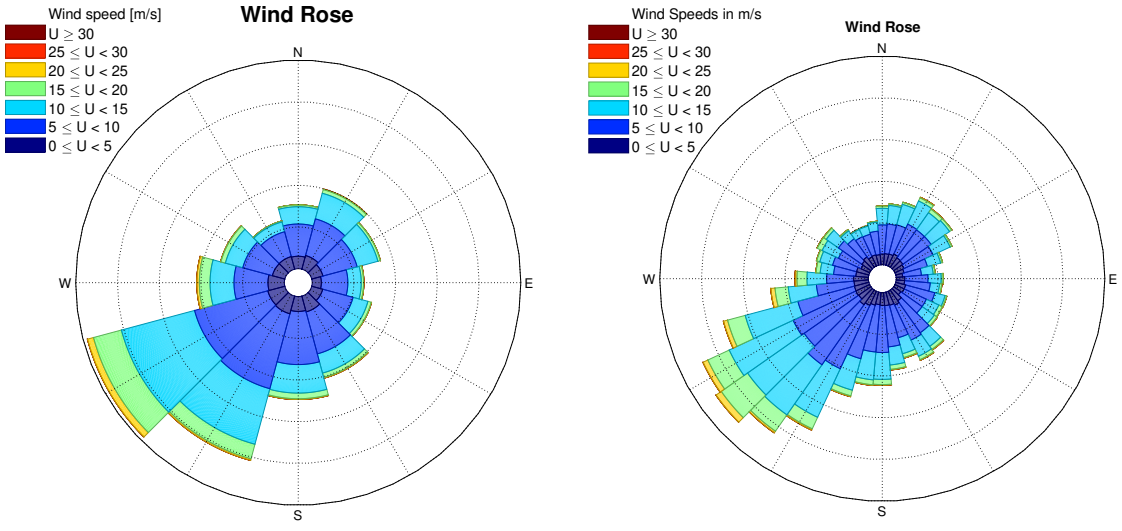

Figure 3.13: Wind rose for the wind farm analysed, left 12 bins, right 36 bins.

The mean free ambient turbulence and its standard deviation are described by quadratic functions of mean wind speed, Eq.3.22. The wind speed statistics are derived from nacelle anemometers readings, as average values taken from the free stream operating WTs depending on the wind direction. The estimation of the second was made by averaging the standard

deviations of the turbulence for each wind speed bin between 4 and 24 m/s, which is the most frequent interval, with a step of 2 m/s. Given the turbulence statistics, its distribution is assumed log-normal conditional on the mean wind speed. The scatter plots in Fig.3.16 show examples of mean turbulence variations for the two dominant directions. In all graphs, fitting was performed by maximum likelihood estimation.

$$\mu_{\sigma_u} = a_1 U^2 + a_2 U + a_3 \tag{3.22}$$

$$\sigma_{\sigma_u} = b_1 U^2 + b_2 U + b_3 \tag{3.23}$$

From Fig.3.16 it can be seen that the turbulence intensity, defined as ration between turbulence and mean wind speed, reaches values around 0.1 for the entire wind speed range. This may be due to the fact that the wind speed profile of offshore sites is not affected by terrain roughness and other obstacles, thus keeping the turbulence values relatively low.

Fig.3.14 displays the differences in wind distributions for 3 different sectors, while Fig.3.15 shows the histograms and Weibull fit for all directions considered.

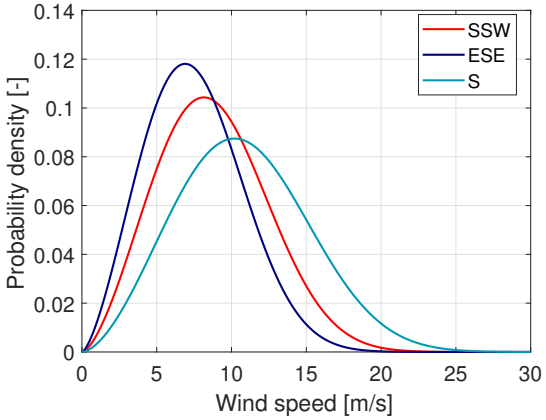

Figure 3.14: Mean wind speed distributions for 3 different directions.

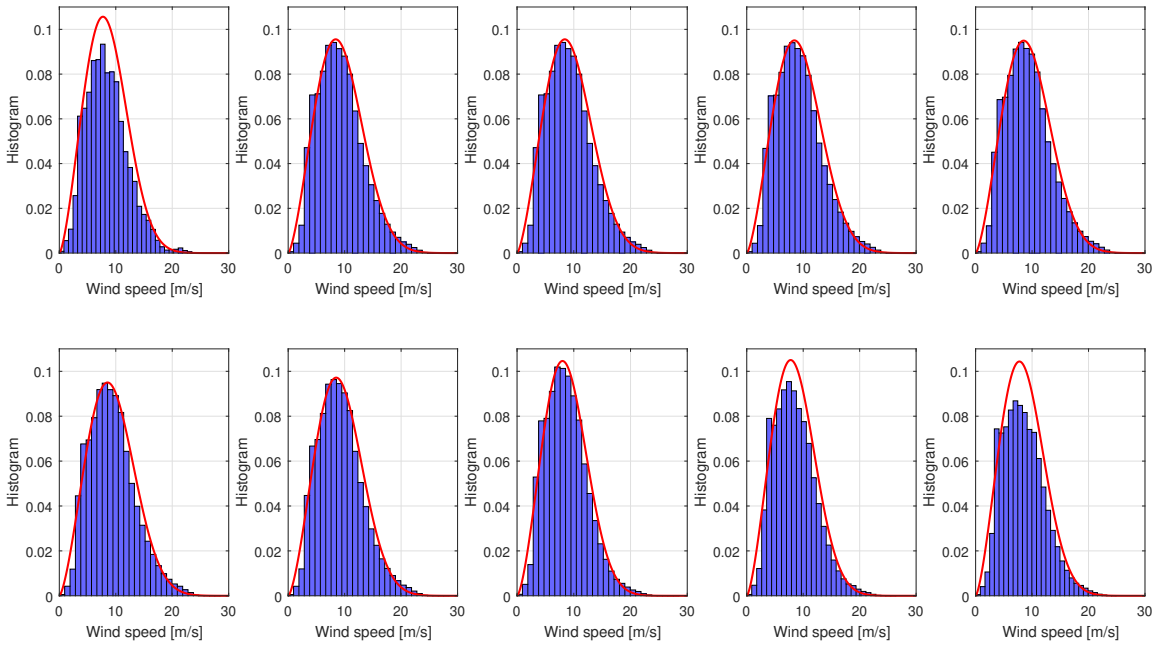

Figure 3.15: Mean wind speed distributions for all the 12 directions considered.

As exemplified in Fig.3.17, the standard deviation of the turbulence may vary significantly depending on the wind direction. This information should be included in the MC sampling to generate realistic loading conditions. However, due to limited amount of data it was not possible to compute the turbulence standard deviation for each wind direction. Tab.3.1 reports the numerical values of the site statistics.

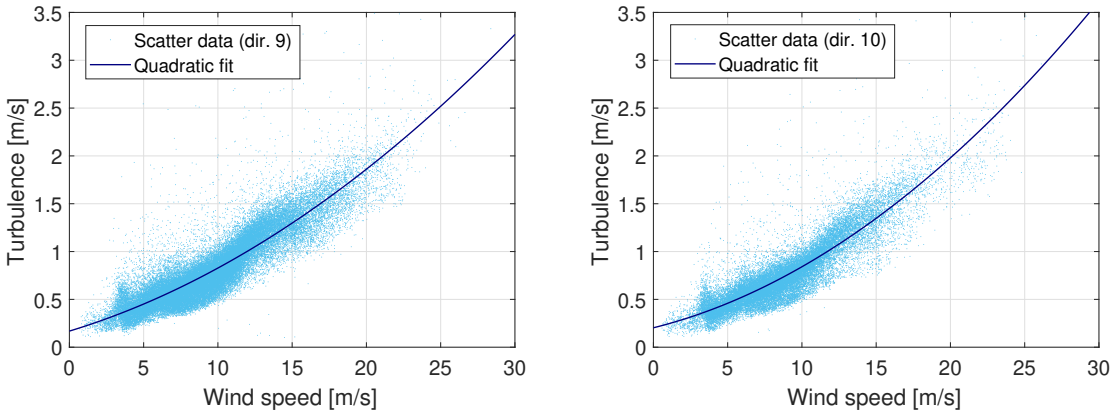

Figure 3.16: Quadratic polynomial fit to the turbulence as function of the 10-minute average wind speed from nacelle anemometer for directions 9 and 10.

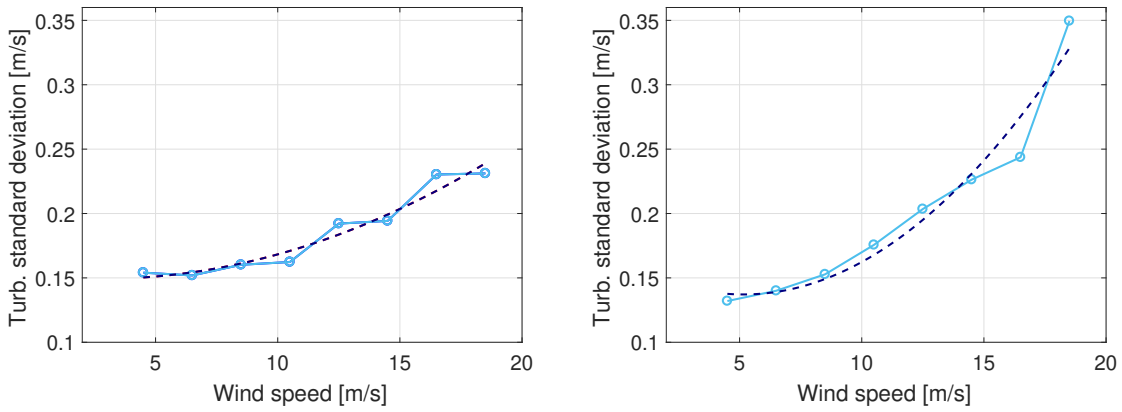

Figure 3.17: Quadratic polynomial fit to the turbulence standard deviation as function of the average wind speed bin from nacelle anemometer for directions 9 and 10.

Table 3.1: Weibull scale and shape parameters A, k, directional distribution and regression coefficients for each wind direction (N - SSE).

	N	NNE	ENE	E	ESE	SSE
A	9.55	9.74	9.88	9.26	8.50	9.87
k	2.49	2.74	2.57	2.63	2.48	2.39
$P(\vartheta)$	0.0471	0.0648	0.0755	0.0582	0.0455	0.0606
a_1	0.0018	0.0028	0.0019	0.0022	0.0022	0.0006
a_2	0.0560	0.0350	0.0487	0.0377	0.0305	0.0616
a_3	0.1658	0.2364	0.1782	0.2324	0.2645	0.1501
b_1	0.0007	0.0006	0.0001	-0.0005	-0.0007	-0.0007
b_2	-0.0090	-0.0091	0.0020	0.0147	0.0230	0.0179
b_3	0.1860	0.2008	0.1455	0.0998	0.0659	0.1185

Table 3.2: Weibull scale and shape parameters A, k, directional distribution and regression coefficients for each wind direction (S - NNW).

	S	SSW	WSW	W	WNW	NNW
A	10.91	12.17	10.92	10.02	9.54	9.64
k	2.17	2.67	2.71	2.59	2.37	2.40
$P(\vartheta)$	0.0798	0.1861	0.1549	0.0937	0.0774	0.0564
a_1	0.0012	0.0017	0.0019	0.0025	0.0025	0.0019
a_2	0.0544	0.0383	0.0472	0.0387	0.0460	0.0543
a_3	0.1360	0.2070	0.1685	0.2032	0.1816	0.1674
b_1	-0.0004	0.0001	0.0004	0.0011	0.0001	0.0007
b_2	0.0135	0.0016	-0.0020	-0.0111	0.0024	-0.0110
b_3	0.0951	0.1646	0.1519	0.1657	0.1111	0.1758

Ultimately, the sea input conditions implemented as showed in Fig.3.18. These are

considered constant for all wind directions, since the interest in this study is not particularly dedicated at foundation loads.

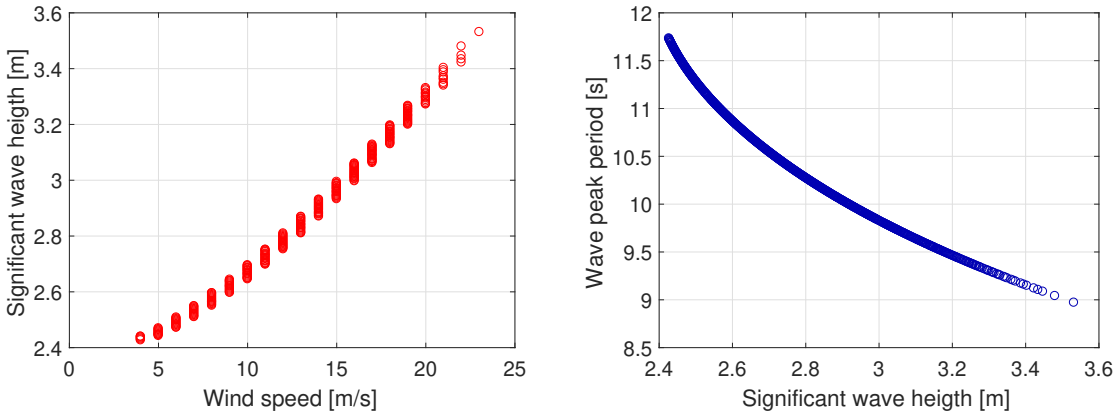

Figure 3.18: Significant wave height as function of the mean wind speed (left), and peak period as function of the significant wave height.

3.6.2 PCE

This paragraph introduces the basic concepts of PCE ([93]). Given a set of random input variables $\mathbf{X}$ and an output function $Y = G(\mathbf{X})$, the PCE is based on fitting a finite number of orthogonal polynomial functions to describe this dependency, through the following mapping $G(\mathbf{X})$

$$Y = G(\mathbf{X}) = \sum_{\boldsymbol{\alpha}} w_{\boldsymbol{\alpha}} \Psi_{\boldsymbol{\alpha}}(\mathbf{X}) \tag{3.24}$$

where Ψ are multivariate polynomials and w their corresponding coefficients. In practice, a finite number for $\boldsymbol{\alpha}$ must be chosen. Most probabilistic models require the input variables $\mathbf{X}$ to be independent and identically distributed (i.i.d.). Thus a Resenblatt transformation [94] followed by normalization to a normal space is performed. This motivates the employment of the Legendre family of univariate orthonormal polynomials, thanks to their interval of definition [-1,1], which is convenient for mapping the bounded random variables $\mathbf{X}$ through their cumulative distribution [95]. According to this, the polynomial basis functions in Eq.3.24 become

$$\Psi_{\boldsymbol{\alpha}}(\mathbf{X}) = \prod_{i=1}^{M} P_{\alpha_i}(\xi_i) \tag{3.25}$$

where P_{α_i} are M-dimensional multivariate polynomials and

$$\xi_i = 2F(X_i) - 1 \tag{3.26}$$

with $F(X_i)$ being the cumulating distribution function of the variable X_i. Eq.3.25 means that each multivariate polynomial $\Psi_{\boldsymbol{\alpha}}(\mathbf{X})$ is expressed as the product of univariate polynomials, where the elements of the vector $\boldsymbol{\alpha}$ are the orders of each univariate polynomial term.

3.6.3 Calibration of the surrogate model

According to Dimitrov et al. [95], the farm loads are obtained by building a surrogate model that based on polynomial basis functions. The procedure allows to determine the wake-induced load variation within a wind farm, by strongly reducing the number of simulation cases of each turbine, which would ne necessary to account for the variability of the input variables. This represent the great benefit of using surrogate models. Alternatively, the load simulations should be set up on the single turbine, which besides large computational expenses, would also require considerable manual work. The main assumptions of the approach is that the relationship between wake-induced loads, wind farm geometry and environmental conditions can be efficiently derived through polynomial fitting, or similarly, with machine learning algorithms.

The surrogate model is based on setting up a set of load simulations for one turbine representative for a specific row of the wind farm, where the stochastic variability of the input variables is considered including wake contributions to turbulence from neighboring turbines. The reason for proceeding in this way is indeed to account for wake turbulence, which varies from row to row of the farm. Once the load simulation results are available, polynomial fitting is performed by taking the indicators as scalar output functions, and using input variables as regressors. The input set normally contains the environemntal variables used as input in the aeroelastic simulator. In this way it becomes possible to map the variation of the output function in every point along the 2-dimensional domain of the wind farm as function of the input set. Since the fitting functions are continuous polynomials, the output is mapped in every point of the domain, in particular where turbines are located.

The output parameters are in this case stress indicators, i.e. blade root DEL (Eq.2.18), ADC (Eq.3.21) and mean friction (Eq.3.18). The latter is obtained by post-processing the load simulations. For the blade root fatigue, a Wöhler exponent $m = 12$ is used for the three directions, flapwise, edgewise and torsion, as recommended by DNV-GL guidelines [96] for glass fiber composites. The DWM [68] is used to compute the wind conditions at each wind farm row.

In Eq.3.24, the selected input functions are mean wind speed U, turbulence σ, wind shear α, turbine spacing S and wake angle ω. The following variable bounds have been selected based on similar studies or derived from available data:

- Mean free wind speed from 4 to 25 m/s (10 min. average)
- 12 wind directions
- Ambient turbulence calculated from available site data
- Wind shear exponent from 0.05 to 0.2
- Spacing between turbines min. $5D_r$, max. $25D_r$ (D_r = rotor diameter)
- Wake angle from -20 to +20 deg

The duration of the time series is 10 minutes and the simulations are performed using the commercially available aeroelastic code HAWC2 [61]. For each row, 500 MC simulation cases are set up, by random sampling the input variables from the joint PDF of the environmental conditions. 12 turbulence seeds are considered for each case. Thus, the number of simulations

per wind farm row is 6000. The polynomial order of Eq.3.24 is set to 6. The total number of polynomials in Eq.3.24 depends on the dimension of the input space and the maximum polynomial degree. For further details, the reader should refer to [95].

The indicators are then projected into cumulative values according to the integral in Eq.3.27, where L_{life} is the numerical value of the indicator and the indexes 1 and 2 stands for upper and lower value, as

$$L_{life} = \left(\int_{U_1}^{U_2} \int_{\sigma_1}^{\sigma_2} \int_{\vartheta_1}^{\vartheta_2} L_i(U,\sigma,\vartheta)^m f(U,\sigma,\vartheta)\ dU\ d\sigma\ d\vartheta \right)^{1/m} \tag{3.27}$$

In Eq.3.27, L_i is the value of the indicator conditional to the environmental conditions, derived through the surrogate model. The main environmental parameters considered are wind speed U, wind direction ϑ and turbulence σ, which probability of occurrence is computed according to the their joint distribution

$$f(U,\sigma,\vartheta) = f(\sigma \mid U,\vartheta) f(u \mid \vartheta) f(\vartheta). \tag{3.28}$$

The resulting vector L_{life} over the wind farm is then normalized with respect to its maximum value. Note that because of this normalization, it is not necessary to average L_{life} over the representative number of cycles or duration of the entire time period considered. Furthermore, due to insufficient amount of data, the turbulence is considered as a deterministic function of the wind speed and wind direction while the wind shear is kept constant to $\alpha = 0.1$, which is normal for offshore sites. Thus, only Eq.3.22 is considered and Eq.3.27 reduces to

$$L_{life} = \left(\int_{U_1}^{U_2} \int_{\vartheta_1}^{\vartheta_2} L_i(U,\vartheta)^m f(U,\vartheta)\ dU\ \ d\vartheta \right)^{1/m} \tag{3.29}$$

Typically, a validation of the PCE against the truth system should be included in the analysis in order to demonstrate whether the fitting is able to predict fatigue loads in this case. Thus, two steps are necessary to argue motivate why this is missing in this dissertation. One step is the validation of the DWM. Although this is not treated in this application, there are in literature several papers demonstrating how the DWM can accurately predict wake-induced loads (see e.g. [68]). Furthermore, the work by Murcia and Dimitrov [97] shows how the surrogate model is indeed good in predicting the output of the DWM model.

3.7 Results

By training the PCE functions in Eq.3.24, the mean friction and ADC turned out to have a coefficient of determination (R-squared) less than 0.8 for every farm row, which indicates an improper polynomial fit. Thus, these two outputs were discarded. Fig.3.19 shows the R-squared for the blade root bending and torsional moments as function of the rows. An error less than 3% is encountered, which is considered satisfactory.

Fig.3.20 displays the normalized blade root cumulative DELs. As expected, the edgewise moment does not vary significantly within the wind farm, unlike flapwise and torsional, since the edgewise moment is mostly driven by gravitational loads, rather than turbulence. In particular, the torsional moment DEL shows greater variation than the flapwise. This variation may be due to the simplified aeroelastic modeling of the blade torsional response, such as

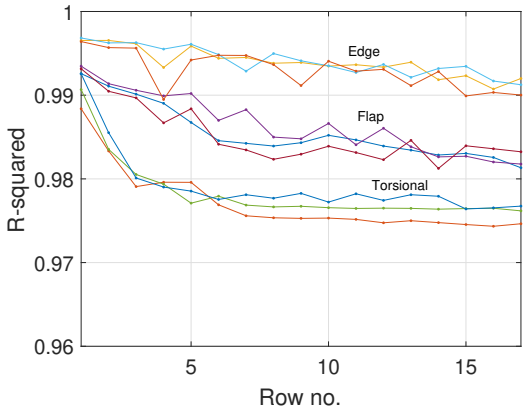

Figure 3.19: Coefficients of determination for blade root bending moment DEL for the 3 blades. In the abscissa the farm row number.

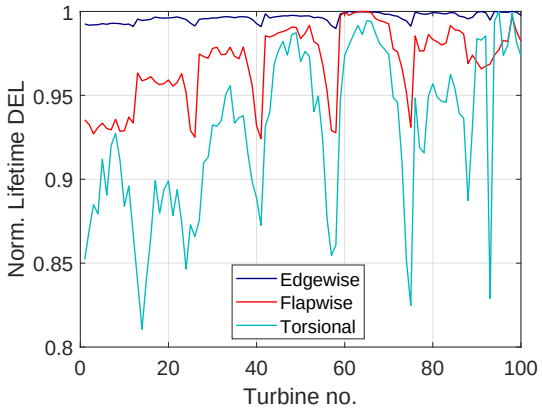

Figure 3.20: Normalized cumulative DEL within the wind farm. Blade root flapwise, edgewise and torsional bending moments averaged over the 3 blades.

not properly adjusted damping properties. However, the first order Sobol indexes of the polynomial function (Eq.3.24), displayed in Fig.3.21, show that for the flapwise, the most important variable is turbulence, while the torsional moment is also affected by wind shear, turbine spacing and wake angle. This may induce larger variations, which are however not investigated here. Each line in Fig.3.21 correspond to a wind farm row.

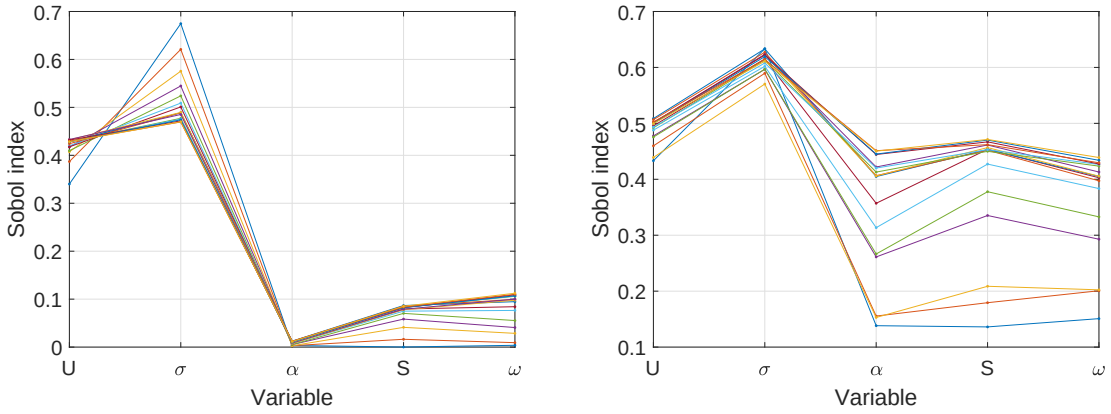

Figure 3.21: Sobol indexes of the DEL polynomial regressors for blade root 1 flapwise bending moment (left) and torsional moment (right) for all the wind farm rows.

It is important to notice that the input variables used to calculate the Sobol indexes are correlated, and thus different results could be obtained bu using more accurate estimations that take into account this correlation (see Ch.4).

Fig.3.22a shows the probability of the pitch alarm events. The following alarms were selected from the alarm-log of the wind farm, which can be considered related to demanding operation, thus to loads:

- Sludge pitch hydraulic station
- High pitch pressure
- Low pressure pitch-block
- Pitch hydraulic temperature too high
- Pitch hydraulic leakages
- Pitch deviations
- Pitch velocity errors
- Pitch errors

In total, circa 1000 alarms were recorded during the time frame analyzed. Fig.3.22 are the load maps showing the normalized DEL of blade root flapwise bending and torsional moments. From Eq.3.18 it can be noticed that the torsion is neither connected to friction nor to possible malfunctions in the hydraulic and pitch systems and thus to any of the alarms listed above, unlike the flapwise bending moment. In addition, the edgewise moment does not show variation along the wind farm, as expected, since it is not driven by turbulence. Thus these two channels are not displayed. In Fig.3.22a, interpolation is obtained by cubic polynomials for graphical display.

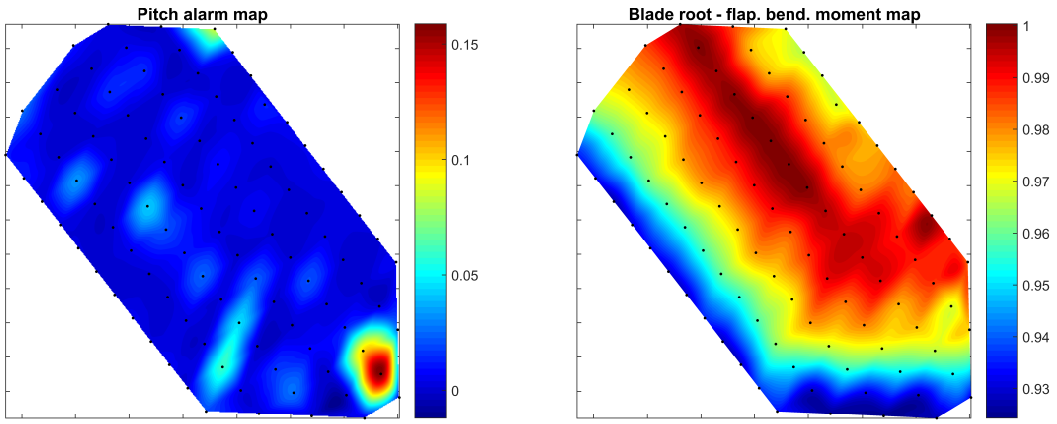

Figure 3.22: Normalized blade root flapwise DEL map and alarm event map of the selected pitch malfunction.

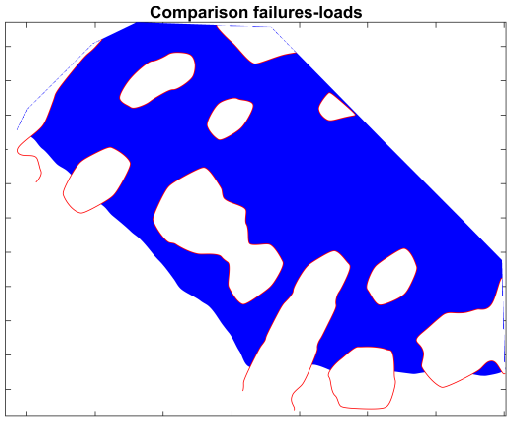

Figure 3.23: Contour regions flapwise bending moment DEL greater than 0.95 and frequency of occurrence of pitch alarms greater than 1% (red edges, white fill).

Fig.3.23 shows a contour plot of the failure areas with frequency of occurrence greater than 1%, and fatigue loads greater than 0.95, from where it emerges that is unclear to define patterns between them. The alarms occured over a period of 5 years, and their distribution is somewhat uniform across the wind farm. Higher fatigue loads are more concentrated in specific regions of the farm, which reflect the wake distribution.

3.8 Conclusions on the load maps

The flapwise bending moment direction can be in this case considered as a good indicator, since it is related to the friction moment in the pitch bearing, and thus to the alarms selected, and carries the variation due to wake effects across the wind farm, as shown from Fig.3.20. The DEL is chosen as a scalar quantity in order to obtain the map, besides being a popular

metric for assessing the cumulative load distribution in real practice. In this work, the flapwise bending moment statistics could have been used as well.

Despite a not clear pattern between alarms and loads, from Fig.3.22 it can be inferred that the alarms are more likely to happen in regions of higher cumulative DEL, greater than 0.95. However, the pitch alarms seem to be uniformly spread around the farm and no correlation can be effectively proven. The row experiencing the least number of alarms is the front row with respect to the prevalent wind direction, being less affected by wakes, as expected. Some unexplained anomalies can be seen in some turbines from Fig.3.22a, which experienced a very high number of alarms. This could depend on the specific loading conditions, which may not be necessarily correlated with an overall picture of the fatigue DEL maps, as well as serial failures or manufacturing defects. The area with stronger wake effects is marked by higher fatigue loads. In particular the 3rd raw from the east direction has also experienced pitch malfunctions.

It can be concluded that in this case the load maps cannot be used as indicative picture to understand the most critical turbines within the farm. However, more detailed analysis would be necessary. For instance, from the operational report of the farm it turned out that the turbines analyzed were heavily curtailed during the period considered for this study, and this condition was not taken into account in the aeroelastic simulations. Introducing one or two levels of curtailment will modify the load distribution across the wind farm, due to varying operational parameters such as blade pitch angle and rotor speed, which in turn will modify the wake produced by the turbines. A more specialized analysis could also include the calculation of the cumulative loads, or other indicators, up to the time of occurrence of the alarms, in order to include the temporal information. This was missing in the analysis, and only cumulative normalised values were considered.

It is important to remark that the scope of this analysis is not to explain the occurrences of shut down events as a direct consequence of excessive loads, but only to provide a qualitative assessment to find out weather fatigue load maps, or any other indicator map, could suggest what regions of the farm layout are more critical in terms of loads, as a consequence of wake turbulence. In this case, fatigue loads was shown, but in practice more specific indicators can be found. In general, however, fatigue loads are not the best indicators for the malfunctions analyzed. The analysis should be continued with more informative quantities such as friction torque and ADC, which have not been shown here due unsatisfactory the polynomial fit.

Chapter 4

Artificial intelligence in wind power

It's no trick to get the answers when you have all the data. The trick is to get the answers when you only have half the data and half that is wrong and you don't know which half.

W. Thomson

The aim of this chapter is to introduce the reader to the analytical concept around predictive maintenance used in this thesis, starting from a discussion about intelligent systems in the context of the 4^{th} industrial revolution, mathematical background of machine learning algorithms and performance metrics for predictive models.

4.1 A brief history of intelligence

The advent of machines taking over repeated human operations is a topic that persists since the first industrial revolution. Now more than ever, this subject keeps inspiring curiosity to further explore deeper functionalities of our brain. Most importantly however, is to understand how biological intelligence has developed over time and to mark the key steps of what today is referred to as AI.

Intelligence is a rather philosophical concept. The early ideas date back to ancient Greeks, who established intelligence as a mean to "rank" all living creatures. Their view was however biased, since it advocated that some humans, specifically educated males, are naturally born with a rational element that allows them to rule over the uncivilized remaining part of the population, including women and animals. For example, Aristotele introduced the concept of master and slave. Although this teaching remained untouched for centuries and represented the foundation of Western philosophy and the base ground of logical thinking, the concept of sovereignty and slavery also stimulated ideas of rulers to differentiate men from women from animals, culture from culture, and even race from race, all according to a scale of superiority based on intellectual skills. Sadly, this often resulted in catastrophic mistakes. Similar conclusions to Aristotele's were reached by Kant centuries later during the Enlightenment. Thus, it can be argued that intelligence was originally deemed as a political tool employed to define what an individual can or cannot do, rather than an inherent faculty common to all

humans. Not far from the modern era, this inspired the idea of quantifying intelligence as any other measurable quantity. An example first appeared in Britain in the early 19th century, when written tests were introduced to evaluate the competences of young students in order to address them in the most suitable scale of society [98].

The argument however made some turns few centuries ago. Perhaps the work published by Charles Darwin on the origin of species provided clear scientific answers of how humans can be differentiated from other living creatures. Darwin did not have an explicit opinion on human evolution, but he indirectly claimed that there are actually no marked behavioral differences with animals [99], except for an extraordinary intellectual capacity. However, the process that led humans to acquire this superior intelligence and dominate over other species is still an open question, seemingly rooted in complex genetic mutations occurred at some point in history that favored brain growth, which specific origins are however still unexplained.

Clearly the discussion could trigger controversial political debates on use and misuse of intelligence to measure human skills, and how this has driven decisions through history. However, this is not the aim of the present work. The interested reader may consult various documents on this subject. The way people perceive this concept nowadays is tremendously different than what philosophers and thinkers argued centuries ago. The methodologies adopted by contemporary institutions to asses the suitability of candidates is free from any apriori classification or rank mentioned above, but purely based on testing individual aptitudes in performing specific tasks. It remains however fascinating to run through the event line that made human beings aware of their own abilities, which eventually resulted in important steps ahead towards the establishment of equality principles, on behalf of of societal progress and mutual respect.

A modern definition regards intelligence as a characteristic common to all living creatures. It includes logical thinking, creativity, problem solving ability to think ahead, plan and learn. Generally speaking intelligence is itself an ability to infer information from the surrounding environment, preserve it and use it in outer contexts. Several different types of intelligence are distinguished, e.g. musical, logical, emotional, linguistic, interpersonal and so on. Furthermore, recent trends deem intelligence as something beyond human cognitive abilities, and this perception helped differentiate biological from artificial forms of intelligence, commonly referred to as AI. The latter are related to the experience of progressive information technologies aimed at improving the quality of life. The advent of data mining has fueled the transition to AI and it is expected that this process will lead the next step of societal change. A historical analogy is the example of the early industrial revolutions started at the turn of the 18th century. These in fact demonstrated how the invention of machines replacing manual work brought in substantial benefits by enabling mass production and faster operations, thanks to auxiliary machines running by burning coal to produce steam, a core element of the early Western industrialization. Among these benefits however, there were also increase of literacy, better working conditions and establishment of faster routes for international trades. Similarly, some believe that the AI-driven revolution will provide people more time to engage in more interesting intellectual subjects, by dissuading them from redundant and repetitive work. Concerns related to empowering AI rather than being empowered by AI arise with the fast-developing abilities of intelligent machines.

In modern societies, a wide range of institutions from private and government organizations, aviation, navy, transportation, medicine, biotechnology and corporations exploit the potential of fast and reliable AI tools to provide services. Most of these, are based on predictive analytic.

4.2 Explanatory versus predictive power

In literature three types of statistical modeling are distinguished, respectively explanatory, predictive and descriptive [100]. In particular, in this dissertation is of primary relevance to clear the difference between explaining and predicting, as a fundamental knowledge for proper statistical modeling. Interpretation refers to the model's ability to find hidden patterns in data to explain causal links between input and output. Prediction on the other hand has a different objective, although the same model can be used for both purposes. The distinction is that boosting the model towards prediction performance typically results in highly complex models, which in turn are poorly interpretable, for obvious reasons. Moreover, some highly performing predictive models are often regarded as *black boxes*, due to their uncontrolled training of internal links. This may also explain why for interpretation purpose, usually simple linear models are preferred, while complex algorithms such as artificial neural networks (ANN) are mostly employed for prediction. It is evident that this distinction suggests the existence of a trade-off between these two different purposes, since the model typically looses its explanatory abilities when performance is prioritized. Thus, it is important that the practitioner is aware of the inner difference between these two faces of the same coin. However, if the purpose of the model is to predict, *it should not matter whether it is a black box or a simple, interpretable model, as long as it can be appropriately validated* [101].

When moving the bar towards prediction performance the model may result in extremely suited functions describing the relationship input-output. The outcome is a model with too optimistic predictions, a problem commonly known as overfitting. When the model is overfitted to the set of data used for training, it looses its generalization abilities and may perform poorly when a new sample is presented to the model that was not present in the training set. To give a honest description of the model performance, cross validation is adopted to prevent overfitting [101, 102].

4.3 Learning paradigms

Machine learning algorithms discover patterns in data and recognize future observations never seen by the them. Thus, their are known to have generalization abilities. Generalization is of primary importance in machine learning, since training is usually performed based on a limited number of observations of a given process. Indeed, the main distinction between learning techniques resides in the type of training process employed to achieve these generalization abilities, which can be:

- **Unsupervised** learning is when the structure of the dataset or similarity between groups of data are identified without a target value. Examples are clustering, data visualization or density estimation.
- **Supervised** learning is when the training process where examples of input and output are presented to the algorithm, which models internal relationship by trying to minimize an error. In probabilistic terms, supervised learning concerns the definition of the conditional probability $p(\text{output} \mid \text{input})$. If the task is to recognize categorical classes, the procedure is called $classification$. If the task is to recognize the behavior of continuous variables, the procedure is called $regression$.

There are also other types of paradigms, such as reinforcement learning, which is based on training through a reward. The nature of this techniques is in between unsupervised and supervised. A further distinction of learning techniques can be made in terms of their mathematical nature, as:

- **Parametric** means that the analytical relationship between input and output is decided apriori, which assumes specific forms based on prior knowledge. This also comprises the statistical distribution of the output variables.
- **Non-parametric** means that the relationship between input and output is not known apriori, but rather constructed based on observations.

The model structure being already fixed, parametric techniques may require less computational effort than the other. This distinction is valid for both regression and classification problems.

4.4 Learning algorithms

This section describes the learning algorithms used throughout this part of the thesis. Specific information and nomenclature are taken from [103]. Unless otherwise specified, the mathematical description refers to N input vectors $\mathbf{x}_n$ collected in a matrix $\mathbf{X}$, where $n = 1, \dots N$, and the dimensionality of the vectors $\mathbf{x}$ is D. Note that in the scientific papers attached to this thesis, the nomenclature may differ, due to ease of interpretation. Further reading is adviced in order to understand specific details of this work, which for the sake of brevity have not been fully addressed.

4.4.1 Linear discriminant analysis

Linear discriminant analysis (LDA) was not explicitly used throughout this work. However, it represents one the simplest classifier, and, on the author's belief, it clearly illustrate the concept of class separability. LDA is a dimensionality reduction technique, in that it reduces D-dimensional vectors into scalar scores. Given a multi-class problem, the vector of linearly transformed scores $\mathbf{y}$ is found as

$$\mathbf{y} = \mathbf{W}^T \mathbf{x} \tag{4.1}$$

where $\mathbf{W}$ is a projection matrix, which is found as described in the following. The within scatter is defined as

$$\mathbf{S}_W = \sum_{k=1}^{K} \sum_{n \in C_k} (\mathbf{x}_n - \boldsymbol{\mu}_k)^T (\mathbf{x}_n - \boldsymbol{\mu}_k) \tag{4.2}$$

where the mean class vectors with N_k are

$$\boldsymbol{\mu}_k = \frac{1}{N_k} \sum_{n \in C_k} \mathbf{x}_n \tag{4.3}$$

where N_k is the number of observations for the class C_k and K the total number of classes. By defining the total mean vector of th entire dataset

$$\boldsymbol{\mu} = \frac{1}{N}\sum_{n=1}^{N}\mathbf{x}_n \tag{4.4}$$

the between scatter matrix is defined as

$$\mathbf{S}_B = \sum_{k=1}^{K} N_k(\boldsymbol{\mu}_k - \boldsymbol{\mu})^T(\boldsymbol{\mu}_k - \boldsymbol{\mu}) \tag{4.5}$$

At this point, the matrix $\mathbf{W}$ is found to maximize the following function

$$J(\mathbf{W}) = Tr\{(\mathbf{W}\mathbf{S}_W\mathbf{W}^T)^{-1}(\mathbf{W}\mathbf{S}_B\mathbf{W}^T)\} \tag{4.6}$$

Once the linear scores are obtained through Eq.4.1, the class membership probability can be found through softmax transform

$$P(y = C_j \mid \mathbf{x}) = \frac{e^{\mathbf{x}^T\mathbf{W}_j}}{\sum_{k=1}^{K} e^{\mathbf{x}^T\mathbf{W}_k}} \tag{4.7}$$

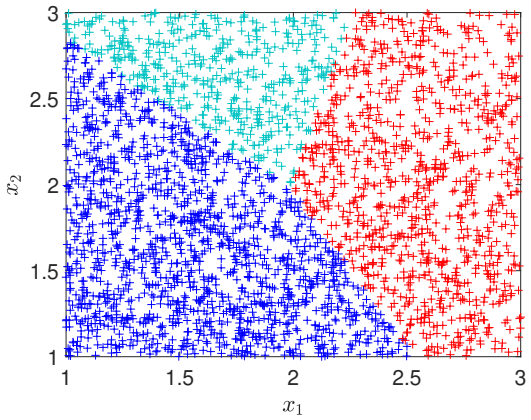

Figure 4.1: Classification of a 2-dimensional normally distributed vector in 3 classes through LDA.

The linear surfaces are also called decision boundaries and their dimensionality is $D-1$. In the example of Fig.4.1, the linear surfaces (straight lines) are clearly distinguished. The plot is obtained through MC sampling of the vector $\mathbf{x} \sim \mathcal{N}(\boldsymbol{\mu}, \boldsymbol{\Sigma})$ where $D = 2$ where the 3 classes have different Gaussian distributed mean vector $\boldsymbol{\mu}$ and covariance matrix $\boldsymbol{\Sigma}$ corresponding to the identity matrix. The data points are subsequently classified through the procedure explained above. To perform successfully, classification requires a certain class separability. For further details the reader should consult [103].

4.4.2 Naïve Bayes

The Naïve Bayes (NB) classifier is the simplest way to account for several input variables. NB is based on the assumption that these variables are conditionally independent given their membership class y. Thus, NB has the structure of a simplified BN. Although this hypothesis is often not realistic in practical examples, the NB classifier nevertheless often performs satisfactorily.

Given a set of random N variables $\mathbf{x}$, a vector of realizations $\mathbf{x} = \{x_1, \dots x_D\}$ and a binary output variable $y = \{0, 1\}$, the joint probability of $\mathbf{x}$ conditional on y is computed from the conditional independence assumption, as

$$P(\mathbf{x} \mid y = C_j) = \prod_i P(\mathbf{x}_i \mid y = C_j) \tag{4.8}$$

where C denotes the class. Recalling the Bayes' rule, the class-conditional probability can be expressed as

$$P(y = C_j \mid \mathbf{x}) = \frac{P(y = C_j)P(\mathbf{x} \mid y = C_j)}{P(\mathbf{x})} \tag{4.9}$$

The class-conditional PDFs can be described in some cases by parametric distributions or non-parametric kernel densities. Given a variable, or covariate, of N observations generically indicated with $X = \{x_1, x_2, \dots, x_N\}$, corresponding to a column of the matrix $\mathbf{X}$ defined above, the univariate kernel density estimate $\hat{p}(x)$ is expressed as

$$\hat{p}(x) = \frac{1}{nh} \sum_{i=1}^{n} k\Big(\frac{x - x_i}{h}\Big) \tag{4.10}$$

where h is the bandwidth and k the kernel basis function.

4.4.3 Linear models

Following the notation used in [103], in general terms a regression model can be written in the form of Eq.4.11, where y is a scalar output, $\mathbf{x} = \{x_1, \dots x_D\}$ is a vector of regressors, $\mathbf{w}$ the vector of coefficients and ϕ are the basis functions, as

$$y(\mathbf{x}, \mathbf{w}) = \sum_{j=0}^{N} w_j \phi_j(\mathbf{x}) \tag{4.11}$$

A linear model (LM) is obtained by setting the basis function as linear, i.e. $\phi(\mathbf{x}) = \mathbf{x}$, which can be written explicitly as

$$y(\mathbf{x}, \mathbf{w}) = w_0 + w_1 x_1 + w_2 x_2 + \dots w_D x_D. \tag{4.12}$$

More precisely, the LM gives an estimate of the variable y given the predictors $\mathbf{x}$, as

$$y_i = w_0 + \sum_{j=1}^{N} w_j x_{ij} + e_i \tag{4.13}$$

where e_i is a Gaussian distributed error. The parameters $\mathbf{w}$ are to be determined. Typically, the least squares are used estimates of the parameters by minimizing the objective function

$$\min_{\mathbf{w}} \sum_{i=1}^{M} \Big(y_i - w_0 + \sum_{j=1}^{N} w_j x_{ij}\Big)^2 \tag{4.14}$$

If N is large, Eq.4.14 admits infinite solutions, and the chances to overfit the model increase. Furthermore, there are two other reasons why an alternative method would be preferable to the least square estimate. The first is the prediction accuracy, which can be improved by

shrinking the values of the regression coefficients, or setting the coefficient of unimportant covariates to zero. The second reason is to interpret the model, i.e. to identify a subset of predictors which best describes the output.

If the predictors are standardized to zero mean and unit variance, the coefficients $\mathbf{w}$ are called standard regression coefficients. The least absolute square and shrinkage operator (LASSO) allows the model regularization, by solving the following problem in the Lagrangian form

$$\min_{\mathbf{w}} ||\mathbf{y} - \mathbf{x}^T\mathbf{w}||_2^2 + \lambda||\mathbf{w}||_1 \tag{4.15}$$

where the index 2 indicated the Euclidean norm, or L2 norm, 1 indicates the L1 norm and $\lambda \geq 0$ is the Lagrangian parameter. LASSO is closely related to the ridge regression, where the L2 norm is used instead of L1. The LASSO regularization can be used for variable selection and sensitivity analysis, in order to improve the model interpretability. For further details, the reader should refer to [104]. In Article III a variable selection method is used to first understand and regularize the model. This latter also prevents overfitting and multicollinearity. A generalized linear model (LM) is a generalization of a linear regression model, where the error distribution can be other than normal. Therefore, given its extension to model different error distributions than normal, LM are suitable for regression and classification. In the first type, the error is normally distributed.

4.4.4 Random forests

Random forests (RF) is a fully data-driven supervised learning technique, which can be used for both classification and regression [105]. RF is based on the concept of bootstrapping the training set, build multiple decision trees and then average their predictions, thus reducing uncertainty and improving performance. For further reading about RF the reader should refer e.g. to [106], from which this text has been rearranged. Given a set of input variables X_i with $i = 1, \dots p$, the decision tree firsts divides the input space into a set of regions, R_j, with $j = 1, \dots J$. Once the classes are built, a similar classification similar to LDA is performed for new samples. The regions or boxes are built by minimizing the error squared, as

$$\sum_{j=1}^{J} \sum_{i \in R_j} (y_i - \hat{y}_{R_j})^2 \tag{4.16}$$

where $\hat{y}_{R_j}$ is the mean of the j-th box. To overcome the problem of heavy computations, the recursive binary splitting, or greedy top-down approach is used. The input space is divided into the regions $\{X \mid X_i < s\}$ and $\{X \mid X_i \geq s\}$, where s is a boundary value.

When RF is performed, several decision trees are created. Here, not only the training dataset is randomly split by bootstrapping, but also the number of predictors is randomly sampled, namely at each bootstrap a number $m < p$ predictors is selected. This operation is performed to eliminate the possibility that the presence of a strong predictor may out-stand over all the remaining predictors. This will reduce the effect of multiple trainings because of correlated resulting trees, and thus the variance will not reduce significantly. RF is said to have decorrelation properties.

4.4.5 Feed-forward artificial neural networks

Linear models can be easily extended to include nonlinearities, by plugging in higher order polynomial terms. However, unless specific knowledge of the process being modeled is available, the user does not know whether the degree suitably describes the process. This is true extrinsically for predicting categorical data. In the context of supervised learning, neural networks (NN) can be regarded as a non-parametric technique. Often they are addressed as artificial, to distinguish them from the real biological neural network [107]. The mathematical steps shown below refer to a single layer perceptron feed forward architecture.

As seen for LM, the relationship between input and output can be expressed as linear combinations of linear or nonlinear basis functions $\phi_j(\mathbf{x})$, as

$$y(\mathbf{x}, \mathbf{w}) = f\Big(\sum_j w_j \phi_j(\mathbf{x})\Big) \tag{4.17}$$

where the operator $f(\cdot)$ is a nonlinear activation function. For example $\phi_(\mathbf{x}) = \mathbf{x}^p$ is a polynomial basis function of order p. NN are a series of basic transformations starting from a the first layer, which defines the following linear activations a_j

$$a_j = \sum_i w_{ji}^{(1)} x_i + w_{j0}^{(1)} \tag{4.18}$$

where $j = 1, \dots M$ with M the maximum number of linear combinations and 1 is the layer where the transformation occurs. The term w_{ji} are the network parameters while w_{j0} its biases. The activations are then transformed using a nonlinear activation function, which corresponds to the basis function ϕ_j in Eq.4.17, as

$$z_j = h(a_j) \tag{4.19}$$

where the function $h(\cdot)$ is the hidden unit activation. Thus, the operation repeats for the output layer as well indicated as (2), where the activation is referred to as output activation function

$$a_k = \sum_j w_{kj}^{(2)} z_j + w_{k0}^{(2)} \tag{4.20}$$

where k is the total number of outputs. Finally, the general expression of the NN can be written as

$$y_k(\mathbf{x}, \mathbf{w}) = \sigma\Big(\sum_j w_{kj}^{(2)} h\Big(\sum_i w_{ji}^{(1)} x_i + w_{j0}^{(1)}\Big) + w_{k0}^{(2)}\Big) \tag{4.21}$$

where y_k is the k-th output variable. It is important to notice that in Eq.4.21 it is

$$\phi(\mathbf{x}) = h\Big(\sum_i w_{ji}^{(1)} x_i + w_{j0}^{(1)}\Big). \tag{4.22}$$

Moreover, in Eq.4.21, the activation function σ is the non linear activation differs for regression and classification models. For the first class, $y_k = a_k$, while for the second class, the output is transformed into a probabilistic quantity through the sigmoid function, which for a binary case is simply

$$\sigma_a = \frac{1}{1+e^{-a}} \tag{4.23}$$

for multiclass classification, the sofmtax transform of type Eq.4.7 is employed. Eq.eq:sigmoid corresponds to the class membership probability.

Thus, training NN is a supervised mode means minimizing the sum of the error squared, given a set of observations of the output $\mathbf{o}_n$, with $n = 1, \dots N$ the number of observations, as

$$E(\mathbf{w}) = \frac{1}{2}\sum_n \|\mathbf{y}(\mathbf{x}_n, \mathbf{w}) - \mathbf{o}_n\|^2 \tag{4.24}$$

To solve the optimization problem in Eq.4.24, gradient information is typically used, to find local stationary points through the condition

$$\nabla E(\mathbf{w}) = 0 \tag{4.25}$$

Regardless the choice of the classification or regression model selected, cross validation is a technique to avoid model overfitting.

4.5 Performance metrics

Although many regression and classification may adopt the same techniques, their performance is measured in different ways, given the nature of the predicted output variable. For the first type, the output is continuous, and typical measure such as the coefficient of determination (R-squared) and root mean square error (RMSE) are used, defined as

$$\mathrm{R}^2 = 1 - \frac{\mathrm{Var}(\hat{y} - y)}{\mathrm{Var}(y)} \tag{4.26}$$

$$\mathrm{RMSE} = \sqrt{\frac{1}{N}\sum_i (\hat{y} - y)^2} \tag{4.27}$$

where y are the real observed values, $\hat{y}$ the predicted values and N the number of samples. A more appropriate metric for binary classifiers is the ROC plot, which displays true positive rate against false positive rate. The curve can be obtained through probabilistic classifiers, namely those that output a probability of the predicted variable belonging to one of the two classes. This is achieved by putting a threshold to the output probability, varying from 0 to 1, and thus spanning the entire ROC space. The probability of detection (POD) and false alarm rate (FAR), are defined as

$$\begin{aligned} \mathrm{POD} &= P(\hat{y} = 1 \mid y = 1) \\ \mathrm{FAR} &= 1 - P(\hat{y} = 0 \mid y = 0) \end{aligned} \tag{4.28}$$

Regardless the choice of the classification or regression model selected, the model performance is evaluated by averaging several trained models. This is accomplished by randomly splitting the entire dataset into a batch used for training the model and a hold-out for testing left apart. The performance metric is then calculated on the testing hold-out. This operation is known as cross validation [101]. Typically, 5 or 10 validations are enough to establish an

unbiased estimate. Cross-validation prevents overfitting, since the model is tested several times on different batches.

In Article II, a multi-training and multi-testing approach is used to quantify the spread around the average ROC curve. This information should be included in reliability analyses as prediction uncertainties, and it provides a way of comparison between different algorithms in terms of reliability of the predictive system. The dataset is first split into k different folds and the algorithm is manually trained k times, by leaving out every time a different batch for testing (10%) and the remaining data for training (90%). An ROC curve is obtained for each testing. The concept of the multi-testing approach is however similar to a bootstrapping, and to some extent, it also provides an indication of overfitting, in case particular hold-outs perform too high.

4.6 Sensitivity analysis

The general scope of a sensitivity study is to identify the importance of an input set of variables with respect to an output variable, and this relationship a functional dependency, which structure can be known a priori or derived from data. Saltelli et al. [108] define a sensitivity analysis as *the study of how uncertainty in the output of a model (numerical or otherwise) can be apportioned to different sources of uncertainty in the model input.* The derivatives of a model, numerical or analytical, is a type of sensitivity which depends on the particular point of the variable space considered, often referred to as local sensitivity.

In this thesis, a global measure of sensitivity is used, which accounts for the uncertainty in the input variables. Thus, the question is, what happens to the variance of the output when a specific input varies? Given a scalar function $Y = f(X_1, \dots X_i)$, where X_i are considered uniformly distributed and independent variables in the unit hypercube, the first order global Sobol indexes measure the contribution of each input variable X_i to the output variance, computed as

$$S_{X_i} = \frac{\mathrm{Var}(E_{\mathbf{X}\sim i}(Y \mid X_i))}{\mathrm{Var}(Y)} \tag{4.29}$$

where $\mathrm{Var}(Y)$ is the total output variance. Note that Eq.4.29 are always between 0 and 1. From the normalized input space, the Resemblant transformation is used to to map the variables in the physical space, by taking into account their joint PDF. For further details refer to [109]. The approach is called global because in Eq.4.29, the dependence on X_i disappears, given the average over all possible values of X_i. Thus, these indexes measure the relative importance of a variable on the output. However, Eq.4.29 is only valid under the assumption of uncorrelated input variables. In case this condition is not fulfilled, the correlation should be taken into account and the analytical expression of the indexes varies, along with the real contribution of each variable.

Chapter 5

Condition-based maintenance

The person who insists on seeing with perfect clearness before deciding, never decides.

H.F. Amiel

This chapter explains the CBM approach used in this work, starting from a description of data-driven technology, types of data available for wind turbine monitoring and some basic notions of decision theory including decision and event trees in the context of predictive maintenance.

5.1 Data-driven condition monitoring

For some applications, as condition monitoring or predictive maintenance of wind turbine components, fully data-driven techniques seem to have gained a large popularity compared to more traditional physics-based methods. Although mathematical models are usually very appealing for their ability to describe a physical phenomenon through differential equations, they also require knowledge about a time depended process. Numerical values of the model's parameters can be updated using evidence from the real world, so to decrease their uncertainty and reach more accurate predictions. While this approach is particularly popular for some class of problems, as for instance fatigue modelling [17], setting up a physical model for complex systems such as operating WT machines is very hard and time consuming. The number of variables into play is enormous and a complete formulation of the physical process can be hardly achieved, often associated with high computational expense. The system's state varies over time-depended on operational conditions, environmental loads, climate and maintenance actions. From the author's experience it emerges that these considerations represent important obstacles that have deterred wind energy practitioners from using highly complex models for monitoring purposes. Although not easier to implement, statistical data-driven models are far simpler to manage.

However, the problem was raised in other industries much earlier than wind energy. The authors in [110] conclude that quantitative model based methods are often not applicable in industrial applications due to the high dimensionality of the data, the system's complexity and nonlinearity, as also argued in [111]. For techniques relying on historical data instead, the

problem is that typically no dataset with all faults is available that would allow to fully learn the fault behavior. On the other hand, data sets with normal behavior are usually available. In those cases data-driven monitoring can be achieved by exploiting the properties of a process in normal operation, typically in supervised learning framework. This is also enabled by the advent of advanced machine learning tools and the outbreak of the new industrial revolution. Early applications of intelligent systems in maintenance programs were set-up by the British airways, however more 30 years ago.

It can be concluded that maintenance management of wind farms belongs to this framework. Clearly, extracting information from collected data to build statistical models seems an approach well tailored for O&M purposes.

5.2 SCADA and vibration technology

Modern multi-MW wind turbines are equipped with SCADA and condition motoring systems (CMS). The first type of system comprise sensors to record operational data such as power output, rotational speed, pitch angles and various temperatures in different components. SCADA systems were initially installed to provide operational data mainly to support control activity of the turbine behaviour in variable speed pitch regulated machines. This is achieved by pitching the blades or controlling the main shaft torque, depending on the power curve region in pitch regulated machines. The second system is dedicated to measuring accelerations or strains and oil particles, and it was initially installed for monitoring mechanical components due to its already well established experience from other industries [13]. Vibration analysis relies on the exaction of features sensitive to a large variety of damages. These features are vibration RMS, kurtosis, impact frequencies wavelet-transform and natural frequencies, which can be extracted through signal processing techniques such as FFT, Envelope and Cepstrum analyses [10]. These techniques can handle typical issues in rotating equipment, such as signal non-stationary and frequency variation as function of the rotational speed. However, most of these quantities require a certain degree of human interpretation, which is not fully desirable for automated procedure typical of machine learning applications. The sampling frequency of CMS is typically in the order of kHz, while the SCADA is in the order of Hz but are commonly stored as 10-minute average values.

Both systems record threshold-based alarms occurring when a specific parameter crosses pre-defined thresholds, typically set by the component manufacturer based on design limits, or by wind farm operators based on their experience.

Although SCADA and CMS have been historically installed separately for distinct purposes, since few years their usefulness for monitoring has been under massive investigation, thanks to the outbreak of machine intelligence [51]. Furthermore, at the moment a standard monitoring system does not exist. Thus, an important step ahead in this area regards standardization and merging of these two sources of information, in order to reduce the amount of data to be stored and processed and to avoid dealing with different types of systems depending on the turbine manufacturer. A detailed review of these techniques and a throughout discussion on the possibilities of merging CMS and SCADA is provided in Article V.

5.3 Decision theory

Despite important steps ahead taken in the area of monitoring WTs, some key questions still need to be answered. AI-based systems in general can provide significantly improved and informed maintenance interventions. However, as any other new technology it becomes crucial for managers to assess the technical and economic risks against the benefit of implementing it. In case of wind farms, this provides the business tools for helping making decisions, in parallel with a fast growing market and large-scale deployment of offshore wind farms. In practice, most wind energy operators are indeed often reluctant in applying new technologies until their effectiveness is demonstrated in terms of costs and this article aims at providing further steps in this direction.

Therefore, after analyzing data and building prediction models, how is the derived information used for supporting decisions? Decision making is step subsequent to prediction. The basic concepts of decision theory are reported in this section, with the primary scope of is to provide an approach to quantify risks and benefits associated with implementing predictive systems, in the context of WT failures.

The theoretical aspects rearranged here are documented in detail in [74, 112, 113]. Decision analyses are employed for several different purposes, from feasibility studies, reassessment of structural integrity, cost-benefit analyses, decommissioning and so on. Decision problems are represented by decisions trees, when the system requires actions to be performed based on a rule, or an event tree, which models the occurrence of a series of events originating from a common event. The event tree lacks of decision nodes. A decision analysis is composed by the following steps

- Identification of decisions and outcomes ϑ. An outcome can have multiple attributes, which are associated to the risk of performing an action or taking a decision, and can vary depending on the applications. Attributes can be for instance cost, net profit, loss of life, lifetime, environmental impact and so on.
- Determination of the probability distribution $f(\vartheta) \mid \mathbf{a})$ conditional on the decision, action or event $\mathbf{a}$. This information is typically retrieved from data and it is possible to update the distributions based on new inference.
- Definition of a utility function $E(u)$, which maps the outcomes of the tree onto numbers.
- Computation of the total expected utility at each decision point as a function of the parameters of the tree.

New inference can come from experimental test or new observations. Often, the role of the decision analysis is also to quantify the benefit of an experimental test, and measure the benefit of the new information gained. To answer this question, the Value of Information is used.

With reference to Fig.5.1, the analysis of the tree concerns computing the expected utilities of all possible decision alternatives. The optimal point is the one providing the maximum expected utility. The optimal decision then, can be found as

$$\mathbf{a}_{opt} = \max_{\mathbf{a}} \mathbf{E}[u(\mathbf{a}, \vartheta) \mid \mathbf{a}] \tag{5.1}$$

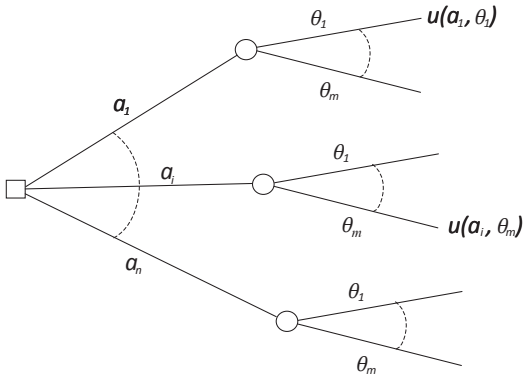

Figure 5.1: An example of decision tree with actions, parameters (or system state) and utilities.

where the expected utility if found by summing all over possible alternatives given a decision, which in the discrete case can be expressed as

$$\mathbf{E}[u(\mathbf{a}, \vartheta) \mid \mathbf{a}] = \sum_{j=1}^{m} u(\vartheta_j, \mathbf{a}) P(\vartheta_j \mid \mathbf{a}) \tag{5.2}$$

The utility function can be used to make cost-optimizations with respect to the system performance. In this thesis, only financial attributes are considered, but it is clear that multi-attribute analyses are not uncommon. Decision trees can be represented graphically through Bayesian networks. If a Bayesian network extended to include utility and decision nodes, it becomes an influence diagram.

5.4 Failure prediction

It has been discussed in Ch.1 that preventive maintenance does not account for the daily-to-daily variation of operational conditions. Thus, predictive maintenance is here deemed as a more suitable policy, especially for monitoring major wind turbine components, which are the main focus of this thesis.

Prediction, refers to the art of building models to predict yet unseen events. Predictive maintenance is being shaped by data mining and applications of AI for the industrial business. This process is well known as Big-data analysis. In the context of failure analysis, Big-data is a terminology introduced in the recent years to indicate the set of tools and techniques employed to mine data, eliminate repetitive data processing and extract information from it, with the ultimate goal to monitoring large amount of operating machines and reduce human interaction with these activities. The core of practicing Big-data lies in reducing to the essential information what appears to be a load of signals. Thus, reducing the input dimensionality also belongs to this world.

Recent research has focused on making predictive systems suitable for large scale applications. As discussed in [114], a condition monitoring system should be highly scalable, this means that human interpretation should be reduced at minimum when large scaled. Fig.5.2 shows the general framework of failure prediction here adopted, based on a CBM approach. In the scenario of a wind farm owner set about building data-driven models to predict and understand failures throughout its fleet, the flow starts from the identification of critical

malfunctions and decision of what type of predictive system to use. Note that this operation is only possible after some years of operations, when

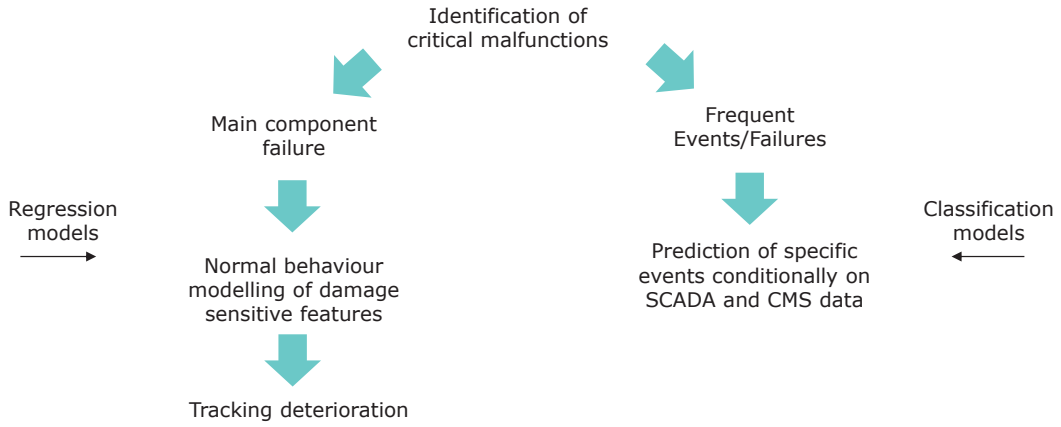

Figure 5.2: Failure prediction using classification and regression techniques.

Two most common machine learning paradigms as explained in Ch.4 are considered, namely regression and classification. These two approaches are exemplified through real applications of failure prediction, based on the following steps

- Identification of critical failure modes
- Data preparation
- Training prediction algorithms
- Decision analysis

With reference to Fig.5.2, the first type of prediction system used is based on regression models. The data-driven model is based on GLM described in Ch.4 to build a NBM of damage sensitive features. In the example provided in Article III, the inner-ring main bearing temperature is chosen to track the degradation of this component. The system is based on building a normal behavior model of the temperature and measure the deviations over time. These deviations are defined as

$$e = y - \hat{y} \tag{5.3}$$

where y and $\hat{y}$ are respectively the real measurement and the model prediction of the temperature. Thus, in order to quantify the PFA, a statistical description of the model deviations is needed. This is achieved by fitting a log-normal distribution to the signal. The Q-Q plot is shown in Fig.5.3 for different levels of the signal filtered through a moving average, in order to eliminate high frequency fluctuations. The plot shows the good agreement between the standard quantiles and those of the log-normal distribution.

An alternative type of prediction system is based on classification of SCADA alarms, which is based on the idea of predicting low-severity events to prevent severe events from happening. These latter are for instance failures of major components or sub-assemblies. The method

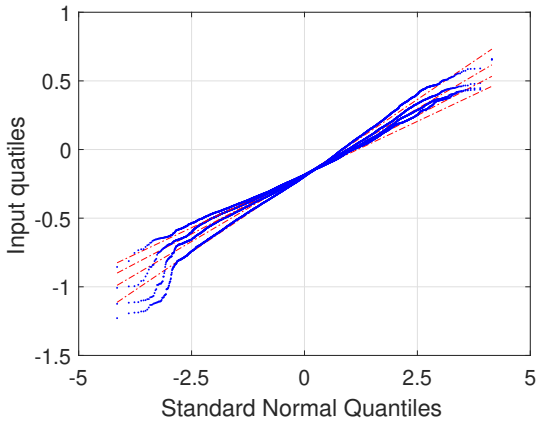

Figure 5.3: Q-Q plot of the log-normal distributed prediction residuals of the main bearing temperature NBM.

is based on a conjecture that the failure space is a subspace of the event space. Events are defined as normal shut-down due to SCADA alarms, which in the long run are indicative of multifunction leading to failure. Thus, it is assumed that the early prediction of these events prevents the main components from operating in critical conditions and void excessive damage. Fig.5.4 exemplifies this concept visually.

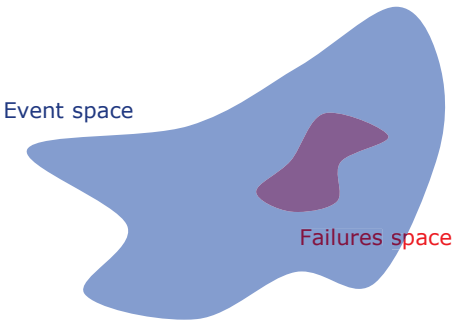

Figure 5.4: Visual concept of event space and failure subspace.

With reference to Fig.5.4, the definition of *event* and *failure* employed in Article II is based on recorded downtime associated to a certain shut-down event, as

- Donwntime $\leq$ 10 seconds = False alarm
- Donwntime $\geq$ 5 minutes = Event (E)
- Donwntime $\geq$ 10 days = Failure (F)

where with false alarm is intended a false in the SCADA alarm system, and should not be confused with false alarms from the classifier, quantified through the PFA. Based on this definition, the a description of the distribution of the SCADA parameters conditional on an event $f(X \mid E)$ and non-event $f(X \mid \bar{E})$ is given. The distribution in normal conditions,

corresponding to $f(X \mid \bar{E})$, is obtained by down-sampling the pool of data in normal conditions, this is to create a balanced dataset and avoid feeding the classifiers with unnecessary data, resulting in high computational time. It is important to notice that performing down-sampling must result in a satisfactory statistical representation of the PDF in normal behaviour, since this generally depends on the number of samples used.

The efficiency of intervention introduced in Article II and used in Article III, is a parameter that affects the probability of failure. If the early intervention is successful, the mechanical component does not fail. Thus, inefficiency means unsuccessful intervention, which turns into a residual probability of failure. In real applications, this parameter can be modelled through a Binomial distribution. Given the random variable $\xi \in [0, 1]$, the Binomial distribution describes the probability of k successes in n trials, $\xi \sim B(n, p)$ expressed as

$$P(\xi = k) = \frac{n!}{k!(n-k)!} p^k (1-p)^{n-k} \tag{5.4}$$

In this case, n is the number of events and k is the number of successful interventions and p the probability of success. Note that Eq.5.4 has a mean and variance, corresponding to

$$\mu(\xi) = np \tag{5.5}$$

$$\sigma^2(\xi) = np(1-p). \tag{5.6}$$

As explained in Ch.2, if n is sufficiently large, the Binomial distribution can be approximated with a normal distribution, which is used in this work. This probability can be updated when new information is available using Bayesian inference, by noting that the Beta distribution is a prior for the Bernoulli distribution.

In Article II, the choice best configuration of the classifier to be adopted can be made by quantifying how the efficiency at 4-hour should be to obtain the same utility of a system trained with 1-hour lead time data. This comparison is given by assuming the respective POD and PFA depending on the classifier adopted. The same comparison can be given in the POD-ξ plot as in Fig.5.6, which displays the 4-hour efficiency and POD locus resulting in the same utility of a 1-hour system. The FAR is in both cases fixed at 0.003 (10 min^{-1}). This plot can be further used by operators to calibrate their classifiers as function of efficiency and POD.

In the analysis presented in Article II, the average values of the cost parameters as well as performance of the predictive system are used. Thus, it may be further of interest to identify how the uncertainty in different parameters affects the final outcome. This question can be addressed by a sensitivity study on the net utility based on the variables listed in Tab.5.1 and their respective uncertainty. A log-normal distribution is adopted for some variables in order to have a positive range.

An arbitrary 5% uncertainty is assigned to $P(E)$, $P(F \mid E)$ and ξ, in order to show their probabilistic impact on the model. The results in Fig.5.5 are generated using a global sensitivity approach, by propagating the uncertainty of the input variables through the scalar output function via Monte Carlo simulations, and thus computing global sensitivity indexes, or first order Sobol indexes [115]. Given a scalar function $Y = f(X_1, \dots X_M)$, these indexes measure the contribution of each input variable X_j to the output variance as

Table 5.1: Numerical quantities for the cost model and associated coefficient of variation (CoV). The mean downtime was estimated from historical data (LN = lognormal, G = Gaussian, D = deterministic).

Name	Distribution	μ	CoV	Description
T_a [h]	LN	1	0.2	Time for intervention
T_d [h]	LN	617	0.55	Failure downtime
$\bar{P}_a$ [MWh/h]	G	0.97	0.2	Hourly mean production
C_r [€]	G	$25 \cdot 10^4$	0.05	Cost of replacement
C_l [€/h]	LN	33	0.2	Cost of labour
C_{el} [€/MWh]	G	100	0.2	Price of electricity
N_w [-]	D	3	-	Number of workers
$P(E)$ [-]	G	$4.7 \cdot 10^{-2}$	0.05	Probability of event
$P(F \mid E)$ [-]	G	$6.9 \cdot 10^{-3}$	0.05	Probability of failure
ξ [-]	G	0.5	0.05	Efficiency

$$S_{X_j} = \frac{\mathrm{Var}(E_{\mathbf{X}\sim j}(Y \mid X_j))}{\mathrm{Var}(Y)} \tag{5.7}$$

where $\mathrm{Var}(Y)$ is the total output variance. Further details can be found in [109].

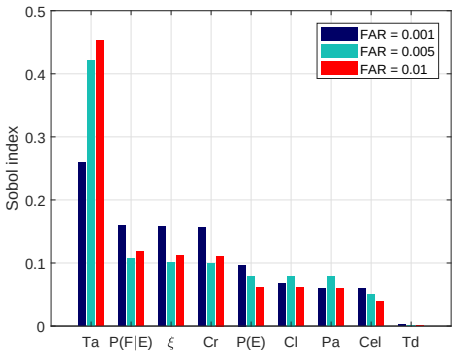

Figure 5.5: First order Sobol indexes of the net utility for different FAR.

Fig.5.5 shows that the net utility is most sensitive to uncertainties in the time for intervention, the probability of failure and the efficiency. As expected, the impact of T_a increases with FAR. The uncertainty in the downtime due to failure does not seem to have a relevant impact, as opposed to the hourly mean production loss $\bar{P}_a$. The sensitivity analysis shows that the uncertainty in these values has a significant impact on the final result.

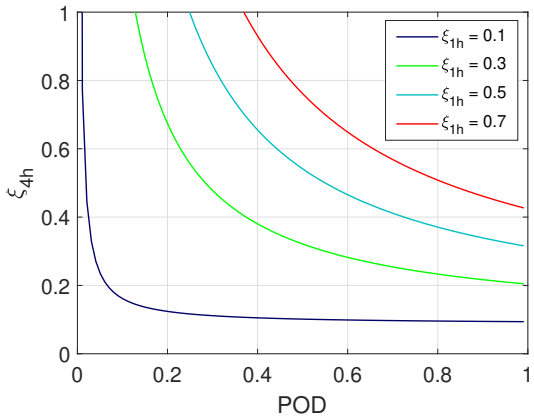

Figure 5.6: Expected utility as function of POD and efficiency of intervention.

Received 26 April 2016; | Revised 6 June 2016; | Accepted 6 June 2016

DOI: xxx/xxxx

ARTICLE TYPE

Predictive repair scheduling of wind turbine drive-train components based on machine learning

L. Colone*[1] | N. Dimitrov[1] | D. Straub[2]

[1]Wind Energy Department, Technical University of Denmark, Frederiksborgvej 399, 4000 Roskilde, Denmark

[2]Engineering Risk Analysis Group, Technical University of Munich, Theresienstr. 90, 80333 Munich, Germany

Correspondence

*L. Colone Email: lcol@dtu.dk

Present Address

Technical University of Denmark, Frederiksborgvej 399, 4000 Roskilde, Denmark

We devise a methodology to predict failures in wind turbine drive-train components, and quantify its utility. The methodology consists of two main steps. The first step is the set-up of a predictive model for shut-down events, which is able to raise an alarm in advance of the fault-induced shut-down. The model is trained on data for shut down events retrieved from the alarm log of an offshore wind farm. Here it is assumed that the timely prediction of low-severity events, typically caused by abnormal component operation, allows for an intervention that can prevent premature component failures. The prediction models are based on statistical classification using only supervisory control and data acquisition (SCADA) data. In the second step, the shut-down prediction model is combined with a cost model, to provide an estimate of the benefits associated with implementing the predictive maintenance system. This is achieved by computing the maximum net utility attainable as a function of the model performance and efficiency of intervention carried out by the user. Results show that the system can be expected to be cost-effective under specific conditions. A discussion about potential improvements of the approach is provided, along with suggestions for further research in this area.

KEYWORDS:

Wind turbine failure, Predictive maintenance, SCADA data analysis, ROC curve, Event tree, Utility function.

1 | INTRODUCTION

The cost of Operation and Maintenance (O&M) of wind power plants is having a significant effect on the levelized cost of energy (LCOE)[1,2]. A key challenge in O&M management is achieving a reliable prediction of mechanical failures. This could enable a better understanding of deterioration mechanisms and provide benefits by allowing a sufficient lead time for making decisions. Early prediction of failures would be especially beneficial for offshore wind farms, where remote location and harsh oceanic weather often impede their accessibility.

The rapid advancements of intelligent data management coupled with large volumes of data[3] have potential for improving maintenance activities on wind turbines (WTs), allowing for more informed and timely decisions. Maintenance based on real-time health assessment of mechanical components is an alternative to more traditional preventive actions[4]. This type of predictive policy is already well established in several industrial fields, known as condition-based or predictive maintenance[5,6]. Detailed analyses on historical O&M costs demonstrate that innovations in this field together with effective offshore operational and logistic strategies can have a high impact in terms of reduction of the LCOE[1].

Modern multi-megawatt wind turbines are equipped with SCADA and vibration based condition monitoring systems, which generate valuable data streams that can be exploited to support maintenance decisions. The analysis of these data received a growing interest in recent years, along with the gain in popularity of data-driven techniques based on regression models of damage-sensitive parameters. A review of these methodologies is provided in e.g.[7,8]. Here we focus on the use of statistical classification for optimizing repair activities in wind turbines.

Statistical classification is commonly used for predictive maintenance. In aerospace, Loyer et al.[9] use machine learning algorithms and parametric techniques for intelligent maintenance scheduling of jet engine sub-components. Cai et al.[10] use support vector machines and association rule mining for fault diagnosis of marine diesel engines. In the area of fault prediction for WTs, Bach et al.[11] implement supervised deep convolutional neural networks to successfully classify acceleration spectral data to detect faults in WT bearings and helical gear-boxes. Their algorithms predict failures long in advance, in the order of several months. In the same work, receiver operator characteristic (ROC) curves are used to quantify the performance of binary classifiers. Another recent study on WTs by Koukura et al.[12], implements decision trees to classify vibration features of faulty WT gears.

Besides the above listed examples applied to real failures, the prediction of warnings is regarded as an alternative monitoring approach (Leahy et al.[13]). Since mechanical failures are generally associated with multivariate processes, which can be treated via a sensor data-fusion[14], the idea of the present study is to capture the information contained in the full set of SCADA data available close to an observed fault-induced event, in order to predict future occurrences of the same type of event. A fault-induced event is defined as an occurrence that leads to a complete turbine shut-down. The fault-induced events considered in this study will be simply referred to as events.

Overall, a significant amount of research has been carried out in the area of monitoring WT components, mainly on improving the performance of prediction models. However, limited effort has been devoted to understanding whether their online implementation can produce cost-effective output, which is the main question of this study. This assessment can be achieved by means of decision analysis tools, which are here used in combination with intelligent condition monitoring. An example of this applications is provided by Colone et al.[15] for normal behaviour models of main mechanical components.

The procedure consists of two main steps: first, a classification technique is derived for early prediction of events, and second, a cost analysis is proposed aimed at demonstrating the potential economic benefits of implementing the predictive maintenance system. The second step involves investigating the optimal configuration of the classifier as a function of performance and efficiency of intervention carried out by the user in case of an alarm triggered by the trained classifier. The problem is similar to other risk engineering applications,[16,17], from which the present approach has drawn inspiration. The main goal of this study is the understanding how available WT data could be used to prevent the occurrence of critical sub-system failures of WTs, along with providing the tools for an economic assessment of the system performance.

The article is organized as follows. Section 2 explains the background and motivation of the work. The methodology section introduces the procedure starting from a description of the variation of the dataset near an event, assumptions, data processing and cost analysis. The latter is based on a decision tree model where ROC curves are used as input performance metric. Results are presented in terms of the maximum net utility obtained. The final section provides a discussion about how operational conditions may increase the risk of failures along with improvements to be addressed in future research.

2 | BACKGROUND AND PROBLEM DEFINITION

Wind farm operators and owners have to deal with different types of failures, depending on the installed capacity of the wind farm, turbine size, site specific environmental conditions, component manufacturer and other factors[18]. Failure of main mechanical components such as e.g. gearbox, main bearing and generator typically lead to significant repair or replacement time. For this problem, data-driven procedures already exist, to track changes in damage-sensitive features based on regression techniques, e.g. normal behaviour modelling[19]. These techniques have been used successful for several failure modes[20]. An additional source of information present in the SCADA data are the component and turbine status alarms, which are here reffered to as events. The occurrence of events results in a shut-down due to certain parameters reaching their operational limit, which is typically set based on the operator's experience, by the component manufacturer or based on other considerations. Although these events are not necessarily severe in terms of downtime and maintenance action, their repeated occurrence in time anticipates, or can be related to, more important failures of major components.

A conjecture used in this study is that the failure space is a subset of the event space, i.e. every failure is preceded by a series of events, and that the timely prediction of these events may help prevent the occurrence of important failures. This means that valuable information is contained in the warning records, which are more numerous than the failure records and thus more suitable for classification and other machine learning techiques. Before model training, a preliminary analysis on the variation of the SCADA data, by comparing their distribution conditionally to an alarm, can provide a first insight into the usefulness of the classification approach as well as a physical interpretation of the operational conditions that led to the issuing of the alarm.

The term alarm in the context of the decision analysis presented below is referred to as the early prediction of an event based on the classification technique developed in this study. This prediction happens by training the classifier with data preceding the occurrence of the shut-down. The shut-down and a potential corrective intervention are associated with a certain downtime, dependent on the damage severity. Thus, the definition of failure is based on the duration of the downtime, as will be clarified in the following.

3 | DATA DESCRIPTION

The data used for the numerical investigation were collected from a large offshore wind farm comprising circa 100 turbines, over a period of 5 years. This period corresponds approximately to the entire operational life of the farm up to the time of the study. The SCADA dataset consists of 48 tags containing 10-minute average records. The data were filtered to select relevant operational conditions by deleting periods of inactivity corresponding to negative and zero active power as well as recording errors. The wind speed is recorded by nacelle anemometers placed on each turbine.

The warning system of the WTs under consideration is based on thresholds set on specific control parameters. Warnings are retrieved from the alarm-log of the wind farm, which was also available for the present study. For the type of system installed, the selected warnings can be considered as indicators of abnormalities in main components. When a parameter reaches its design threshold, the component may experience higher degree of deterioration if the turbine keeps operating in these critical conditions. Events related to main component malfunctions, such as gearbox, generator and generator bearings, were considered. More specifically, the description of the events identified as critical include high gear-oil temperature, gear-oil level too high or too low, unstable gear-oil pressure, low gear water level, high generator bearing temperature, high generator slip-ring temperature, and generator water temperature too high. The recorded events are categorized in Tab.1 in terms of associated and maintenance action performed. In the absence of historical information on the type of maintenance action performed, the latter has been deduced from the associated downtime.

TABLE 1 Number of events categorised according to the associated downtime.

Downtime	Number of events	Category
$\geq$ 5 min	1910	Automatic restart
$\geq$ 1 day	90	Manual restart
$\geq$ 3 days	28	Minor repair
$\geq$ 10 days	14	Major replacement

Events associated with a downtime greater than 10 days are defined as failures, where it is assumed that a major replacement of at least one sub-component among the ones analysed was performed in practice. Similar considerations were made in [21].

4 | METHODOLOGY

We develop a methodology to predict event data based on statistical classification, and derive the optimal configuration of the classifier based on a decision analysis. Statistical classification is a supervised learning technique, which uses a function to map a set of instances $\mathbf{x} \in \mathcal{X}$ onto one of the class labels $y \in \{0, 1, \dots K\}$, where K is the total number of classes and $\mathcal{X}$ the feature space. As opposed to hard classifiers based on optimal decision rules, probabilistic classifiers explicitly produce a continuous class membership probability of the instance $P(y = j \mid \mathbf{x})$. In binary classification the class vector becomes $y \in \{0, 1\}$, where $y = 0$ and $y = 1$ here indicate respectively a normal condition and an event. In the present study, two types of classifiers are used: a Naïve Bayes (NB) classifier, and a Neural Network (NN). The NB classifier is conceptually easy and computationally inexpensive, even for a large number of predictors. NN classifiers require more efforts to set up, but are versatile and can provide good performance in a wide range of applications. The theoretical background on classification briefly summarized here can be found in more details in e.g. [22,23,24].

In this section, $k \in \{1 \dots K\}$ is used for indexing the class number, $i \in \{1 \dots N\}$ is used for indexing the observation where N is the total number of observations per feature, $j \in \{1 \dots M\}$ is used for indexing the feature number, where M is the total number of features.

4.1 | Class distributions

In general, the performance of a classifier depends on the discriminatory power between the classes, which can be quantified by computing the statistical difference between two conditional probability density functions (PDFs) of the SCADA parameter, conditional on normal condition and

on the occurrence of an event. This measure is here chosen as the relative entropy between the two PDFs, the Kullback-Leibler divergence (KLD)[25]. The two conditional distributions are $s(x) \coloneqq p(X \mid y = 1)$ and $q(x) \coloneqq p(X \mid y = 0)$ estimated by Eq.4, and the KLD is

$$\mathrm{KLD}(s \mid\mid q) = \int_{-\infty}^{\infty} s(x) \log\Big(\frac{s(x)}{q(x)}\Big)\, dx. \tag{1}$$

Other distance measures could be also used such as density overlap or in case of normally distributed variables the Fisher's ratio, as in[26]. The KLD does not only account for the class overlap, but also the different shape of the distributions compared.

4.2 | Kernel-based Naïve Bayes classifier

A simple way to take into account multiple input variables is to assume that they are conditionally independent given their membership class y, which is the main assumption behind the NB classifier. Although this hypothesis is obviously not fulfilled in practice, the NB classifier nevertheless often performs satisfactorily. A sketch of the NB network is displayed Fig.1. From the conditional independence assumption, the joint probability of $\mathbf{x}$ conditional on y is computed as

$$P(\mathbf{x} \mid y = k) \prod_{j=1}^{M} P(x_j \mid y = k) \tag{2}$$

Recalling Bayes' rule, the class-conditional probability can be expressed as

$$P(y = k \mid \mathbf{x}) = \frac{P(y = k)P(\mathbf{x} \mid y = k)}{P(\mathbf{x})} \tag{3}$$

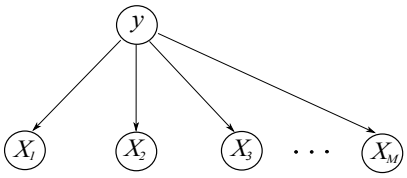

FIGURE 1 A Naïve Bayes' network. The features are conditionally independent given the class.

In Eq.2 and 3, $\mathbf{x} = \{x_1, x_2, \ldots, x_j, \ldots x_M\}$ is the instance feature vector. The class-conditional PDFs can be described in some cases by parametric distributions. However, when data do not respect such condition, non-parametric kernel densities should be employed[27]. Given a feature j of N observations $X = \{x_{j1}, x_{j2}, \ldots, x_{ji}, \ldots x_N\}$, its univariate kernel density estimate $\hat{p}(x)$ can be expressed as

$$\hat{p}(x) = \frac{1}{Nh} \sum_{i=1}^{N} \varphi\Big(\frac{x_j - x_{ji}}{h}\Big) \tag{4}$$

where $\varphi(\cdot)$ is the kernel base function taken here as Gaussian[23], and h the bandwidth parameter selected according to[28]. The NB classifier directly computes a class membership probability.

4.3 | Neural network classifier

The high flexibility of NN is in their ability to model nonlinear complex relationships between input and output, categorical or continuous. NN is here used for prediction purposes. A single hidden layer architecture is used, wherein the number of hidden nodes is set as the average number between input and output nodes. This choice, which is common in NN-based machine learning[24], is based on testing different configurations and engineering judgment. Fig.2 shows the structure of the network adopted.

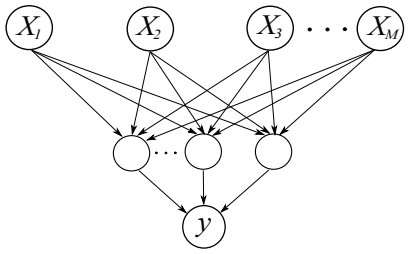

FIGURE 2 A Neural network configuration for binary classification with one input layer, one hidden layer and one binary output layer.

The probabilistic output of the network is obtained in this case by a logistic sigmoid activation function on the binary output layer [22,29]. The logistic function $\sigma(\alpha)$ is a nonlinear transformation of the activations α, Eq.5:

$$\sigma(\alpha) = \frac{1}{1+e^{-\alpha}} \tag{5}$$

The resulting output of the two-layer network can be interpreted as a class membership probability, expressed as

$$P(y = k \mid \mathbf{x}) = \sigma(\mathbf{w}_1^T \tanh(\mathbf{w}_0^T \mathbf{x} + \mathbf{b}_0) + \mathbf{b}_1) \tag{6}$$

where $\mathbf{w}$ are the network's weights, $\mathbf{x}$ the instance feature vector and $\mathbf{b}$ are constant vectors. Note that Eq.6 can be interpreted as the class membership probability $P(y = 1 \mid \mathbf{x})$, where $P(y = 0 \mid \mathbf{x}) = 1 - P(y = 1 \mid \mathbf{x})$ [22]. A multilayer feed-forward NN algorithm for binary classification is used.

Training a network consists of minimizing the error function and estimating the parameters $\mathbf{w}$ and $\mathbf{b}$. Note that by definition the class membership probability is given by a Bernoulli distribution [22], as

$$p(y \mid \mathbf{w}, \mathbf{x}) = \hat{y}(\mathbf{w}, \mathbf{x})^y (1 - \hat{y}(\mathbf{w}, \mathbf{x}))^{1-y}. \tag{7}$$

Thus, for classification, a cross-entropy error function is employed, Eq.8.

$$E(\mathbf{w}) = -\sum_{i=1}^{N} \Big(y_i \ln(\hat{y}_i(\mathbf{w}, \mathbf{x})) + (1 - y_i) \ln(1 - \hat{y}_i(\mathbf{w}, \mathbf{x})) \Big) \tag{8}$$

The trainig optimization problem is solved by backpropagation, using the deep learning tools described in [30].

4.4 | Training process

The training process is sketched in the flow chart of Fig.3. The data are first filtered and normalized to zero mean and unit variance. Afterwards, normal and event records in the form of class labels defined in the previous sections are synchronized with SCADA data. The classifiers are trained using data points picked before the real event record, to understand whether it is possible to obtain an earlier prediction of the event. Two time lags are chosen, 1 hour and 4 hours. These time lags will be referred to as lead times in the remainder of the paper. The lead time is introduced to understand whether the SCADA dataset manifests a certain degree of variation earlier than the actual adverse event, which could be exploited to issue a timely warning. These specific values are assumed to be sufficient for the component to avoid excessive damage, by stopping the turbine earlier than the actual shut-down and perform an online intervention. Whether this assumption is true in real life cannot be retrieved from the information available for the present study. By proceeding in this way, it is important to make sure that consecutive events occur at intervals greater than the selected lead times.

Since normal operation observations outnumber event data, random down-sampling without replacement is applied to reduce the normal operation pool of data from approximately 30 million to 1 million data points. The PDFs of the predictors are compared before and after down-sampling, to verify that this operation does not introduce any loss of information. Another reason to apply down-sampling at this stage is to improve computational efficiency during training and to allow for a faster data handling while retaining the statistical information of the complete dataset. Data falling into the 98$^{\text{th}}$ percent confidence interval of their Mahalanobis squared distance D^2 [31], are considered as normal behaviour data (Eq.9).

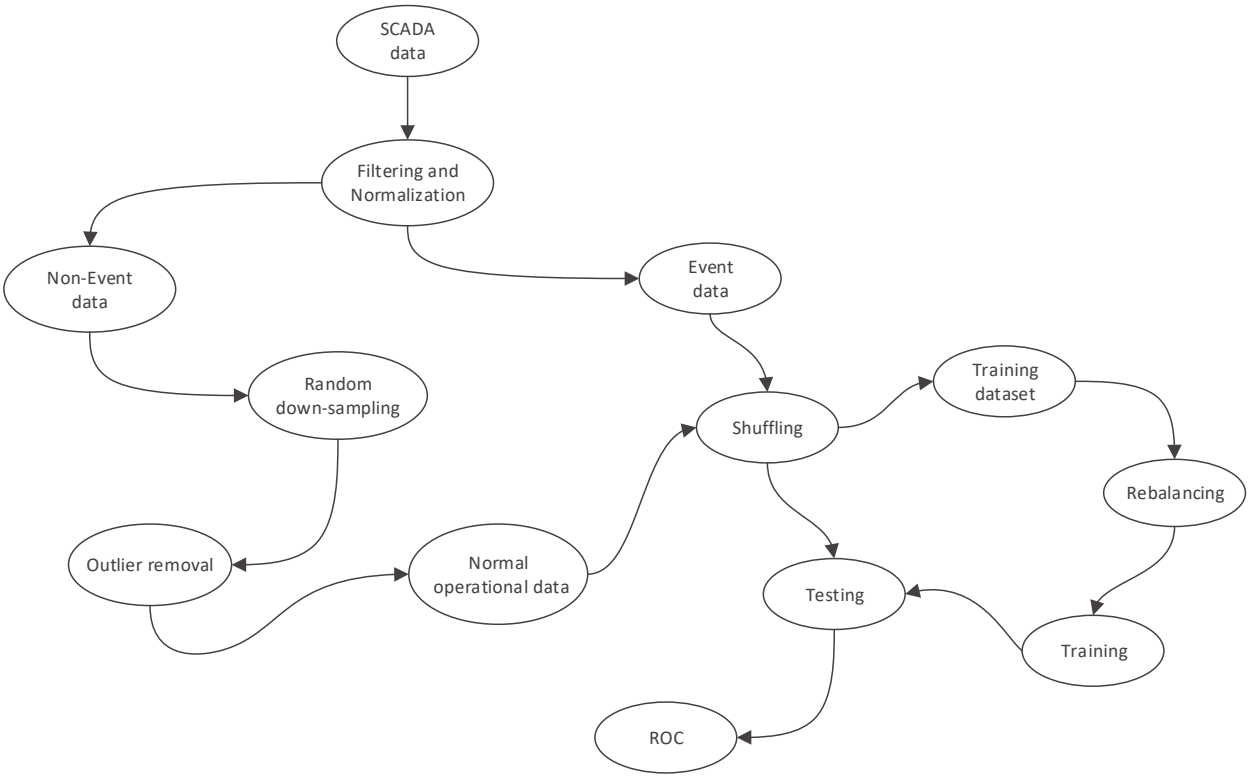

FIGURE 3 Summary of the SCADA processing flow from the database to training and testing.

A similar approach for selection of data in normal operation was used in[32]. This filter helps to remove outliers as well as other fault-induced observations not considered in this study.

$$D^2 = (\mathbf{x} - \mu_{\mathrm{x}})\Sigma_{\mathrm{xx}}^{-1}(\mathbf{x} - \mu_{\mathrm{x}}) \tag{9}$$

In Eq.9, μ_{x} is the mean of the observation vector and Σ_{xx} the correlation matrix of the dataset. The entire dataset is then randomly shuffled, to redistribute the class labels uniformly within the dataset. This is equivalent to assuming that for training the classifiers, events are independent of each other. In the records it was found that consecutive events are more likely to happen than a single event within days, weeks or months from each other. Therefore, a more accurate modelling would require to take into account the correlation in time of these events. However, this would imply the modelling of the conditional probability of consecutive events, which would require a greater amount of observations. The lack of extensive event data thus motivates the independence assumption.

The data points are picked before shuffling, since the latter breaks the chronological order of the data. The dataset is split into 90% for training the model and 10% for blind testing. This operation is repeated 10 times where the two batches of 90% training and 10% test data are randomly selected. At this step, random shuffling ensures that the number of event data in the testing dataset is comparable for each holdout, to avoid misinterpretations due to the different number of events. Further down-sampling to normal data is applied in order to rebalance the classes to a ratio 20% of $y = 1$ to 80% of $y = 0$,[29,33]. This ratio is specifically chosen to be able to explore the sensitivity of the classifier in the low false alarm rate (FAR) region. Likewise, a test on the PDF before and after down-sampling was performed. This procedure generates an ROC curve for each holdout, with the aim to provide an estimate of the uncertainty in the prediction and be able to assess the performance of different models. A 5-fold cross validation (CV) is applied during model training to prevent overfitting.

4.5 | Performance measures

ROC curves are used to measure the performance of the algorithms, which is a suitable metric for binary classification [34]. It is obtained by varying the threshold to the predicted class posterior probabilities. The following statistical performance measures can be calculated

$$\begin{aligned} sensitivity &= P(\hat{y} = 1 \mid y = 1) = \mathrm{POD} \\ specificity &= P(\hat{y} = 0 \mid y = 0) = 1 - \mathrm{FAR} \end{aligned} \tag{10}$$

where the variable $\hat{y}$ is the estimated class label, the quantity $1 - specificity$ is the false alarm rate (FAR) and $sensitivity$ corresponds to the probability of detection (POD). The ROC curve displays the POD against FAR. A scalar quantity used to summarise the information contained in an ROC plot is the area under the curve (AUC), which corresponds to the probability of ranking randomly chosen positive instances higher than negative ones. The AUC of a random classifier is 0.5, resulting from a straight line in the ROC plot. Any useful classifier must perform higher than this value. However, the AUC alone is not a sufficient summary of performance. In fact, a classifier with a high AUC may still perform poorly in some regions of interest for specific cases. The selection of the optimal parameters of the ROC curve and thus the threshold value is made according to a cost analysis by specifying the utility as function of the performance metrics, as presented in the following.

4.6 | Decision analysis

The scope of the decision analysis is to devise a criterion for deciding on whether or not to use the SCADA-based predictive system and to identify the optimal configuration of the classification algorithm. This is achieved by a simple cost model based on an event tree. We denote with E the events and with F the event of a failure. The occurrence of an event would eventually trigger a shut-down by the default warning system, and the role of the classifier is to issue an early prediction of this event. This early alarm is indicated as A. The analysis is performed on an hourly basis. N_E is the observed number of events corresponding to categories 1 to 4 in Tab.1, N_F is the observed number of failure events corresponding to category 4 in Tab.1 and $N_y = 5$ is the number of operational years for which data are available. $P(E)$ and the conditional $P(F \mid E)$ are estimated as

$$P(E) \approx \frac{N_E}{8760\ N_y}, \qquad P(F \mid E) \approx \frac{N_F}{N_E}, \tag{11}$$

where 8760 is the number of hours in a year. The event tree illustrated in Fig.4 explores the entire space of possible sequences resulting from the occurrence of a warning and models the action to reduce or mitigate the consequences of the initiating event. Fig.4 also shows the influence diagram associated to the event tree, which explains the relationships between alarm A, event E and failure F as well as the associated costs. The event tree assumes a fixed decision policy, which consists of stopping the turbine and performing an intervention whenever the system raises an alarm and the user performs an intervention. No action is performed in case of no alarm $\bar{A}$.

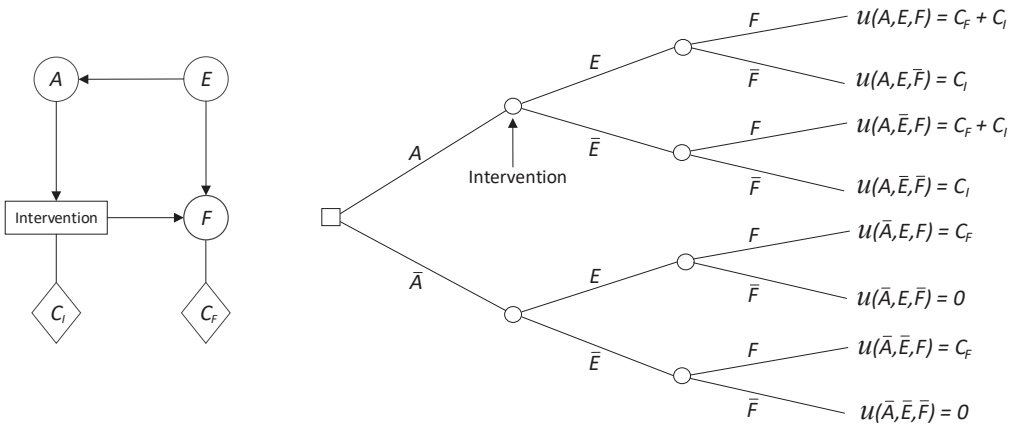

FIGURE 4 Influence diagram and event tree for the risk analysis of the classification system.

When the turbine stops, the operator proceeds to check if the operational data can provide evidence of malfunction, resulting in a positive or negative occurrence of the event. A utility function $u()$ is associated with each outcome of the tree. The only attribute considered in this study are economic losses. Therefore, with reference to Fig.4, the utilities are

$$\begin{aligned} u(A,E,F) &= C_F + C_I & u(\bar{A},E,F) &= C_F \\ u(A,E,\bar{F}) &= C_I & u(\bar{A},E,\bar{F}) &= 0 \\ u(A,\bar{E},\bar{F}) &= C_I & u(\bar{A},\bar{E},F) &= C_F \\ u(A,\bar{E},F) &= C_F + C_I & u(\bar{A},\bar{E},\bar{F}) &= 0 \end{aligned} \tag{12}$$

The intervention cost C_I and failure costs C_F in Eq.12 are estimated as

$$\begin{aligned} C_I &= N_w\, T_a\, C_l + T_a\, \bar{P}_a\, C_{el} \\ C_F &= C_r + T_D\, \bar{P}_a\, C_{el} \end{aligned} \tag{13}$$

The cost of failure is equal to the replacements costs C_r plus the power loss due to downtime, where $\bar{P}_a$ is the average power loss, C_{el} the price of electricity and T_D the downtime due to failure. T_a is the time for an online analysis after an alarm when the turbine is stopped, C_l the price of labour and N_w the total number of workers employed in the analysis. More accurate analyses could also include the material cost for the online intervention, if any. Numerical values and description of the quantities in Eq.13 are reported in Tab.3 in the result section.

The discrete branch probabilities are computed according to the conditional probability rule, as expressed in Eq.14 for one of the branches.

$$P(A \cap E \cap F) = P(F \mid E \cap A)\; P(E \mid A)\; P(A) \tag{14}$$

A failure is a subset of the event space, hence $P(F \mid \bar{E}) = 0$. It follows that $P(A \cap \bar{E} \cap F) = 0$ and $P(\bar{A} \cap \bar{E} \cap F) = 0$. The potential outcomes (success or failure) of the mitigation action are modelled by introducing an efficiency function. The probability of failure conditional on E and the alarm A, which systematically implies an intervention (see Fig.4), are expressed as a function of the efficiency as

$$P(F \mid E \cap A) = P(F \mid E \cap \bar{A})\; (1 - \xi) \tag{15}$$

where the efficiency $\xi \in [0, 1]$ reduces the probability of failure linearly from 0 to 1. For $\xi = 1$, the probability of failure after intervention is 0. For $\xi = 0$, the probability of failure stays $P(F \mid E \cap \bar{A})$. The remaining conditional probabilities in Eq.14 can be derived from Bayes' rule and expressed as a function of the POD and FAR, as

$$P(E \mid A) = \frac{P(A \mid E)\; P(E)}{P(A)} = \mathrm{POD}\frac{P(E)}{P(A)} \tag{16}$$

$$P(E \mid \bar{A}) = \frac{P(\bar{A} \mid E)\; P(E)}{P(\bar{A})} = (1 - \mathrm{POD})\frac{P(E)}{P(\bar{A})} \tag{17}$$

and likewise

$$P(\bar{E} \mid A) = \mathrm{PFA}\frac{(1 - P(E))}{P(A)} \tag{18}$$

where $P(\bar{E}) = 1 - P(E)$, $P(\bar{F}) = 1 - P(F)$ and the probability of false alarm (PFA) is approximated by FAR times 1 hour. For a discrete event probability tree, the expected utility is found as the sum of the utilities times the probability of occurrence of the respective branches over all possible consequences. The expected utility given the adoption of the monitoring system can be thus obtained, Eq.19.

$$\begin{aligned} &E[U \mid \text{system}] = P(F \mid E)(1-\xi)P(E)\mathrm{POD}(C_F + C_I) + \Big[1 - P(F \mid E)(1-\xi)\Big]P(E)\mathrm{POD}(C_F + C_I) + \\ &+ (1 - P(E))\mathrm{PFA}C_I + P(F \mid E)P(E)(1 - \mathrm{POD})C_F = \\ &= P(F \mid E)P(E)\mathrm{POD}(C_I\xi + C_F) + (1 - P(E))\mathrm{PFA}C_I + P(F \mid E)P(E)C_F \end{aligned} \tag{19}$$

Not implementing the classifier has also an associated utility, which corresponds to the positive cost of failure times its probability of occurrence, when no intervention is performed, expressed by Eq.20.

$$E[U \mid \text{no system}] = P(F \mid E)P(E)C_F \tag{20}$$

Therefore, the net utility is defined as the difference between Eq.19 and Eq.20, as

$$U_{net} = E[U \mid \text{system}] - E[U \mid \text{no system}] \tag{21}$$

Note that Eq.21 is linear in the efficiency. Since the net utility in Eq.21 can be expressed as function of POD and FAR, the maximum net utility attainable from the classifier, for a given efficiency ξ can be obtained as

$$U_{net,max}(\xi) = \max_{\text{POD,FAR}\in\text{ROC}} E[U(\text{POD}, \text{FAR}, \xi)] \tag{22}$$

where the maximization is over all pairs of POD and FAR as defined by the ROC curve.

5 | RESULTS

The KLD plot of the SCADA dataset in Fig.5 reflects the changes in the environmental and operational parameters close to an event. The larger the KLD, the larger the relative change in the distribution with the occurrence of the event. Fig.5 shows that the PDFs of many parameters before the event differ from the respective normal operation PDFs. This behavior is observed for the 10-minute mean values but also for the standard deviations of some environmental parameters. The KLD of the dataset provides an initial assessment of the data and helps understanding whether this information can be used for classification.

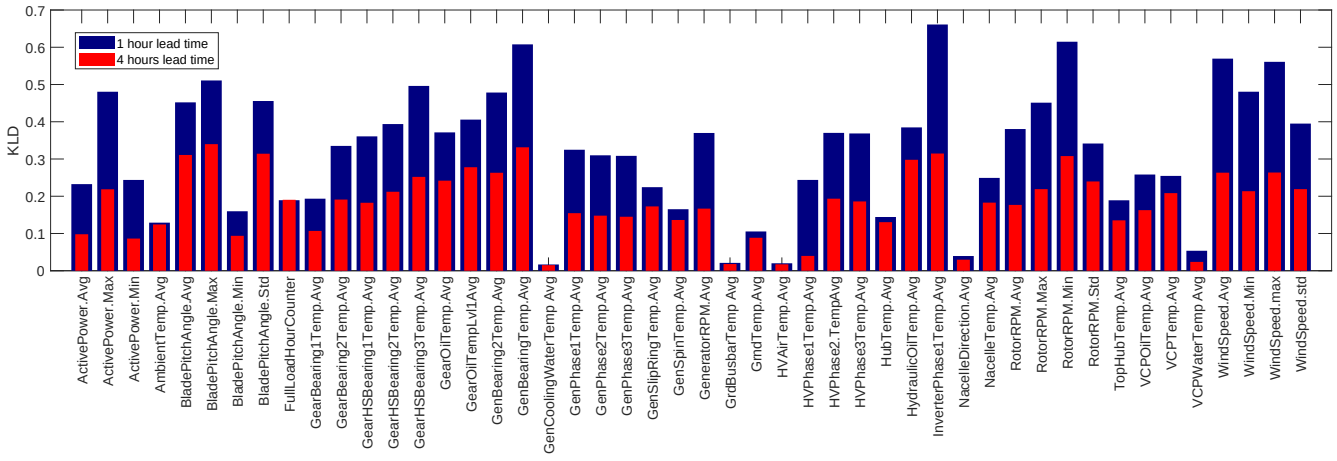

FIGURE 5 Kullback-Leibler distance (KLD between distributions in normal conditions and prior to an event, with different lead times.)

The wind speed statistics close to an event, as shown in Fig.6 and 7a, manifest an increase compared to normal operation. This indicates that these events are associated with operational conditions on average more demanding than normal operation, driven by stronger inflow conditions. The results are in agreement with findings of recent studies [18], where the impact of environmental conditions such as relative humidity, turbulence and temperature variations was found to contribute to the overall turbine reliability, especially of main components such as gearboxes. However, the dataset used in the present study did not comprise other environmental parameters than ambient temperature and wind speed. Note that Fig.6 to 8 refer to normalized quantities with zero mean and unit variance, for confidentiality reasons.

From the comparison between the PDFs it can be inferred that the events are more likely to occur around the rated wind speed, and the wind speed statistics such as minimum, maximum and standard deviation are also higher than average. Turbulence carries the contribution of free stream and farm wakes. Moreover, the picture of the operational conditions of the faulty turbines may suggest that these events mostly occur during power curtailment as inferred for instance by the distributions of the full load hour counter and active power in Fig.7c. Given the wind speed conditions shown in Fig.6a, the turbines should be expected to operate in the design full load region.

Other environmental factors such as the mean ambient temperature do not seem to show significant differences. Internal parameters such as specific components and oil temperatures show higher mean value, see Fig.8, which confirms that the turbines are operating under stressed conditions. This also plays a role in the performance of the prediction algorithms.

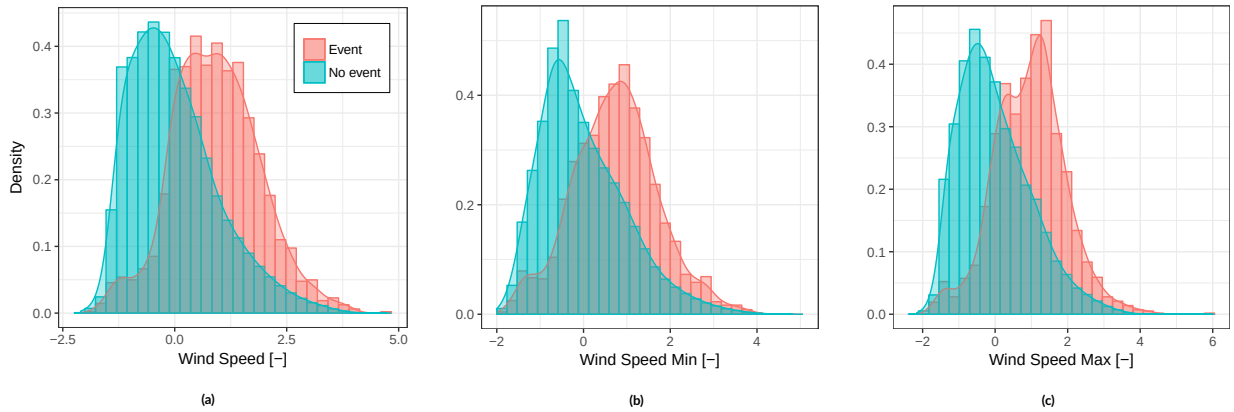

FIGURE 6 Distributions of mean wind speed, maximum and minimum in normal operation 4 hours before an event. Quantities are normalised to zero mean and unit variance in normal conditions. The KLDs are respectively 0.28, 0.24, 0.28 from left to right.

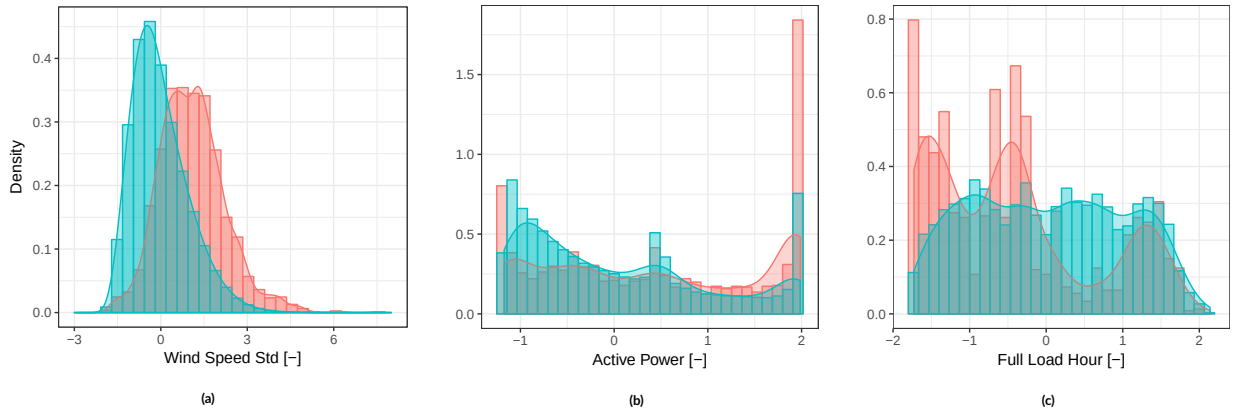

FIGURE 7 Distributions of turbulence, active power and full load counter in normal operation 4 hours before an event. Quantities are normalised to zero mean and unit variance in normal conditions. The KLDs are respectively 0.23, 0.09, 0.19 from left to right.

The next analysis concerns the training of the classifiers. In terms of predictions, some features could be removed out because of redundancy. However, variable selection and model reduction were not performed here, since the computational performance is not an objective of the present study, but rather a comparison between techniques and demonstration of a cost analysis. Fig.9,10 highlight important differences in the classifiers in terms of performance. It is clear from Fig.5 that 4 hours before an event the SCADA parameters show less variation from the normal conditions than 1 hour before an event, resulting in poorer performance of both algorithms for this lead time. Furthermore, the ROC curves show that NN is able to provide less uncertain predictions than NB. This consideration is useful in practice, since it allows an evaluation of the confidence level of the prediction model adopted. Tab.2 is a summary of the performance measures, where AUC is determined from the average ROC curve computed from testing data of each of the 10 hold-outs.

TABLE 2 Performance table of the different classifiers at different lead times.

Lead time	AUC
1 hrs NN	0.947
4 hrs NN	0.867
1 hrs NB	0.854
4 hrs NB	0.771

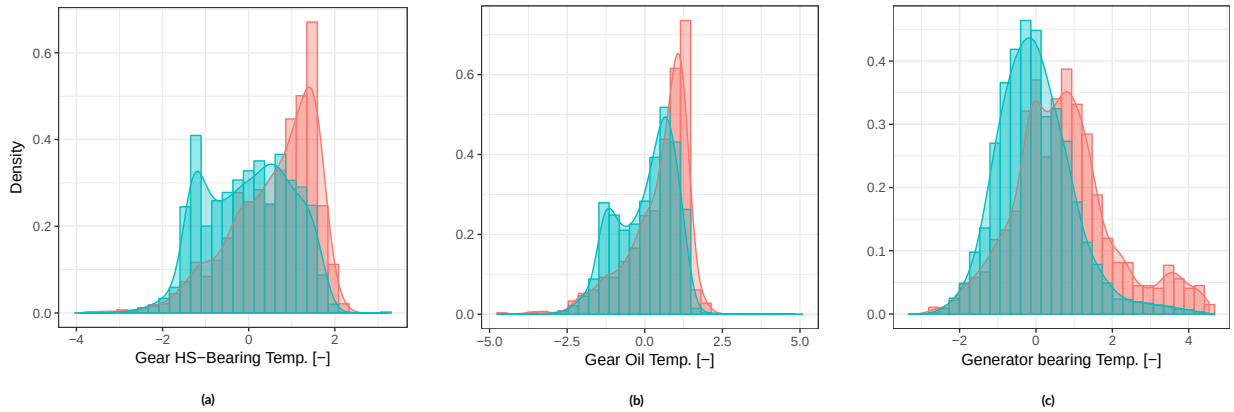

FIGURE 8 Distributions of high speed bearing, gear oil and generator bearing temperatures in normal operation 4 hours before an event. Quantities are normalised to zero mean and unit variance in normal conditions. The KLDs are respectively 0.18, 0.25, 0.33 from left to right.

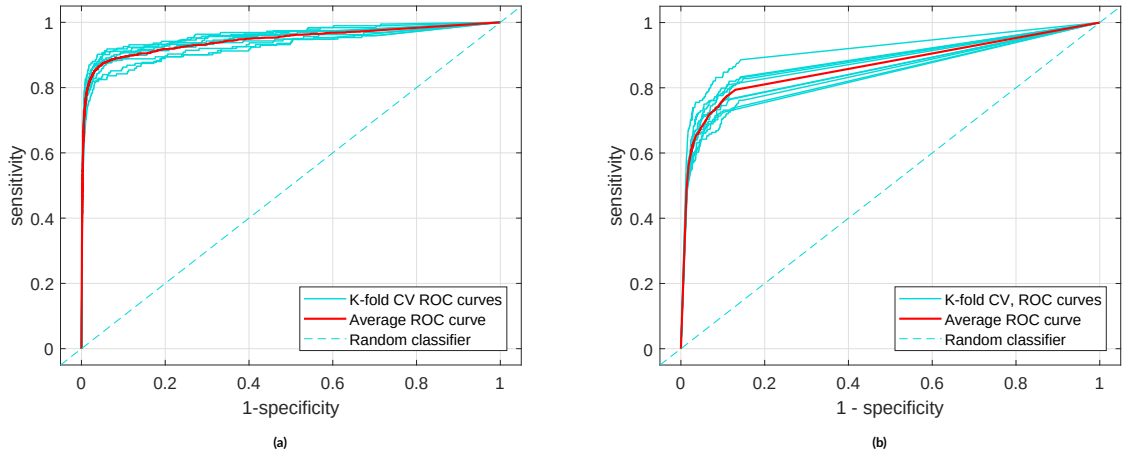

FIGURE 9 Cross validated and average ROC curves for obtained by using 1 hour shifted back in time data for NN (left) and NB (right).

Tab.3 lists the numerical parameters used in the cost model. The downtime T_d is obtained directly from data. It is assumed that the lost power production corresponds to the mean production per turbine per hour $\bar{P}_a$, estimated by the available annual power production data of a reference year. Note that this is an actual value, which is lower than the one obtained by estimating the theoretical annual energy production per turbine. The price of electricity C_{el} is taken from [35]. The cost of replacement C_r is taken as the average cost of replacing a major drive-train component based on literature [35,21] and expert knowledge. This covers material costs, crew and vessel required. For analysing the alarms, a crew of 3 workers is considered and the cost per hour taken as the average European labour cost in 2017.

The average performance of the classifiers is displayed along with the contour lines of the net utility in Fig.11, obtained by using the mean values of the random variables defined in Tab.3, except for the efficiency ξ, which is in this case set equal to 1. The dots represent the optimal points. The log-scale is used to highlight the low FAR intervals. The sensitivity of the classifier in these intervals depends on the number of observations per class label, as well as the algorithm employed. It is important to notice that these values, which are assumed constant in this study, should vary with the lead time.

NN clearly outperforms NB. Besides the fact that the AUC values in Tab.2 differ by 10% between the two classifiers, important differences in terms of performance can be observed in the low FAR region, as seen from Fig.11. This is the region where the highest utility is achieved. Therefore, the maximum net utility along the performance curves is displayed in Fig.12a against the efficiency of intervention.

Fig.12a shows $U_{net,max}(\xi)$; for efficiencies greater than 0.3 all investigated classifiers provide positive net utility. The maximum net utility increases with the efficiency of intervention. The optimal configuration of the online classifier concerns selecting a threshold from which POD and FAR can be computed, resulting in a specific point on the curve.

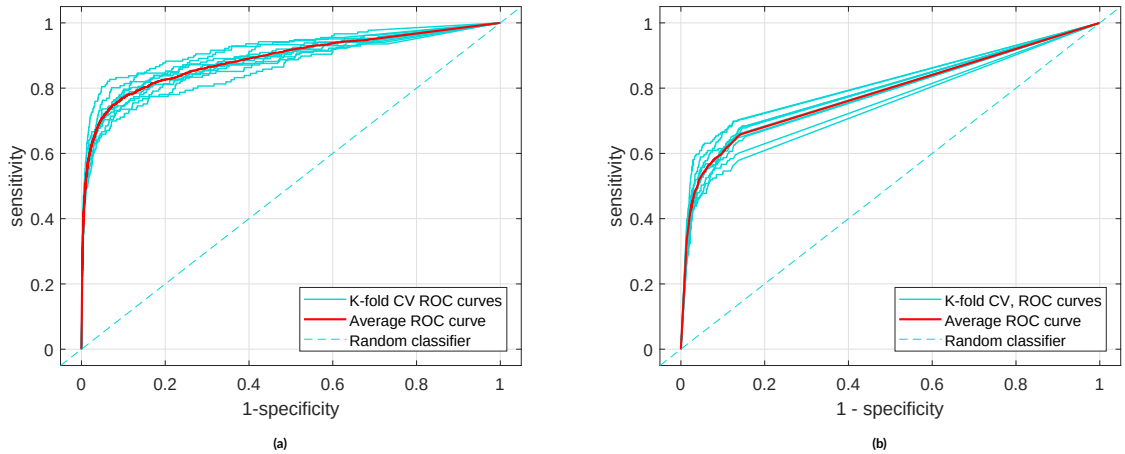

FIGURE 10 Cross validated and average ROC curves for obtained by using 4 hours shifted back in time data for NN (left) and NB (right).

TABLE 3 Numerical quantities for the cost model and associated coefficient of variation (CoV). The mean downtime was estimated from historical data (LN = lognormal, G = Gaussian, D = deterministic).

Name	Value	Description
T_a [h]	1	Time for intervention
T_d [h]	617	Failure downtime
$\bar{P}_a$ [MWh/h]	0.97	Hourly mean production
C_r [€]	$25 \cdot 10^4$	Cost of replacement
C_l [€/h]	33	Cost of labour
C_{el} [€/MWh]	100	Price of electricity
N_w [-]	3	Number of workers
$P(E)$ [-]	$4.7 \cdot 10^{-2}$	Probability of event
$P(F \mid E)$ [-]	$6.9 \cdot 10^{-3}$	Probability of failure
ξ [-]	0.5	Efficiency

Fig.12b makes a comparison in terms of performance at the two different lead times. The figure shows an estimate of the efficiency of a 4h lead time system which would be required to match the utility of a 1h lead time system. The computation is done for a fixed FAR of 0.003 (10 min^{-1}) and its corresponding POD, computed by the ROC curves respectively for the NN and NB classifiers. The plot shows that for the NN, higher efficiency is required for the 4h lead time system to achieve the same utility of a 1h system. Moreover, if 60% efficiency can be achieved with the a 1h system, the 4h system becomes obsolete, as it will require an efficiency of more than 1 to achieve the same utility. The higher performance of NN over NB can be inferred by noting that a lower efficiency at 1h would be required given the same level of the efficiency at 4h.

6 | DISCUSSION

We presented a methodology for assessing the economic viability of using monitoring data for predictive maintenance and repair. It also facilitates the optimization of the applied machine learning algorithms and the threshold values utilized to decide on repair actions. While the employed decision model is simple, it is deemed sufficiently realistic for these purposes. However, the parameters utilized in the case studies, in particular the times for intervention and the cost values, should be reexamined prior to an application of the methodology in practice. It is pointed out that a FAR = 10^{-3} $(10\ \text{min})^{-1}$, which corresponds to FAR = $6 \cdot 10^{-3}$ h^{-1}, implies approximately one false alarm every week. However, the optimal configuration of the system identified in the case study leads to FAR of around $6 \cdot 10^{-2}$ h^{-1}, which is 10 false alarms per week on average. This indicates that the cost for an intervention are selected as too low in our case study.

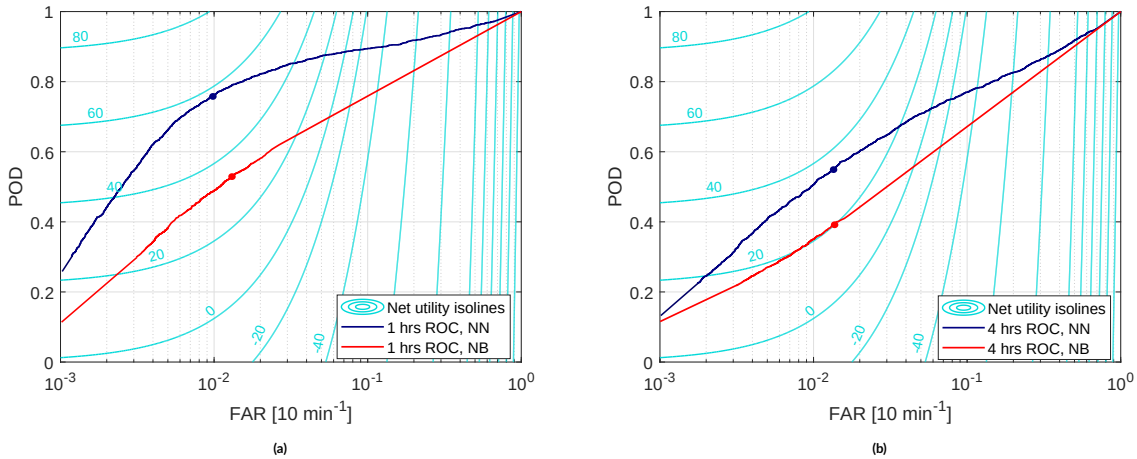

FIGURE 11 Isolines of the net utility U_{net} as a function of the FAR and POD given efficiency $\xi = 1$, and respective classifier output performance for 1 hour lead time (left) and 4 hours (right). The dots are the optimums.

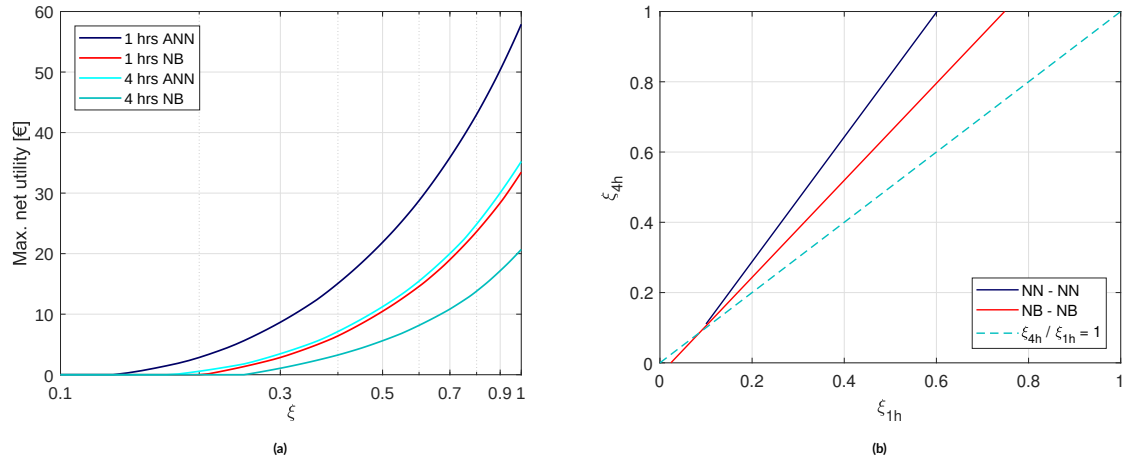

FIGURE 12 a) Maximum net utility as a function of the efficiency of intervention derived from the ROC curves for different lead times. b) Efficiency of intervention at 4 hours resulting in the same utility of a system with an efficiency at 1 hour given the same FAR, for the NB and NN classifiers.

More robust predictions can be achieved by using more specialized data. For instance, the use of vibration data is promising for classification of damaged WT components. In particular, vibration data can provide higher performance for longer lead times, as for instance demonstrated in [11]. Longer lead times enable additional decision policies, as opposed the fixed decision policy adopted in this study. Prediction performance can be also increased by training the classifiers at different operational regimes, by dividing the operational conditions into a finite number of classes, e.g. rotor speed and active power, as for instance proposed in [36]. Moreover, restricting the detection to specific components is expected to result in higher prediction performance, but this would result in a problem of retrieving sufficient failure data, which could represent a challege. Significant differences in terms of performance between the two classifiers used in this study suggest that the choice of the algorithm plays an important role for the performance of the system. We also note that the overall performance may vary when modeling times series, as opposed to random shuffling [37,13].

Some characteristics of the failure events can be inferred from the analysis, by noting that the events experienced occur mostly during wind speeds around the rated speed. Generally, the transition from below to above rated power, is a critical operational range for the turbine, because of repeated pitch activation, which may result in high dynamic loading of the machine. This condition is especially intensified during periods of higher than average turbulence, as observed in this study. Moreover, the operational report states that during the analyzed period, the wind farm was heavily curtailed, for about 38% of the time at different curtailment levels. However, the interaction between WT control strategies, external

factors, and the reliability of the wind farm, is out of the scope of the present study. A more detailed analysis should be performed preferably using higher frequency data, supported by aeroelastic simulations.

7 | CONCLUSIONS

The research presented in this article demonstrates an application of SCADA data for improving the alarm system for indicating malfunctions of main WT components such as gearbox, generators and bearings considered in this study, and eventually leading to failure. In practice, the approach could prevent the turbine from operating during periods of high component degradation. A risk analysis based on a fixed decision policy was set up to quantify the economic benefit of implementing the monitoring system. The resulting maximum net utility shows that it is possible to achieve positive utilities. To summarize, the main contributions of this work can be highlighted as follows:

- A method is devised for avoiding the occurrence of critical failures by predicting warnings and intervene in a timely manner with a certain efficiency, potentially leading to improved wind farm operations and smooth running conditions
- Coupling machine learning prediction with event-trees to quantify the reliability of data-driven monitoring systems to provide a criterion to select a risk-based threshold for on-line classifiers
- Modelling of the reduced probability of failure of mechanical components given maintenance intervention and quantification of its effect on the maximum net utility

The novelty of the approach resides in the combination of the prediction ability of machine learning techniques with probabilistic modelling and optimization of maintenance practice applied to wind energy. A discussion on performance and reliability of the monitoring system was provided. Results demonstrate that SCADA data alone could already represent a valuable source of information to help the industry transition from preventive to predictive maintenance policies. The study also showed the importance of recording data statistics and the implementation of advanced machine learning techniques, which resulted in higher performance and less prediction uncertainty. This should encourage maintenance practitioners to record statistics beyond mean values, which is the current practice for most signals.

ACKNOWLEDGEMENT

This project has received funding from the European Union's Horizon 2020 research and innovation programme under the Marie Sklodowska-Curie grant agreement No 642108 (Advanced Wind Energy Systems Operation and Maintenance Expertise, http://awesome-h2020.eu/).

References

1. Poulsen Thomas, Hasager Charlotte Bay, Jensen Christian Munk. The Role of Logistics in Practical Levelized Cost of Energy Reduction Implementation and Government Sponsored Cost Reduction Studies: Day and Night in Offshore Wind Operations and Maintenance Logistics. *Energies*. 2017;10(4):464.
2. May Allan. Operational expenditure optimisation utilising condition monitoring for offshore wind parks. *PhD thesis, University of Strathclyde*. 2016;.
3. Meeker William Q, Hong Yili. Reliability meets big data: opportunities and challenges. *Quality Engineering*. 2014;26(1):102–116.
4. Jardine Andrew KS, Lin Daming, Banjevic Dragan. A review on machinery diagnostics and prognostics implementing condition-based maintenance. *Mechanical systems and signal processing*. 2006;20(7):1483–1510.
5. Randall Robert Bond. *Vibration-based Condition Monitoring: Industrial, Aerospace and Automotive Applications*. Chichester, UK: John Wiley & Sons, Ltd; 2011.
6. Peng Ying, Dong Ming, Zuo Ming Jian. Current status of machine prognostics in condition-based maintenance: a review. *The International Journal of Advanced Manufacturing Technology*. 2010;50(1):297–313.

7. Tautz-Weinert Jannis, Watson Simon J. Using SCADA data for wind turbine condition monitoring–a review. *IET Renewable Power Generation*. 2016;11(4):382–394.

8. Zaher ASAE, McArthur SDJ, Infield DG, Patel Y. Online wind turbine fault detection through automated SCADA data analysis. *Wind Energy*. 2009;12(6):574–593.

9. Loyer Jean-Loup, Henriques Elsa, Wiseall Steve. Comparison of binary classifiers for data-driven prognosis of jet engines health. 2014;:1–12.

10. Cai Chengtao, Weng Xiangyu, Zhang Chuanbin. A novel approach for marine diesel engine fault diagnosis. *Cluster Computing*. 2017;:1–12.

11. Bach-Andersen Martin, Rømer-Odgaard Bo, Winther Ole. Deep learning for automated drivetrain fault detection. *Wind Energy*. 2017;.

12. Koukoura Sofia, Carroll James, McDonald Alasdair. Wind turbine intelligent gear fault identification. *Annual Conference of the PHM Society*. 2017;.

13. Leahy Kevin, Gallagher Colm, Bruton Ken, O'Donovan Peter, O'Sullivan Dominic TJ. Automatically Identifying and Predicting Unplanned Wind Turbine Stoppages Using SCADA and Alarms System Data: Case Study and Results. In: :012011IOP Publishing; 2017.

14. Li Xiaochuan, Duan Fang, Mba David, Bennett Ian. Multidimensional prognostics for rotating machinery: A review. *Advances in Mechanical Engineering*. 2017;9(2):1687814016685004.

15. Colone Lorenzo, Reder Maik, Dimitrov Nikolay, Straub D. Assessing the Utility of Early Warning Systems for Detecting Failures in Major Wind Turbine Components. In: :032005IOP Publishing; 2018.

16. Sättele Martina, Krautblatter Michael, Bründl Michael, Straub Daniel. Forecasting rock slope failure: how reliable and effective are warning systems?. *Landslides*. 2016;13(4):737–750.

17. Sättele Martina, Bründl Michael, Straub Daniel. Reliability and effectiveness of early warning systems for natural hazards: Concept and application to debris flow warning. *Reliability Engineering & System Safety*. 2015;142:192–202.

18. Reder Maik, Yürüşen Nurseda Y, Melero Julio J. Data-driven learning framework for associating weather conditions and wind turbine failures. *Reliability Engineering & System Safety*. 2018;169:554–569.

19. Zaher ASAE, McArthur SDJ, Infield DG, Patel Y. Online wind turbine fault detection through automated SCADA data analysis. *Wind Energy*. 2009;12(6):574–593.

20. Tautz-Weinert Jannis, Watson Simon. Condition monitoring of wind turbine drive trains by normal behaviour modelling of temperatures. In: :359BoD–Books on Demand; 2017.

21. Carroll James, McDonald Alasdair, McMillan David. Failure rate, repair time and unscheduled O&M cost analysis of offshore wind turbines. *Wind Energy*. 2016;19(6):1107–1119.

22. Bishop Christopher M.. *Pattern Recognition and Machine Learning (Information Science and Statistics)*. Secaucus, NJ, USA: Springer-Verlag New York, Inc.; 2006.

23. Alpaydin Ethem. *Introduction to machine learning*. MIT press; 2014.

24. Friedman Jerome, Hastie Trevor, Tibshirani Robert. *The elements of statistical learning*. Springer series in statistics New York; 2001.

25. Kullback Solomon, Leibler Richard A. On information and sufficiency. *The annals of mathematical statistics*. 1951;22(1):79–86.

26. Regan Taylor, Beale Christopher, Inalpolat Murat. Wind Turbine Blade Damage Detection Using Supervised Machine Learning Algorithms. *Journal of Vibration and Acoustics*. 2017;139(6):061010.

27. John George H, Langley Pat. Estimating continuous distributions in Bayesian classifiers. 1995;:338–345.

28. Scott David W. *Multivariate density estimation: theory, practice, and visualization*. John Wiley & Sons; 2015.

29. Kuhn Max, Johnson Kjell. *Applied predictive modeling*. Springer; 2013.

30. Candel Arno, Parmar Viraj, LeDell Erin, Arora Anisha. *Deep learning with h2o*. 2015.

31. Huberty Carl J. Mahalanobis distance. *Wiley StatsRef: Statistics Reference Online.* 2005;.

32. Mazidi Peyman, Du Mian, Bertling Tjernberg Lina, Sanz Bobi Miguel A. A health condition model for wind turbine monitoring through neural networks and proportional hazard models. *Proceedings of the Institution of Mechanical Engineers, Part O: Journal of Risk and Reliability.* 2017;:1748006X17707902.

33. López Victoria, Fernández Alberto, García Salvador, Palade Vasile, Herrera Francisco. An insight into classification with imbalanced data: Empirical results and current trends on using data intrinsic characteristics. *Information Sciences.* 2013;250:113–141.

34. Fawcett Tom. An introduction to ROC analysis. *Pattern recognition letters.* 2006;27(8):861–874.

35. Dinwoodie Iain, Endrerud Ole-Erik V, Hofmann Matthias, Martin Rebecca, Sperstad Iver Bakken. Reference cases for verification of operation and maintenance simulation models for offshore wind farms. *Wind Engineering.* 2015;39(1):1–14.

36. Ha Jong M, Oh Hyunseok, Park Jungho, Youn Byeng D. Classification of operating conditions of wind turbines for a class-wise condition monitoring strategy. *Renewable Energy.* 2017;103:594–605.

37. Cody Tyler, Dempsey Paula J. Application of Machine Learning to Rotorcraft Health Monitoring. 2017;.

IOP Conf. Series: Journal of Physics: Conf. Series **1037** (2018) 032005 doi:10.1088/1742-6596/1037/3/032005

Assessing the Utility of Early Warning Systems for Detecting Failures in Major Wind Turbine Components

L Colone[1,*], M Reder[2], N Dimitrov[1], D Straub[3]

[1] Technical University of Denmark, Frederiksborgvej 399, 4000 Roskilde, Denmark
[2] CIRCE - University of Zaragoza, C/ Mariano Esquillor 15, 50018, Zaragoza, Spain
[3] Technical University of Munich, Theresienstr. 90, 80333 Munich, Germany

E-mail: lcol@dtu.dk

Abstract. This paper provides enhancements to normal behaviour models for monitoring major wind turbine components and a methodology to assess the monitoring system reliability based on SCADA data and decision analysis. Typically, these monitoring systems are based on fully data-driven regression of damage sensitive-parameters. Firstly, the problem of selecting suitable inputs for building a temperature model of operating main bearings is addressed, based on a sensitivity study. This shows that the dimensionality of the dataset can be greatly reduced while reaching sufficient prediction accuracy. Subsequently, performance quantities are derived from a statistical description of the prediction error and used as input to a decision analysis. Two distinct intervention policies, replacement and repair, are compared in terms of expected utility. The aim of this study is to provide a method to quantify the benefit of implementing the online system from an economic risk perspective. Under the realistic hypotheses made, the numerical example shows for instance that replacement is not convenient compared to repair.

1. Introduction

The significant maintenance cost associated with failures of large wind turbine (WT) components calls for improved operation and maintenance (O&M) decision support systems. Such systems are increasingly drawing the attention of operators, especially in the offshore sector [1]. Maintenance actions are necessary to ensure a certain level of reliability of a machine throughout its lifetime. Maintenance strategies can be broadly categorised into corrective and preventive [2, 3]. The second type can in turn be divided into scheduled and condition based maintenance (CBM), with the latter being a predictive policy. CBM is helpful to avoid early replacement of healthy components while identifying critically worn-out components. Wind energy, especially offshore, is still a maturing industry and the scenario around CBM poses some new and unique challenges. The lack of extensive datasets containing run-to-failure data often does not allow the adoption of supervised learning techniques [4]. Moreover, realistic physics-based deterioration models are not generally available due to the complexity of the machine behaviour under operation and its dependence on multiple physical variables. To deal with this problem some studies have suggested to derive a fully data-driven normal behaviour model (NBM) of specific damage-sensitive features [5]. This process refers to building a model characterizing the behaviour of a system directly from measured data. Such NBMs are regularly used to detect anomalies in wind turbine behaviour, as demonstrated in [6, 7]. Since the model variables

are typically continuous, prediction models are based on linear or nonlinear regression. This approach seems to be well tailored for main components, thanks to its simplicity of application with regards to the data requirements and scalability [8]. From an operator's perspective it is important to understand the economic benefit of implementing predictive systems. This can be achieved by defining a performance measure to quantify the reliability of early detection warnings, followed by a cost-benefit analysis. Often, when dealing with rare events, a sufficient number of failure observations is not available and thus not allowing to establish performance statistics, as for instance used in [8]. Hence, this indicates the need for alternative metrics. In the present study, the lead time to failure events against the probability of false alarms (PFA) is analysed, in order to assess the system performance from an economic perspective. Considerations about the nature of failure are taken into account to identify suitable detection thresholds. A case study of main bearing failures from an onshore wind farm is carried out and analysed. The system output is condensed into a scalar anomaly measure to track the component deterioration. Furthermore, a sensitivity study selecting the most important input variables is carried out, in order to enhance NBM. Each section explains the methodology adopted and uses information previously derived. From section 3 on, results are presented in a progressive order without a dedicated result section. The paper concludes with a discussion on the contribution and future research in the area.

2. Model

The analytical model used herein has the structure of a hierarchical NBM between input vectors $\mathbf{x}$ and output $\hat{\mathbf{y}}$. For modelling the main bearing temperature in the form $\hat{\mathbf{y}} = g(\mu(\mathbf{x})) + \mathbf{e}$, a generalised linear model (GLM) with mean μ, a Gaussian error distribution $e_i \sim \mathcal{N}(0, \sigma_{e,i})$ and an identity link function $g(\cdot)$ is used [9], so that, for the i^{th} output variable, $g(\mu_i) = \mu_i = E(\hat{y}_i)$, where E is the expected value operator. The model is expressed in scalar form as

$$E(\hat{y}_i) = \hat{\alpha}_{0i} + \sum_{j=1}^{K} \hat{\alpha}_{ij} x_j + e_i, \tag{1}$$

where $\hat{\alpha}$ is assumed to be $\hat{\alpha} \sim \mathcal{N}(\bar{\alpha}, \sigma_\alpha)$, with $\bar{\alpha}$ and σ_α being respectively mean and standard deviation of the model parameters and K the number of explanatory variables, or covariates. The error between the model output $\hat{\mathbf{y}}$ and the measurements $\mathbf{y}$ has zero mean, and the appearance of bias indicates deviation from the normal behaviour. The parameter estimation is based on a least-squares optimization with a least absolute shrinkage and selection operator (Lasso) [10]. This regularisation method uses a penalisation on the $\mathcal{L}_1$ norm, and is an effective technique for subset selection in high dimensional multivariate models. The Lasso solves the following optimisation problem, where the penalisation parameter λ is introduced:

$$\hat{\alpha}_{lasso}(\lambda) = \arg\min_{\hat{\alpha}^*} \|\mathbf{y} - \mathbf{x}\hat{\alpha}^*\|_2^2 + \lambda \|\hat{\alpha}^*\|_1 , \tag{2}$$

where $\mathbf{x}$ is the vector of model covariates and λ is the penalisation parameter. The remaining terms are the same as in Eq.1. Lasso is applied here by virtue of its ability to achieve high prediction quality with the minimum number of covariates. The relative importance of covariates is measured for the training with the coefficient of determination (R-squared), and for the predictions with the mean absolute error (MAE) and root mean squared error (RMSE). In this manner, the herein used techniques have practical utilization.

3. Training

A set of SCADA data from an onshore wind farm with more than 10 turbines is available over a period of 5 years. During this period 3 turbines, WT1, WT2 and WT3, experienced main bearing failures. This component has been identified in previous studies as one of the most critical WT components in terms of failure frequency and downtime [11]. The full SCADA dataset consists of 74 channels given as 10 minutes average values. Operational data only are selected from the dataset by removing unnecessary observations, corresponding to power less or equal than zero as well as measurement errors.

The training dataset is built by selecting normal behaviour data from 6 turbines including the 3 having experienced failures. In these latter, NBM data are selected until 6 months before the failure event, in order to not introduce degradation information into the training dataset. From the selected training pool of normal behaviour data, random down-sampling is applied in order to reduce its size while conserving the variability of the data coming from different turbines and their operational conditions. In total, $N = 3 \cdot 10^5$ samples are employed for training, corresponding to the equivalent of 6 years of data from 1 turbine. All the SCADA variables are normalised between 0 and 1. The turbine validation demonstrates that the NBM has more universal applicability and ensures that the failure detection does not rely on conditions specific to the turbines that have experienced the event. The GLM was trained with a 10-fold cross validation.

4. Variable Selection and sensitivity study

Model reduction is an important step in improving the model speed and usability when dealing with large datasets. Although the GLM is computationally efficient, reducing the number of covariates will lead to further benefits as it will reduce the data storage requirements and data processing. A certain degree of model reduction is ensured by the Lasso approach, as the penalization function leads to some model coefficients being reduced towards zero, which allows their elimination from the model. This is performed through a variable importance analysis by comparing the standardised coefficient magnitudes for each input variable obtained through the estimation process. The model predicts the main bearing temperature using the full set of variables in the SCADA dataset. The 15 most important variables obtained are displayed in Fig.1. Blue colour indicates a positive effect on the model result, which means that with increasing values for the coefficient of this covariate the model response also increases. Red bars indicate the inverse relationship.

Interestingly, the first top 10 covariates are temperature measurements, which may suggest a correlation between abnormal bearing temperature rise, which eventually leads to failure, and high operational demand, as shown in Fig.1. Rising brake temperature, lower external temperature and lower non-drive-end (NDE) generator bearing temperatures contributed to the increasing main bearing temperature. At first glance, this might seem contradictory. However, lower external temperatures are usually related to higher wind speeds, which affect the failure bahaviour of certain components [12,13]. At this step, further analysis could be carried out such as Chi-square tests or ANOVA, in order to further reduce the number of input parameters, [14].

Fig.2 displays the model RMSE, the MAE and R-squared performance metrics as function of the number of model covariates. To obtain the figure, the model is first trained using the full set of variables, then retrained subsequently by adding one variable at the time from the most important to least important variable to establish the variable importance. The x-axis indicates the number of input covariates ordered according to the standardized model coefficients from the most important (number 1) to the least important variable (number 74). Including more covariates to a model implies higher model complexity and longer model evaluation times. Thus, a compromise between the number of model covariates and model accuracy has to be found. It is shown in the graph that by including the 15 most important covariates the R-squared reaches

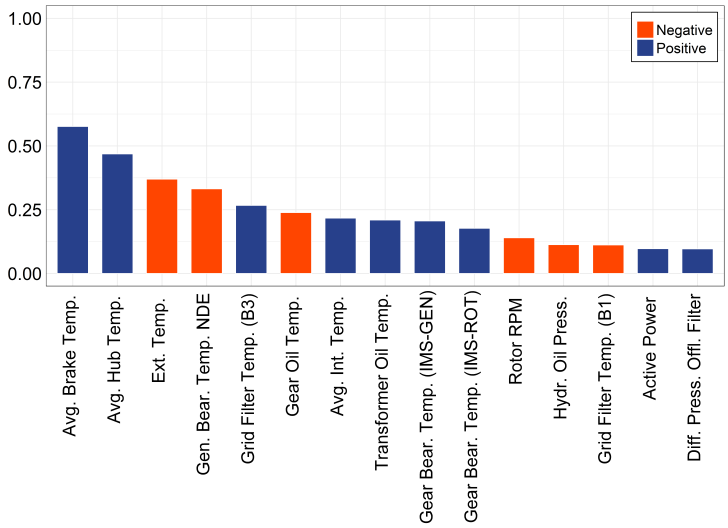

Figure 1: Top-15 standardised regression coefficient with respect to main bearing temperature from Lasso

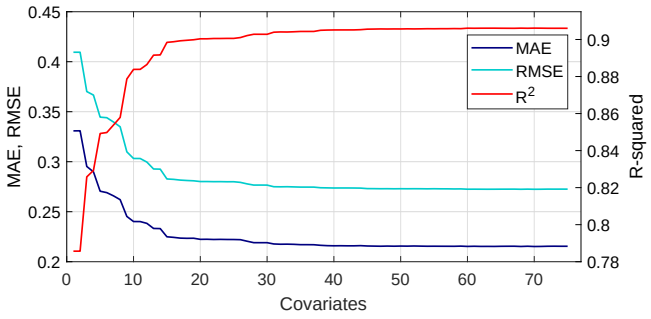

Figure 2: The R-squared of the model and the prediction errors MAE and RMSE using different numbers of inputs.

a value of approximately 0.91, along with a sufficiently low prediction error.

5. Damage detection

The set of covariates obtained in the previous section is selected for building the model and testing it on the damaged turbines. In the case of a single model output (e.g. inner-ring temperature), the deviation function is a univariate measure, which is here selected as the RMSE, namely RMS of 10 consecutive samples of the model residuals, corresponding to an effective operating time $\Delta t = 100$ minutes. Previous studies e.g. [6], suggested to average the discordance measure over 3 days in order to reduce the occurrence of false alarms. In the present study, however, shorter time periods are achieved by applying a low-pass filter, a centered moving average, to the model residuals. In Eq.3, the parameter η is the window size of the filter.

$$e_f(i) = \frac{1}{2\eta + 1} \sum_{j=0}^{2\eta} h(e(i + \eta - j)) \tag{3}$$

In this way, a more robust performance is ensured. The raw and filtered RMSE in normal behaviour are displayed in Fig.3a, while Fig.3b shows their distributions at different filtering levels, where a log-normal distribution is fitted, which is the distribution that resulted in the best fit. As can be noticed, the uncertainty decreases with the level of filtering. This information is useful to quantify the reliability of the monitoring system.

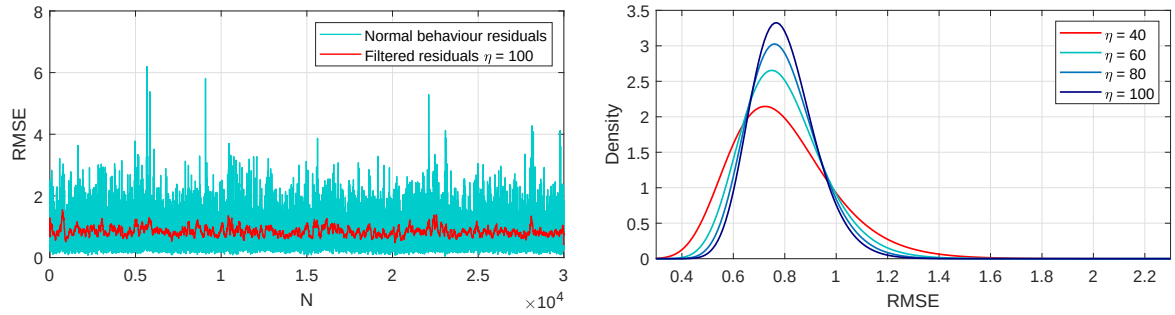

(a) (b)

Figure 3: *a*) Raw and filtered RMSE from the normal behaviour dataset. *b*) Log-normal distributions of the filtered RMSE from normal behaviour data.

In general a multivariate discordance metric can be used as degradation function, if for instance the output set is composed of a correlated set of damage-sensitive features. For instance, Fig.4 shows the main bearing vertical acceleration RMS, temperature, and tower-top acceleration RMS in an example case of failure. The interaction between these variables could be exploited to obtain earlier and more robust predictions. However, this study only focuses on SCADA data, leaving out the vibration analysis.

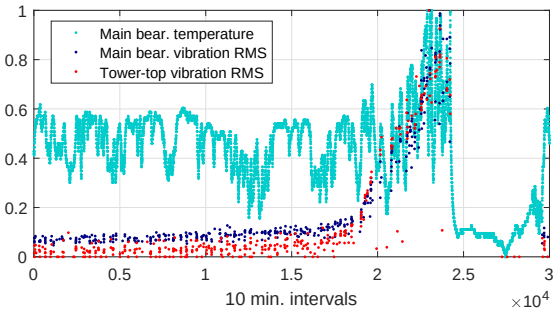

Figure 4: Main bearing temperature, acceleration RMS and tower-top acceleration RMS close a main bearing failure event (WT1).

Fig.5a and 5b show the trend of the filtered RMSE for the damaged dataset on the three turbines. The damage progression can be readily identified and an NBM-based alarm is issued when the failure threshold is crossed.

The lead time is here defined as the time lag between the first warning issued by the model and the first threshold-based alarm from the SCADA system. The selection of the NBM-based alarm threshold is a tradeoff between lead time and probability of false alarms (PFA), where

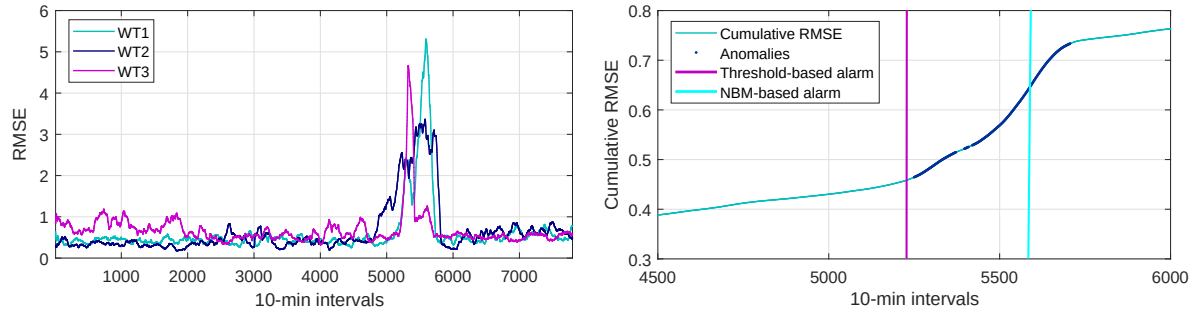

(a) (b)

Figure 5: *a*) Filtered RMSE of the damaged (testing) dataset. *b*) Normalised cumulative RMSE and alarms issued by threshold-based and NBM-based system (WT2)

for a given reference period the PFA equals the probability of exceeding the threshold under normal, stationary conditions. The PFA can thus be found as $P[\text{RMSE} > T]$, where T is a threshold.

6. Decision analysis

The decision analysis has the aim to assess the economic advantage of using the system based on field data. Since the analysis is based on simple cost considerations, it is best suitable for preliminary assessments. A utility function is derived by associating a cost to a false alarm and a saving to detecting a failure early. The NBM-based threshold is chosen such that the lead time is long enough to cover the entire mobilization time, needed for preparing the crew and hiring the crane vessel. Only consequences associated with direct financial losses are considered, i.e. human injuries, environmental effects and similar are not taken into account. The decision tree is sketched in Fig.6, which shows all possible alternatives originating from an NBM-based alarm A. In the simplest case, when an alarm is issued, the turbine keeps running and a site inspection is performed, which can result in false case ($\bar{E}$) or a true case (E). It is assumed that the inspections are perfect. As shown in Fig.6, if the inspection reveals a developing failure, an intervention a is performed, corresponding to a repair r or full component replacement R and their associated costs. In case of repair $C_a = C_r$, and in case of replacement $C_a = C_R$. These two cases are studied separately, as if the adopted policy is constrained to be only one of them.

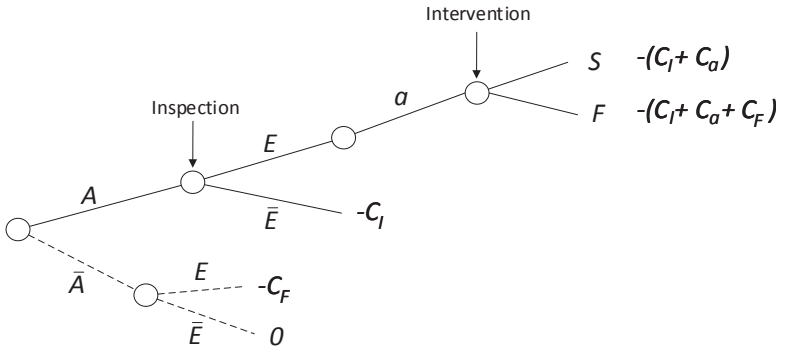

Figure 6: Decision tree associated to the detection of rare events and corresponding utility functions for each outcome.

Two discrete states: failure (F) and functional, or safe, (S) are considered after the intervention is performed. In order to model the possibility that a repair fails to eliminate the component damage, an efficiency coefficient $\psi \in [0, 1]$ is introduced as formerly developed in [15]. The possible outcomes of the maintenance action are considered binary, i.e., the component is either restored to its original undamaged state, or its state remains equivalent to its current damaged state. The efficiency term specifies the probability that the repair action is successful and the component health is fully restored, as

$$P(F \mid E \cap A \cap a) = P(F \mid E)(1 - \psi) = (1 - \psi), \tag{4}$$

where the assumption $P(F \mid E) = 1$ means that a true case is always associated with a developing failure, regardless of the maintenance policy adopted. Therefore, the repair action influences the probability of failure of the component by making it decrease linearly with the increasing repair efficiency. In real applications, a similar function could be derived from historical data. With reference to Fig.6, the discrete probabilities can be readily written as

$$\begin{aligned} P(F \cap E \cap A \cap a) &= P(F \mid E \cap A \cap a)P(E \mid A)P(A) = (1 - \psi)\lambda_0 \\ P(S \cap E \cap A \cap a) &= [1 - P(F \mid E \cap A \cap a)]P(E \mid A)P(A) = \psi\lambda_0 \end{aligned} \tag{5}$$

which make use of the following quantities expressed as functions of PFA and efficiency, derived from the Bayes rule

$$P(E \mid A) = \frac{P(A \mid E)P(E)}{P(A)} = \frac{\lambda_0}{P(A)} \tag{6}$$

$$P(\bar{E} \mid A) = \frac{P(A \mid \bar{E})P(\bar{E})}{P(A)} = \frac{\mathrm{PFA}(1 - \lambda_0)}{P(A)}. \tag{7}$$

Note that in Fig.6, the alternative $\bar{A}$ (dashed) is associated with zero utility, because $U(\bar{E} \mid \bar{A}) = 0$ and $P(E \mid \bar{A}) = 0$. $P(A \mid E) = 1$ because it is assumed the system always issues an NBM-based alarm in case a failure is present. This is equivalent to assuming a probability of detection equal to 1. Further information on this probability could not be inferred from available data.

The tree includes the utilities u_i associated to each possible outcome. Note that the quantity $P(A) \neq 0$ does not need to be explicitly determined, since it cancels out when Eq.6 is inserted into Eq.5.

The analysis is performed on a hourly basis, namely all the probabilities are expressed with respect to 1 hour. A constant event rate $P(E) = \lambda_0$ is assumed, derived as a frequentistic rate from historical data, where 3 events on three different turbines were reported over the period analysed of 5 years. Note that the hourly PFA is derived from the PFA computed for 100-minute sampling windows by scaling with the ratio between the length of the sampling periods (see Fig.3). To perform a repair comes at a cost C_r, while the inspection costs are C_I. These quantities were retrieved from available literature [16].

The cost of replacement is equal to the material cost plus the crew costs (which means the possibility that the lead time is shorter than the mobilization time for crew and equipment is neglected), while the cost of failure comprises the cost of replacement plus the power loss during the mobilization time and replacement time. With reference to Tab.1, these quantities are expressed as

Table 1: Numerical quantities employed in the decision analysis.

Parameter	Value	Description
C_I [€]	2500	Cost of inspection
C_r [€]	$10 \cdot 10^3$	Cost of repair
$\bar{P}$ [MWh/h]	1.05	Hourly average production
C_m [€]	$15 \cdot 10^4$	Material cost
N_w [€]	10	Number of workers
C_{el} [€/MWh]	100	Price of electricity
C_l [€/h]	33	Cost of labour
MTTR [h]	240	Mean time to replacement
MT [h]	170	Mobilization time

$$\begin{aligned} C_R &= C_m + \text{MTTR}\ C_l\ N_w \\ C_F &= C_R + (\text{MTTR} + \text{MT})\ \bar{P}\ C_{el}. \end{aligned} \tag{8}$$

The current electricity price from offshore wind was taken from [17]. Due to the absence of cost parameters and time to repair for this specific case, the quantities found in [1] were adopted, corresponding to the replacement of an equivalent main component, the gearbox. The total expected utility is found as

$$U = \sum_i P_i u_i - U_0, \tag{9}$$

where $U_0 = \lambda_0 C_F$ is the utility associated with not implementing the system. This comprises the average power production losses, replacement or repair costs and labour costs, part of which could be saved when a sufficient lead time and repair efficiency can be provided by the system. Fig.7a shows the lead time as a function of the PFA where the jumps are due to the small sample size. The changes in lead time and PFA are a direct function of the chosen error threshold, T. The figure shows that achieving longer lead time requires lowering the error threshold and hence increasing PFA. Conceptually, for a specifically chosen error threshold the lead time would be a random variable, and there is a non-zero likelihood for the lead time to be shorter than the required mobilization time. This is associated with a certain cost, which has a trade-off with the cost of false alarms, as reducing the threshold will mean increasing the lead time but also increasing the false alarm rate. It is possible to search for an optimal threshold that results in the lowest overall cost, however this is not considered in the present study. Instead, a suitable error threshold level is chosen such that the average lead time equals 23 days for filtering level $\eta = 100$. Based on this choice, the corresponding PFA is obtained (Fig.7).

Fig.7b displays the expected utility in case of repair $U_a(\psi)$, which is positive already for a large span of the efficiency domain. The plot displays that low-pass filtering the error deviations lead to lower PFA and thus higher benefit, besides providing positive utility at lower efficiency values. In this numerical example, the replacement policy is not cost-effective compared to repair, with $U_a = -15.9$ € and $U_a = -18.6$ € respectively for the maximum and minimum levels of error filtering as shown in case of repair in Fig.7b).

7. Discussion

The positive standardized coefficient of the brake temperature could be due to thermal conduction from the bearing to the brake, possibly indicating a cross-correlation between

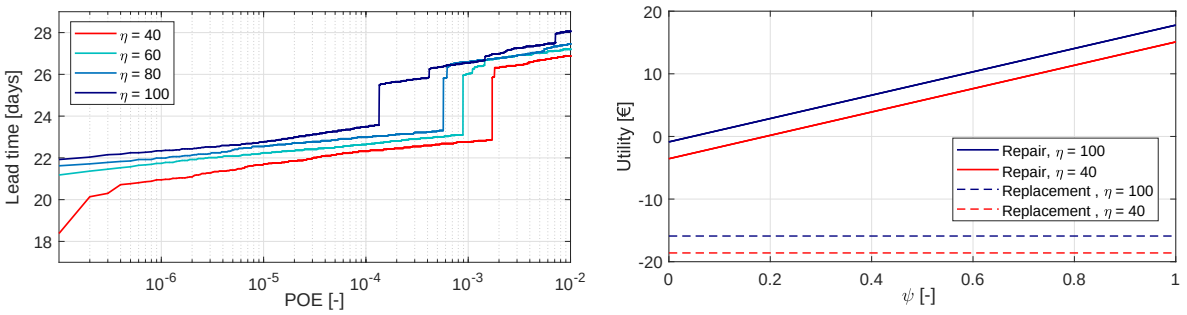

(a) (b)

Figure 7: *a*) Lead time against probability of exceedance (POE) averaged over 3 failure cases, for different filter levels. POE is equivalent to PFA. *b*) Repair utility as a function of the efficiency of intervention.

the bearing temperature, the brake temperature and failure. For example, a high bearing temperature combined with high brake temperature might mean normal operation under heavy load. The NDE generator bearing located on the opposite end of the drive train compared to the main bearing, is able to maintain lower temperatures. The increasing hub temperature might instead be a consequence of the main bearing temperature raise, by thermal conduction through the main shaft.

Main bearing failures as the ones analysed here, which show a clear temperature rise over time, may be related to high friction, probably due to lack of proper grease lubrication. This justifies the utilization of a repair policy.

More detailed cost models should be used in the decision analysis to include site accessibility, parameter uncertainty [18], discount rate, updated probability of failure. Furthermore, advanced models of inspections would be desirable [16], which will trigger more decision alternatives. In this paper, perfect inspection was assumed. However these details are case-specific and thus showing their value mainly in real applications.

Regarding the probability of failure in case of replacement, more detailed models would allow for an updated probability of event or failure based on condition, rather than considering the same measured event rate after replacement as done in this work. This is to account for the increased probability of failure due to usage, as opposed to new.

A further improvement would be to incorporate lifetime prediction models as for instance proposed in other structural components [19], in order to give an estimate of the remaining life of the component. In this case, the latter can be achieved by for instance setting a maximum temperature threshold at which the component is considered to be in failed state. In this way, information about progressive failures can be obtained and included in the decision model, which in real cases is expected to be more advanced.

8. Conclusions

This research has highlighted improvements in NBM of WT components and the definition of a performance metric in case of rare events was defined. Thus, a model of the normal main bearing inner-ring temperature is trained by using turbines other than the ones experiencing the damage analysed (turbine validation). A linear model is used and a sensitivity study is performed to select the most important variables. The Lasso-based model reduction successfully eliminated unimportant input variables and provided an understanding of the failure mechanisms related parameters. Brake temperature, hub temperature, external temperature and generator bearing

(NDE) temperature were found to be the most important model covariates. The decision analysis has shown that a replacement policy would not result in cost-effective solutions, while a repair policy would be more suitable. These types of problems should be addressed by wind farm operators in order to advance in maintenance management and make the wind energy market more competitive with conventional energy generation. The approach can be implemented for any kind a major wind turbine subsystems such as gear box, generators or blades. Thus, future research will need to cover failure detection of main mechanical components and quantify the benefit of using multivariate over single parameter approaches.

Acknowledgements
This project has received funding from the European Union's Horizon 2020 research and innovation program under the Marie Skłodowska-Curie grant agreement No 642108 (AWESOME). Furthermore, the authors wish to thank Vattenfall for the support provided.

References

[1] Carroll J, McDonald A and McMillan D 2016 *Wind Energy* **19** 1107–1119
[2] Randall R B 2011 *Vibration-based condition monitoring: industrial, aerospace and automotive applications* (John Wiley & Sons)
[3] Rausand M and Arnljot H 2004 *System reliability theory: models, statistical methods, and applications* vol 396 (John Wiley & Sons)
[4] Bishop C M 2006 *Pattern Recognition and Machine Learning (Information Science and Statistics)* (Secaucus, NJ, USA: Springer-Verlag New York, Inc.) ISBN 0387310738
[5] Tautz-Weinert J and Watson S J 2016 Comparison of different modelling approaches of drive train temperature for the purposes of wind turbine failure detection *Journal of Physics: Conference Series* vol 753 (IOP Publishing) p 072014
[6] Bangalore P and Tjernberg L B 2015 *IEEE Transactions on Smart Grid* **6** 980–987
[7] Mazidi P, Bertling Tjernberg L and Sanz Bobi M A 2017 *Proceedings of the Institution of Mechanical Engineers, Part O: Journal of Risk and Reliability* **231** 121–129
[8] Bach-Andersen M, Winther O and Rømer-Odgaard B 2015 Scalable systems for early fault detection in wind turbines: a data driven approach *Annual Conference of the european Wind Energy Association*
[9] Nelder J A and Baker R J 1972 *Generalized linear models* (Wiley Online Library)
[10] Tibshirani R 1994 *Journal of the Royal Statistical Society, Series B* **58** 267–288
[11] Reder M, Gonzalez E and Melero J J 2016 *Journal of Physics: Conference Series* **753** 072027 ISSN 1742-6588
[12] Reder M and Melero J J 2017 *Journal of Physics: Conference Series* **926** 012012 ISSN 1742-6588
[13] Reder M, Yürüşen N Y and Melero J J 2018 *Reliability Engineering & System Safety* **169** 554–569 ISSN 09518320
[14] Friedman J, Hastie T and Tibshirani R 2001 *The elements of statistical learning* vol 1 (Springer series in statistics New York)
[15] Colone L, Dimitrov N and Straub D *(Unpublished)*
[16] Nielsen J J and Sørensen J D 2010 *Proceedings of the Reliability and Optimization of Structural Systems, München, Germany* 7–10
[17] Dinwoodie I, Endrerud O E V, Hofmann M, Martin R and Sperstad I B 2015 *Wind Engineering* **39** 1–14
[18] Seyr H and Muskulus M 2016 *Journal of Physics: Conference Series* **753** 092009
[19] Nielsen J S and Sørensen J D 2017 *Energies* **10**

Chapter 6

Conclusions

You will always find a clear blue sky,
even beyond the heaviest cloud.

The author

6.1 Main contributions

The present thesis addressed relevant topics in offshore wind farm O&M. The ultimate objective of the work was to achieve a cost reduction through predictive maintenance and improving load assessment models. Although it was demonstrated that it is possible to achieve cost-effective solutions through advanced statistical modelling, many issue still remain unsolved. First, the main conclusions and implications of this work can be readily listed as follows:

- It is possible to achieve less conservative designs of offshore WT monopiles by reducing the fatigue equivalent turbulence percentile than the level suggested by current standards. In terms of their probability of failure, wave kinematic and turbulence models can have an impact on reliability against fatigue damage up to 15%, despite the estimated model uncertainties not being as important as other uncertainties, for instance in the aerodynamic model. This result can lead to more accurate load predictions for both initial design and load reassessment of aging turbines.

- The qualitative assessment between blade root flapwise bending DEL map and probability map of pitch malfunctions experienced cannot confirm a direct correlation between loads and failures. However, the approach could be potentially be used to achieve a better configuration of the farm to account for possible financial losses due to and eventual failures, which probability of occurrence increases in higher DEL zones. Alternatively, the information could be used to adjust the operational conditions of critical turbines by building a time varying fatigue load map.

- When building NBMs for damage sensitive features, such as for inner-ring main bearing temperature adopted in this work, it is possible reduce the dimensionality of the input dataset through a variable selection criteria, saving cumbersome data processing and

time consuming model training. The LASSO regularization can also provides a physical understanding of the failure process by correlating the input variables with the damage-sensitive feature adopted. This result can help practitioners select the least number of covariates and therefore achieve more reliable models. For this class of problems based on regression, the decision tree allows to estimate the utility of the learning system adopted prior its online implementation, by considering all possible decision policies, realistic failure rates and false alarm rate. This approach can be used as a tool to assess the viability of different maintenance policies of newly deployed wind farms given historical information on similar wind farms or major mechanical component.

- Prediction systems based on early classification of SCADA alarms resulting in shut-down events, can be coupled with decision trees to provide a criteria to select a risk-based threshold for online classifiers to achieve an optimal configuration of the predictive system. On this purpose, the quantification of the prediction uncertainty becomes important. The introduction of an efficiency of intervention allows to model the CBM effectiveness and thus estimate the utility-based threshold. Furthermore, the analysis of the SCADA data for this study prior a shut-down event revealed that these events mostly happen during periods of higher than average wind speed statistics, which may suggest that failures are also driven by demanding environmental conditions. The average statistics correspond to normal behaviour distributions, i.e. obtained by selecting data far in time from the occurrence of an alarm. Outliers are excluded through a filter based on Mahalanobis distance.

In connection with these conclusive statements, the study highlights practical and technical recommendations for a potential cost-reduction of wind farms O&M. These are:

- Improve the technology by boosting the performance of machine learning algorithms, reduce prediction uncertainties, improve POD versus PFA of online classifiers.
- Standardize monitoring systems by combining SCADA and CMS data. This will enable large-scale deployments of monitoring systems and enable a fast and reliable the data process from raw measurements into actionable maintenance information.
- Exploit sensor-fusion and variable selection for online predictive systems to reduce amount of data. As by direct author's experience, the labor cost associated with data processing accounts for a considerable portion of the total costs of building and running predictive systems.
- Careful tracking of field data, namely maintenance history, efficiency of intervention, SCADA data, CMS data, costs and downtimes are necessary to be able to provide an economic assessment of prediction models.
- Operators should exploit the warranty period to gather all the information necessary and build prediction models based on history or recorded events.

Given the challenges encountered in terms of data gathering during these studies, a closer collaboration towards more effective agreements between manufacturers and operator is highly encouraged. Ambitious targets and closer communication will consent to achieve high reliability levels in wind energy industry industry. This however, will be a blend of improved design, materials and maintenance practice.

6.2 Limitations

The benefit associated with this work is the gain in knowledge about the next generation of problems the industry will face in terms of O&M planning of large offshore wind farms. The up-scaling trend of WT means larger components to be replaced in case of failures, which may increase the level of complexity of offshore operations. The analysis carried out in this work are applicable to all kind of wind farms and show potential to be scaled up on large fleets. The reader can understand the extent to which the problem is applicable, as well as some important limitations.

The fact that changing environmental models for fatigue load assessment leads to substantially different results raises many questions about the suitability of models for lifetime reassessment. Careful analyses of site conditions should be made to determine the most suitable environmental models that better describe the site. This choice helps reduce both conservatism in design and improved lifetime reassessment, by reducing the model uncertainties. However, for broader objectives such as lifetime extension, load analysis through aeroelastic simulations should be complemented with measured loads and inspections.

In case of strong wakes, the turbulence percentile related to the free stream ambient turbulence will play a lower role, since wake turbulence will be predominant. In this cases, the percentile reduction is not expected to provide significant benefit to current load estimation. The trend shows that wind farms are constantly trying to occupy the least space possible, thus trying to minimize the distance between turbines. This consequently increases the wake effects.

When working on load maps, it is important to remark that a possible correlation should be understood only between load-driven failures and loads or other stress indicator. Generally speaking, failures are not only due to operating conditions, but also serial defects of mechanical parts, for example.

The use of SCADA data is still very appealing for the industry. Although in this work it was demonstrated that SCADA alarms can be predicted by suitably trained classifiers, their implementation provided insufficient performance for practical applications at long lead times. More robust predictions by using more specialized failure data to achieve higher POD against lower PFA and longer lead times are necessary, as well as more realistic and detailed cost models. Specialized data are for instance vibration records, detailed maintenance history, information on the structure and policy of the organization, periodic maintenance activities, failure downtimes and failure rates. The assumptions made in this work, although realistic, may play a substantial role on the final outcome. This also remarks the importance of gaining advanced expert knowledge to reduce the uncertainty on maintenance decisions.

A further disadvantage of data-driven monitoring systems is their dependencies on experienced failures and large amount of data, especially for classification. In this work for instance, historical failures were used, which implies that training the algorithms was only possible based on a sufficient historical database of aged wind farms. This may represent a limitation to assess the utility of monitoring systems when prior information is still not available.

These challeges must be tackled in real applications, in order for advanced analytics models to be valuable from an financial perspective.

6.3 Future work

The entity of the subject treated in this work is large, and this document only provides few answers. Therefore, there are a number of points that deserve further focus, which are here discussed.

In relation to offshore foundation loads, interest should be posed on quantifying the impact of different environmental models on extreme loads besides fatigue, and provide a description conditional to the significant wave height and wind speed required by IEC standards. This can be achieved by for instance inverse-FORM techniques.

The failure maps should be explored further by including different scenario, as for instance failure and no-failure, and obtain maps based on respective environmental conditions. This will better reveal whether metrics such as DEL, ADC, friction and so on can actually indicate areas of the farm layout with higher risk of failure. Furthermore, degradation models should be included, to explain how the failure maps can evolve over time. For instance, in the example developed in this work, the dynamic of the pitch actuator should comprise friction. An interesting comparison should be made in terms of failure maps and recorded vibration history, since the latter could potentially give a better description of the level of stress in mechanical components. A probabilistic study is also adviced, in order to consider the variability of the full set of environmental parameters more deeply.

For online classifiers, the inclusion of detailed vibration data into prediction models is recommended. Vibrations can provide more robust predictions at longer lead times (see Article V), which would increase the benefit significantly. Furthermore, in online applications, time varying classifiers as for instance based on Markov models [116] should be preferred over static classification. Scaling-up data-driven monitoring systems at a wind farm level will enable flexible learning, allowing pair-wise comparison between turbines.

Further research is also necessary towards standardization of monitoring systems, by combining CMS and SCADA data. This will enable a less amount of data to process, less sensors to install and easier interpretation by the user. Moreover, given N occurrences of the same type of SCADA alarm, it may be of interest to quantify after how many alarms the system experiences failure.

The decision models should be extended to include longer lead times, thus allowing for more actions and different consequences. Pre-posterior decision analyses could be implemented, in order to find optimal maintenance decisions based on observed failures and updated parameters in the decision models.

A final suggestion for future work is the continuation of the implementation of the friction model into the actuator motion based on forces. The friction contribution into the turbine dynamic could potentially reveal interesting connections between failures of hydraulic pitch systems and loads.

Collaborative work

Article IV, V

The following articles have been made in collaboration with other PhD students in the AWESOME project, Jannis Tautz-Weinert, Loughborough University, UK, and Maik Reder, CIRCE - University of Zaragoza, Spain. The initial idea of the work was defined during an industrial workshop hosted by Rambøll in Berlin, Germany, in February 2016. The objective of the workshop was to promote communication between the PhD researchers and industrial experts, in order to solve practical problems of interest for the industry.

Available online at www.sciencedirect.com

ScienceDirect

Energy Procedia 137 (2017) 571–578

Energy Procedia

www.elsevier.com/locate/procedia

14th Deep Sea Offshore Wind R&D Conference, EERA DeepWind'2017, 18-20 January 2017, Trondheim, Norway

Optimisation of Data Acquisition in Wind Turbines with Data-Driven Conversion Functions for Sensor Measurements

L. Colone [*,a], M. Reder[*,b], J. Tautz-Weinert[*,c], J.J. Melero[b], A. Natarajan[a], S.J. Watson[c]

[*] *Shared first authorship - authors contributed equally to the publication and are presented in alphabetical order.*

[a] *Technical University of Denmark, Frederiksborgvej 4000, Roskilde, Denmark*
[b] *CIRCE - Universidad de Zaragoza, C/ Mariano Esquillor 15, 50018, Zaragoza, Spain*
[c] *CREST - Loughborough University, Holywell Park, Loughborough, LE113TU, UK*

Abstract

Operation and Maintenance (O&M) is an important cost driver of modern wind turbines. Condition monitoring (CM) allows the implementation of predictive O&M strategies helping to reduce costs. In this work a novel approach for wind turbine condition monitoring is proposed focusing on synergistic effects of coexisting sensing technologies. The main objective is to understand the predictability of signals using information from other measurements recorded at different locations of the turbine. The approach is based on a multi-step procedure to pre-process data, train a set of conversion functions and evaluate their performance. A subsequent sensitivity analysis measuring the impact of the input variables on the predicted response reveals hidden relationships between signals. The concept feasibility is tested in a case study using Supervisory Control And Data Acquisition (SCADA) data from an offshore turbine.

Peer-review under responsibility of SINTEF Energi AS.

Keywords: Wind Turbine, Condition Monitoring, SCADA, Data Optimisation, Data Mining, Operation and Maintenance (O&M);

1. Introduction

The costs associated with Operation and Maintenance (O&M) of wind turbines account for about 10-15% of the overall energy generation cost for onshore [1] and 25-30% for offshore wind turbines [2]. For wind farms approaching the end of life the O&M costs may rise up to 35% [3]. Currently, the wind industry is incurring significant numbers of main component failures, causing large downtimes and consequently loss of power production [4], [5], [6]. Throughout many years of experience in other industrial sectors, condition based maintenance (CBM) has become an established and cost-effective maintenance strategy [7], [8]. The need for cost-effective maintenance is further intensified

[*] Corresponding authors
E-mail address: lcol@dtu.dk, mreder@fcirce.es, j.tautz-weinert@lboro.ac.uk

1876-6102
Peer-review under responsibility of SINTEF Energi AS.
10.1016/j.egypro.2017.10.386

by the increasing installation of wind turbines offshore, where logistics are more difficult. This implies an increased reliance on remote sensing systems for health assessment in the transition from corrective to predictive maintenance.

Early condition monitoring of wind turbines was based on the high frequency signals provided by a dedicated Condition Monitoring System (CMS), in particular acceleration measurements (cf. [7]). The advantages and economic benefits of CMS in the wind energy sector were analysed for instance in [9]-[10]. Current trends also provide clear evidence of an increasing exploitation of Supervisory Control And Data Acquisition (SCADA) data for monitoring purposes, thanks to its economic advantages and well established online data management. Following the latest development in the field with regards to wind energy applications, artificial intelligence systems are receiving greater consideration. An example of application is presented by Kusiak and Verma where genetic programming is employed to predict blade pitch faults as early as an hour before occurrence [11]. Bangalore and Tjernberg detected gearbox bearing damage with artificial neural networks (ANNs) one week earlier than the CMS [12]. A comprehensive review of the main advances in this area is provided in [13].

There is a potential to widen the monitoring concept by taking advantage from combined information of operational and condition monitoring data. However, wind farm operators and manufacturers claim to gather extensive data from wind farms while lacking the capability to translate data into useful information for decision making. This motivates further research for optimisation and standardisation of monitoring systems [14]. In this context, less effort has been made to investigate synergistic effects of coexisting sensing technologies, e.g. SCADA and CMS. Hence, modern approaches should focus on analysing the correlation between signals, in the attempt to enable better understanding of the measurement data and eventually exclude irrelevant input variables.

The initial idea of the concept presented in this paper was developed during the 1st *Joint Industrial Workshop* (JIW) within the European Union's H2020 project AWESOME, as documented in [15]. This work is a continuation and extension of the main idea presented in the workshop. A case study is carried out testing different techniques on field data. The primary objective is the optimisation of the data acquisition by taking advantage of correlated signals and mining algorithms. The base of the methodology is the prediction of certain variables using a set of conversion functions between measurements. The approach is fully data driven, which implies that it is not relying on physical models. The next section of this paper includes an outline of the proposed approach, followed by details of a case study and results. The last section provides an outlook of ongoing and recommended future research in this field.

2. Methodology

A framework is proposed to investigate relationships between coexisting measurements to reveal potentially helpful correlations and synergistic effects. This hidden information will be identified by the evaluation of data-driven conversion functions. To allow all possible interactions, selecting the input-output relations is not limited to a physical understanding of the system. On the contrary, each available signal $x_1, x_2, x_3 ... x_{n-1}$ has to be used as an input for modelling one of the other signals (x_i). Only the target signal itself is excluded from the input set, in order to discard trivial conversion functions. Each signal acts once as the target, resulting in n multiple input and single output conversion functions predicting with an error ϵ.

$$x_i = f_i(x \in X \setminus x_i) + \epsilon_i \qquad \text{with } X = \{x_1, x_2, x_3, ..., x_n\} \text{ and } i = 1, 2, 3, ..., n \tag{1}$$

Figure 1 illustrates a single exemplary conversion function in a wind turbine drive train. The investigation of synergistic effects is based on three main steps:

1. Pre-process and extract features of training data,
2. Build n conversion functions,
3. Evaluate conversion functions.

In the first step, measurement data are prepared to be used to set up and feed the conversion functions. Preprocessing has to include checking for missing signals and invalid values. Duplicated or non-working sensors are excluded. As SCADA signals, which are commonly provided in 10 minute resolution, will be combined with dedicated CMS measurements at high sampling rate, a common working frequency has to be determined. It might be

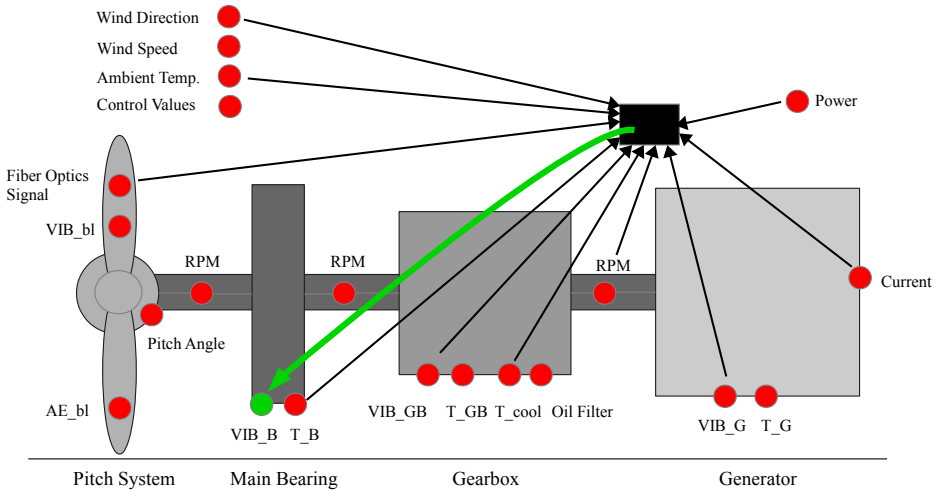

Fig. 1. Exemplary scheme for modelling the main bearing vibration (VIB_B, green dot) with the conversion function (black box). The input signals for the conversion function are depicted with red dots. T: temperature, VIB: vibration, RPM: rotational speed, AE: acoustic emission, bl: blade, B: main bearing, GB: gearbox, G: generator.

reasonable to further normalise the temperatures, speeds or or oil particle counts, calculating amplitudes in characteristic frequency bands for accelerations or use amplitudes or energy measures for acoustic emission.

In the second step, conversion functions are trained with measured data. The conversion function f needs to be capable of modelling non-linear relationships. A suitable regression technique has to be selected according to the properties of the signal as techniques might perform differently for predicting different kinds of signals. The selected training window must be representative for the behaviour of the turbine and sufficiently long.

In the final step, the conversion functions are evaluated in terms of the prediction accuracy. If all possible inputs are used then the prediction performance can be assessed to determine whether a signal is independent. If it is representable by a function of the other signals, the contribution of the individual inputs has to be evaluated with a sensitivity study to identify hidden relationships.

3. Case study

A brief case study with only SCADA data is conducted to test the proposed procedure. Although, the intention is to combine SCADA and CMS signals for a full analysis, this application to real data demonstrates the methodology. In the absence of a full set of signals, six SCADA sensor signals from an offshore wind turbine provided as 10-minute average are available as listed in Table 1. In this simple case, pre-processing of signals as the step 1 of the procedure can be reduced to a validity check as feature extraction is not required.

Table 1. SCADA signals used in the analysis provided as 10 minute average.

Variable	Unit
Rotor speed (low speed shaft)	rpm
Pitch angle	deg
Yaw angle	deg
Tower-top acceleration in x-direction (fore-aft)	m/s^2
Tower-top acceleration in y-direction (side-side)	m/s^2
Active power	MW

In order to find the most suitable tool for building the conversion functions in step 2, four different regression techniques are tested on two of the signals: (i) Random Forests (RF), (ii) Generalized Linear Model (GLM), (iii) Gradient Boost Machine (GBM) and (iv) Artificial Neural Networks (ANNs).

GLMs are flexible generalised linear regression models, formulated by Nelder & Wedderburn [16]. These types of model allow the error to be a distribution other than the normal distribution. A canonical link function for a gaussian distribution is used. Maximum likelihood estimation is used to fit the model to the data.

GBM is a regression and classification technique that originated from the idea of gradient boosting in order to create an optimisation algorithm on a cost function in Breiman [17]. The regression gradient boosting algorithm was developed by Friedman et al.[18]. GBM builds a stage-wise prediction model that consists of a combination of weak prediction models, such as e.g. decision trees.

RF is a machine learning algorithm, which is also frequently used for classification and regression analysis. The main idea was firstly developed in 1995 by Ho et al. [19] and later Breiman et al. [20] introduced the actual algorithm known as random forests. The latter uses a combination of tree predictors and an out-of-bag error as estimate for the generalisation error. The predictor variable importance is then obtained using permutation.

ANNs are a widely used tool for learning non-linear relationships inspired by the human brain. In a network of layers of nodes, each node's output is fed to all nodes in the next layer. In this study, an architecture of feed-forward network with one input, one hidden and one output layer with 20 neurons in the hidden layer is trained by Levenberg-Marquardt backpropagation [21]. Each neuron in the hidden layer produces an output with a hyperbolic tangent sigmoid transfer function. ANNs have been applied successfully to wind turbine condition monitoring, e.g. [12].

The performance is evaluated for different training times. For this purpose, three datasets, as explained in Table 2, corresponding to cases *(A)*, *(B)* and *(C)* are used. Each set is divided into a training and a testing subset.

Table 2. Definition of training and testing subsets for increasing length of the dataset.

	Case *(A)*	**Case *(B)***	**Case *(C)***
Training	48 days	108 days	156 days
Testing	16 days	36 days	52 days
Total	64 days	144 days	208 days

In order to evaluate the performance of the conversion functions in step 3, the performance metrics root mean square error (RMSE), mean absolute error (MAE) and the coefficient of determination R^2 are used, defined as:

$$RMSE = \sqrt{\frac{1}{N}\sum_{i=1}^{N}(\hat{y}_i - y_i)^2}, \qquad MAE = \frac{1}{N}\sum_{i=1}^{N}\sqrt{(\hat{y}_i - y_i)^2}, \qquad R^2 = 1 - \frac{\sigma(\hat{y} - y)^2}{\sigma(y)^2}; \tag{2}$$

where $\hat{y}$ is the predicted variable, y its true value and σ denotes the standard deviation.

The sensitivity of the conversion function accuracy to the different inputs is analysed by training and testing of conversion functions for all possible combinations of inputs (31 combinations for 5 possible predictors for each target) based on case *(C)*.

4. Case study results

In this section the results are presented for the comparison of modelling techniques and the input sensitivity study.

Comparison of modelling techniques

Table 3 and Table 4 summarise the blind testing results for the predictions of the active power and the tower acceleration in x-direction using the four different techniques and three different datasets. The values for *MAE* and *RMSE* are all normalised to the rated power of the turbine or the maximum tower acceleration in x-direction, respectively. It can be seen, that the GLM did not perform well in predicting the active power and thus it will not be considered further. RF, GBM and ANNs performed well and showed similar results. An extended training time seemed to influence the performance of RF and GBM positively, resulting in lower values for MAE and RMSE and higher ones for R^2. ANNs showed the best model metrics for case *(B)*. Thus, their performance did not necessarily enhance with higher amounts of input data.

Table 3. Results for the MAE, RMSE and R^2 with different training input sizes for predicting the active power (MAE and RMSE normalised to rated power).

Technique	**Case *(A)***			**Case *(B)***			**Case *(C)***		
	MAE	RMSE	R^2	MAE	RMSE	R^2	MAE	RMSE	R^2
GLM	0.139	0.170	0.781	0.160	0.187	0.768	0.167	0.194	0.759
RF	0.021	0.035	0.990	0.017	0.032	0.993	0.016	0.031	0.994
GBM	0.017	0.030	0.993	0.015	0.031	0.994	0.014	0.028	0.995
ANNs	0.021	0.035	0.991	0.019	0.030	0.994	0.020	0.034	0.993

Table 4. Results for the MAE, RMSE and R^2 with different training input sizes for predicting the Tower acceleration in the x-direction (MAE and RMSE normalised to maximum value).

Technique	**Case *(A)***			**Case *(B)***			**Case *(C)***		
	MAE	RMSE	R^2	MAE	RMSE	R^2	MAE	RMSE	R^2
GLM	0.194	0.230	0.301	0.210	0.251	0.245	0.207	0.247	0.273
RF	0.103	0.142	0.740	0.091	0.130	0.809	0.091	0.127	0.811
GBM	0.084	0.132	0.790	0.070	0.115	0.851	0.073	0.115	0.850
ANNs	0.050	0.094	0.884	0.039	0.075	0.933	0.054	0.093	0.899

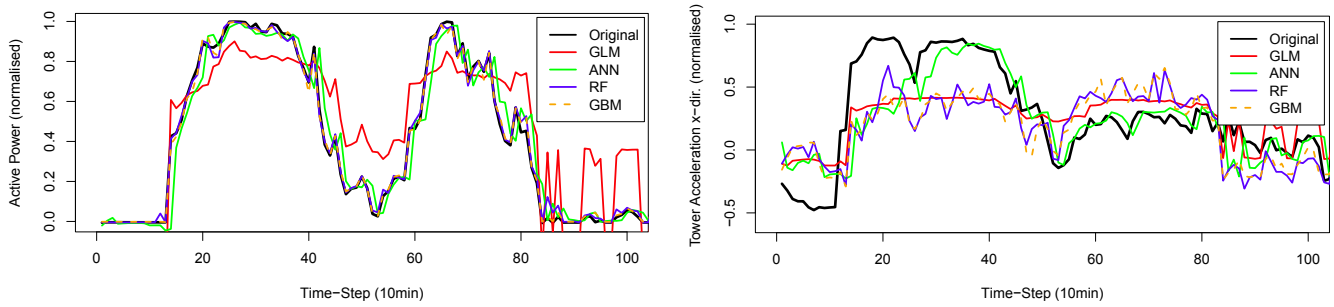

(a) (b)

Fig. 2. Original and predicted *(a)* power production and *(b)* tower acceleration in the x-direction for 100 time-steps based on case *(C)*.

As shown in Table 4, for the blind testing of the tower acceleration prediction the ANNs clearly showed the best results for all three cases. Regarding the training time, GBM and ANNs showed both a slightly better performance for input case *(B)*. Figure 2a shows the original and predicted active power using the four different techniques, normalised to the turbine's rated capacity. Figure 2b shows the original and predicted tower acceleration in the x-direction normalised to the maximum value of the original data set. Due to limited space only a selection could be displayed, thus, both figures show the first 100 time-steps of the blind testing based on case *(C)*. The better prediction of the active power compared to the acceleration is due to the strong correlation of the active power to all variables employed in the analysis. For the tower acceleration this is not the case, as discussed in the subsequent sensitivity analysis.

Input sensitivity study

As ANNs performed well for both the prediction of the active power and the tower accelerations, the sensitivity study on the variable importance is carried out with ANNs. Figures 3 - 5 show the results of the input sensitivity study. As there are five possible inputs for each predicted signal, 31 combinations are given on the abscissa. The performance of each input combination is given as the testing R^2 on the ordinate based on case *(C)*. The composition of each combination is displayed by overlaying different markers for the inputs. It can be seen that rotor speed and pitch angle are the most important signals for predicting the active power. If these two are combined, adding

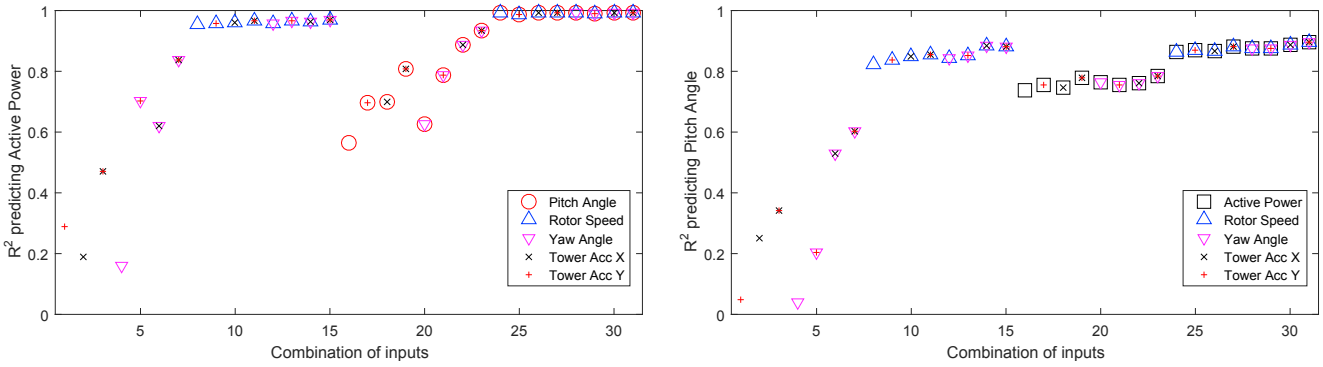

(a) (b)

Fig. 3. Modelling accuracy for all possible input combinations if predicting *(a)* active power and *(b)* pitch angle.

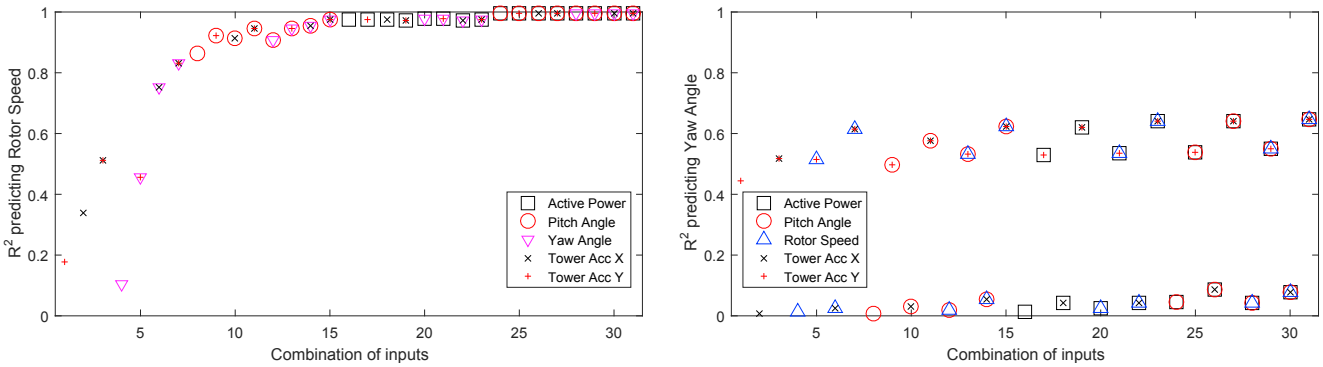

(a) (b)

Fig. 4. Modelling accuracy for all possible input combinations if predicting *(a)* rotor speed and *(b)* yaw angle.

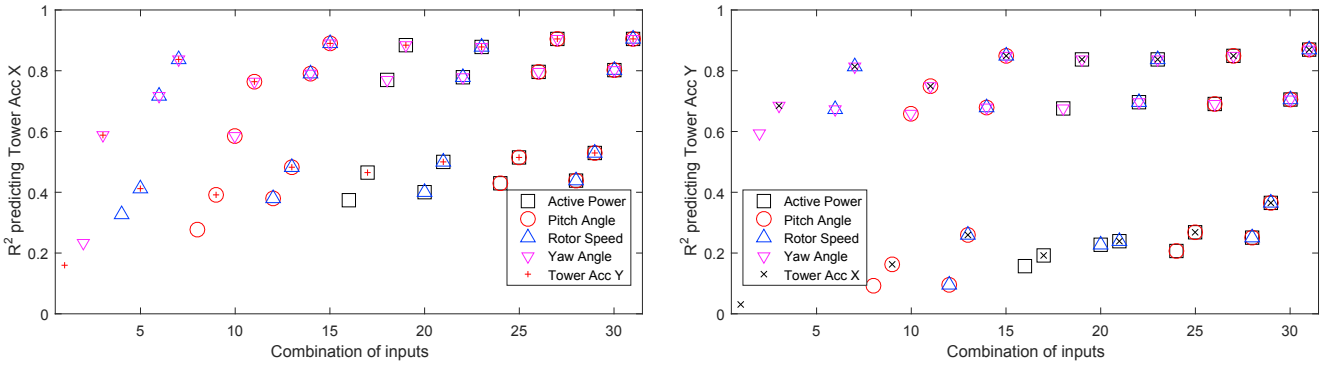

(a) (b)

Fig. 5. Modelling accuracy for all possible input combinations if predicting *(a)* tower-*x* acceleration and *(b)* tower-*y* acceleration.

the remaining signals does not contribute to a significantly better accuracy. Similarly, only active power and rotor speed are necessary to predict the pitch angle. The active power is also the best single input predictor for the rotor speed. Surprisingly, predicting the yaw angle is possible if the tower acceleration in the *y*-direction is included in the inputs. This might reveal the presence of site-specific effects of misalignments causing this relationship. The tower acceleration in the *x*-direction is best modelled in all cases by a single input if again active power is chosen. However, adding yaw angle as an input is a clear benefit in all cases. The strong relationship of tower acceleration in the *y*-direction and yaw angle can also be seen if the tower *y* acceleration is predicted.

Figure 6 visualises the identified relationships of the SCADA signals. An arrow from one node to another stands for a prediction of the target node signal using the start node signal. The thickness of the connections between the

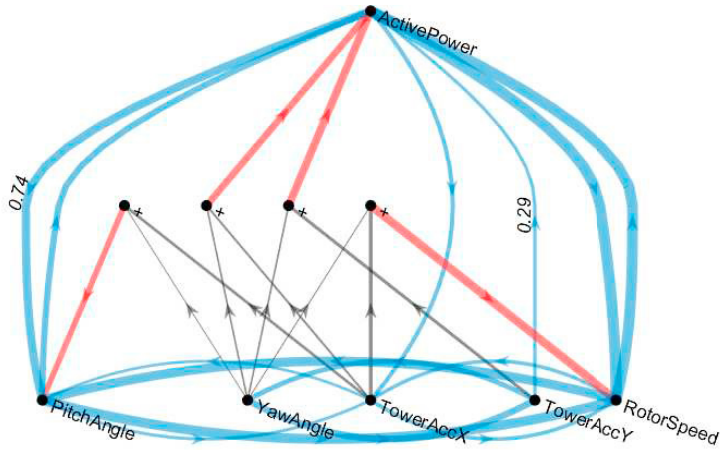

Fig. 6. Diagram of the relationship between investigated SCADA signals in terms of correlation measure R^2. Blue arrows depict single-input predictions (with $R^2 > 0.25$ for clarity), grey arrows contribute to a combination of two inputs in a node marked with + and red arrows combined predictions significantly better than individual modelling.

nodes depicts the accuracy of prediction in terms of R^2. The strong relationship of active power, pitch angle and rotor speed is easily identifiable. Synergistic effects are shown by adding accuracies of predictions with two combined inputs, which are significantly better than predicting with the individual inputs. The strongest synergistic effects are seen in combining yaw angle with the tower accelerations.

5. Conclusions and outlook

In this work a novel approach for wind turbine condition monitoring was presented focusing on synergistic effects between measured signals. The concept is based on predicting certain sensor signals using the information of other sensors at different locations in the turbine. Conversion functions are employed in order to make these predictions. In this work four machine learning algorithms: generalised linear models (GLM), gradient boosting machine (GBM), random forests (RF) and artificial neural networks (ANN) are tested for the conversion functions. Their performance was evaluated in a case study using 10 minute average SCADA data from an offshore wind farm. Three different sizes of the training dataset were used in order to analyse the effects of different training times on the quality of the outcome.

The results show that for predicting each of the parameters the different algorithms performed differently. GBM, RF and ANNs showed very good results for both of the presented predictions. Nonetheless, ANNs showed slightly better results, especially for predicting the tower acceleration, and were used to carry out a sensitivity study demonstrating the variable importance of the predictors and the predicted parameters. The sensitivity study suggests how to interpret the synergistic effects of combined measurements to predict a specific response.

The presented approach has shown to work well and will be extended in future studies. As the case study only contained a limited sample data set, the machine learning algorithms will have to be tested on different datasets and a sensitivity study has to be carried out for the contained parameters. These can contain for instance CMS data in combination with SCADA data. The challenge here will be to understand how signals can be analysed at different sampling frequencies, time windows and continuity in time. Also, the optimal training time should be investigated, as it has been stated that especially ANNs are very sensitive to the latter and do not necessarily show better results with more input data. Furthermore, extending the conversion functions so that measurements from one wind turbine are used to model the status of other turbines in the wind farm, could reduce monitoring costs even further.

In conclusion, further development of this novel approach may result in several benefits for wind farm O&M practice. These range from possible economic benefits by omitting costly sensors in condition monitoring systems, as their information could be predicted using other measurements, to controlling the accuracy of certain sensor outputs by modelling their supposed thresholds. Nevertheless, additional research is also needed to quantify the real economic benefit of O&M by the method proposed.

Acknowledgements

The authors thank the participants of the 1st *Joint Industrial Workshop* (JIW) within the AWESOME project, in particular Estefania Artigao, Ravi Pandit, Lisa Ziegler, Michael Muskulus and Ursula Smolka, who contributed to the development of the idea.

This project has received funding from the European Union's Horizon 2020 research and innovation programme under the Marie Sklodowska-Curie grant agreement No 642108.

References

[1] Lu, B., Li, Y., Wu, X., Yang, Z.. A review of recent advances in wind turbine condition monitoring and fault diagnosis. 2009. In: *2009 IEEE Power Electronics and Machines in Wind Applications*;(1):1-7.

[2] Rademakers, L., Braam, H., Obdam, T., Pieterman, R.. Operation and maintenance cost estimator (OMCE) to estimate the future O&M costs of offshore wind farms. *European Offshore Wind 2009 Conference* 2009;(1):14–16.

[3] Tchakoua, P., Wamkeue, R., Ouhrouche, M., Slaoui-Hasnaoui, F., Tameghe, T., Ekemb, G.. Wind Turbine Condition Monitoring: State-of-the-Art Review, New Trends, and Future Challenges. *Energies* 2014;7(4):2595–2630.

[4] Carroll, J., McDonald, A., McMillan, D.. Failure rate, repair time and unscheduled O&M cost analysis of offshore wind turbines. *Wind Energy* 2016;19(6):1107–1119.

[5] ReliaWind, . Project final report - RELIAWIND - Reliability - Focused Research on Optimizing Wind Energy System Design, Operation and Maintenance: Tools, Proof of Concepts, Guidelines & Methodologies for a new Generation Funding. Tech. Rep.; 2011. URL: *http://cordis.europa.eu/result/rcn/55560_es.html*. Last Accessed: 12/01/2017.

[6] Reder, M.D., Gonzalez, E., Melero, J.J.. Wind Turbine Failures - Tackling current Problems in Failure Data Analysis. *Journal of Physics: Conference Series* 2016;753(072027):1–11.

[7] Randall, R.B.. *Vibration-based Condition Monitoring: Industrial, Aerospace and Automotive Applications*. Chichester, UK: John Wiley & Sons, Ltd; 2011.

[8] Davies, A., editor. *Handbook of Condition Monitoring*. Dordrecht: Springer Netherlands; 1998.

[9] Nilsson, J., Bertling, L.. Maintenance Management of Wind Power Systems Using Condition Monitoring Systems& Life Cycle Cost Analysis for Two Case Studies. *IEEE Transactions on Energy Conversion* 2007;22(1):223–229.

[10] Besnard, F., Nilsson, J., Bertling, L.. On the economic benefits of using condition monitoring systems for maintenance management of wind power systems. 2010. In: *IEEE 11th International Conference on Probabilistic Methods Applied to Power Systems*;(1):160–165.

[11] Kusiak, A., Verma, A.. A Data-Driven Approach for Monitoring Blade Pitch Faults in Wind Turbines. *IEEE Transactions on Sustainable Energy* 2010;2(1):87–96.

[12] Bangalore, P., Tjernberg, L.B.. An Artificial Neural Network Approach for Early Fault Detection of Gearbox Bearings. *IEEE Transactions on Smart Grid* 2015;6(2):980–987.

[13] Tautz-Weinert, J., Watson, S.J.. Using SCADA data for wind turbine condition monitoring - a review. *IET Renewable Power Generation* 2016;In Press. URL: *http://dx.doi.org/10.1049/iet-rpg.2016.0248*. Last Accessed: 04/04/2017.

[14] European Technology and Innovation Platform on Wind Energy, . Strategic research and innovation agenda 2016. Tech. Rep. September; 2016. URL: *https://etipwind.eu/*. Last Accessed: 12/01/2017.

[15] Artigao, E., Colone, L., Pandit, R., Reder, M., Weinert, J., Ziegler, L.. Optimisation of data acquisition in wind turbines with data-driven conversion functions for measurements. Tech. Rep.; 2016. Melero, J.J., Muskulus, M., Smolka, U., editors. In: *1 st Joint Industry Workshop Scientific report*; Zaragoza, Spain; URL: *http://awesome-h2020.eu/1st-joint-industry-workshop-scientific-report/*. Last Accessed: 12/01/2017.

[16] Nelder, J., Wedderbu, R.. Generalized Linear Models. *Journal of the Royal Statistical Society, Series A-General* 1972;135(3):370–384.

[17] Breiman, L.. Arcing the edge. Tech. Rep.; Statistics Department - University of California; Berkeley, CA; 1997. URL: *https://www.stat.berkeley.edu/ breiman/arcing-the-edge.pdf*. Last Accessed: 12/01/2017.

[18] Friedman, J.H... Greedy Function Approximation : A Gradient Boosting Machine. *The Annals of Statistics* 2001;29(5):1189–1232.

[19] Ho, T.K.. Random Decision Forests. 1995. In: *Proceedings of the 3rd International Conference on Document Analysis and Recognition*;1:278–282.

[20] Breiman, L.. Random Forests. Tech. Rep.; Statistics Department - University of California; Berkeley, CA; 2001. URL: *http://link.springer.com/10.1023/A:1010933404324*. Last Accessed: 12/01/2017.

[21] Marquardt, D.W.. An Algorithm for Least-Squares Estimation of Nonlinear Parameters. *Journal of the Society for Industrial and Applied Mathematics* 1963;11(2):431–441.

Automated Fault Detection Algorithms for Wind Turbines using CMS and SCADA Data

Maik Reder[a], Jannis Tautz-Weinert[a,b], Lorenzo Colone[c], Simon J. Watson[d], Julio J. Melero[a,*]

[a] *CIRCE – Universidad de Zaragoza, C/ Mariano Esquillor Gómez 15, 50018, Zaragoza, Spain*
[b] *CREST – Loughborough University, Holywell Park, Loughborough, LE113TU, UK*
[c] *Technical University of Denmark, Frederiksborgvej 4000, Roskilde, Denmark*
[d] *DUWIND – Delft University of Technology, Kluyverweg 1, 2629 HS Delft, Netherlands*

Abstract

Wind turbines are commonly monitored by analysing spectral properties of high frequency (kHz range) vibrations using a dedicated Condition Monitoring System (CMS) or by applying machine learning techniques to low frequency (ten-minute) operational data from the Supervisory Control And Data Acquisition (SCADA) system. So far, these two approaches have been investigated separately, but there could be benefits in combining the data sources for simplified data processing and improved understanding of the required data for failure prediction. In this paper, a framework is developed for merging the CMS vibration records and respective alarms with ten-minutely SCADA data to build a consistent database. The main objective is to develop automated fault detection. Based on real data from an onshore wind farm, this is carried out by, firstly, applying clustering and distance-based techniques to investigate relationships between different signals. Secondly, an automated tool is developed to evaluate vibration measurements considering a comparison at farm level. And thirdly, failure prediction is performed with four classification techniques and different input data combinations. The results show the power of both automated and machine learning frameworks for failure predictions, which outperform the alarms of the commercial CMS for the discussed main bearing failures and can predict failures up to 119 days before they occur.

Keywords: Wind turbine, Operation and Maintenance, Condition Monitoring, Machine Learning, CMS, SCADA

1. Introduction

Over the past years, wind turbine (WT) Operation and Maintenance (O&M) has become an emerging field of research. Operators are interested in finding new ways to anticipate wind turbine component failures and to optimise their maintenance strategies. A coordinated shift towards condition-based maintenance could significantly lower the costs related to O&M. Supervisory control and data acquisition (SCADA) systems are standard in modern WTs. However, WTs are increasingly being equipped with condition monitoring systems (CMS), which in many cases is a requirement for certification and insurance purposes.

In this paper, novel automated failure detection techniques based on combining data from both SCADA and CMS, are presented. Furthermore, the relationship between the two data types with the aim of enhancing predictive O&M is investigated. In the following, the motivation and objectives of this work are discussed in more detail. Section 2 gives an overview of failure detection with CMS and SCADA data, before Section 3 introduces the analysed data. Sections 4 and 5 explain the used approach and observed results, respectively. The discussion of the findings is gathered in Section 6. Section 7 concludes this paper and lists tasks for future work.

*Corresponding author (J.J. Melero).
Email addresses: mreder@fcirce.es (M. Reder), jannis.tautz-weinert@ramboll.com (J. Tautz-Weinert), lcol@dtu.dk (L. Colone), s.j.watson@tudelft.nl (S.J. Watson), melero@unizar.es (J.J. Melero)

1.1. Motivation

While CMS have been used in several industries over many years, only recently have WT operators started to install dedicated CMS. This is due to the fact that installing CMS is rather expensive [1, 2], and thus, might not be profitable for all wind farms. It could, however, be a financially attractive investment if the benefits of early failure detection can outweigh the initial installation cost. At the same time, as SCADA systems are installed in nearly all operating WTs, recent research has focused on using exclusively SCADA data for WT condition and performance monitoring, implying no additional installation cost for CMS.

CMS and SCADA data have been compared for failure detection [2, 3] but to the authors' knowledge, combining data from these two sources has not been explored as yet. There have been efforts to combine SCADA and vibration measurements [4, 5], but this has been limited to the time-domain information in vibrations also recorded in the SCADA system. The synergies within different SCADA channels have previously been analysed by the authors in [6]. In the present paper, the aim is to use both SCADA and full CMS data, which could eventually lead to advanced knowledge of the WT health and remaining lifetime as pointed out previously, [7].

There are many reasons for combining CMS and SCADA in one database to enhance industrial O&M practice. Both data sources contain important information on the turbine health and the operational and environmental conditions at different level of detail. Most intuitively, the fact that one of the systems can fail at any time and that the fault indicating sensor information of one system might not be available when needed [8], calls for including different information sources to ensure a reliable fault detection. In several meetings with European wind farm operators, it was observed that there are currently problems related to the CMS and SCADA data processing, merging the information contained in both sources and automating the failure detection process, [9]. Furthermore, installing CMS as well as storing and analysing their data is often quite expensive and time consuming. Hence, failure detection based on SCADA data could be used as a first and fast method to find faulty components. Since CMS data usually contain more detailed information on the components' health, the techniques based on vibration measurements can be used to reduce uncertainty in the failure detection and to further specify the failure modes. Nonetheless, also SCADA data contain information, which is not present in the CMS data, such as operational variables like pitch angles, active power production, temperatures, overloads, rotational speed, curtailment, etc. These could be very important inputs for the failure detection algorithms of certain components, and thus, could enhance the failure prediction. In addition, for extending the turbine lifetime or making decisions on component maintenance, not only knowledge from vibration data are necessary, but the entire operational history.

This paper extends the current state of the art in WT failure detection, firstly, by providing a new method for merging the data of two distinct sources, i.e. CMS and SCADA. Furthermore, the development of automated failure detection algorithms using either one or a combination of both sources provides new insight on how data can be used for this purpose. New tools are proposed that can complement and automate conventional failure detection. However, the overall aim is not to replace conventional CMS or the analyses of their data, but rather to explore the possibilities for automated failure detection. This could significantly enhance the operators' ability to react to emerging component failures and consequently decrease the cost related to O&M. In addition, it can be imagined that, due to operational or financial reasons, the CMS might not constantly be in operation and SCADA data might provide primary monitoring based on learned relationships.

1.2. Objectives of the paper

Firstly, this paper proposes a framework for merging CMS vibration data with the ten-minute recordings from the SCADA system to provide useful input to data analyses and machine learning algorithms. The processed data are then used for the following objectives:

- *Understanding relationships between data:* explore similarities of different signals in the merged data set.
- *Distance-based automated vibration evaluation:* develop an algorithm for automated failure detection based on CMS data.
- *Prediction of CMS alarms:* evaluate the possibility of giving earlier warnings than the CMS system based on data-driven learning. The following approaches are considered:

– *Count of alarms:* predict the number of alarms only with SCADA data to investigate the possibility of substituting CMS.
– *Time dependent probability of alarm:* predict the probability of failures as an approach for early warnings based on only SCADA data.
– *Alarm time shifting:* predict the alarm in a classification set-up as an alternative approach for early warnings, focussing also on the benefit of adding CMS data to the prediction.

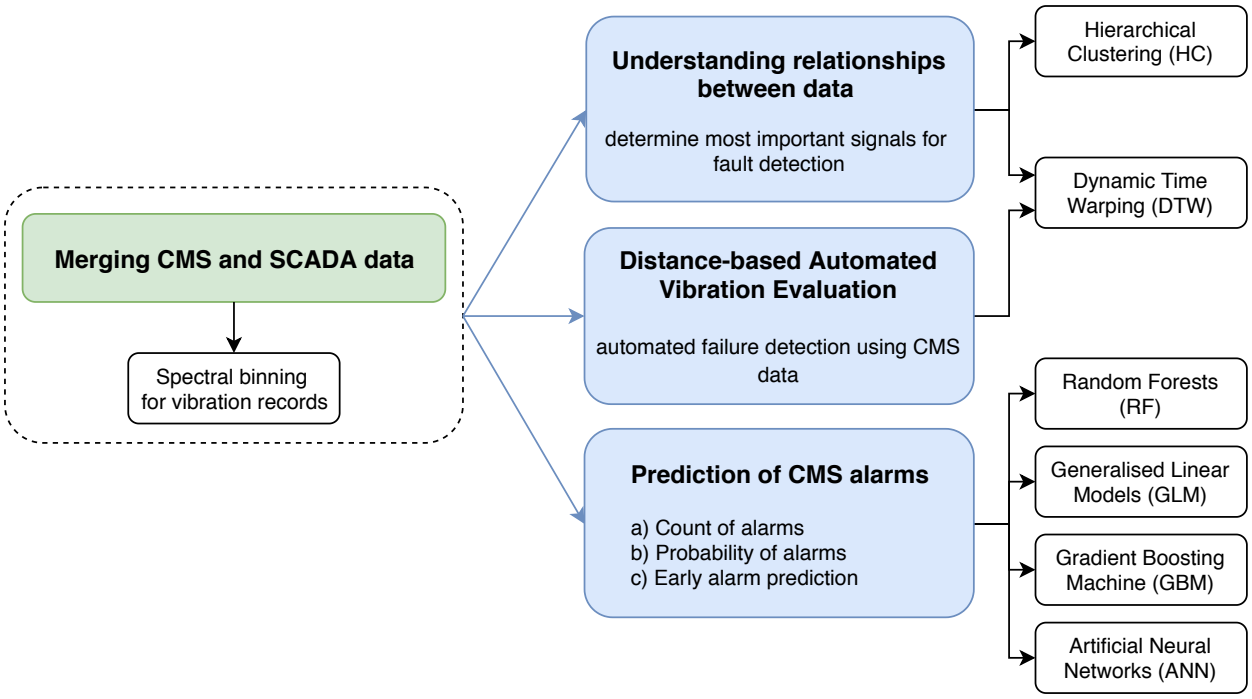

Figure 1: Application of the merged data for different purposes

Figure 1 illustrates the different objectives of this paper with the techniques applied. The overall aim is to provide the basis for further research on how SCADA and CMS data can be combined and used to optimise WT maintenance. As this work is primarily intending to explore the possibilities of automated failure detection using either SCADA, CMS data, or both data sources, the objectives presented in Figure 1 are not necessarily building on each other, but should be treated as separate approaches.

2. Background

This section details the state of the art in condition monitoring with CMS and SCADA data, which provides the background for this study.

2.1. Condition monitoring with CMS data

In general, a CMS consists of sensors installed at different locations in the WT with the purpose of e.g. vibration analysis, acoustic measurements, oil analysis and strain measurement, [10]. This paper will focus on vibration analysis as it is the most widely used technique in WT condition monitoring, due to the profound experience obtained in other industries for rotating machinery, [2]. Accordingly, in this paper, the term CMS data will be used to refer exclusively to vibration data obtained from the CMS.

Manual analysis of raw vibration data is a rather difficult task and has limited benefit for failure detection. Common processing techniques include time-domain analysis, such as Hilbert transform, statistical analysis (root mean square

(RMS)) and Envelope analysis; frequency domain techniques like the Fast-Fourier-Transform (FFT) and Cepstrum analysis, as well as time-frequency techniques, e.g. wavelet-transform, [11]. Commercial CMS usually send out alarms, when the component's vibration level indicated by the Envelope, FFT, Cepstrum or RMS exceeds a predefined threshold.

2.1.1. Fast-Fourier-Transform (FFT) for fault detection

The FFT is the most widely used technique to obtain the frequency spectrum and then relate certain frequencies directly to degradation processes or specific WT component faults, [12, 13]. An FFT can be used to discover faults in stationary signals, but non-stationary signals might result in indistinct FFT results. As WTs operate in highly non-stationary conditions, several approaches have been developed to ensure stationarity before applying an FFT, [14, 15].

2.1.2. Envelope analysis for fault detection

Another frequently applied signal processing technique is called Envelope analysis, which helps to detect fault frequencies that might not be present in the spectrum generated by the FFT, such as shock impulse repetition and their harmonics, [16]. A bandpass filter is applied to the time domain signal that centres on the desired frequency energy region. Then amplitude demodulation is performed on the filtered time signal to extract the repetition rate of the impact. By taking the FFT of the enveloped signal, the characteristic 'impact frequencies' and their modulations, such as sidebands, can be derived.

2.1.3. Cepstrum analysis for fault detection

Cepstrum analysis [17, 18] is carried out by taking the inverse Fourier transform of the logarithmic power spectrum. This is very similar to auto-correlation analysis, with the difference that it is performed on the logarithmic scale of the power spectrum. Thus, it mainly emphasizes lower level frequencies, [12, 19, 20].

2.1.4. State of the art: Commercial and automated vibration analysis

In rotating machinery, fault frequencies can usually be distinguished from other frequencies by identifying harmonics or sidebands. While Envelope analysis is performed to find sidebands through amplitude demodulation, Cepstrum analysis is used to distinguish between the different harmonic families, [21]. Combining techniques such as FFT, Envelope and Cepstrum analysis can lead to good failure detection, as they are able to identify distinct failure types. Hence, many commercially available solutions for vibration analysis for WT condition monitoring rely on RMS, FFT, Envelope and Cepstrum analysis for fault diagnosis, [22]. These tools usually require an expert to interpret the results and decide whether a fault is apparent. In [12, 20, 23], extensive reviews on the latest research in condition monitoring based on vibration analysis are given.

Only few researchers, have tried to automate fault detection with CMS data, e.g. by deriving features like side band energy and kurtosis [24], applying deep learning convolutional networks [25], or proposing a monitoring strategy based on a classification with wind and rotor speeds, [26]. However, there is still a need for more generic approaches for fault detection with CMS data and machine learning techniques, which require the least possible human interaction.

2.2. Condition monitoring with SCADA data

As opposed to CMS, SCADA data were initially intended for operation and performance monitoring only. For this reason, only average statistics are recorded to describe the wind conditions (wind speed, direction), the operation (rotational speed, pitch angles, yaw angle, currents, power output) and the component health. The latter can be indicated by the SCADA system with temperatures and, possibly, vibrations. Due to the historical aim of describing the wind conditions, the measurements have a sampling frequency of usually 1 Hz, but only ten-minute statistics are saved. Additionally, all alarms issued by the SCADA system are logged.

An overview of various SCADA-based condition monitoring approaches is given in Tautz-Weinert and Watson, [27]. Research on condition monitoring with SCADA data has investigated the use of the alarm logs [28–31], and shown the effect of weather on the WT failure behaviour, [32]. Wind turbine controller based fault detection using SCADA data was analysed e.g. in [33–35], taking into account how the SCADA signals are influenced by the WT control system. Furthermore, damage models based on SCADA records were investigated, [36, 37]. However, most

attention has been dedicated to the potential of temperature measurements to detect drive-train problems. Some work has tried to observe trends in the relationships between signals [1, 3] and other research has used clustering approaches [38], but the most promising results have been achieved using the normal behaviour modelling of temperatures. These models can be based on artificial neural networks [39, 40], adaptive neuro-fuzzy inference systems [41], or various other regression techniques, [42]. After data-driven training, residuals of measured and modelled temperatures act as indicators for increased energy loss and consequently possible imminent failure. In one case study, it was shown that this approach can detect problems even before a commercial CMS raises an alarm, [43]. However, there is still a need to fully assess the potential of SCADA data for failure detection purposes.

3. Data

This section explains the origin and properties of the measurements and failure documentation that was used to develop and test the proposed algorithms.

This study is carried out using data from 13 WTs (referred to as T01 to T13) located in an onshore wind farm in Denmark. All WTs are three bladed and pitch regulated machines with 2.3 MW rated capacity. The data were recorded throughout an observation period from January 2013 to December 2016. The data set is comprised of:

- SCADA data with 155 channels of 10-minute resolution.
- A log containing the alarms produced by the SCADA system.
- CMS vibration data consisting of multiple FFT, Envelope (Env), Cepstrum and RMS records in non-uniform sampling intervals. The data are obtained from a modern commercial CMS, which is installed in all 13 WTs. The vibration records are labelled with characteristic sampling frequencies and bandwidths, e.g. 'FFT1000' for an FFT with frequencies between 0 and 1000 Hz. For the data processing, it had to be ensured that the vibrations were obtained under stationary conditions. Alternatively, if the data were obtained under non-stationary conditions, techniques to re-sample vibration records could have been applied to achieve the same objective. In the commercial CMS system used for this study, the measurements were taken in seven different active power intervals to classify them under quasi-stationary load and operating conditions. The vibrations of seven WT components were measured:
  1. Generator Drive End (GDE),
  2. Generator Non-Drive End (GNDE),
  3. High Speed Shaft (HS),
  4. Intermediate Speed Shaft (IMS),
  5. Main Bearing (MB),
  6. Planet (P),
  7. Tower top acceleration, which only contained their root mean squared (RMS) amplitude.
- Alarms per component as triggered by the commercial CMS.

This study uses information on component failures and replacements, provided by the operator, and the CMS and SCADA records obtained prior to these failures. In the present case, main bearing failures in turbine T01, T03 and T08 were indicated by both CMS and SCADA systems and were followed by significant downtime. There were no further confirmed major maintenance interventions (e.g. replacements) or main bearing failures during the observation period, but various CMS alarms of different severity. The SCADA alarms used in this study are high temperature alarms related to the main bearing, which were raised automatically by the SCADA system when a critical temperature value was reached. As this component failed shortly after, it is assumed that the related SCADA alarms are no false alarms. The CMS alarms were triggered when the vibration level of the component indicated by the Envelope, FFT, Cepstrum or RMS exceeded a certain threshold. In the present case of main bearing failures, the CMS used the RMS as an indicator.

Note, that for better readability 'spectra' and 'frequency' are used subsequently to describe CMS records, but these terms shall also imply the equivalents in Cepstrum analysis.

4. Methodology

In this section the techniques used to achieve the different objectives of this paper, as displayed in Figure 1, are discussed. Firstly, the data merging process is explained, which lays the foundation for the subsequent applications. Then, the techniques used to understand the relationships between the different data types are introduced. Subsequently, the framework for the automated failure detection is presented. Finally, the data-driven CMS alarm prediction is explained.

4.1. Merging CMS and SCADA

CMS and SCADA data usually have different temporal resolutions. While SCADA measurements are often averaged over 10-minute intervals, CMS measurements are taken once a day or once a week. Hence, the data need to be processed to build a uniform database for thorough analysis and the application of data-driven prediction algorithms.

The different spectra can give information on deteriorating components, indicated by spectral peaks such as their fault frequencies, side-bands and harmonics. For analysing the deterioration of a component, it is necessary to examine the evolution of the amplitudes of different spectral peaks over time to determine whether there a notable trend in their behaviour.

At present, this is done manually by experts, by using plots similar to Figure 2, which shows an example for an Envelope spectrum obtained before and after a main bearing failure. One can clearly see that the amplitude rises for certain frequencies continuously until the failure occurs (in April 2016).

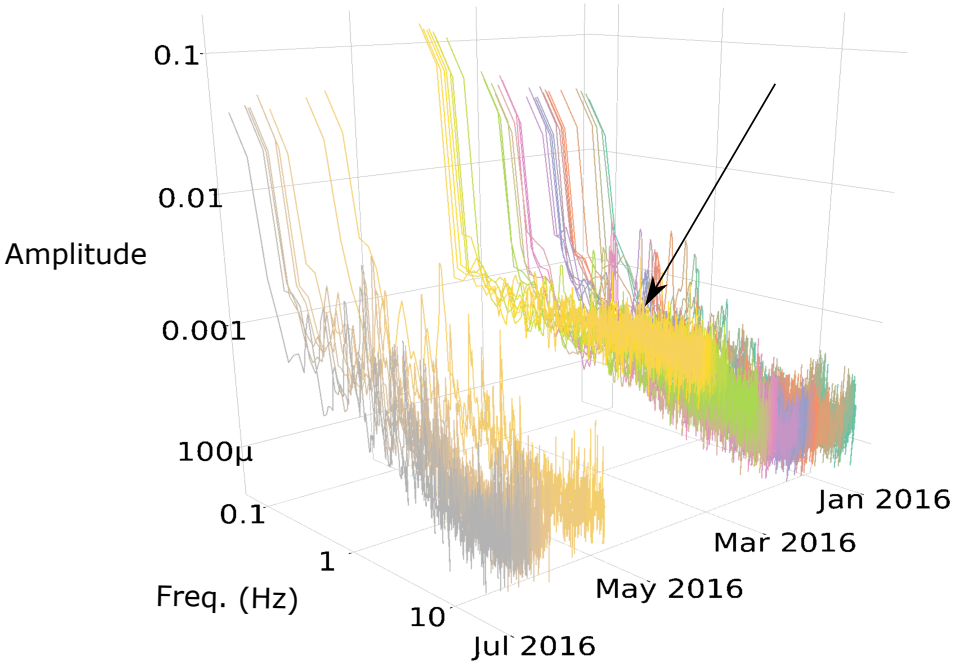

Figure 2: Example of Envelope records plotted in the time-frequency domain (log-log axes) for manual analysis by experts. Significant failure indicators happening in April 2016 are shown.

If the CMS records like FFT, Cepstrum and Envelopes are going to be used in a machine learning application, a complexity reduction is advisable. Furthermore, including the entire spectrum in the algorithms would lead to an excessively high number of channels.

A binning approach is chosen to pre-process the CMS records. Each FFT spectrum, Cepstrum or Envelope record is split into bins of frequencies and subsequently the integral of each bin is calculated. After analysing the different CMS records (FFT, Cepstrum and Envelope), a total number of 17 bins was selected. With this resolution, it is possible

to capture the different peaks in the spectrum, which indicate different fault frequencies, harmonics and side-bands, while still reducing the sprectrum's dimensionality. The bins are labelled in alphabetical order *A,B,...,Q*. Figure 3 visualises this process.

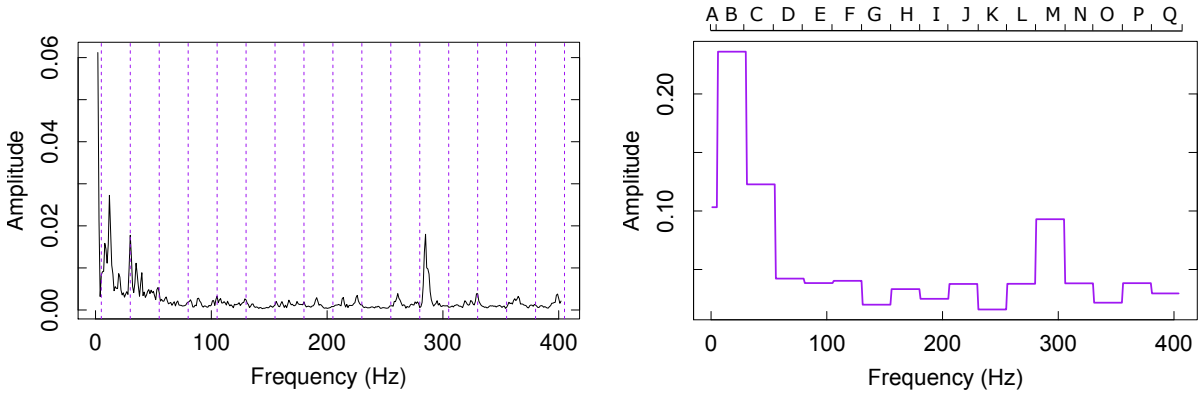

(a) Spectral binning

(b) Binned spectrum

Figure 3: The binning process visualised.

Figure 4 shows Box-Whisker plots of the binned Envelope and FFT spectra obtained in a healthy and faulty state of a WT main bearing. Here, the mean values and the variations obtained in a faulty state differ from those obtained in healthy condition. As both techniques, however, treat the raw signal differently, the changes occur in different regions of the spectra. Thus, the binning approach allows a significant dimensionality reduction of the spectra, whilst being sensitive to condition changes.

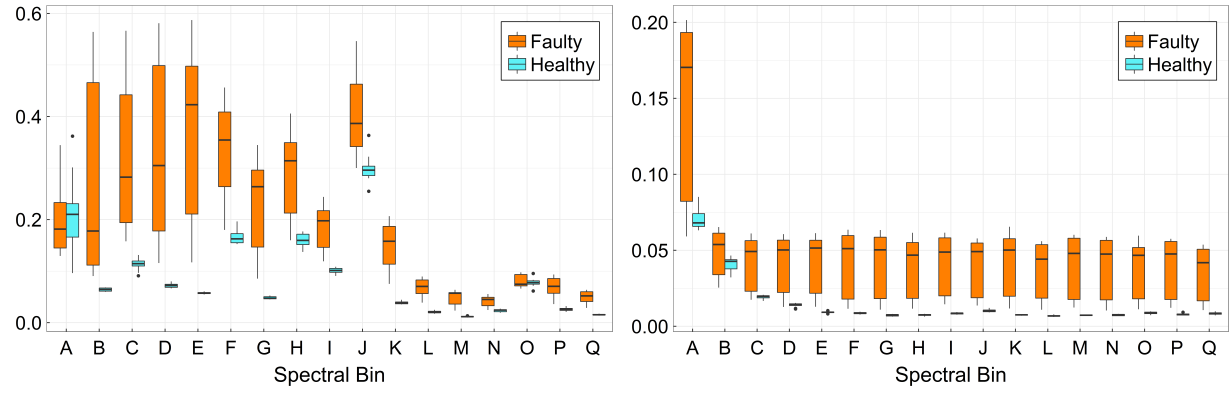

(a) FFT

(b) Envelope

Figure 4: Comparing binned FFT and Envelope records in a healthy and faulty state of a wind turbine main bearing.

For the final merging of the processed CMS records with the SCADA data, the temporal resolution needs to be matched. As the measurement vibration intervals are distinct from those of the SCADA data and fewer CMS measurements are available, the CMS values are kept constant (i.e. assumed not to change) if no measurements are available and are updated as soon as there are new measurements. Both, SCADA and CMS data were standardised for all applications discussed in the following sections.

4.2. Understanding relationships between data

Relationships between SCADA and CMS data are analysed with a focus on how the similarities change in the case of a component failure. This knowledge can help to understand which signals are appropriate for data-driven failure

detection and which signals can be omitted. Simple correlation analyses are susceptible to failure due to the irregular temporal CMS data resolution and the large number of signals. Instead, Hierarchical Clustering (HC) and Dynamic Time Warping (DTW) are applied.

HC is a basic unsupervised machine learning tool to group data either bottom-up (agglomerative) or top-down (divisive), [44]. In this paper, an agglomerative HC is used with the average linkage method and Euclidean distances.

DTW is a method to measure similarities in two time-dependent signals which may have characteristics that are out of phase. The algorithm, originally developed for speech recognition, [45] re-aligns the signals by finding the best 'warping' path that results in the lowest sum of pairwise distances. The warping path is required to be monotonic and boundaries might be set to limit the adjustment. Here, DTW is applied with a Euclidean distance and a maximum adjustment window of two weeks. Groups of data are compared by a 2-dimensional DTW distance that stretches all signals of each group together.

4.3. Distance-based automated vibration evaluation

This section addresses the second objective of this study, namely a methodology to automate fault detection using CMS data. The distance-based automated vibration evaluation (DAVE) tool presented in this paper is a generic tool for WT health assessment based on the fact that it is unlikely that all WTs in a farm have failures simultaneously. It detects deviations in the vibration records measured at a WT component from 'healthy' behaviour by calculating the pairwise DTW distances of vibration records of all WTs. The DAVE concept can be used for automated failure detection and as an early warning system.

The procedure involves, firstly, defining the initial detection setup using recorded data. Here, the CMS records for each component are analysed separately. This setup is then used for the actual failure detection with online measurements obtained for the same component. This is exemplified in this paper for the main bearing, for which several failures were recorded in the data base. Figure 5 visualises the automated failure detection process.

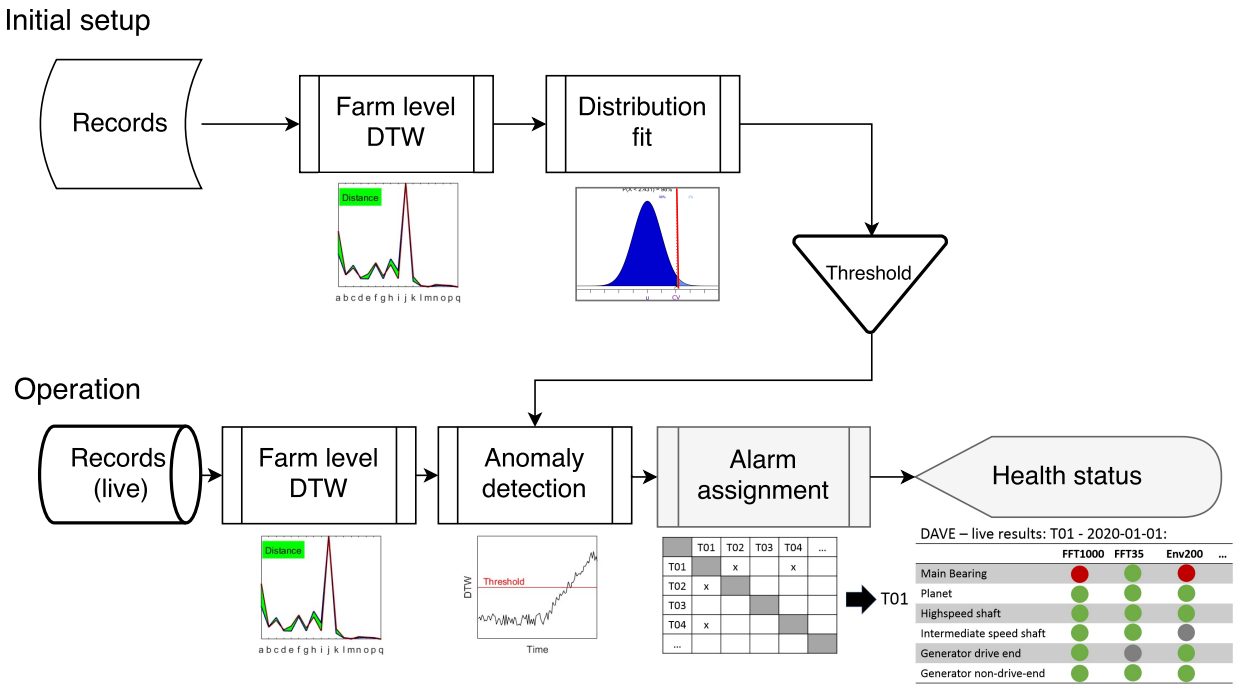

Figure 5: Distance-based Automated Vibration Evaluation (DAVE) workflow.

The procedure involves the following steps:

1. *Initial setup:* In this phase, thresholds are derived to identify anomalies from normal operation. This could be done by an expert or be data-driven. The data-driven approach uses data obtained during 'healthy' operation and includes two sub-tasks:
   (a) *Farm-level DTW calculation:* At each time step t, the spectra of the vibration measurements of two WTs are compared (e.g. the record of turbine T01 is compared to the one of T02, T03, etc.). Thus, for each point in time and each combination of WTs the similarity of two binned vibration spectra is assessed using DTW distances. Here, the flexibility of the DTW algorithm is used to identify similar trends even if there are slightly different peaks in the spectra. Accordingly, the warping window is limited to a maximum adjustment of two neighbouring bins (one at each side of the actual bin) to allow a slight shift of peaks without considering peaks at opposite ends of the spectra as corresponding.
   (b) *Distribution fit and threshold definition:* By fitting a distribution to the distances and setting a threshold for the healthy condition, anomalies are defined for the subsequent on-line application. The threshold represents a critical value, which is set to a certain percentile of the distribution. Thus, values higher than this critical value will subsequently be flagged as anomalous.
2. *Operation:* The on-line data recorded during operation are then used for the following steps:
   (b) *Farm-level DTW calculation:* For each point in time, a distance matrix of all WTs is set up by calculating all pairwise distances, analogous to step 1 (a).
   (c) *Anomaly detection:* Based on the threshold defined during the initial setup, anomalies within the pairwise distances are identified.
   (d) *Alarm assignment:* To determine whether an alarm has to be triggered and to which turbine it corresponds, the number of anomalies from pairwise comparisons is counted for each turbine (at each time step). If the count is larger than one, an alarm is issued. The alarm is assigned to the turbine with the highest count.
   (e) *Health status:* Based on the above, alarms are generated for each turbine, component and CMS record. The overall health status can be visualised with a dashboard summarising all alarms.

4.4. Prediction of CMS alarms

CMS alarms are often triggered significantly before the component actually fails. Being able to predict these CMS alarms could lead to notable benefits with regards to early failure predictions. This third objective is addressed with a classical machine learning approach. As there have been observed failures in three WTs, we focus here only on main bearing (MB) alarms. For the CMS alarm prediction, three different approaches are investigated: (1) The CMS alarm count is modelled. (2) The probabilities of having an alarm over time are obtained. (3) The alarms are predicted in a classification set-up with an alarm time shifting approach.

In this part of the work four probabilistic regression and classification techniques are used:

- A Generalised Linear Model (GLM) [46] is applied with a penalised likelihood estimation technique using the least absolute shrinkage and selection operator (LASSO), [47]. The obtained standardised coefficient magnitudes serve then as indicators for the importance of each input variable. The GLM is a generalisation of the ordinary linear model and can be used with error distributions other than the Gaussian distribution. In this paper two distinct error distributions are applied. At first, for modelling the count of alarms, a Poisson distributed GLM with logarithmic link function is used. The probability density function (pdf) of the Poisson distribution is given by:

$$Pr(y_i \mid x_i) = \frac{\mu_i^{y_i}}{y_i!} e^{-\mu_i} \quad , \tag{1}$$

  where y is the response variable and x_i are the model covariates for each observation i. The conditional mean and variance of the distribution are given by $E(y_i \mid x_i) = Var(y \mid x_i) = \mu_i = \exp(x_i \beta_i)$, with the estimation coefficients β_i. The logarithmic link function is denoted as:

$$g(\mu_i) = log(\mu_i) \quad . \tag{2}$$

Secondly, for modelling the time dependent probability of alarms, a GLM with a binomial error distribution and a *logit* link-function is used. The pdf of the binomial distribution is given as:

$$f(y \mid k) = \binom{k}{y} p^y (1-p)^{k-y} \quad , \tag{3}$$

where y is the number of successes when running k trials, and p is a model parameter. The *logit* link-function is defined as:

$$g(p) = logit(p_i) = \frac{p_i}{1-p_i} \quad . \tag{4}$$

During the parameter estimation process the LASSO sets unimportant covariates to zero to reduce the number of model covariates.

- A Random Forest (RF), [48], is an ensemble of single decision tree predictors, of which each one is considered a weak learner. Using a combination of these weak learners results in an enhanced prediction. The RF is trained using the so called Bootstrap Aggregation (bagging) algorithm, [49]. Here, subsets of the whole database are randomly generated and full trees for each random sub-set are grown. Subsequently, each decision tree of the RF is used to predict the response variable with the testing data. The overall RF prediction is the response that was predicted by the majority of the decision trees (for classification problems) or the mean of the predicted counts (for regression problems). In this study an RF with 60 individual decision trees is used. The importance of each covariate is estimated via permutation, which investigates how the prediction accuracy, indicated by e.g. the coefficient of determination R^2, mean absolute error (MAE) or root mean squared error (RMSE), decreases if one particular feature is not present.

- A Gradient Boosting Machine (GBM), [50], is also a prediction model based on weak learners. In contrast to the RF, which uses fully grown trees, the GBM uses very shallow decision trees. By virtue of their setup, these shallow trees have low variance and high bias and a 'boosting' algorithm is used to reduce this bias. The boosting is a sequential process, which in each iteration adds a decision tree to the existing one, and thus, enhances the predictive ability of the model.

  For the gradient boosting, a loss function is defined (e.g. an error metric such as the mean squared error (MSE)), which is minimised by continuously adding weak learners to the model, while leaving the existing ones unchanged. In this paper a GBM with 100 decision trees is applied, with a maximum depth of 10 values each. Again, permutation is used to obtain the significance of the different variables.

- Artificial Neural Networks are among the most popular machine learning algorithms that are frequently used for classification and regression problems. These networks consist of several layers containing nodes (often called neurons), which are interconnected with weighted paths, the so called 'synapses'. The importance of a connection for predicting the outcome depends on the assigned weight to the respective synapses.

  In this paper, a feed-forward Artificial Neural Network (ANN) is trained, implying that the nodes are only connected in one direction: from the input layer towards the output layer. Three hidden layers of 50, 40 and 20 nodes are used respectively. This setup showed the best performance in an iterative testing of different configurations starting with one hidden layer and a small number of nodes.

  Levenberg-Marquardt backpropagation [51] is used for training the ANN, which changes the internal structure of the ANN (i.e. the weights and biases at each node) to minimise a given cost function, commonly the MSE. In this process, at first the weights of the neural network are selected randomly and the response is calculated using only one input variable. The cost function indicates then how close the predicted values are to the observed ones. Then, the output is propagated back through the ANN to determine the error of all hidden and output neurons, and the neurons' weights and biases are modified accordingly.

  Finally, the variable importance is determined using functional analysis of the weight matrix, as introduced in literature, [52].

4.4.1. Count of alarms

As the alarms are directly issued by the CMS, only SCADA data are used for prediction. SCADA channels containing constant or cumulative values were eliminated for this task, as they would contain unnecessary information. Two different concepts of defining training and testing data are investigated:

- Random sampling of all data from all WTs with a ratio of 80% training and 20% testing (labelled *random sampling* subsequently).
- Training with data from all WTs except one and blind testing on the remaining turbine, i.e. approx. 92% training and 8% testing (labelled *blind testing* subsequently).

As the number of time-steps containing entries for alarm events is much lower than the time-steps where no alarms were observed, the class distribution needs to be adjusted using a method called 'under-sampling'. The resulting training data set is under-sampled limiting the number of time-steps without alarm to 80% of the data, to re-balance the representation of different targets, [53].

For this task, the mentioned algorithms are used in a regression setup, i.e. predicting a discrete quantity output for the alarm count. Thus, the GLM is set with a Poisson distribution and logarithmic link function. The other algorithms are used as explained above in Section 4.4. The best performing model is determined by comparing the evaluation metrics: coefficient of determination R^2, mean absolute error (MAE) and root mean squared error (RMSE) on the training and testing data. The R^2 is a standard evaluation metric and indicates how well the model explains the variance in the response based on the input variables of a given data set. The R^2 reaches from 0 to 1, while 0 states that the model fails to accurately represent the data, 1 indicates a perfect fit. The MAE and RMSE are also standard evaluation metrics for regression problems and represent the average magnitude of the prediction error. Ranging from 0 to infinity, lower numbers indicate better predictions. As the RMSE is slightly more sensitive to outliers than the MAE, both metrics are included in the analysis to thoroughly compare the model accuracy.

4.4.2. Time dependent probability of alarms

In this section, the aim is to generate a time-dependent probability of getting a CMS alarm in a classification approach. Again, only SCADA data are used for the predictions. For the training, these are under-sampled to a ratio of 80% and 20% for the two respective classes {0,1}, which stands for {'no alarm','alarm'}. The *blind testing* approach is applied, as any random sampling and testing would hinder a time-dependent evaluation. In this case, the algorithms introduced in Section 4.4 are used to solve a classification problem. Hence, GLM is applied with a binomial error distribution and a *logit* link-function. Also, when modelling binary response variables, the other learning algorithms can be used as probabilistic classifiers. The output from the predictions is then a posterior class probability at each point in time, [54]. To provide a comparison, the probabilistic output of the classifiers is analysed for WTs with and without failure.

4.4.3. Alarm time shifting

Again, a binary classification approach is used. Prediction is performed by shifting the data set to an earlier time step, and thus, training the model with shifted data. Zero lead time corresponds here to modelling the alarm, while higher lead times correspond to alarm prediction in advance. Although, this is a static way to represent a dynamic process, it can provide useful information about the classifiers' performances before the actual occurrence of an event.

Several combinations of input sources are investigated, namely 1) SCADA, 2) SCADA and RMS and 3) 'all data'. 'All data' stands here for SCADA, RMS and all MB spectra from one active power interval. This procedure allows the evaluation of the contribution of each data source regarding the prediction accuracy. Data from all WTs are used with random sampling and are again under-sampled, as described in the previous section. The classifiers employed in this section are RF and ANN.

A 10-fold cross validation is carried out on the data leading to 10 distinct predictions, which are then gathered to provide an average performance.

5. Results

In this section, the results for the application of the processed and merged CMS and SCADA data are presented for the three separate objectives of this paper: (1) understanding relationships between the data, (2) automated failure detection (DAVE) and (3) predicting the CMS alarms.

5.1. Understanding relationships between Data

The results of the HC analysis of all data per turbine are given in Figures 6 - 7 with simplified dendrograms and statistics of the most separated clusters. In general, a cluster analysis can show which signals are similar, i.e. joined in a cluster, and which signals are more different, i.e. in separated clusters. In agglomerative HC, the process of building the clusters is more important than the final result due to the fact that all signals are eventually joined to one cluster. A dendrogram visualises how clusters are formed by connecting two 'leaves', i.e. sub-clusters, to form the next cluster. Here, the x-axis represents the sub-clusters or in the lowest level all signals. Due to the high number of signals (3375), the lowest level is not shown, but the dendrograms were cut at 20 leaves. The height in the y-axis represents the difference of the two joined sub-clusters in terms of the Euclidean distance, i.e. a dendrogram with vertically close clusters indicates very similar signals.

Figure 6a shows that there was no significant cluster separation for fault-free time periods. The two clusters that are joined at the top of the dendrogram consisted here of one big cluster and one smaller cluster with only a few signals (the most separated cluster). The second most separated cluster (which is not a sub-cluster of the most separated cluster) showed a similarly small number of signals. In case of the MB failures, however, there was a clear separation of more signals (Figures 6b and 7). Here, the two most separated clusters were formed by many MB signals for T03 and T08. This proved that a number of signals shows clearly deviating features before the failures. Noticeably, there were mainly GNDE and not MB contributors in the case of the MB failure in T01.

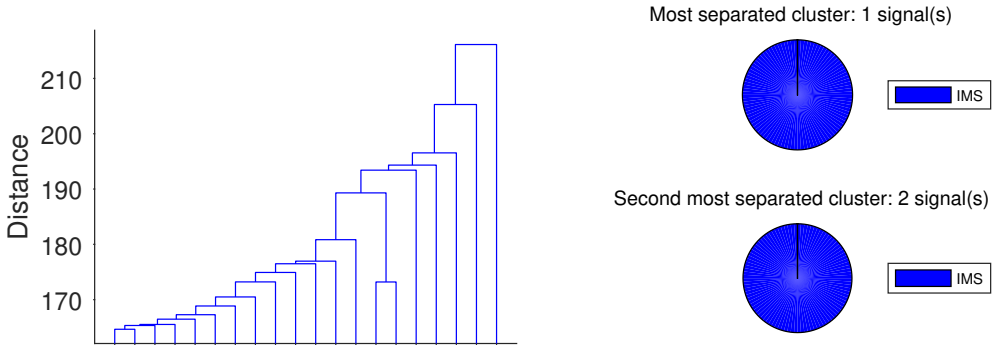

(a) fault-free example (T01, Oct-Dec 2015)

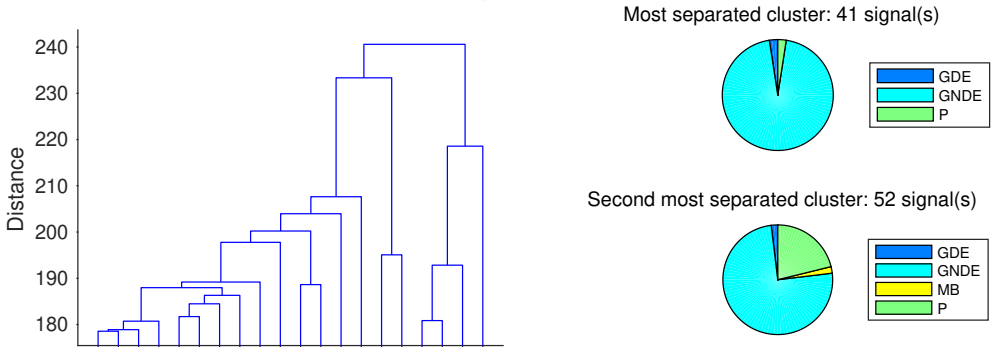

(b) Imminent MB failure in T01 (Jan-Mar 2016)

Figure 6: Simplified dendrogram and contribution to most separated clusters in T01.

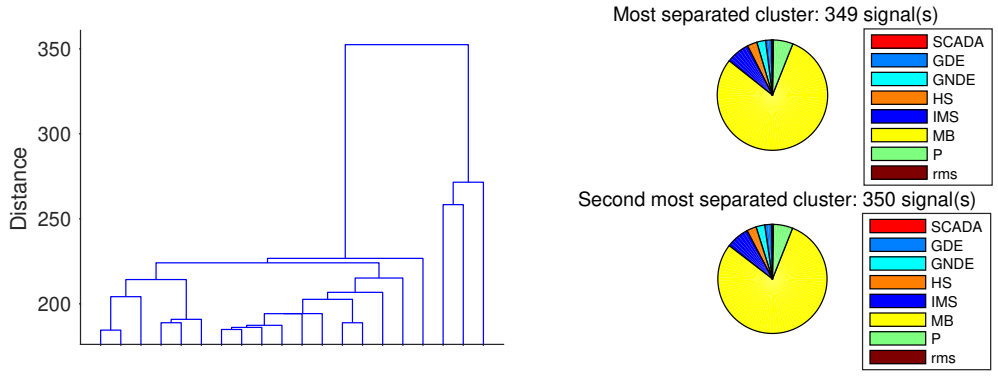

(a) Imminent MB failure in T03 (Apr-Jun 2015)

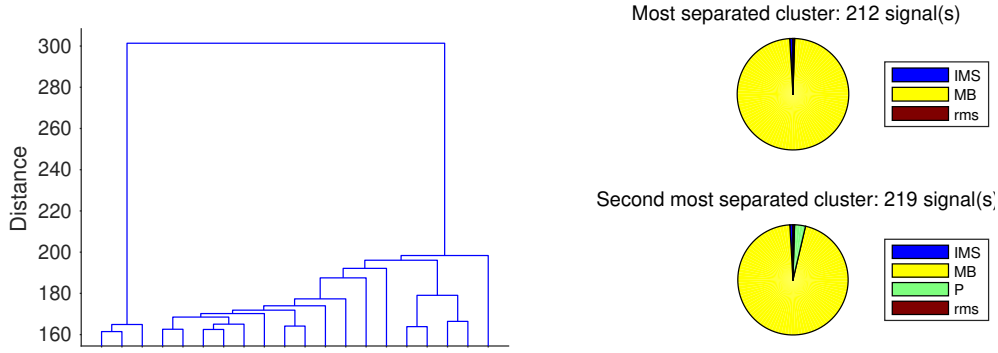

(b) Imminent MB failure in T08 (Oct-Dec 2015)

Figure 7: Simplified dendrogram and contribution to most separated clusters in case of MB failure for WTs T03 and T08.

In a second step, the relationships between the CMS records for different active power intervals were evaluated with DTW distances. Each spectrum was taken as a group of signals in this case without differentiation of the individual bins. The DTW distance was then calculated by comparing with another spectrum measured in a different active power interval. Here, the calculated distance is normalised by the number of samples in the signal for better readability. The complete analysis resulted in pairwise distances for three different spectra FFT1000, Env200 and FF35, (names indicate the signal type as well as its sampling frequencies and bandwiths – e.g. FFT35 stands for an FFT signal with frequencies between 0 and 35 Hz) and seven active power intervals (<38%, 38-48%, 48-58%, 58-69%, 69-79% and >90% of rated power). For each spectra-to-spectra relationship, a distance matrix T is described by defining the element at position i, j as

$$T_{i,j}(rs) = d_{DTW}(r^i, s^j) \quad , \tag{5}$$

with the DTW distance d_{DTW}, r and s as the two selected spectra, superscripts describing the active power bin and $i = 1, 2, 3, \ldots, 7$, $j = 1, 2, 3, \ldots, 7$. This means, for each of the r-s relationships a 7×7 matrix can be written. As an example, the FFT1000-Env200 relationship for the period of failure in T08 (Oct-Dec 2015) results in the following:

$$T(\text{FFT1000}, \text{Env200}) = \begin{bmatrix} 0.137 & 0.144 & 0.145 & 0.142 & 0.137 & 0.141 & 0.167 \\ 0.113 & 0.112 & 0.118 & 0.114 & 0.109 & 0.109 & 0.179 \\ 0.115 & 0.116 & 0.119 & 0.115 & 0.111 & 0.110 & 0.181 \\ 0.102 & 0.101 & 0.109 & 0.103 & 0.099 & 0.106 & 0.175 \\ 0.103 & 0.107 & 0.110 & 0.107 & 0.106 & 0.109 & 0.178 \\ 0.109 & 0.107 & 0.116 & 0.111 & 0.105 & 0.116 & 0.188 \\ 0.221 & 0.223 & 0.220 & 0.222 & 0.224 & 0.215 & 0.219 \end{bmatrix} \tag{6}$$

Six matrices were derived for each turbine and selected time window. Note that for certain relationships the matrix was symmetric and filled with zeros on the diagonal (e.g. FFT1000-FFT1000). The pairwise comparison of spectra of different active power intervals showed that in case of MB failures, spectra from all active power intervals became relatively similar with some normalised distances as low as 0.05-0.15. In contrast, for fault-free operation, normalised distances were usually >0.2. The information for varying bins is further visualised in Figures 8 and 9 by using directed graphs. The distance matrix T is split into two adjacency matrices for the upper and lower triangle, respectively. In the directed graph, each set of seven nodes represents the seven active power intervals. The heading above each set of nodes identifies the two compared record types according to the direction of the arrows connecting the nodes (always starting at the lower number). The colour of the arrows shows the similarity of the two connected spectra, as indicated by the DTW distance. With this, higher distances imply higher dissimilarities.

Noticeably, some spectra were only similar for certain power intervals as shown in Figure 8 for T01. Very low distances and accordingly similar features were seen for all intervals in the FFT1000 spectra. In contrast, interval 1 appeared to have unique features for Env200 spectra, as they are not connected to any other node. If the different record types are compared, the FFT1000 and Env200 are more similar, but the two FFT records FFT1000 and FFT35 are less similar. Figures 9a and 9b show the DTW distances for the MB failures in T03 and T08, respectively. The identified relationships in T08 are comparable to T01, except for interval 7 with unique features (instead of interval 1). However, all FFT1000 and Env200 distances were slightly larger in T08 – a trend that was amplified in T03 with even higher distances. All in all, the DTW analysis confirmed that the CMS records from the different active power intervals showed mostly similar features, i.e. using data from only one active power interval is a reasonable compromise to handle a large number of records. Thus, in the further, the study is based on data from the fourth active power interval corresponding to 58-69% rated capacity.

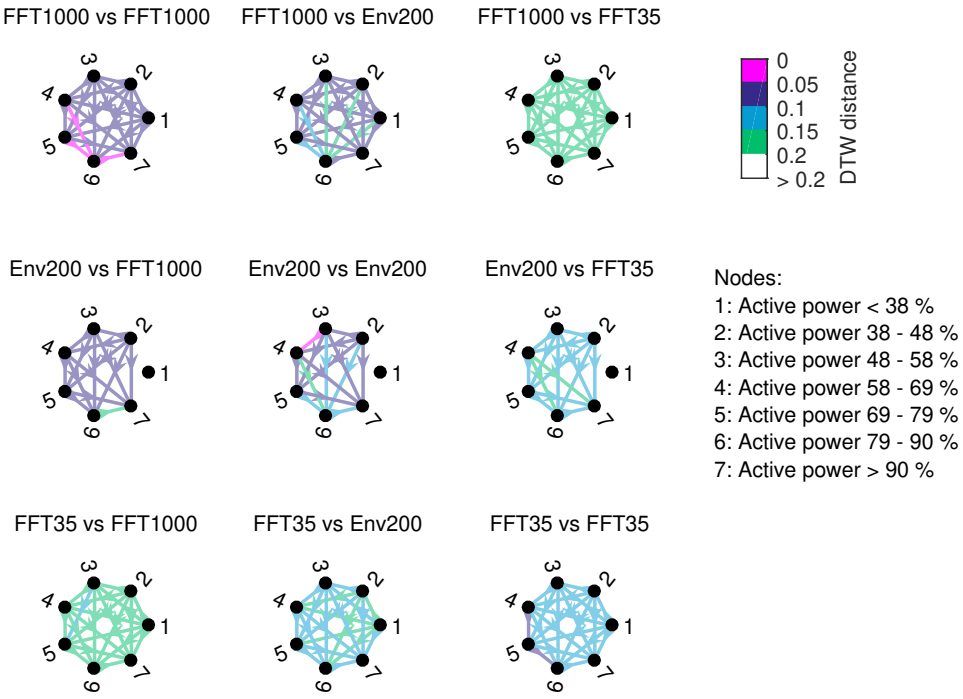

Figure 8: DTW distances for various MB records with different active power intervals in the case of a MB failure for T01 (Jan-Mar 2016).

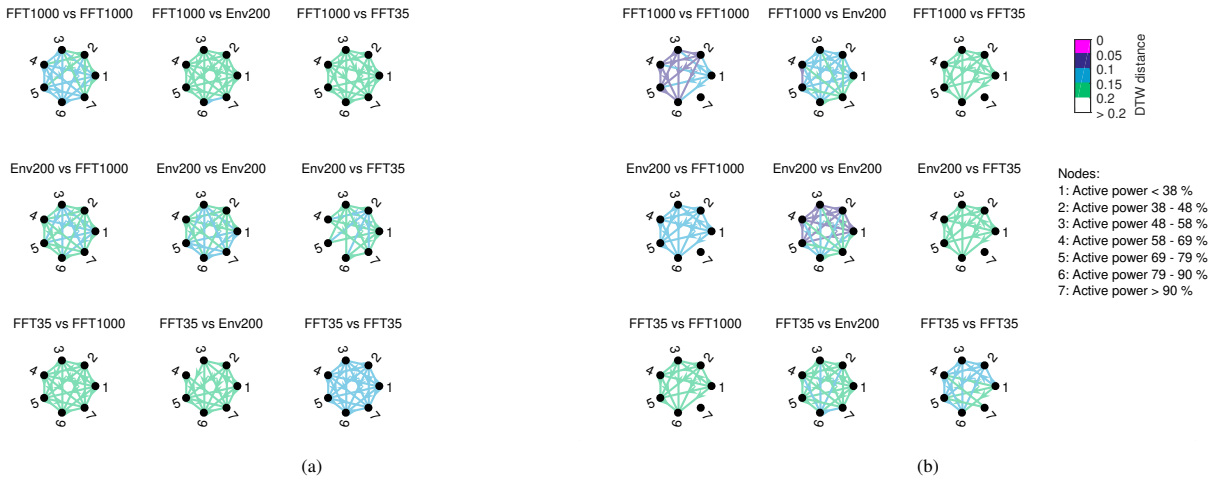

(a) (b)

Figure 9: DTW distances for various MB records with different active power intervals in the case of a MB failure for (a) T03 (Apr-Jun 2015) and (b) T08 (Oct-Dec 2015).

5.2. Distance-based automated vibration evaluation

The performance of the automated failure detection is demonstrated in this section for CMS records obtained for the main bearing.

For the initial setup of DAVE, the first two observed (healthy) years of the entire data set were used to derive the thresholds directly from the WT data. In this context, a Weibull distribution showed the best fit to the calculated distances. The threshold for the anomaly was set to the 99.9^{th} percentile of the distribution. Figure 10 shows the alarms, triggered by CMS, SCADA and DAVE (for FFT1000), and the downtime caused by the failure during an observation period of four years. WTs T09 to T13 are not shown in this graph as none of them had either CMS or SCADA alarms. Also, DAVE did not indicate any alarms for these latter WTs. DAVE showed very early alarms for the three MB failures in T01, T03 and T08. Additionally, no false positives or false negatives were recorded during the four year period. The other MB records, Env200 and FFT35 gave less reliable warnings. Table 1 shows the number of days DAVE was able to anticipate the component problem in comparison to the CMS and SCADA alarms. Figure 10 and Table 1 show that DAVE was capable of detecting the problems up to 72 days prior to the CMS and 119 days before the actual failure event.

Table 1: Number of days the different systems triggered alarms before failure.

WT	**DAVE**			**CMS**	**SCADA**
	FFT1000	FFT35	Env200		
T01	106.5	11.8	-	34.5	9.3
T03	119.9	-	105.1	110.1	0
T08	65.1	-	93.8	5.5	0

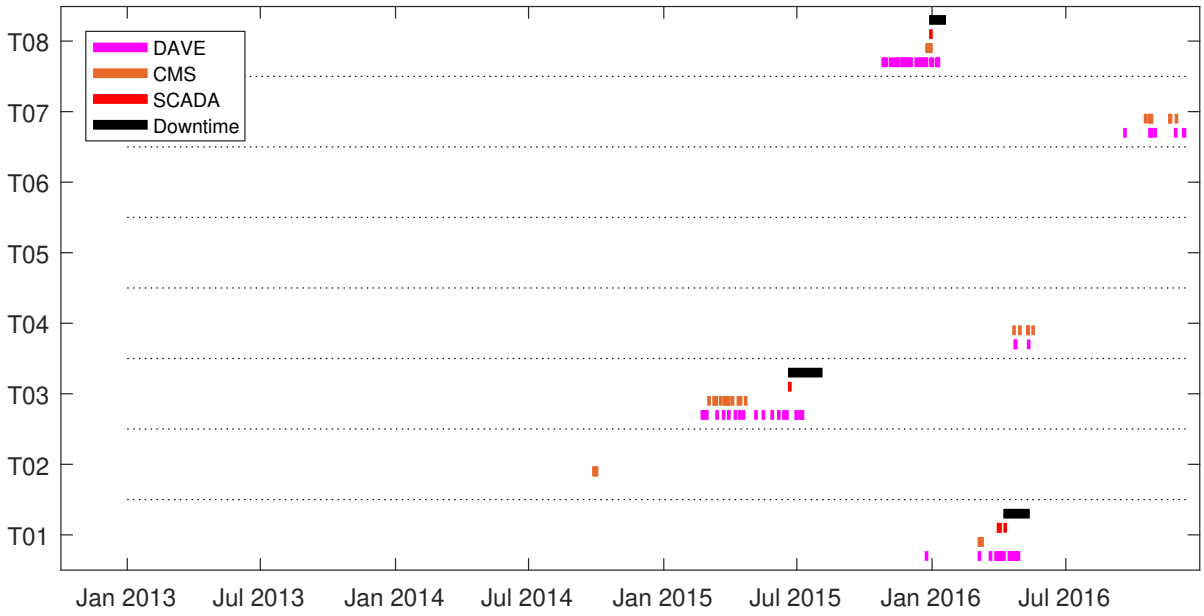

Figure 10: Results for the automated failure detection. Comparing CMS, SCADA and DAVE (FFT1000) alarms.

5.3. Prediction of CMS alarms

This section presents the results of the three approaches to predict CMS alarms in supervised learning frameworks. At first, the results for modelling the number of CMS alarms are shown including a sensitivity study to determine the most important input parameters. Then, the time dependent probability of having a CMS alarm is presented. Finally, the alarms are shifted towards an earlier time step and predicted. For the latter, the performance of different input data combinations is evaluated.

5.3.1. Count of alarms

In the following, the results for modelling the number of CMS alarms by only using SCADA data are presented. The performance of the different algorithms is evaluated with the Coefficient of Determination (R^2), the mean absolute error (MAE) and the root mean squared error (RMSE). The most important model covariates for each set-up are determined. The evaluation metrics for training and testing of each technique using *random sampling* are shown in Table 2. Figure 11 shows the recorded CMS alarms and the predictions obtained from each model. RF and GBM performed best, ANN showed intermediate results, while GLM resulted in poor performance. Figure 12 shows the importance of the different variables in each model, indicating the most important model covariate, which was in all cases the main bearing temperature.

Table 2: Evaluation metrics for modelling CMS alarm counts using only SCADA data with random sampling.

	Metric	**RF**	**GBM**	**GLM**	**ANN**
Train	R^2	0.893	0.942	0.142	0.610
	MAE	0.151	0.192	0.982	0.388
	RMSE	1.261	0.929	3.573	2.438
	Metric	**RF**	**GBM**	**GLM**	**ANN**
Test	MAE	0.149	0.224	0.982	0.379
	RMSE	1.151	1.182	3.592	2.468

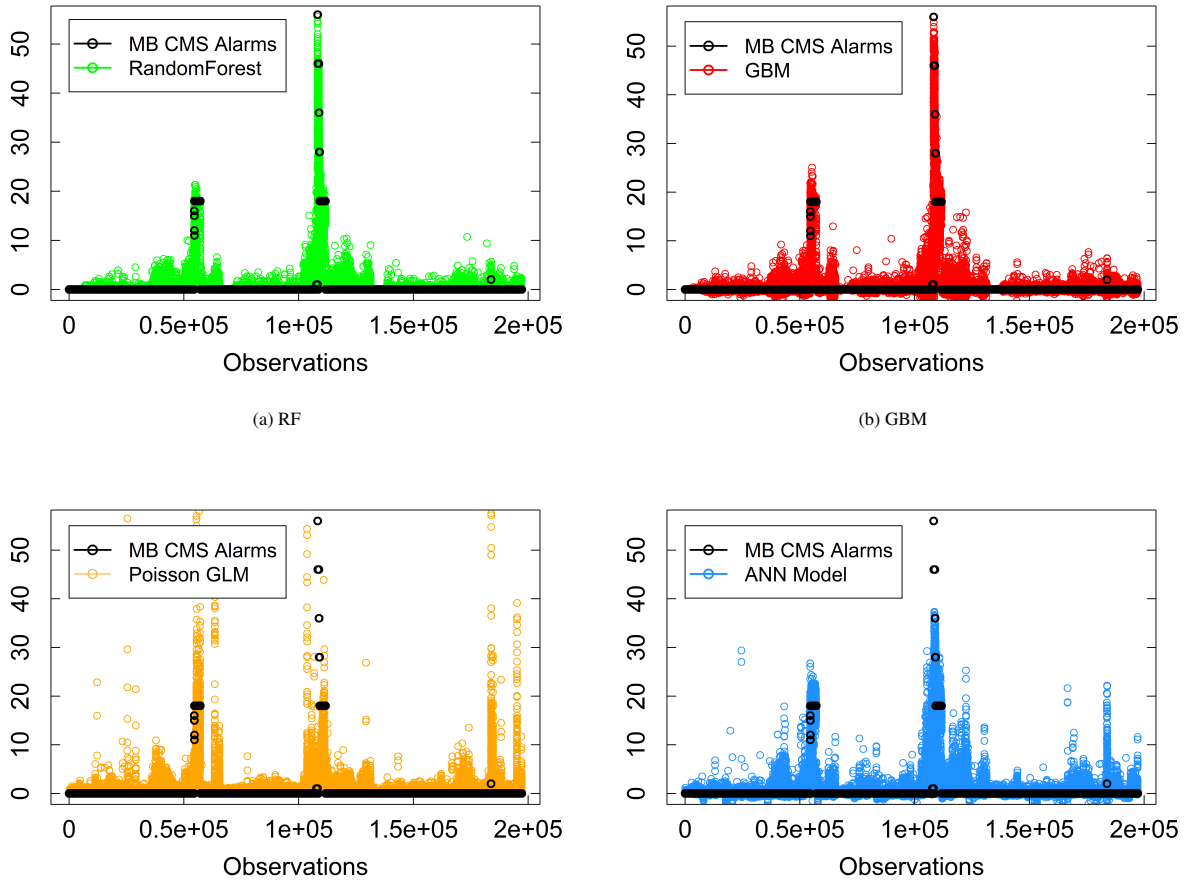

(a) RF

(b) GBM

(c) GLM

(d) ANN

Figure 11: Results for modelling of CMS alarm counts with random sampling.

The results for *blind testing* are displayed in Figure 13 and Table 3. During the training phase, RF and GBM performed better than ANN and GLM. The predictions using the testing data set were characterised by much higher errors than in the previous section. This may be due to turbine-dependent operational and environmental conditions, since it is difficult to capture all of these variations if one turbine is left out.

Table 3: Evaluation metrics for modelling CMS alarm counts using only SCADA data with blind testing.

	Metric	**RF**	**GBM**	**GLM**	**ANN**
Train	R^2	0.979	0.989	0.218	0.549
	MAE	0.028	0.053	0.504	0.195
	RMSE	0.364	0.256	2.211	1.672
	Metric	**RF**	**GBM**	**GLM**	**ANN**
Test	MAE	0.974	0.950	1.350	1.079
	RMSE	4.698	4.689	5.640	5.498

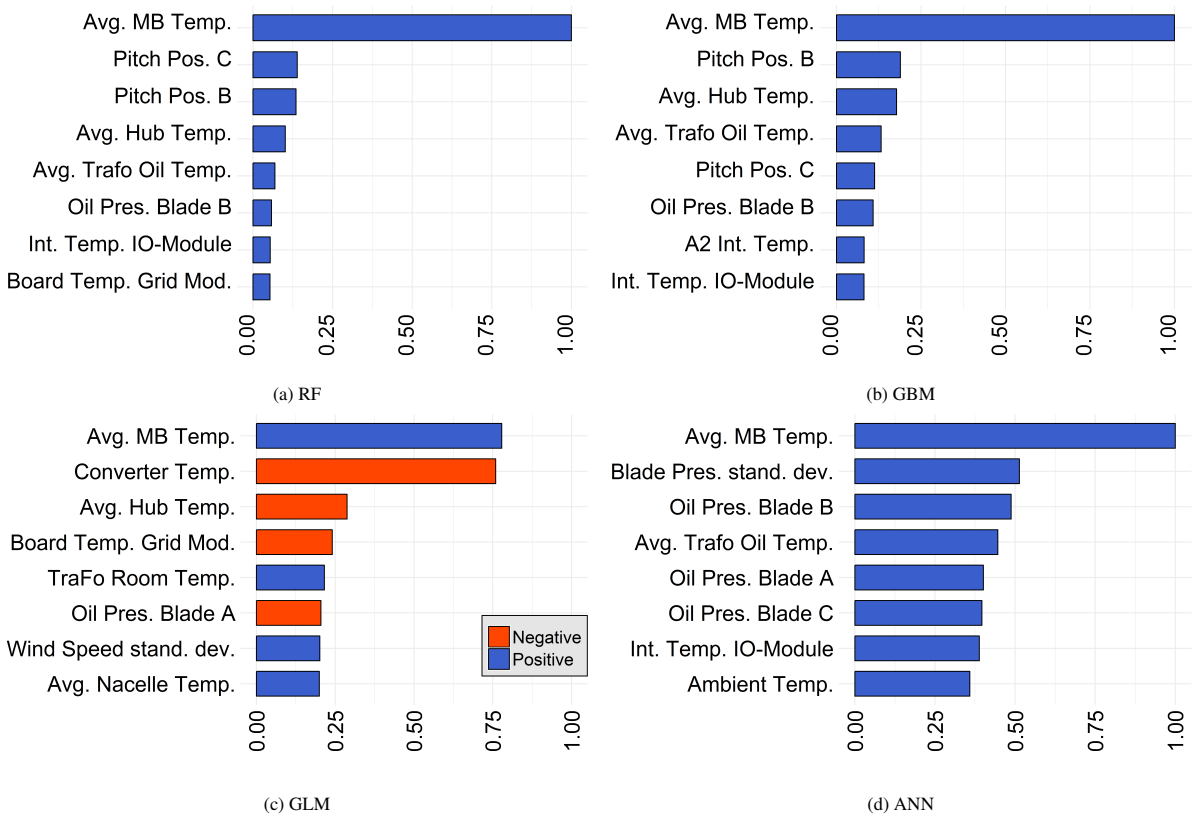

(a) RF

(b) GBM

(c) GLM

(d) ANN

Figure 12: Variable importance for the algorithms used for random sampling.

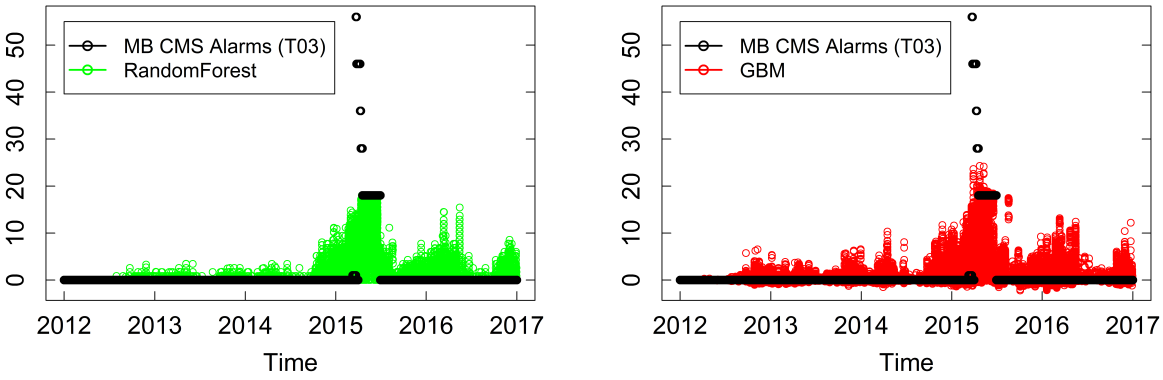

(a) RF

(b) GBM

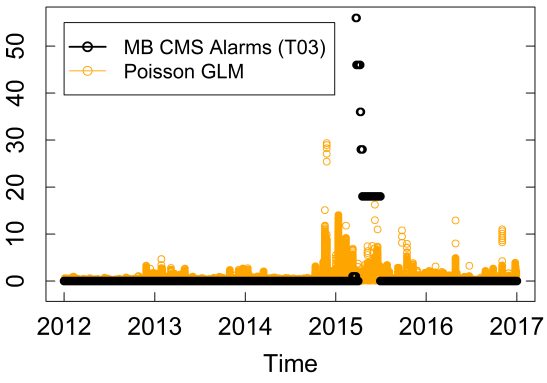

(c) GLM

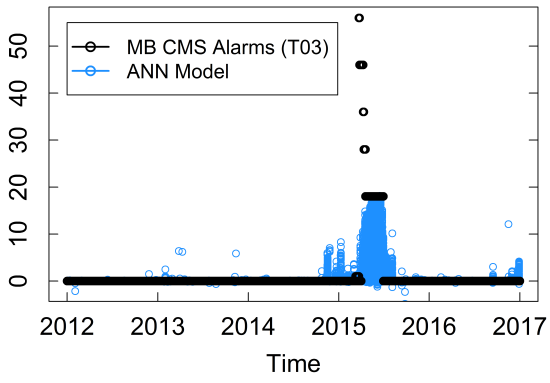

(d) ANN

Figure 13: Results for modelling of CMS alarm counts with blind testing.

5.3.2. Time dependent probability of alarms

This section is concerned with predicting how the probability of having a CMS alarm is evolving over time, based only on SCADA data. The results are evaluated graphically by plotting the predicted probabilities over time, as well as the alarm event. It is investigated how the probabilities behave before the event and which algorithm was able to indicate an upcoming alarm more reliably. Figure 14 shows the results for WTs T01, T03 and T08, for which MB CMS alarms were recorded throughout the observation period. Furthermore, WTs T06, T10 and T11, which did not experience any main bearing CMS alarms, are displayed. For easier interpretation of the graphs, the probabilities over time are smoothed using a moving average filter.

It can be seen that GBM performed best. It indicated a rising probability towards the time of occurrence of the actual alarms for all WTs, while resulting in a near-zero probability for WTs T06, T10 and T11, which did not experience any CMS alarms. The results for GLM and RF indicate a relatively high probability of alarm occurrence for T06. GLM performed overall poorly for all cases. A certain seasonality was observed for the ANN predictions of T01 and T06 as well as the GLM predictions of T01, T10 and T11. GBM and RF showed a peak in probability approximately one year before the failure in T08, which could be caused by seasonality or a separate problem in the MB. Further investigation is required to fully understand the observed trends.

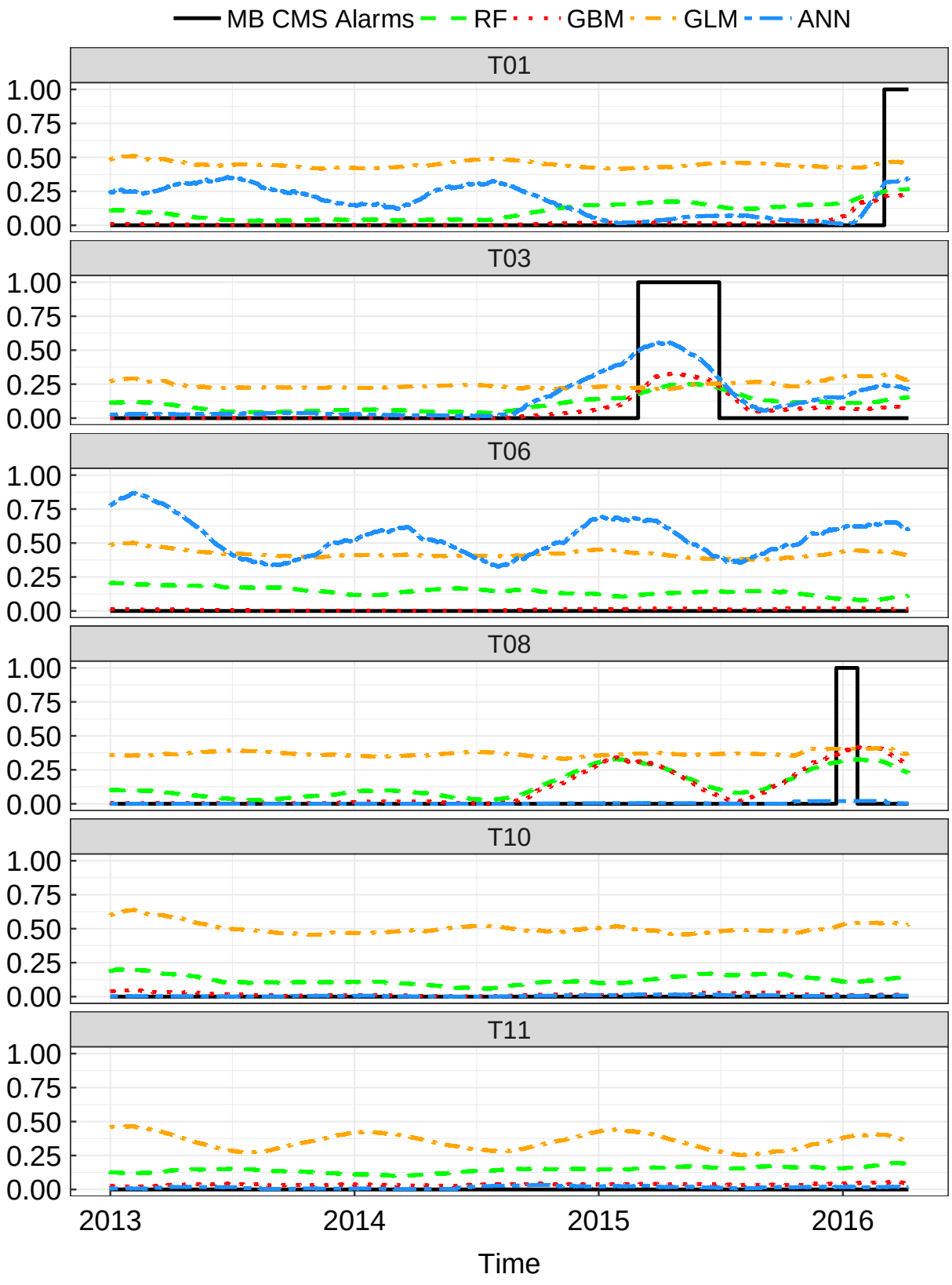

Figure 14: Probability of having a CMS alarm.

5.3.3. *Alarm time shifting*

The performance of the predictions using alarm time shifting is evaluated by receiver operator characteristic (ROC) curves at different fixed lead times. ROC curves show the hit rate (probability of detection - POD) versus the false alarm rate (FAR) as a function of the threshold for an alarm in a probabilistic setting. Figures 15a and 15b show the results for the predictions made using ANN and RF with a lead time of 0 hours. These consist of ten different ROC curves for each of the predictions made during cross validation. The red line indicates the average ROC curve.

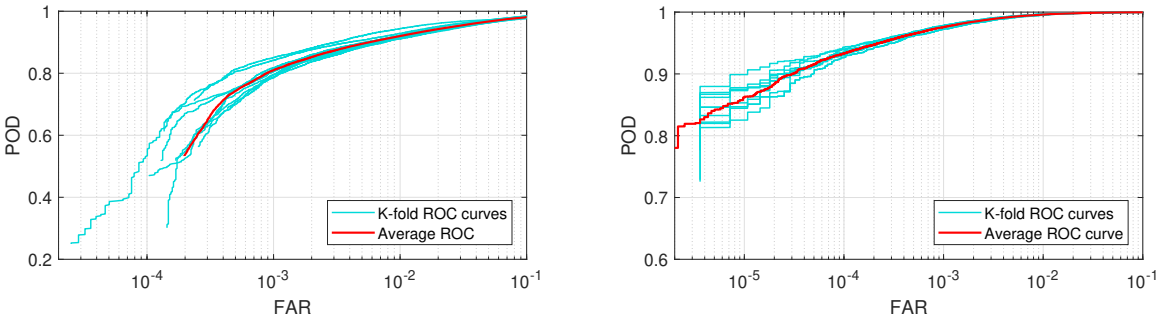

(a) ANN (b) RF

Figure 15: Example of variation in the results of the 10-fold cross-validation.

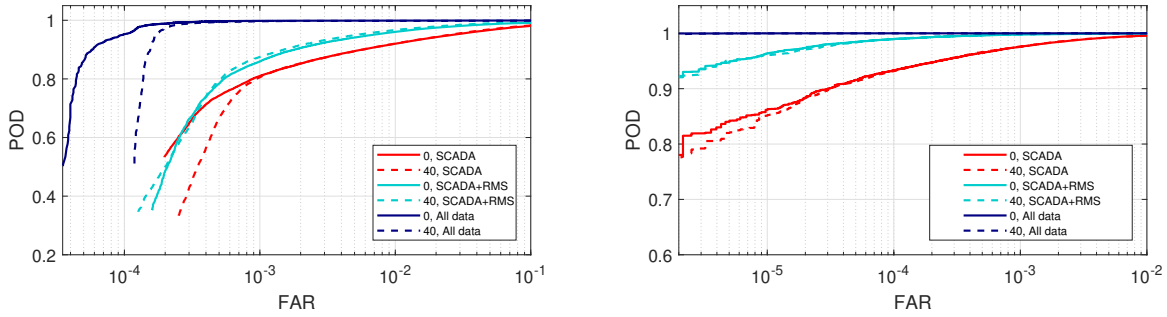

(a) ANN (b) RF

Figure 16: Average ROC curves for ANN and RF at lead times 0 and 40 hours.

In Figures 16a and 16b the average ROC curves for different input combinations and different lead times are displayed. Notice that in the figures, different axis scales are used to emphasise the difference between different data combinations, rather than comparing the performance of the two classifiers. Here, 'all data' denotes the input set comprised of SCADA, RMS, FFT and Envelope records. The RF algorithm performed considerably better than the ANN in all cases. Interestingly, the POD of both algorithms in predicting CMS alarms by only using SCADA data is high. Nonetheless, using more data improved the predictions. As expected, the combination of all CMS and SCADA data performed best followed by the combined SCADA and RMS data. This demonstrates that the added value of CMS data for failure detection is large. The temperature as sole fault indicator might not be sensitive to all failure modes and damages and vibration records can provide a more sensitive measure for the automated failure detection. Furthermore, it is shown that with zero lead time the predictions for all combinations of input data are better. This was also an expected result, since closer to an actual event the separability between the classes increases. It is worth noting that the order of the POD and FAR displayed is affected by the pre-processing approach used for the data, in particular the fact that the CMS records are kept constant if there was no measurement.

6. Discussion

In this section, the different results of this work will be further discussed. Several methods for WT failure detection based on a database of merged CMS and SCADA data have been explored. The proposed merging procedure resulted in a complexity reduction without losing fault relevant information (peaks, harmonics, sidebands, etc.) and was intended to be a generic solution for various CMS records and possible failure modes. However, future work needs to validate the suitability for fault features not studied in this work and explore alternative solutions for merging the data.

The HC analysis on one turbine highlighted that there is no strong cluster separation in case of normal conditions, but separation of signals in case of imminent failures. This confirmed that failures are clearly reflected in a number of CMS signals, not only recorded at the failing part but also at other locations. For some failures, SCADA signals were assigned to the same cluster, indicating a change in behaviour. This gave first evidence of overlapping information in CMS and SCADA data. Further refining of the clustering analyses, e.g. by cutting into shorter windows, could have potential for failure prediction, but classification setups were considered to be more efficient for this purpose.

The evaluation of DTW distances of different CMS records showed that the information contained in the MB records is mostly similar for various active power intervals. This fact might be beneficial in industrial practice to limit the monitoring efforts. However, the results also indicated some dissimilarities for certain records and active power intervals, which should be investigated in more detail.

The application of the DAVE framework to MB failures showed that an automated evaluation of the FFT and Envelope records, emitted by several WTs within the same wind farm, works well for early failure prediction in this component. Future research needs to validate DAVE with other failure modes beside MB. It would be helpful to establish the required similarity in the wind farm, e.g. will it work in complex terrain?

For predicting the CMS alarms, three distinct approaches were chosen to accomplish different objectives. This helped to understand that it can be possible to anticipate the CMS alarms by only using SCADA data. The blind testing results indicated that the exact number of alarms is difficult to predict. It can be argued, that this is not necessarily required in practice, but rather a prediction of the failure by means of a probability.

The probability of having a CMS alarm over time was calculated only based on SCADA data. It was found for instance that the GBM algorithm reliably indicated a rise in the probability of having an alarm several months ahead of the alarm. This setup could be used by operators as a monitoring system, if CMS are not continuously available, or as an additional early warning system. However, it should be investigated why the different classification techniques performed so differently and whether GBM gives reliable results also with other data.

Finally, the CMS alarms were predicted using alarm time shifting. The results here showed that the combination of SCADA and CMS performed better than using the single sources, which may suggest that the mutual information between them could provide prediction synergies. Nonetheless, only using SCADA data still led to relatively low false alarm rates. Future work needs to establish what lead times are feasible, i.e. how much in advance the alarms can be predicted.

An important point emerging from this research is how the different time-based or static learning techniques can be used to provide information about progressive damage. In particular, reducing the dimensionality of the data set can be achieved in several different ways, depending on the nature of failure. For instance, the techniques employed in this paper led to substantially different results and considerations, that took into account relationships between data, turbines and mechanical components as well. It seems likely that it is impossible to define a standard procedure to extract information from data for WT failure detection that will be valid for all failure modes and site-specific properties. Further explorative analyses are recommended, thus taking into account the nature of historical information, e.g. whether labelled or unlabeled data are available to develop adequate automated processes for commercial O&M practice.

When looking at the overall results of this paper, it could be argued that failure prediction can be carried out exclusively based on SCADA data, avoiding expensive CMS. This might hold true in certain cases and failure modes, nonetheless, using both data sources enhances the failure detection. Hence, merging SCADA and CMS may lead to standard monitoring systems calibrated for detecting a larger variety of failures, eliminating redundancy, decreasing costs of equipment and increase data reliability (in case one system fails) and facilitate their processing.

7. Conclusion

This paper proposed a method for merging CMS, SCADA and alarm data and a thorough analysis was carried out on the possible applications with respect to enhancing predictive O&M practice. Automated failure detection algorithms using both data sources have been developed and tested, which to the authors' knowledge has not been subject to previous research. As this work was intended to give new practical solutions, it started off from an industry perspective by considering data of a commercial monitoring system. The aim of this study was not to substitute CMS experts, but to provide them with useful tools to draw faster and more reliable conclusions regarding the necessary O&M actions.

This research addressed optimisation of predictive O&M with the following novel contributions:

- A new method for merging CMS and SCADA data was presented to overcome issues with the different temporal resolutions of both sources and to reduce the dimensionality for the use in machine learning algorithms.
- The relationships between the two data sources were analysed using hierarchical clustering (HC) and dynamic time warping (DTW).
- A tool for automated failure detection on wind farm level was developed for using vibrational data of all WTs: distance-based vibration evaluation (DAVE).
- Algorithms for automated data-driven CMS alarm prediction were introduced. Here, three different approaches were carried out: predicting the number of alarms, predicting the probability of having an alarm over time and predicting failures with an alarm time shifting setup.

The analysis of the merged data utilising HC showed that signal relationships changed before main bearing (MB) failures. It became apparent, that not only dedicated CMS records for the MB might indicate the problem, but also other CMS records of other components and SCADA signals. The CMS data taken in various active power intervals were found to be similar.

The application of the DAVE tool proved that reliable failure detection is feasible based on pair-wise comparisons of vibration spectra. Three MB failures were detected up to 119 days in advance of the failure. DAVE gave consistently earlier alarms than the commercial CMS.

The application of machine learning frameworks showed that after learning with CMS alarms, SCADA data alone could give a reasonably accurate failure prediction – in terms of the alarm count (used as failure indicator) and also the time-dependent probability. However, the ratio of true and false alarms was clearly improved if CMS data were also used.

It can be concluded that the herein presented automated failure detection algorithms based on both SCADA and CMS data, have shown to perform very well and could contribute to lowering the costs related to maintenance actions.

For future studies, there are several possibilities to build upon this work. This could include:

- Further analysis of data relationships should consider the detailed cluster composition and DTW similarities inside these clusters.
- The DAVE framework should be evaluated for other failure modes and components.
- The probabilities of having an alarm could be integrated into an online monitoring framework.
- The CMS alarm prediction could be extended using other learning algorithms, maximising the possible lead times for several components.
- The effectiveness of the classification based predictions should be evaluated from a risk perspective.
- The different approaches presented in this work could be merged, e.g. by predicting alarms generated by DAVE.
- The proposed algorithms should be validated against traditional CMS analysis.

In general, the synergies between CMS and SCADA data should be better explored. Direct data processing in the turbine should be the final aim to avoid high frequency time series storage.

Acknowledgements

This project has received funding from the European Union's Horizon 2020 research and innovation programme under the Marie Skłodowska-Curie grant agreement No 642108, known as the AWESOME consortium. The authors would like to thank Vattenfall for the data and support provided.

References

References

[1] W. Yang, R. Court, J. Jiang, Wind turbine condition monitoring by the approach of SCADA data analysis, Renewable Energy 53 (2013) 365–376, DOI: 10.1016/j.renene.2012.11.030.

[2] W. Yang, P. J. Tavner, C. J. Crabtree, Y. Feng, Y. Qiu, Wind turbine condition monitoring: technical and commercial challenges, Wind Energy 17 (5) (2014) 673–693, DOI: 10.1002/we.1508.

[3] Y. Feng, Y. Qiu, C. J. Crabtree, H. Long, P. J. Tavner, Monitoring wind turbine gearboxes, Wind Energy 16 (5) (2013) 728–740, DOI: 10.1002/we.1521.

[4] A. Kusiak, Z. Zhang, Analysis of Wind Turbine Vibrations Based on SCADA Data, Journal of Solar Energy Engineering 132 (3) (2010) 031008, DOI: 10.1115/1.4001461.

[5] P. Lind, L. Vera-Tudela, M. Wächter, M. Kühn, J. Peinke, Normal Behaviour Models for Wind Turbine Vibrations: Comparison of Neural Networks and a Stochastic Approach, Energies 10 (12) (2017) 1944, DOI: 10.3390/en10121944.

[6] L. Colone, M. Reder, J. Tautz-Weinert, J. J. Melero, A. Natarajan, S. J. Watson, Optimisation of Data Acquisition in Wind Turbines with Data-Driven Conversion Functions for Sensor Measurements, Energy Procedia 137 (2017) 571–578, DOI: 10.1016/j.egypro.2017.10.386.

[7] G. A. M. van Kuik, J. Peinke, R. Nijssen, D. Lekou, J. Mann, J. N. Sørensen, C. Ferreira, J. W. van Wingerden, D. Schlipf, P. Gebraad, H. Polinder, A. Abrahamsen, G. J. W. van Bussel, J. D. Sørensen, P. Tavner, C. L. Bottasso, M. Muskulus, D. Matha, H. J. Lindeboom, S. Degraer, O. Kramer, S. Lehnhoff, M. Sonnenschein, P. E. Sørensen, R. W. Künneke, P. E. Morthorst, K. Skytte, Long-term research challenges in wind energy - a research agenda by the European Academy of Wind Energy, Wind Energy Science 1 (1) (2016) 1–39, DOI: 10.5194/wes-1-1-2016.

[8] S. Dienst, J. Beseler, Automatic Anomaly Detection in Offshore Wind SCADA Data, WindEurope Summit 2016, 2016, pp. 1–6.

[9] E. Artigao, L. Colone, E. Gonzalez, E. Nanos, R. Pandit, M. Reder, H. Seyr, J. Tautz-Weinert, L. Valldecabres, N. Yilidirim, L. Ziegler, 1st Joint Industry Workshop Scientific report, Tech. rep., melero, J J, Muskulus, M and Smolka, U (editors). URL: `http://awesome-h2020.eu/2016/02/20/1st-joint-industry-workshop-scientific-report/` Last accessed: 05/06/2018. (2016).

[10] F. P. García Márquez, A. M. Tobias, J. M. Pinar Pérez, M. Papaelias, Condition monitoring of wind turbines: Techniques and methods, Renewable Energy 46 (2012) 169–178, DOI: 10.1016/j.renene.2012.03.003.

[11] W. Qiao, D. Lu, A Survey on Wind Turbine Condition Monitoring and Fault Diagnosis - Part II: Signals and Signal Processing Methods, IEEE Transactions on Industrial Electronics 62 (10) (2015) 6546–6557, DOI: 10.1109/TIE.2015.2422394.

[12] K. Fischer, D. Coronado, Condition Monitoring of Wind Turbines : State of the Art , User Experience and Recommendations, Tech. rep., Fraunhofer Institute for Wind Energy and Energy System Technology, Bremerhaven, Germany, URL: `https://www.vgb.org/vgbmultimedia/383_Final+report-p-9786.pdf`. Last accessed: 10/02/2018 (2015).

[13] GL Renewables Certification, Rules and Guidelines, IV: Industrial Services; 4: Guideline for the certification of condition monitoring systems for wind turbines (2013).

[14] X. Gong, W. Qiao, Bearing Fault Diagnosis for Direct-Drive Wind Turbines via Current-Demodulated Signals, Industrial Electronics, IEEE Transactions on 60 (8) (2013) 3419–3428, DOI: 10.1109/TIE.2013.2238871.

[15] Y. Guo, X. Chen, S. Wang, R. Sun, Z. Zhao, Wind Turbine Diagnosis under Variable Speed Conditions Using a Single Sensor Based on the Synchrosqueezing Transform Method, Sensors 17 (6) (2017) 1149, DOI: 10.3390/s17051149.

[16] B. Geropp, Envelope Analysis - A Signal Analysis Technique for Early Detection and Isolation of Machine Faults, IFAC Proceedings Volumes 30 (18) (1997) 977–981, DOI: 10.1016/S1474-6670(17)42527-4.

[17] B. P. Bogert, J. R. Healy, J. W. Tukey, The Quefrency Analysis of Time Series for Echoes: Cepstrum, Pseudo-Autocovariance, Cross-Cepstrum, and Saphe Cracking, Proceedings of the Symposium on Time Series Analysis, 1963, pp. 209–243.

[18] M. P. Norton, D. G. Karczub, Fundamentals of Noise and Vibration Analysis for Engineers, Cambridge University Press, 2003.

[19] N. J. Wismer, Gearbox Analysis using Cepstrum Analysis and Comb Liftering, Tech. Rep. 403, Application Note Brüel & Kjaer, URL: `https://www.bksv.com/media/doc/bo0440.pdf`. Last accessed: 10/02/2018 (2003).

[20] S. Sheng, Wind Turbine Gearbox Condition Monitoring Round Robin Study - Vibration Analysis, Tech. rep., National Renewable Energy Lab. (NREL), Golden, CO (United States), DOI: 10.2172/1048981 (2012).

[21] Specra Quest Tech Note, Rotating Machinery Faulty Diagnosis Techniques - Envelope and Cepstrum Analyses, Tech. rep., Spectra Quest, Inc., Richmond, VA , USA, URL: `http://spectraquest.com/technote_display/?technote_id=23`. Last accessed: 10/02/2018 (2006).

[22] C. J. Crabtree, D. Zappalá, P. J. Tavner, Survey of Commercially Available Condition Monitoring Systems for Wind Turbines, Tech. rep., Durham University School of Engineering and Computing Sciences and the SUPERGEN Wind Energy Technologies Consortium, URL: `http://dro.dur.ac.uk/12497/`. Last accessed: 10/02/2018 (2014).

[23] R. Uma Maheswari, R. Umamaheswari, Trends in non-stationary signal processing techniques applied to vibration analysis of wind turbine drive train - A contemporary survey, Mechanical Systems and Signal Processing 85 (2017) 296–311, DOI: 10.1016/j.ymssp.2016.07.046.

[24] S. Koukoura, J. Carroll, A. Mcdonald, Wind Turbine Intelligent Gear Fault Identification, Annual Conference of the PHM Society, St. Petersburg, United States, 2017, pp. 1–7.

[25] M. Bach-Andersen, B. Rømer-Odgaard, O. Winther, Deep learning for automated drivetrain fault detection, Wind Energy 21 (1) (2018) 29–41, DOI: 10.1002/we.2142.
[26] J. M. Ha, H. Oh, J. Park, B. D. Youn, Classification of operating conditions of wind turbines for a class-wise condition monitoring strategy, Renewable Energy 103 (2017) 594–605, DOI: 10.1016/j.renene.2016.10.071.
[27] J. Tautz-Weinert, S. J. Watson, Using SCADA data for wind turbine condition monitoring – a review, IET Renewable Power Generation 11 (4) (2017) 382–394, DOI: 10.1049/iet-rpg.2016.0248.
[28] A. Kusiak, W. Li, The prediction and diagnosis of wind turbine faults, Renewable Energy 36 (1) (2011) 16–23, DOI: 10.1016/j.renene.2010.05.014.
[29] B. Chen, P. C. Matthews, P. J. Tavner, Wind turbine pitch faults prognosis using a-priori knowledge-based ANFIS, Expert Systems with Applications 40 (17) (2013) 6863–6876, DOI: 10.1016/j.eswa.2013.06.018.
[30] E. Gonzalez, M. Reder, J. J. Melero, SCADA alarms processing for wind turbine component failure detection, Journal of Physics: Conference Series 753 (072019), DOI: 10.1088/1742-6596/753/7/072019.
[31] M. Reder, E. Gonzalez, J. J. Melero, Wind Turbine Failures - Tackling current Problems in Failure Data Analysis, Journal of Physics: Conference Series 753 (072027), DOI: 10.1088/1742-6596/753/7/072027.
[32] M. Reder, N. Y. Yürüşen, J. J. Melero, Data-driven learning framework for associating weather conditions and wind turbine failures, Reliability Engineering & System Safety 169 (2018) 554–569, DOI: 10.1016/j.ress.2017.10.004.
[33] S. M. Tabatabaeipour, P. F. Odgaard, T. Bak, Fault detection of a benchmark wind turbine using interval analysis, in: 2012 American Control Conference (ACC), 2012, pp. 4387–4392, DOI: 10.1109/ACC.2012.6315162.
[34] P. F. Odgaard, S. E. Shafiei, Evaluation of Wind Farm Controller based Fault Detection and Isolation, in: 9th IFAC Symposium on Fault Detection, Supervision and Safety for Technical Processes SAFEPROCESS 2015, Vol. 48, 2015, pp. 1084 – 1089, DOI: 10.1016/j.ifacol.2015.09.671.
[35] H. Badihi, Y. Zhang, S. Rakheja, P. Pillay, Model-Based Fault-Tolerant Pitch Control of an Offshore Wind Turbine, in: 10th IFAC Symposium on Advanced Control of Chemical Processes ADCHEM 2018, Vol. 51, 2018, pp. 221 – 226, DOI: 10.1016/j.ifacol.2018.09.303.
[36] C. S. Gray, S. J. Watson, Physics of Failure approach to wind turbine condition based maintenance, Wind Energy 13 (5) (2010) 395–405, DOI: 10.1002/we.360.
[37] Y. Qiu, L. Chen, Y. Feng, Y. Xu, An Approach of Quantifying Gear Fatigue Life for Wind Turbine Gearboxes Using Supervisory Control and Data Acquisition Data, Energies 10 (8) (2017) 1084, DOI: 10.3390/en10081084.
[38] K. Kim, G. Parthasarathy, O. Uluyol, W. Foslien, S. Sheng, P. Fleming, Use of SCADA data for failure detection in wind turbines, no. PARTS A, B, AND C in ASME 5th Int. Conf. Energy Sustain., 2011, pp. 2071–2079, DOI: 10.1115/ES2011-54243.
[39] P. Sun, J. Li, C. Wang, X. Lei, A generalized model for wind turbine anomaly identification based on SCADA data, Applied Energy 168 (2016) 550–567, DOI: 10.1016/j.apenergy.2016.01.133.
[40] P. Bangalore, M. Patriksson, Analysis of SCADA data for early fault detection, with application to the maintenance management of wind turbines, Renewable Energy 115 (2018) 521–532, DOI: 10.1016/j.renene.2017.08.073.
[41] M. Schlechtingen, I. F. Santos, S. Achiche, Wind turbine condition monitoring based on SCADA data using normal behavior models. Part 1: System description, Applied Soft Computing 13 (1) (2013) 447–460, DOI: 10.1016/j.asoc.2013.09.016.
[42] J. Tautz-Weinert, S. J. Watson, Comparison of different modelling approaches of drive train temperature for the purposes of wind turbine failure detection, Journal of Physics: Conference Series 753 (2016) 072014, DOI: 10.1088/1742-6596/753/7/072014.
[43] P. Bangalore, L. B. Tjernberg, An Artificial Neural Network Approach for Early Fault Detection of Gearbox Bearings, IEEE Transactions on Smart Grid 6 (2) (2015) 980–987, DOI: 10.1109/TSG.2014.2386305.
[44] L. Rokach, O. Maimon, Clustering Methods, in: Data Mining and Knowledge Discovery Handbook, Springer-Verlag, New York, 2005, pp. 321–352.
[45] H. Sakoe, S. Chiba, Dynamic programming algorithm optimization for spoken word recognition, IEEE Transactions on Acoustics, Speech, and Signal Processing 26 (1) (1978) 43–49, DOI: 10.1109/TASSP.1978.1163055.
[46] J. A. Nelder, R. W. Wedderbu, Generalized Linear Models, Journal of the Royal Statistical Society, Series A-General 135 (3) (1972) 370–384, DOI: 10.2307/2344614.
[47] R. Tibshirani, Regression Shrinkage and Selection Via the Lasso, Journal of the Royal Statistical Society, Series B 58 (1994) 267–288.
[48] L. Breiman, Random Forests, Tech. rep., Statistics Department - University of California, Berkeley, CA, URL: `http://link.springer.com/10.1023/A:1010933404324`. Last accessed: 06/01/2018 (2001).
[49] L. Breiman, Bagging predictors, Machine Learning 24 (2) (1996) 123–140. `doi:10.1007/BF00058655`.
[50] J. H. Friedman, Greedy function approximation: A gradient boosting machine., Ann. Statist. 29 (5) (2001) 1189–1232, DOI: 10.1214/aos/1013203451.
[51] D. W. Marquardt, An Algorithm for Least-Squares Estimation of Nonlinear Parameters, *Journal of the Society for Industrial and Applied Mathematics* 11 (2) (1963) 431–441.
[52] T. D. Gedeon, Data Mining of Inputs: Analysing Magnitude and Functional Measures, International Journal of Neural Systems 08 (02) (1997) 209–218, DOI: 10.1142/S0129065797000227.
[53] N. V. Chawla, Data Mining for Imbalanced Datasets: An Overview, in: Data Mining and Knowledge Discovery Handbook, Springer US, Boston, MA, 2009, pp. 875–886.
[54] C. M. Bishop, Pattern Recognition and Machine Learning (Information Science and Statistics), Springer-Verlag New York, Inc., Secaucus, NJ, USA, 2006.

Bibliography

[1] J. Cook, N. Oreskes, P. T. Doran, W. R. L. Anderegg, B. Verheggen, E. W. Maibach, J. S. Carlton, S. Lewandowsky, A. G. Skuce, S. A. Green, D. Nuccitelli, P. Jacobs, M. Richardson, B. Winkler, R. Painting, K. Rice, Consensus on consensus: a synthesis of consensus estimates on human-caused global warming, Environmental Research Letters 11 (4) (2016) 048002.
URL http://stacks.iop.org/1748-9326/11/i=4/a=048002

[2] I. E. C. IEC, Wind Turbines - Part III: Design Requirements for Offshore Wind Turbines - IEC 61400-3.

[3] S. T. Frandsen, Turbulence and turbulence-generated structural loading in wind turbine clusters, Technical University of Denmark, Risø National Laboratory for Sustainable Energy, 2007.

[4] W. Europe, Wind in power 2017. annual combined onshore and offshore wind energy statistics.

[5] Block island wind farm, https://www.nrdc.org/stories/wind-farm-great-lakes-lets-give-it-twirl.

[6] Example wind turbine configuration, https://www.windpowerengineering.com/bearings/large-offshore-wind-turbines-challenging-bearing-designs/.

[7] World economic forum, https://www.weforum.org/.

[8] The economist, https://www.economist.com/news/leaders/21721656-data-economy-demands-new-approach-antitrust-rules-worlds-most-valuable-reso

[9] W. Q. Meeker, Y. Hong, Reliability meets big data: opportunities and challenges, Quality Engineering 26 (1) (2014) 102–116.

[10] R. B. Randall, Vibration-based condition monitoring: industrial, aerospace and automotive applications, John Wiley & Sons, 2011.

[11] M. Rausand, H. Arnljot, System reliability theory: models, statistical methods, and applications, Vol. 396, John Wiley & Sons, 2004.

[12] T. Bedford, R. Cooke, Probabilistic Risk Analysis: Foundations and Methods, Cambridge University Press, 2001.
URL https://books.google.at/books?id=46dx50PoWcwC

[13] A. K. Jardine, D. Lin, D. Banjevic, A review on machinery diagnostics and prognostics implementing condition-based maintenance, Mechanical systems and signal processing 20 (7) (2006) 1483–1510.

[14] A. Guillén, A. Crespo, M. Macchi, J. Gómez, On the role of prognostics and health management in advanced maintenance systems, Production Planning & Control 27 (12) (2016) 991–1004. arXiv:https://doi.org/10.1080/09537287.2016.1171920, doi:10.1080/09537287.2016.1171920.
URL https://doi.org/10.1080/09537287.2016.1171920

[15] J. Lee, C. Jin, Z. Liu, H. D. Ardakani, Introduction to data-driven methodologies for prognostics and health management, Probabilistic Prognostics and Health Management of Energy Systems (2017) 9–32doi:10.1007/978-3-319-55852-3_2.

[16] J. R. Sifonte, J. V. Reyes-Picknell, Reliability Centered Maintenance–Reengineered: Practical Optimization of the RCM Process with RCM-R®, CRC Press, 2017.

[17] D. Straub, Generic approaches to risk based inspection planning for steel structures, Vol. 284, vdf Hochschulverlag AG, 2004.

[18] J. S. Nielsen, Risk-based operation and maintenance of offshore wind turbines, River Publishers, 2013.

[19] M. K. Hovgaard, Incorporating structural health monitoring in the design of slip formed concrete wind turbine towers, Ph.D. thesis, River Publishers (2015).

[20] T. D. Nielsen, F. V. Jensen, Bayesian networks and decision graphs, Springer Science & Business Media, 2009.

[21] C. A. Walford, Wind turbine reliability: understanding and minimizing wind turbine operation and maintenance costs., Tech. rep., Sandia National Laboratories (2006).

[22] M. D. Esteban, J. J. Diez, J. S. López, V. Negro, Why offshore wind energy?, Renewable Energy 36 (2) (2011) 444 – 450. doi:https://doi.org/10.1016/j.renene.2010.07.009.
URL http://www.sciencedirect.com/science/article/pii/S0960148110003332

[23] T. J. Stehly, D. M. Heimiller, G. N. Scott, 2016 cost of wind energy review, Tech. rep., National Renewable Energy Lab.(NREL), Golden, CO (United States) (2017).

[24] C. Namovicz, Assessing the economic value of new utility-scale renewable generation projects, in: EIA energy conference, 2013.

[25] F. Besnard, On maintenance optimization for offshore wind farms, Chalmers University of Technology, 2013.

[26] P. Tavner, J. Xiang, F. Spinato, Reliability analysis for wind turbines, Wind Energy 10 (1) (2007) 1–18.

[27] M. Reder, J. J. Melero, Modelling the effects of environmental conditions on wind turbine failures, Wind Energy – (–) (2018) –. doi:DOI:10.1002/we.2201.
URL http://stacks.iop.org/1742-6596/926/i=1/a=012012

[28] T. Poulsen, C. B. Hasager, C. M. Jensen, The role of logistics in practical levelized cost of energy reduction implementation and government sponsored cost reduction studies: Day and night in offshore wind operations and maintenance logistics, Energies 10 (4) (2017) 464.

[29] S. Bhattacharya, Challenges in design of foundations for offshore wind turbines, Engineering & Technology Reference 1 (1).

[30] L. Castro-Santos, A. Filgueira-Vizoso, I. Lamas-Galdo, L. Carral-Couce, Methodology to calculate the installation costs of offshore wind farms located in deep waters, Journal of Cleaner Production 170 (2018) 1124–1135.

[31] L. Ziegler, E. Gonzalez, T. Rubert, U. Smolka, J. J. Melero, Lifetime extension of onshore wind turbines: A review covering germany, spain, denmark, and the uk, Renewable and Sustainable Energy Reviews 82 (2018) 1261–1271.

[32] G. DNV, Lifetime extension of wind turbines, Edition March (2016) 2016–03.

[33] Megavind. strategy for extending the useful lifetime of a wind turbine., http://www.vindmoellegodkendelse.dk/media/1163/strategy-for-extending-the-useful-lifetime-of-a-wind-turbine.pdf.

[34] T. Rubert, D. McMillan, P. Niewczas, A decision support tool to assist with lifetime extension of wind turbines, Renewable Energy.

[35] W. Weijtens, N. Noppe, T. Verbelen, A. Iliopoulos, C. Devriendt, Offshore wind turbine foundation monitoring, extrapolating fatigue measurements from fleet leaders to the entire wind farm, in: Journal of Physics: Conference Series, Vol. 753, IOP Publishing, 2016, p. 092018.

[36] W. Weijtjens, T. Verbelen, E. Capello, C. Devriendt, Vibration based structural health monitoring of the substructures of five offshore wind turbines, Procedia Engineering 199 (2017) 2294–2299.

[37] L. Ziegler, U. Smolka, N. Cosack, M. Muskulus, Brief communication: Structural monitoring for lifetime extension of offshore wind monopiles: can strain measurements at one level tell us everything?, Wind Energy Science 2 (2) (2017) 469.

[38] A. RP2A-LRFD, Recommended practice for planning, designing and constructing fixed offshore platforms-load'and resistance factor design, American Petroleum Institute, Washington.

[39] P. Tavner, C. Edwards, A. Brinkman, F. Spinato, Influence of wind speed on wind turbine reliability, Wind Engineering 30 (1) (2006) 55–72.

[40] M. Reder, J. J. Melero, Modelling wind turbine failures based on weather conditions, Journal of Physics: Conference Series 926 (1) (2017) 012012.
URL http://stacks.iop.org/1742-6596/926/i=1/a=012012

[41] N. T. Garabedian, B. J. Gould, G. L. Doll, D. L. Burris, The cause of premature wind turbine bearing failures: Overloading or underloading?, Tribology Transactions 0 (0) (2018) 1–10. arXiv:https://doi.org/10.1080/10402004.2018.1433345, doi:10.1080/10402004.2018.1433345.
URL https://doi.org/10.1080/10402004.2018.1433345

[42] A. Rasekhi Nejad, Z. Gao, T. Moan, Fatigue reliability-based inspection and maintenance planning of gearbox components in wind turbine drivetrains.

[43] C. Galinos, N. Dimitrov, T. J. Larsen, A. Natarajan, K. S. Hansen, Mapping wind farm loads and power production-a case study on horns rev 1, in: Journal of Physics: Conference Series, Vol. 753, IOP Publishing, 2016, p. 032010.

[44] A. Kusiak, Z. Song, Design of wind farm layout for maximum wind energy capture, Renewable energy 35 (3) (2010) 685–694.

[45] P.-E. Réthoré, P. Fuglsang, G. C. Larsen, T. Buhl, T. J. Larsen, H. A. Madsen, Topfarm: Multi-fidelity optimization of wind farms, Wind Energy 17 (12) (2014) 1797–1816.

[46] A. C. Pillai, J. Chick, L. Johanning, M. Khorasanchi, Offshore wind farm layout optimization using particle swarm optimization, Journal of Ocean Engineering and Marine Energy 4 (1) (2018) 73–88.

[47] J. Carroll, A. McDonald, D. McMillan, Failure rate, repair time and unscheduled o&m cost analysis of offshore wind turbines, Wind Energy 19 (6) (2016) 1107–1119.

[48] J. Tautz-Weinert, S. Watson, Condition monitoring of wind turbine drive trains by normal behaviour modelling of temperatures, in: Conference for Wind Power Drives 2017: Tagungsband zur Konferenz, Vol. 3, BoD–Books on Demand, 2017, p. 359.

[49] P. Bangalore, L. B. Tjernberg, An artificial neural network approach for early fault detection of gearbox bearings, IEEE Transactions on Smart Grid 6 (2) (2015) 980–987.

[50] E. Gonzalez, B. Stephen, D. Infield, J. Melero, On the use of high-frequency scada data for improved wind turbine performance monitoring, in: Journal of Physics: Conference Series, Vol. 926, IOP Publishing, 2017, p. 012009.

[51] J. Tautz-Weinert, S. J. Watson, Using scada data for wind turbine condition monitoring–a review, IET Renewable Power Generation 11 (4) (2016) 382–394.

[52] M. Bach-Andersen, B. Rømer-Odgaard, O. Winther, Flexible non-linear predictive models for large-scale wind turbine diagnostics, Wind Energy 20 (5) (2017) 753–764.

[53] K. Leahy, C. Gallagher, K. Bruton, P. O'Donovan, D. T. O'Sullivan, Automatically identifying and predicting unplanned wind turbine stoppages using scada and alarms system data: Case study and results, in: Journal of Physics: Conference Series, Vol. 926, IOP Publishing, 2017, p. 012011.

[54] M. Bach-Andersen, B. Rømer-Odgaard, O. Winther, Deep learning for automated drivetrain fault detection, Wind Energy.

[55] J. Daily, J. Peterson, Predictive maintenance: How big data analysis can improve maintenance, in: Supply Chain Integration Challenges in Commercial Aerospace, Springer, 2017, pp. 267–278.

[56] G. G. Hassan, A guide to uk offshore wind operations and maintenance, Scottish Enterprise and The Crown Estate (2013) 21.

[57] DNV-GL, Loads and site conditions for wind turbines, DNV-GL, 2016.

[58] N. Dimitrov, J. Staerdahl, P. Friis-Hansen, C. Berggreen, Structural reliability of wind turbine blades: Design methods and evaluation, Ph.D. thesis (2013).

[59] J. F. Manwell, J. G. McGowan, A. L. Rogers, Wind energy explained: theory, design and application, John Wiley & Sons, 2010.

[60] F. Rasmussen, M. H. Hansen, K. Thomsen, T. J. Larsen, F. Bertagnolio, J. Johansen, H. A. Madsen, C. Bak, A. M. Hansen, Present status of aeroelasticity of wind turbines, Wind energy 6 (3) (2003) 213–228.

[61] T. J. Larsen, A. M. Hansen, How 2 hawc2, the user's manual, Tech. rep., Risø National Laboratory (2007).

[62] I. Abdallah, Assessment of extreme design loads for modern wind turbines using the probabilistic approach, Ph.D. thesis, DTU Wind Energy (2015).

[63] J. Journée, W. Massie, Offshore hydromechanics, TU Delft, 2000.

[64] A. Natarajan, Influence of second-order random wave kinematics on the design loads of offshore wind turbine support structures, Renewable Energy 68 (2014) 829–841.

[65] P. Agarwal, L. Manuel, Incorporating irregular nonlinear waves in coupled simulation and reliability studies of offshore wind turbines, Applied Ocean Research 33 (3) (2011) 215–227.

[66] G. DNV, DNV-OS-J101–design of offshore wind turbine structures, DNV GL.

[67] J. Morison, J. Johnson, S. Schaaf, et al., The force exerted by surface waves on piles, Journal of Petroleum Technology 2 (05) (1950) 149–154.

[68] G. C. Larsen, H. A. Madsen, K. Thomsen, T. J. Larsen, Wake meandering: a pragmatic approach, Wind Energy: An International Journal for Progress and Applications in Wind Power Conversion Technology 11 (4) (2008) 377–395.

[69] H. S. Toft, L. Svenningsen, W. Moser, J. D. Sørensen, M. L. Thøgersen, Wind climate parameters for wind turbine fatigue load assessment, Journal of Solar Energy Engineering 138 (3) (2016) 031010.

[70] D. N. Veritas, Fatigue design of offshore steel structures, No. DNV-RP-C203 30.

[71] O. Standard, Design of offshore wind turbine structures, DET NOR SKE VERITAS.

[72] D. Kallehave, B. W. Byrne, C. L. Thilsted, K. K. Mikkelsen, Optimization of monopiles for offshore wind turbines, Phil. Trans. R. Soc. A 373 (2035) (2015) 20140100.

[73] W. NJOMO WANDJI, Probabilistic design of wind turbine structures: Design studies and sensitivities to model parameters, Ph.D. thesis, Denmark (2017). doi:10.11581/DTU:00000026.

[74] M. H. Faber, Statistics and probability theory: in pursuit of engineering decision support, Vol. 18, Springer Science & Business Media, 2012.

[75] S. Schløer, L. G. Castillo, M. Fejerskov, E. Stroescu, H. Bredmose, A model for quick load analysis for monopile-type offshore wind turbine substructures, in: Journal of Physics: Conference Series, Vol. 753, IOP Publishing, 2016, p. 092008.

[76] N. Veritas, Structural reliability analysis of marine structures, Det Norske Veritas, 1992.

[77] A. M. Hasofer, N. C. Lind, Exact and invariant second-moment code format, Journal of the Engineering Mechanics division 100 (1) (1974) 111–121.

[78] O. Ditlevsen, H. O. Madsen, Structural reliability methods, Vol. 178, Wiley New York, 1996.

[79] M. Reder, N. Y. Yürüşen, J. J. Melero, Data-driven learning framework for associating weather conditions and wind turbine failures, Reliability Engineering & System Safety 169 (2018) 554–569.

[80] M. Reder, E. Gonzalez, J. J. Melero, Wind turbine failures-tackling current problems in failure data analysis, in: Journal of Physics: Conference Series, Vol. 753, IOP Publishing, 2016, p. 072027.

[81] K. Ogata, Y. Yang, Modern control engineering, Vol. 4, Prentice hall India, 2002.

[82] E. A. Bossanyi, Individual blade pitch control for load reduction, Wind Energy 6 (2) (2003) 119–128. doi:10.1002/we.76.
URL http://dx.doi.org/10.1002/we.76

[83] P. F. Odgaard, J. Stoustrup, M. Kinnaert, Fault tolerant control of wind turbines–a benchmark model, IFAC Proceedings Volumes 42 (8) (2009) 155–160.

[84] J. Ringwood, S. Simani, Overview of modelling and control strategies for wind turbines and wave energy devices: Comparisons and contrasts, Annual Reviews in Control 40 (2015) 27 – 49. doi:https://doi.org/10.1016/j.arcontrol.2015.09.003.
URL http://www.sciencedirect.com/science/article/pii/S1367578815000371

[85] S. S. Rao, F. F. Yap, Mechanical vibrations, Vol. 4, Prentice Hall Upper Saddle River, 2011.

[86] M. H. Hansen, B. S. Kallesøe, Servo-elastic dynamics of a hydraulic actuator pitching a blade with large deflections, Journal of Physics: Conference Series 75 (1) (2007) 012077.
URL http://stacks.iop.org/1742-6596/75/i=1/a=012077

[87] T. J. Larsen, A. M. Hansen, Influence of blade pitch loads by large blade deflections and pitch actuator dynamics using the new aeroelastic code hawc2 (2006).

[88] J. Berroth, G. Jacobs, T. Kroll, R. Schelenz, Investigation on pitch system loads by means of an integral multi body simulation approach, in: Journal of Physics: Conference Series, Vol. 753, IOP Publishing, 2016, p. 112002.

[89] R. Erde, Rothe erde® slewing bearings, Rothe Erde, Dortmund.

[90] M. Stammler, F. Schwack, N. Bader, A. Reuter, G. Poll, Friction torque of wind-turbine pitch bearings–comparison of experimental results with available models, Wind Energy Science Discussions 2017 (2017) 2017 (2017) 1–16.

[91] SKF, The SKF model for calculating the frictional moment.
URL http://www.skf.com/group/splash/index.html

[92] C. Tibaldi, M. H. Hansen, L. C. Henriksen, Optimal tuning for a classical wind turbine controller, in: Journal of Physics: Conference Series, Vol. 555, IOP Publishing, 2014, p. 012099.

[93] S. Marelli, R. Schöbi, B. Sudret, Uqlab user manual–structural reliability, Tech. rep., Technical report, Chair of Risk, Safety and Uncertainty Quantification, ETH Zurich. Report UQLab-V1. 0-107 (2017).

[94] M. Rosenblatt, Remarks on a multivariate transformation, Ann. Math. Statist. 23 (3) (1952) 470–472. doi:10.1214/aoms/1177729394.
URL https://doi.org/10.1214/aoms/1177729394

[95] N. Dimitrov, M. Kelly, A. Vignaroli, J. Berg, From wind to loads: wind turbine site-specific load estimation using databases with high-fidelity load simulations, Wind Energ. Sci. Discuss.

[96] G. DNV, Rotor blades for wind turbines, Tech. rep., Standard DNVGL-ST-0376 (2015).

[97] J. P. Murcia, P.-E. Réthoré, N. Dimitrov, A. Natarajan, J. D. Sørensen, P. Graf, T. Kim, Uncertainty propagation through an aeroelastic wind turbine model using polynomial surrogates, Renewable Energy 119 (2018) 910 – 922. doi:https://doi.org/10.1016/j.renene.2017.07.070.
URL http://www.sciencedirect.com/science/article/pii/S0960148117306985

[98] Aeon, https://aeon.co/essays/on-the-dark-history-of-intelligence-as-domination.

[99] M. Ruse, Charles darwin on human evolution, Journal of Economic Behavior & Organization 71 (1) (2009) 10–19.

[100] G. Shmueli, et al., To explain or to predict?, Statistical science 25 (3) (2010) 289–310.

[101] M. Kuhn, K. Johnson, Applied predictive modeling, Vol. 26, Springer, 2013.

[102] J. Friedman, T. Hastie, R. Tibshirani, The elements of statistical learning, Vol. 1, Springer series in statistics New York, 2001.

[103] C. M. Bishop, Pattern Recognition and Machine Learning (Information Science and Statistics), Springer-Verlag New York, Inc., Secaucus, NJ, USA, 2006.

[104] T. Hastie, R. Tibshirani, M. Wainwright, Statistical learning with sparsity: the lasso and generalizations, CRC press, 2015.

[105] L. Breiman, Random forests, Machine learning 45 (1) (2001) 5–32.

[106] G. James, D. Witten, T. Hastie, R. Tibshirani, An introduction to statistical learning, Vol. 112, Springer, 2013.

[107] M. Titterington, Neural networks, Wiley Interdisciplinary Reviews: Computational Statistics 2 (1) (2010) 1–8. doi:10.1002/wics.50.
URL http:https://doi.org/10.1002/wics.50

[108] A. Saltelli, S. Tarantola, F. Campolongo, M. Ratto, Sensitivity analysis in practice: a guide to assessing scientific models, John Wiley & Sons, 2004.

[109] T. A. F. C. J. C. D. G. M. S. A. Saltelli, M. Ratto, S. Tarantola, Global Sensitivity Analysis. The Primer, John Wiley & Sons, 2008.

[110] V. Venkatasubramanian, R. Rengaswamy, S. N. Kavuri, K. Yin, A review of process fault detection and diagnosis: Part iii: Process history based methods, Computers & chemical engineering 27 (3) (2003) 327–346.

[111] R. Isermann, Fault diagnosis of machines via parameter estimation and knowledge processing—tutorial paper, Automatica 29 (4) (1993) 815–835.

[112] D. Straub, I. Welpe, Decision-making under risk: a normative and behavioral perspective, in: Risk-A Multidisciplinary Introduction, Springer, 2014, pp. 63–93.

[113] A. Gelman, J. B. Carlin, H. S. Stern, D. B. Dunson, A. Vehtari, D. B. Rubin, Bayesian data analysis, CRC press, 2013.

[114] M. Bach-Andersen, O. Winther, B. Rømer-Odgaard, Scalable systems for early fault detection in wind turbines: a data driven approach, in: Annual Conference of the european Wind Energy Association, 2015.

[115] I. M. Sobol, Global sensitivity indices for nonlinear mathematical models and their monte carlo estimates, Mathematics and computers in simulation 55 (1-3) (2001) 271–280.

[116] T. Cody, P. J. Dempsey, Application of machine learning to rotorcraft health monitoring.

Technical University of Denmark
Department of Wind Energy
Frederiksborgvej 399
Building 118
4000 Roskilde
Denmark
Telephone 46 77 50 85

info@vindenergi.dtu.dk
www.vindenergi.dtu.dk